

Structural basis for reversible, oxidative inhibition of PTEN phosphatase activity

Dissertation

**For the achievement of the academic degree of the
doctor rerum naturalium
(Dr. rer. nat.)**

Submitted to

Department of Chemistry and Chemical Biology
Technical University Dortmund

by

M. Sc. Chang Uk Lee

Dortmund 2016

Structural basis for reversible, oxidative inhibition of PTEN phosphatase activity

Dissertation

zur Erlangung des akademischen Grades

doctor rerum naturalium

(Dr. rer. nat.)

eingereicht an der

Fakultät für Chemie und Chemische Biologie

der Technischen Universität Dortmund

von

M. Sc. Chang Uk Lee

Dortmund 2016

1st Examiner

Prof. Dr. Herbert Waldmann

Department of Chemistry and Chemical Biology
Technical University Dortmund, Dortmund, Germany
and

Department of Chemical Biology
Max Planck Institute of Molecular Physiology, Dortmund, Germany

2nd Examiner

Prof. Dr. Tom N. Grossmann

VU University Amsterdam
Department of Chemistry & Pharmaceutical Sciences
De Boelelaan 1083, 1081 HV, Amsterdam, The Netherlands

The present work has been performed in the research group of Prof. Dr. Tom N. Grossmann at the Chemical Genomics Centre of the Max Planck Society from February 2012 to January 2016.

Parts of this dissertation have been published in the following journal article:

Redox modulation of PTEN phosphatase activity by hydrogen peroxide and bisperoxidovanadium complexes.

C.-U. Lee, G. Hahne, J. Hanske, T. Bange, D. Bier, C. Rademacher, S. Hennig, T. N. Grossmann, *Angew. Chem. Int. Ed.* **2015**, *54*, 13796-13800.

Acknowledgement

First of all, I am very grateful to Prof. Dr. Waldmann for accepting the supervision of my Ph.D. program and for his valuable advices and scientific inputs about our publication. I also thank Prof. Dr. Tom N. Grossmann very much for his all-around supervision, support and direction of my project. I am grateful to all the members of the Chemical Genomics Centre (MPI Dortmund) and especially those of the Grossmann lab for a great working atmosphere. Among others, I appreciate members of the previous PTEN team, Dr. Gernot Hahne, Arne Küpper, Carolin Müller, and Sandra Bäcker, for their excellent works on the individual as well as on the cooperative level. I am grateful to Dr. Gernot Hahne, Christiane Junk, and Carolin Müller for the proof-reading of this thesis. In particular, I would like to deeply thank Dr. Gernot Hahne and Adrian Glas for their encouragement, fruitful discussion, and friendship. My deepest gratitude also goes to Dr. Sven Hennig for his scientific support and encouragement. His suggestions and advices led to significant advances in many aspects during this project. I appreciate Dr. Ingrid Vetter, Georg Holtermann and the X-ray team at MPI Dortmund for their support in protein crystallography, fruitful discussions and maintenance of the X-ray facility. I am grateful to Dr. Tanja Bange, Franziska Müller, Jonas Hanske and Dr. Christoph Rademacher for the constructive collaboration in mass spectrometric and NMR spectroscopic analyses. I thank Dr. Stefan Heinrichs for providing the *pten* gene for the efficient start of this project. I express my deepest gratitude to Prof. Dr. Robert Huber, Dr. Martin Augustin, Dr. Junghoon Lee and all employees of Proteros Biostructures GmbH for giving me a tremendous chance to get into biochemistry. I cannot imagine successfully finishing my Ph.D. program in a structural biology field without experiences and lessons I had at that time.

In addition, I appreciate GoogleTM, PubMed, and Protein Data Bank very much for allowing people to have an easy access to extremely large amount of information as well as all scientists who are willing to share their knowledge and know-hows in the internet as an open-source.

At last, I am deeply grateful to my family, particularly to my parents and my wife Bohye. With their encouragement and love, I am now able to finish this long chapter of my life.

Table of contents

| | |
|--|------------|
| Acknowledgement | iii |
| Table of contents | iv |
| Zusammenfassung | v |
| 1 Introduction | 1 |
| 1.1 Protein tyrosine phosphatases | 1 |
| 1.2 PTEN | 3 |
| 1.3 Reactive oxygen species | 12 |
| 1.4 Bisperoxidovanadium-based PTEN inhibitors | 18 |
| 2 Aim of the thesis | 19 |
| 3 Results and discussion | 20 |
| 3.1 Protein expression and purification | 20 |
| 3.2 Effects of PIP ₂ /PIP ₃ -derivatives on phosphatase activity | 30 |
| 3.3 Oxidative modification of PTEN by hydrogen peroxide and bpV-phen | 34 |
| 3.4 Crystal structure of reduced PTEN | 39 |
| 3.5 Crystal structure of H ₂ O ₂ -treated PTEN | 53 |
| 3.6 Structural impact of PTEN inhibition by bpV-phen | 60 |
| 3.7 Discussion | 70 |
| 4 Summary | 75 |
| 5 Material and methods | 77 |
| 5.1 Materials and equipments | 77 |
| 5.2 Quantative analytical methods | 86 |
| 5.3 Molecular biological methods | 87 |
| 5.4 Protein expression using Bac-to-Bac [®] baculovirus expression system | 94 |
| 5.5 Recombinant protein expression in Escherichia coli | 97 |
| 5.6 Isolation of the recombinantly expressed proteins and their purification | 97 |
| 5.7 Protein crystallization and structure determination | 103 |
| 5.8 Malachite green activity assay | 107 |
| 5.9 Sample preparation for mass-spectrometric methods | 110 |
| 6 References | 111 |
| 7 Appendices | 126 |
| 7.1 pFH1-Vector | 126 |
| 7.2 Sequencing results | 128 |
| 7.3 SDS-PAGE and SEC analyses of the protein purification | 135 |
| 7.4 Detection of disulfide formation using HPLC-MS and MS/MS | 137 |
| 7.5 Influence of tartrate on oxidative inhibition and reactivation | 141 |
| 7.6 SDS-PAGE and SEC analyses of the protein purification | 142 |
| 8 Abbreviations | 143 |

Zusammenfassung

PTEN (phosphatase and tensin homolog deleted on chromosome 10) ist eine dualspezifische Protein-Tyrosin-Phosphatase (PTP). Als Tumorsuppressor spielt PTEN im Bezug auf zelluläre Homöostase eine wichtige Rolle. Die PTEN-Aktivität wird im physiologischen Zusammenhang von H_2O_2 inhibiert, das durch einen Redox-Signalweg und oxidativen Stress produziert wird. Die oxidative Inhibition durch H_2O_2 führt zur Disulfidbildung zwischen dem katalytischen Cystein C124 und dem räumlich benachbarten Cystein C71. Die Auswirkung der Disulfidbildung auf die Proteinstruktur ist jedoch bisher unbekannt. Um die Effekte der PTEN-Inhibition zu untersuchen, dienen Bisperoxidovanadium (bpV) Komplexe als wichtige Modellverbindungen. Diese bpV Komplexe weisen bei neuronalen und myokardialen Verletzungen einen regenerativen Effekt auf und besitzen damit Potential für deren Behandlung. Allerdings blieb deren Wirkungsweise auf PTEN unklar. Daher wurden in der vorliegenden Arbeit molekulare Effekte von H_2O_2 und bpV-phen auf PTEN mithilfe von Aktivitätsmessungen, Massenspektrometrie und Röntgenkristallographie untersucht.

Sowohl H_2O_2 als auch bpV-phen führen durch oxidative Inhibition am aktiven Zentrum von PTEN zu einer Disulfidbindung zwischen C124 und C71, was aber nur geringe strukturelle Änderungen zur Folge hat. Im Vergleich zu bekannten PTP-Strukturen im oxidierten Zustand ist dies zwar analog zur lymphoiden Tyrosinphosphatase, jedoch unterscheidet es sich von CDC25B und PTP1B, die signifikante Konformationsänderungen des aktiven Zentrums zeigen. Ausserdem zeigt PTEN auch unter stringenter H_2O_2 -Behandlung eine hohe Reaktivierbarkeit, wogegen CDC25B und PTP1B auch irreversible Oxidation erfahren. Damit besitzt PTEN möglicherweise einen effizienteren Schutzmechanismus gegen irreversible Modifikationen als andere PTPs. Desweiteren wurde mit ^{51}V -NMR Spektroskopie die Reaktion von PTEN mit bpV-phen näher untersucht. Die oxidative Inhibition führt zur Bildung eines Orthovanadatmoleküls, das eine schwache Affinität zum aktiven Zentrum des oxidierten PTEN aufweist. Im Gegensatz zu einigen anderen Phosphatasen zeigt Orthovanadat keine inhibitorische Wirkung auf die Enzymaktivität von PTEN, was bestätigt, dass die durch bpV-phen vermittelte PTEN-Inhibition auf die Disulfidbildung zurückzuführen ist. Die hier nachgewiesene reversible Inhibition durch bpV-phen könnte sich positiv auf therapeutische Anwendungen auswirken, da irreversible Inhibition dieses zentralen Tumorsuppressors systemische Störungen verursachen könnte. In dieser Hinsicht können die neuen Erkenntnisse über die Wirkungsweise von bpV-phen zur weiteren Entwicklung dieser Inhibitoriklasse beitragen.

1 Introduction

1.1 Protein tyrosine phosphatases

The reversible phosphorylation of proteins is of central importance to the regulation of numerous physiological processes in living organisms^{1,2}. As one of the post-translational modifications, phosphorylation involves covalent functional modifications of proteins, which results in alteration of their biological activity, stability, subcellular localization and protein-protein interaction properties among others¹. In particular, phosphorylation of a tyrosine residue plays a crucial role in growth control, as it is deeply implicated in transmembrane signaling^{3,4}. Indeed, cellular tyrosine phosphorylation increases during oncogenic transformation (total tyrosine phosphorylation of proteins from 0.01 % to 2 %.)^{5,6}. Tightly regulated phosphorylations are essential in maintaining cellular homeostasis and aberrant protein phosphorylation is associated with the development of many human diseases such as cancer, diabetes, rheumatoid arthritis, hypertension and neurodegeneration^{2,4,6,7}.

Protein phosphorylation is governed by two classes of enzymes. Protein kinases convey phosphorylation at serine/threonine and tyrosine residues of their protein substrates. Protein phosphatases reverse this action. Particularly, protein tyrosine phosphatases (PTPs), a subgroup of protein phosphatases, downregulate the tyrosine phosphorylation in signaling pathways. PTPs harbor a characteristic phosphate-binding loop (P-loop) in their active site involving a structural motif with the consensus sequence: HCXXGXXR^{8,9}. The conserved cysteine residue is responsible for the catalytic activity^{8,9}. In addition, the active site of PTPs exhibits an acidic microenvironment^{8,9}, which supports efficient recognition of negatively charged phosphotyrosine in their protein substrates. This acidic property promotes the presence of a deprotonated version of the catalytic cysteine at neutral pH¹⁰. The resulting protein thiolate is more nucleophilic than its protonated version, but susceptible to oxidation¹⁰. During phosphatase reaction, the catalytic cysteine in the active site P-loop nucleophilically attacks the phosphorous atom of the phosphotyrosine (Figure 1)¹¹. Upon obtaining a proton from a catalytic aspartic acid in the WPD (Trp-Pro-Asp)-loop, the protein substrate with the dephosphorylated tyrosine residue is released from the active site. The remaining cysteinyl-phosphate intermediate is stabilized by the neighboring arginine residue in the P-loop and subsequently hydrolyzed by a water molecule in the release of a free phosphate.

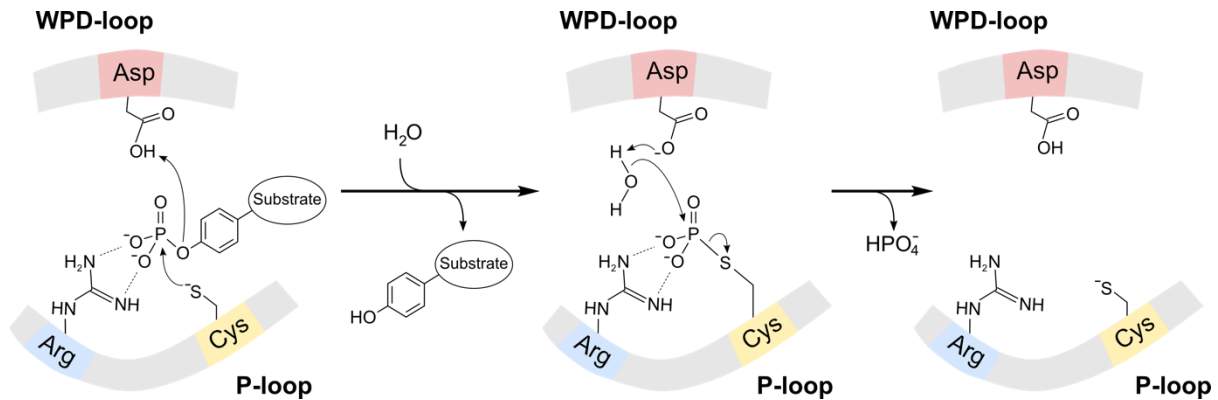


Figure 1 | Catalytic mechanism of dephosphorylation of phosphotyrosine by PTP. Catalytic cysteine in P-loop nucleophilically attacks the phosphate group of the phosphotyrosine and releases the dephosphorylated protein substrate. A water molecule activated by an aspartate in WPD-loop subsequently hydrolyzes the phosphocysteine, liberating an orthophosphate. The figure is based on Zhao *et. al.* (2014)¹¹.

The PTP superfamily including 107 human PTPs can be divided into four classes based on the amino acid sequence of their catalytic domains^{2,12,13}. Class I cysteine-based PTPs involve the majority of this superfamily with 38 classical PTPs and 61 dual-specificity protein tyrosine phosphatases (DUSPs)^{2,12,13}. Compared to classical PTPs with specific phosphotyrosine recognition, DUSPs are able to catalyze dephosphorylation of both tyrosine and serine/threonine substrates. The class II cysteine-based PTPs in the human genome comprises a single member, which is low-molecular weight PTP^{2,12,13}. Its catalytic domain is structurally related to bacterial arenate reductases^{12,13}. The class III cysteine-based PTPs contain three members, CDC25A, CDC25B, and CDC25C^{12,13}. These cell cycle regulators are dual-specific for phosphothreonine and -tyrosine residues on their substrates cyclin-dependent kinases. Compared to cysteine-based PTPs, the class IV involves aspartate as a key catalytic residue^{12,13}. Four *eya* genes belong to this group and have been shown to have tyrosine and serine phosphatase activity^{12,14-16}.

1.2 PTEN

1.2.1 Phosphatase PTEN

As a member of class I cysteine-based PTPs, PTEN (phosphatase and tensin homolog deleted on chromosome 10) is a dual-specificity protein tyrosine phosphatase and one of the most important tumor suppressors¹⁷⁻¹⁹. PTEN governs a wide spectrum of physiological processes including proliferation, cell size determination, differentiation, cell fate specification and energy metabolism^{20,21}. Frequently found loss-of-function mutations of *pten* gene in human cancers implicate its importance in the regulation of cellular survival signaling. Beside its crucial role as a gatekeeper in tumorigenesis, PTEN constitutes a critical factor in regenerative processes²²⁻²⁴ (Chapter 1.2.5). Both implications are mainly related to its inhibitory effect on PI3-K/Akt signaling pathway²⁵ (Figure 2).

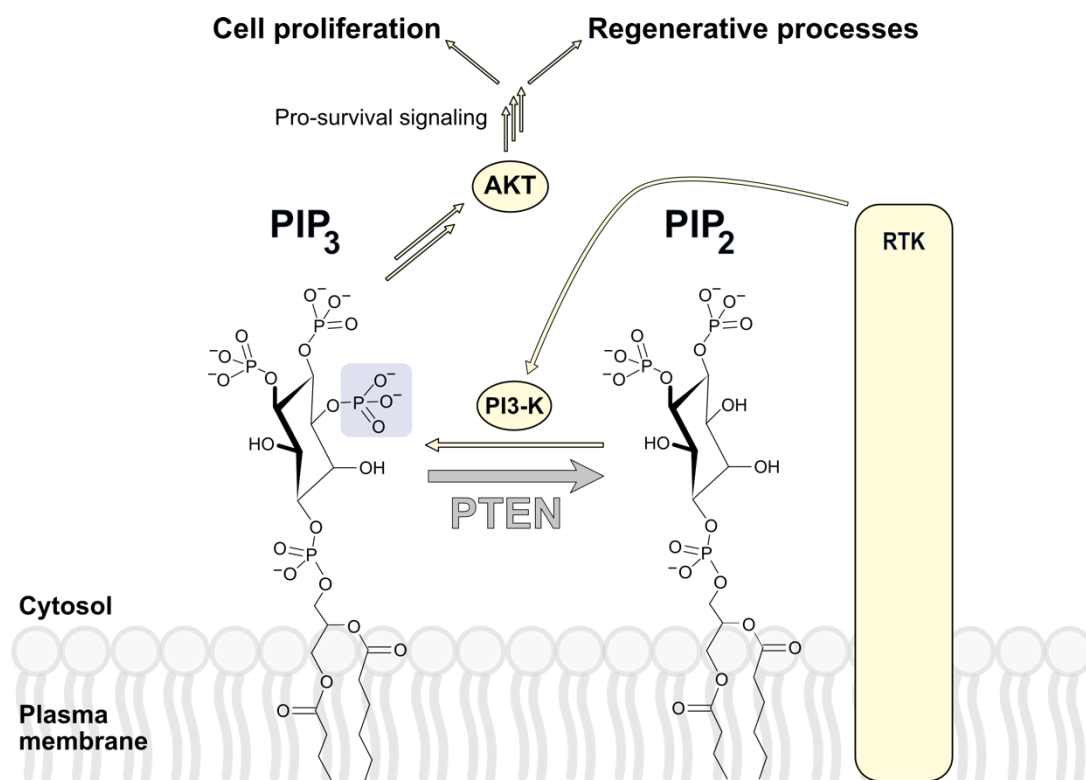


Figure 2 | PTEN antagonizes PI3-K/Akt signaling pathway. The activated PI3-K/Akt pathway is involved in cell proliferation, growth and regenerative processes via pro-survival signaling. PTEN inhibits this signal transduction by catalyzing dephosphorylation of PIP₃ to PIP₂.

The signal transduction of PI3-K/Akt pathway is initiated by binding of insulin or growth factors to receptor tyrosine kinase (RTK) on the cell surface, which promotes phosphorylation of insulin receptor substrate 1 (IRS-1) and subsequently phosphoinositide 3-kinase (PI3-K)^{26,27}. The activated PI3-K catalyzes phosphorylation of phosphatidylinositol (4,5)-bisphosphate (PIP₂) to (3,4,5)-trisphosphate (PIP₃) at the plasma membrane^{26,27}. PIP₃ production induces activation of downstream proteins including PDK1²⁸, Akt^{29,30} and mTORC1³¹. The following pro-survival signaling leads to enhanced glucose metabolism, cell growth and proliferation (Figure 2). As an antagonist in this pathway, PTEN reverses the action of PI3-K by converting PIP₃ to PIP₂ and prevents PIP₃ accumulation^{25,32,33}. In consequence, PTEN inhibits PI3-K/Akt signaling and modulates cell cycle progression and cell survival³³. Thereby, the lipid phosphatase activity of PTEN is a critical factor for thorough regulation of this signaling and the cellular homeostasis.

Although the lipid phosphatase activity is the main enzymatic function of PTEN, it also has the capability of dephosphorylating protein substrates. As a member of DUSP (Chapter 1.1)³⁴, PTEN exhibits substrate specificity towards a phosphoserine/threonine and -tyrosine. For instance, PTEN inhibits focal adhesion kinase (FAK) by dephosphorylating phosphotyrosine (pY397), which is phosphorylated in response to integrin-mediated cell adhesion^{35,36}. As a result, PTEN hinders cell migration, invasion, spreading, and focal adhesions^{35,37,38}. Protein phosphatase activity of PTEN has also been demonstrated by its action on IRS-1³⁹. Dephosphorylating two phosphotyrosine residues (pY612, pY989), PTEN inhibits the insulin signaling mediated by IRS-1 in PI3-K/Akt pathway. Finally, PTEN manifests an autodephosphorylation feature. As a highly regulated enzyme, cellular activity of PTEN is controlled by its intramolecular phosphorylation. Autodephosphorylation at pT366 on PTEN's regulatory C-tail has been suggested to promote the membrane targeting for its antagonistic function in PI3-K/Akt pathway⁴⁰.

1.2.2 PTEN structure

PTEN is a non-redundant and evolutionary conserved tumor suppressor containing 403 amino acids^{25,41}. PTEN consists of four functional domains involving central phosphatase and C2 domains flanked by two *N*- and *C*-terminal regulatory polypeptide regions (Figure 3a). Detailed insight into protein folding of the central globular domains was provided by the crystal structure of Lee *et al.* (1999) (PDB⁴² 1D5R)⁴³ (Figure 3b). However, structural information of the full-length PTEN is still missing, which would allow us to understand the functional regulation of this tumor suppressor.

Phosphatase domain of PTEN consists of 170 amino acids (residues 16-185) (Figure 3b). As a member of DUSPs, PTEN contains the wide and deep active site compared to classical PTPs with a small and deep pocket for a substrate specificity⁴⁴. Notably, PTEN exhibits an even larger phosphatase active site than the structurally similar DUSP human vaccinia H1-related phosphatase (VHR)^{43,44}. Given the lipid phosphatase activity of PTEN, the enlarged width of the active site might be a crucial feature to accommodate PIP₃ substrate that is bulkier than phosphorylated tyrosine, serine or threonine residues⁴³. Moreover, the P-loop motif of PTEN includes two lysines (residues 123-HCKAGKGR-130) that are conserved in the tensin-type lipid phosphatases^{43,45}. These basic amino acids may stabilize PIP₃ substrate binding by interacting with the phosphate groups at position D1 and D5 of the inositol ring^{43,45}.

C2 domain of PTEN, including 165 amino acids (residues 186-350), is mainly composed of an antiparallel β -sandwich structure (Figure 3b). This domain exhibits structural homology to the classical C2 domain that mediates membrane association in a Ca²⁺-dependent manner⁴³. However, PTEN C2 domain lacks two out of three conserved Ca²⁺-binding loops (CBR1, CBR2, CBR3) and is unlikely to bind Ca²⁺. Nonetheless, five lysine residues with net +5 charge in the present CBR3-loop (residues 260-269) might serve to mimic Ca²⁺-binding and promote interaction with phospholipids in the plasma membrane⁴³. PTEN C2 domain has an additional structural element with solvent-exposed basic residues. Ca2 (residues 326-335) closely located to the active site harbors three lysines and one arginine. This structural element may contribute to membrane recruitment together with the CBR3-loop⁴³. Another structural feature in PTEN C2 domain is the D-loop (residues 286-309) involving 24 amino acids. This region was not included for the protein crystallization, due to its flexible nature⁴³. In addition, very little is known about the functional role of this loop. So far, it has been shown that the D-loop is affected by caspase-3-dependent proteolytic cleavage and

ubiquitination at D301 and K289, respectively^{46,47}.

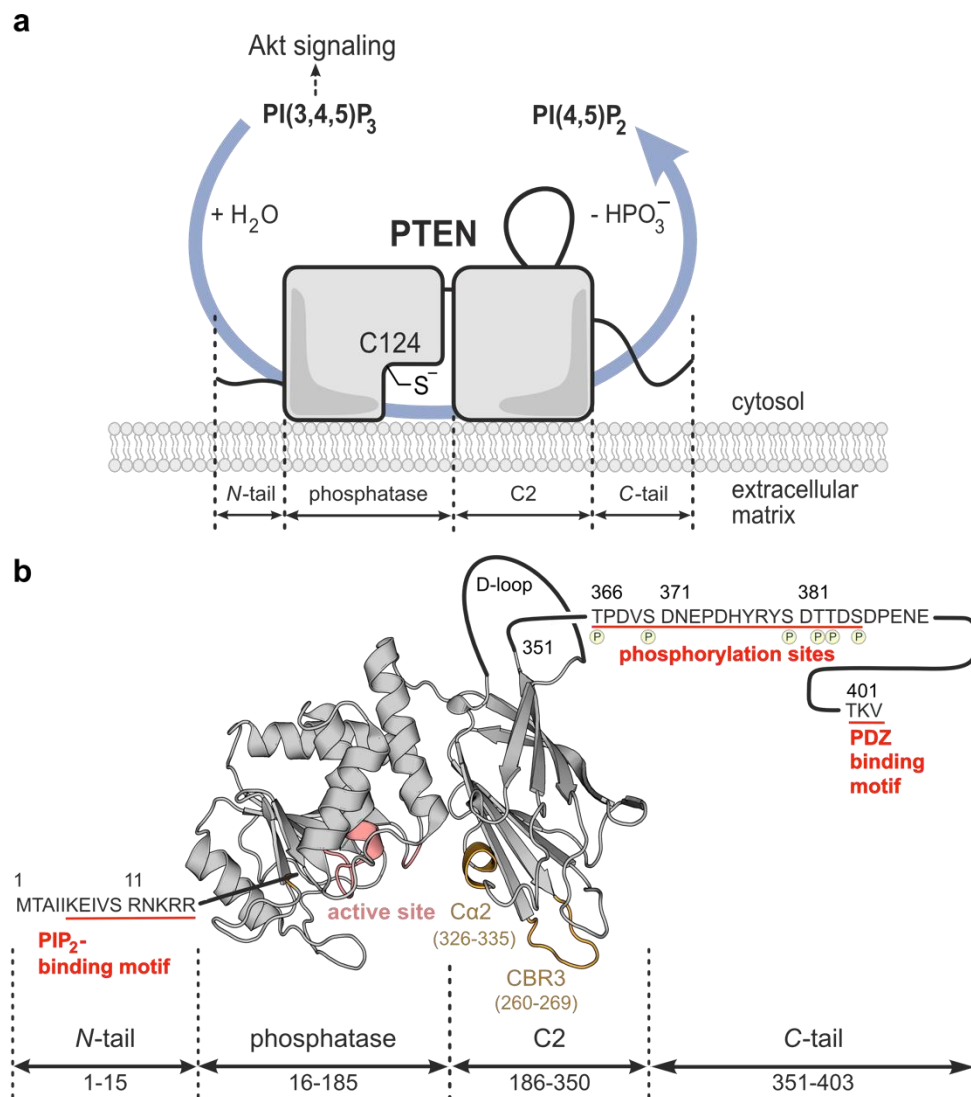


Figure 3 | Domain architecture and structure of PTEN. (a) PTEN consists of four functional domains. The active site in the phosphatase domain contains a catalytic cysteine (C124), which is essential for its lipid phosphatase activity at the plasma membrane. (b) Only phosphatase and C2 domains are structurally elucidated, while structural information of the regulatory *N*- and *C*-tails is still missing.

The *N*-tail comprises 15 amino acids including the proposed PIP₂-binding motif (residues 6-KEIVSRNKRR-15) (Figure 3b)⁴⁸. The densely located basic amino acids are suggested to interact with the negatively charged head group of PI-(4,5)-P₂, which is the dephosphorylation product of PI-(3,4,5)-P₃ by the lipid phosphatase activity of PTEN⁴⁸. Notably, previous *in*

vitro and *in vivo* studies show that this motif is essential for the catalytic activity and plasma membrane localization^{45,48-55}.

The C-tail consists of 52 amino acids (residues 352-403) (Figure 3b). This structurally flexible domain is responsible for the conformational change via post-translational modification and the following subcellular localization (Chapter 1.2.3). Upon phosphorylation, PTEN undergoes a conformational change to the “closed and inactive” state and resides in the cytosolic compartment^{56,57}. PDZ-binding motif (residues 401-403) located at the end of the C-tail contributes to the formation of a signaling complex at the plasma membrane^{58,59}.

A translational variant of PTEN was recently discovered by two independent groups involving an alternative translation initiation site CUG upstream to the canonical start codon AUG^{60,61}. This isoform, called PTEN-L, constitutes a longer form of PTEN with 173 additional amino acids at the N-terminus. This extended region is predicted to be intrinsically disordered⁶⁰⁻⁶³. Notably, PTEN-L is able to be secreted and also to enter adjacent cells^{60,61}. It has been suggested that this feature be attributed to the presence of a poly-arginine stretch R⁶ (residues 47-52), which is similar to the poly-basic sequences found in cell-permeable peptides⁶⁰.

1.2.3 Post-translational modification of PTEN

PTEN activity is regulated by multiple post-translational modifications including phosphorylation, ubiquitination, acetylation, and oxidation (Figure 4). Among others, phosphorylation of PTEN is the most heavily studied modification. It serves as a critical factor to modulate cellular tumor-suppressing activity of PTEN by determining subcellular localization. PTEN is mainly phosphorylated at serine/threonine clusters of the C-tail (S362, T366, S370, S380, T382, T383, S385)^{64,65} by CK2^{57,66,67}, GSK-3 β ^{67,68}, and PICT-1⁶⁹. Upon phosphorylation, the negatively charged C-tail domain undergoes intramolecular interaction with the positively charged central globular domains, interfering with the electrostatic interaction between the core domains and the plasma membrane^{55,70,71}. The resulting closed conformation leads to the cytosolic localization of PTEN in its inactive, but more stable state (Figure 5)^{56,72}. On the contrary, previous mutation studies demonstrated that the open and active state of PTEN is induced by alanine substitution at these phosphorylation sites^{70,71}. This dephosphorylation mimicry results in the increased membrane recruitment and nuclear

localization⁷³. Other phosphorylation modifications on PTEN C2 domain have also been reported. Phosphorylation at S229, T232, T319, and T321 catalyzed by ROCK promotes membrane localization of PTEN in chemoattractant-treated leukocytes⁷⁴. In addition, phosphorylation at Y336 conveyed by RAK protects PTEN from ubiquitin-mediated proteolysis⁷⁵.

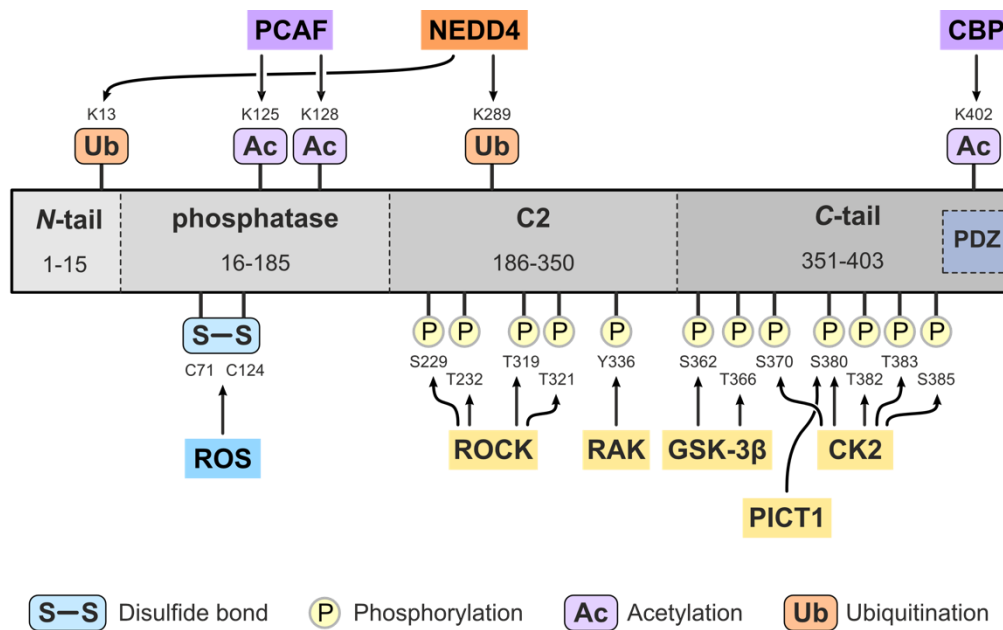


Figure 4 | Post-translational modifications of PTEN. Ubiquitination regulates subcellular localization and protein levels of PTEN, while phosphorylation and acetylation affect its enzymatic activity. In addition, reactive oxygen species induces catalytic impairment of PTEN via disulfide bond formation. The figure is reconstructed based on Shi *et al.* (2012) and Worby *et al.* (2014)^{64,65}.

Ubiquitination regulates subcellular localization and protein levels of PTEN (Figure 5). Monoubiquitination mediates the nuclear import of PTEN and enables its tumor suppressor function in phosphatase-independent manner (Chapter 1.2.4)⁴⁷. However, polyubiquitination directs PTEN to proteasomal degradation⁷⁶. This is consistent with low protein levels of PTEN observed in cancer cells, which is in coincidence with aberrant overexpression of ubiquitin ligase (*e.g.* NEDD4-1)^{77,78}. So far, three E3 ligases (*e.g.* NEDD4-1⁷⁷, WWP2⁷⁶, and XIAP⁷⁹) have been identified to promote this modification. Analogous to ubiquitination on other proteins, this modification occurs on solvent-exposed lysines of PTEN such as K13 and K289 (Figure 4).

Acetylation of PTEN is associated with its activity regulation and protein-protein interaction. Lysine acetyltransferase PCAF promotes acetylation of PTEN at K125 and K128 in response

to growth factor stimulation⁸⁰. As both residues are located within the active site P-loop, enzymatic activity of PTEN is reduced consequently⁸⁰. PTEN is also acetylated on its C-terminal PDZ binding motif (K402). This has been suggested to have an influence on physical interaction between PTEN and PDZ-domain-containing proteins^{64,65,81}.

Phosphatase activity of PTEN is regulated by oxidation (Chapter 1.3.4). It has been reported that H₂O₂-treatment or endogenously produced reactive oxygen species inactivate PTEN^{82,83}. In both cases, disulfide formation between cysteines C124 and C71 was observed^{82,83}. In addition to phosphatase inhibition, oxidative stress promotes nuclear localization of PTEN via phosphorylation at the C-tail (pS380)⁸⁴. Nuclear PTEN contributes to increase of p53 levels in the phosphatase-independent manner, which leads to p53-mediated G₁ cell growth arrest, cell death, and a reduction in cellular ROS production^{65,84}.

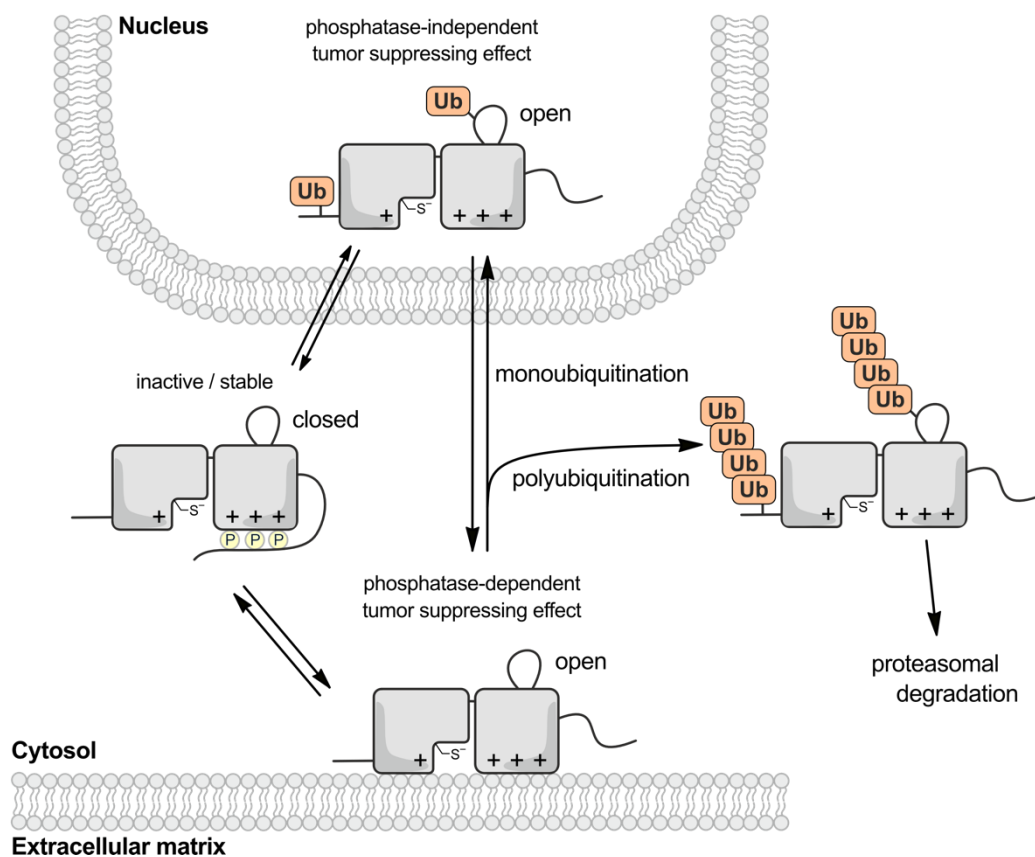


Figure 5 | Subcellular localization of PTEN. Phosphorylation triggers the conformational closure and leads to the cytosolic localization in the inactive state. Upon activation, PTEN is translocated to the plasma membrane. Subcellular localization and cellular protein level of PTEN are also controlled by ubiquitination. Monoubiquitination of PTEN promotes its nuclear import, while polyubiquitination induces proteasomal degradation.

1.2.4 Tumor suppressing effects of nuclear PTEN

As previously described, PTEN constitutes a key negative regulator in the PI3-K/Akt signaling and attenuates pro-survival signal (Chapter 1.2.1). This feature is attributed to its lipid phosphatase activity at the plasma membrane. However, growing evidence supports the functional importance of PTEN, also, in the nucleus. Contrary to its cytoplasmic activity, nuclear PTEN exerts tumor suppression function in a phosphatase-independent manner by controlling genomic stability and cell cycle progression^{21,85,86}. PTEN maintains chromosomal integrity by physical association with centromere protein C1 (CENPC1)⁸⁵. Under genotoxic stress, PTEN contributes to DNA double-strand repair by inducing the expression of RAD51⁸⁵. Nuclear PTEN also promotes formation of a complex between an E3 ubiquitin ligase APC/C and CDH1. The resulting protein complex recruits its specific substrates (*e.g.* PLK1, Aurora A, CDC20, SKP2) for ubiquitin-mediated proteolysis, which are overexpressed in the tumor progression⁸⁷. In addition, cooperative effects of two major tumor suppressors PTEN and p53 have been demonstrated in earlier studies. Direct interaction of PTEN with p53 regulates the protein levels of p53 and also leads to overexpression of PTEN itself via an autoregulating mechanism^{88,89}. PTEN also enhances the acetylation of p53 and thereby activates this tumor suppressor by inducing tetramerization⁹⁰.

1.2.5 PTEN in regenerative processes

Axons in the mammalian adult central nervous system (CNS) are not able to regenerate spontaneously after nerve injury²². This property is ascribed to the extracellular inhibitory environment and the reduced intrinsic growth ability^{22,24}. For this reason, enzymatic removal of axon regrowth inhibitors (*e.g.* chondroitin sulphate proteoglycans, myelin-associated inhibitors) occurring in the extracellular matrix after nerve injury has been demonstrated to promote axonal regeneration^{91,92}. However, this strategy shows regeneration effect only to a small extent^{91,92}. Another approach includes modulation of the intrinsic growth control. This is based on two findings, which are increased axon outgrowth by amplification of PI3-K/Akt pathway^{93,94} and extensive expression of the antagonist PTEN in peripheral neurons, including those that have been injured⁹⁵. Indeed, genetic deletion of PTEN has been reported to promote neuronal survival and robust axon regeneration after nerve injury by activating the downstream protein mTOR²². Regenerative effects of PTEN inhibition are also highlighted in terms of cardioprotection. This is due to the fact that, analogous to nerve injury, activation of PI3-K/Akt signaling pathway significantly reduces ischemia/reperfusion injury^{*}, which consequently leads to myocardial infarction (heart attack)^{96,97}. Consistently, PTEN inhibition promotes myocardial[†] survival and limits infarct size^{97,98}. These implications in cellular regeneration make PTEN a pharmacological target for the treatment of nerve injury, stroke and myocardial infarction. However, due to potential tumorigenesis from the long-term knock-down, pharmacological inhibition of PTEN would be confined to acute treatment. Nevertheless, research on the pharmacological effect of PTEN inhibition is still in its infancy and requires further investigation.

^{*} Ischemia refers to the state, in which the blood supply to tissues and organs is restricted. Reperfusion refers to the restoration of blood supply after a period of ischemia.

[†] Relating to the muscular tissue of the heart.

1.3 Reactive oxygen species

1.3.1 Occurrence and effect of reactive oxygen species

Reactive oxygen species (ROS) are a collective term for chemically reactive molecules containing oxygen. Hydrogen peroxide (H_2O_2), hydroxyl radical (OH^\bullet), superoxide ($\text{O}_2^{\bullet-}$), nitric oxygen (NO^\bullet) and singlet oxygen ($^1\text{O}_2$) belong to these species (Figure 6). ROS are produced in a wide range of physiological processes⁹⁹. ROS are formed as a natural byproduct of metabolic processes, while ROS levels can also increase by exposure to extrinsic stress factors (*e.g.* UV, γ -radiation, chemicals). ROS formation is furthermore involved in certain physiological circumstances (*e.g.* hypoxia, oncogene activation) and the following oncogenic transformation¹⁰⁰. The resulting ROS have diverse effects depending on their cellular level¹⁰⁰. Low levels of ROS promote cell survival and proliferation particularly via growth factor-induced signaling events (Chapter 1.3.2). In this controlled metabolic state, normal cells utilize antioxidants (*e.g.* thioredoxin, reduced glutathiones) to regulate intracellular ROS content within nontoxic range¹⁰¹. However, once ROS levels become exceedingly high, they can exert detrimental oxidative stress ranging from tumorigenesis to apoptosis^{100,102}. Notably, cancer cells thoroughly control and maintain the household of ROS at moderate level, so that they escape from the cell death but further induce ROS-related mutations¹⁰⁰. Moreover, ROS also activate various transcription factors (*e.g.* NF- κ B, AP-1, HIF-1 α , STAT3) and downregulate expression of tumor suppressor proteins (*e.g.* p53, Rb, PTEN)¹⁰³. In this regard, thorough regulation of ROS levels is very important for cellular homeostasis.

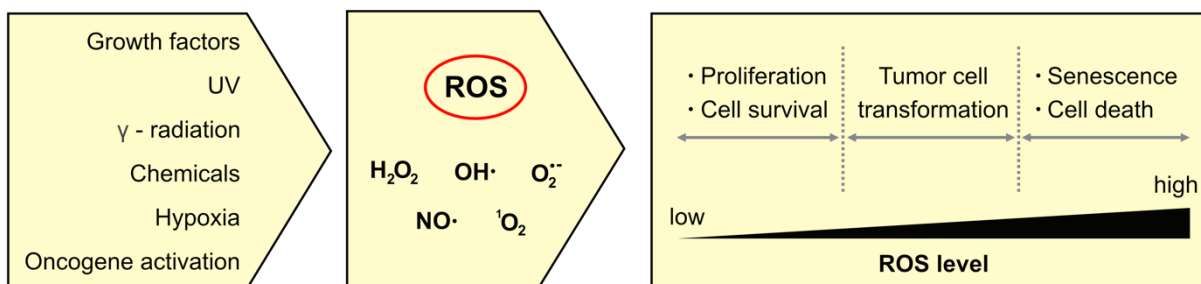


Figure 6 | Reactive oxygen species (ROS). ROS are generated by various sources ranging from metabolic to extrinsic factors. Depending on the level of ROS, different potential cellular outcomes occur ranging from cell survival through tumorigenesis up to cell death. The figure is reconstructed based on Cairns et al. (2011)¹⁰⁰.

1.3.2 Growth factor-induced hydrogen peroxide generation

H_2O_2 is the most abundant ROS (about 10^{-7} M in the steady state)^{104,105}. Among the different ROS, H_2O_2 is relatively stable with cellular half-life of about 1 ms¹⁰⁴. H_2O_2 is diffusible through membranes with its small molecular size and non-polarity^{104,105}. Furthermore, H_2O_2 exhibits selective reactivity, especially to PTPs^{104,105}. Its cellular concentration can be controlled by the antioxidant defense system¹⁰⁵. Collectively, these properties make H_2O_2 suitable to act as a second messenger in different redox signaling pathways, unless its concentration is exceedingly high to exert an oxidative stress^{106,107}. In particular, H_2O_2 plays a crucial role in the PI3-K/Akt signaling. Once external signals stimulate receptor tyrosine kinase with growth factors (*e.g.* EGF, PDGF, VEGF, insulin), NADPH oxidase 1 (NOX1) is activated in the downstream signaling event and produces H_2O_2 (Figure 7)¹⁰⁵. The elevated level of H_2O_2 potentiates the inactivation of PTPs including PTEN, since the local inactivation of these antagonists is required to increase the accumulation of PIP_3 to a sufficient level for the downstream events^{108,109}. As a result, subsequent activation of Akt kinase leads to cell survival and proliferation. Given that PTEN is a key antagonist of this pathway, oxidative inhibition of PTEN by H_2O_2 in response to cell stimulation might be an important determinant of PIP_3 generation in timing and localization for the effective regulation of a signal transduction¹⁰⁹. In this respect, PTEN requires efficient redox regulation involving a highly reversible character of oxidative inactivation and selective switching between oxidized and reduced states.

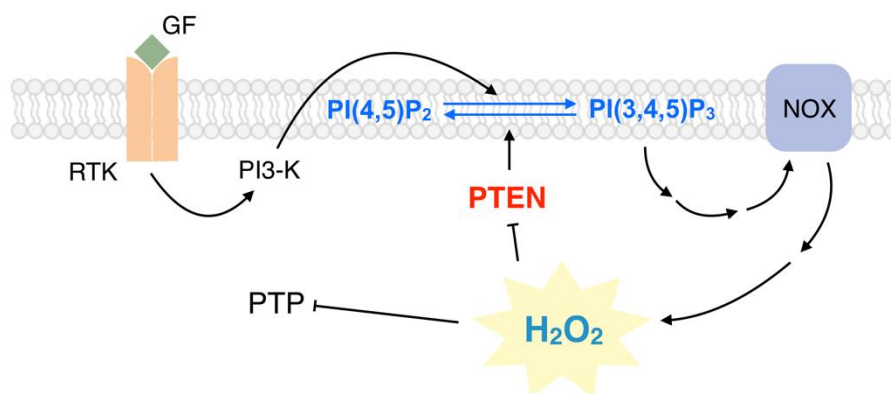


Figure 7 | H_2O_2 generation in response to a growth factor in PI3-K/Akt pathway. Cellular stimulation via various growth factors reinforces the PI3-K/Akt signaling via H_2O_2 production, which in turn inhibits its negative regulator PTEN. GF: growth factor, RTK: receptor tyrosine kinase, PI3-K: Phosphoinositide 3-kinase, PTP: protein tyrosine phosphatase, NOX: NADPH oxidase. The figure is reconstructed based on Kwon *et. al.* (2004)¹⁰⁹.

1.3.3 Molecular consequences of PTPs upon hydrogen peroxide

Cysteines play a crucial role in numerous biological processes. They are involved in stabilization of protein structures (*e.g.* disulfide formation), regulation of protein functions (*e.g.* post-translational modifications), coordination with metals (*e.g.* Fe, Zn, Cu), and enzymatic reactions (*e.g.* active site cysteines)^{110,111}. This stems from unique features of thiols, for instance from their high reactivity, polarizability, high affinity for metals, redox-mediated modification, and responsiveness to local environments¹¹². Such versatile properties make cysteine residues special in protein chemistry, although they are one of the least abundant amino acids in proteins (1 – 2 %) ¹¹¹. In particular, the catalytic cysteine in the active site of PTPs is sensitive to oxidative inhibition by ROS. This is due to the fact that the active site manifests an acidic environment with an unusually low pK_a value ($pK_a = 4.7 - 5.4$), whereas the thiol group of most cysteines exhibits pK_a at about 8.5¹¹³. As a result, the catalytic cysteine residue in PTPs is present in the deprotonated form as a protein thiolate, which is stabilized by polar or positively charged amino acids in the active site P-loop^{8,9,105,114}. The charged nature of the protein thiolate makes them more nucleophile but susceptible to oxidation^{10,115-117}. Upon exposure to H_2O_2 , the protein thiolate is initially oxidized to sulfenic acid, which is located at a crossroad of reversible and irreversible oxidative modifications (Figure 8a). This highly reactive sulfur species can be further oxidized to sulfinic or sulfonic acid, resulting in irreversible catalytic impairment. Alternatively, in the presence of another proximal cysteine (Figure 8b) or an activated main-chain amide (Figure 8c), sulfenic acid undergoes an intramolecular condensation reaction to form disulfide or sulfenyl-amide bond. These modifications constitute a protective mechanism from further irreversible inactivation of the protein and enable the restoration of the active form under reductive conditions¹⁰.

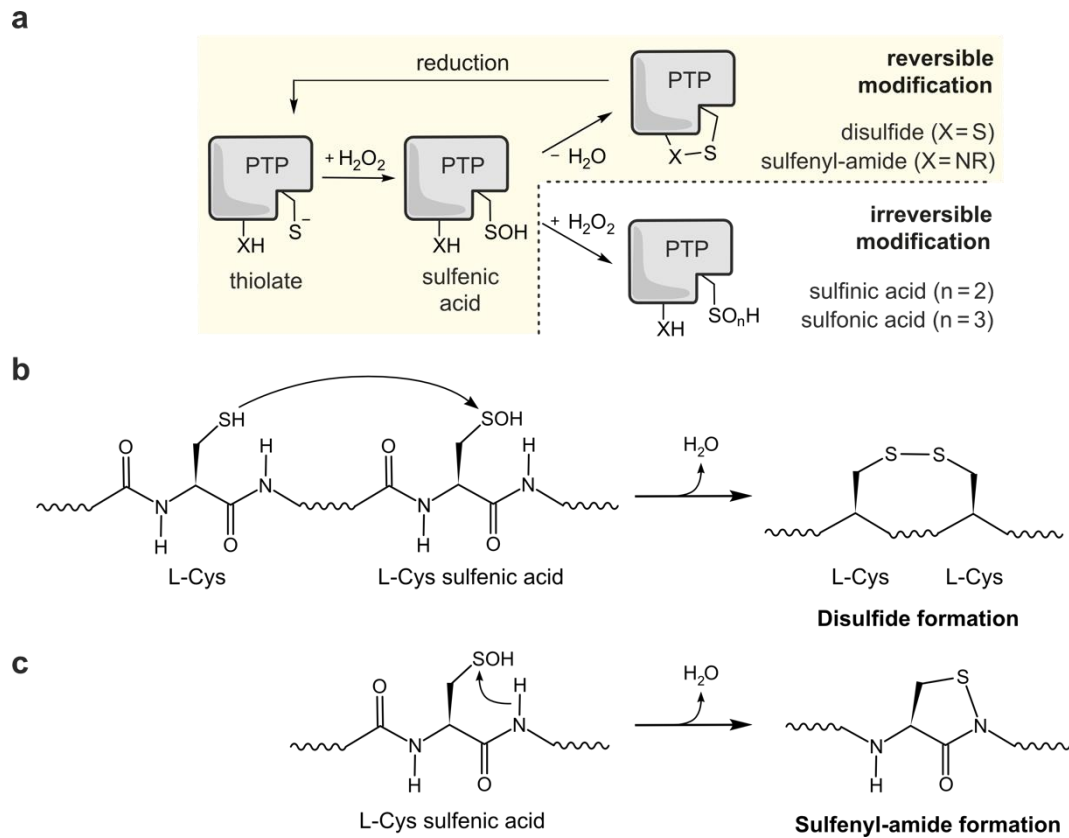


Figure 8 | Molecular consequences of protein thiolates upon H₂O₂ oxidation. **a)** The catalytic cysteine in PTP is present as thiolate that is particularly susceptible to oxidation. Upon exposure to H₂O₂, cysteine thiolate at the active site of PTP is converted to sulfenic acid, which subsequently undergoes disulfide or sulfenyl-amide formation in the presence of cysteine or activated amide in the neighborhood. Alternatively, additional equivalent of H₂O₂ can facilitate irreversible oxidative modification of sulfenic acid to sulfinic or sulfonic acid. **b)** Intramolecular disulfide formation. **c)** Intramolecular sulfenyl-amide formation.

1.3.4 Structural changes of PTPs upon oxidation

PTPs take advantage of the reversible nature of disulfides and sulfenyl-amides to switch between active and inactive forms, while these chemical modifications simultaneously have a protective effect against irreversible abrogation of their catalytic activity. Depending on the underlying mechanisms, the reversible modifications can be categorized into three different classes¹¹⁸, although they have the initial oxidation of the catalytic cysteine to sulfenic acid in common. First, reversible sulfenyl-amide formation is promoted by a nucleophilic attack from the main chain amide of the next residue to the sulfenic acid. As observed in the crystal structures of PTP1B, this intramolecular five-membered ring extensively distorts the P-loop conformation (Figure 9, PDB 2HNP vs. 1OEM)¹¹⁹⁻¹²³. Second, disulfide formation occurs between two cysteine residues separated by several amino acids in the primary sequence. A representative example is the low molecular weight protein tyrosine phosphatase (*i, i+5* for LMW-PTP)^{124,125}. The last mechanism also involves disulfide formation. However, the intramolecular condensation reaction is induced by the spatial proximity of two cysteine residues, even though both are located far apart from each other in the primary sequence^{82,126-128}.

So far, there are two human PTPs of which the structural impact of the disulfide formation is elucidated with crystal structures. These are CDC25B¹²⁶ and LYP¹¹⁸. Interestingly, CDC25B undergoes a significant conformational change of the active site P-loop upon disulfide formation (PDB 1YMK vs. 1YS0), whereas LYP maintains the backbone structure (PDB 2P6X vs. 3H2X) (Figure 9). Dual-specificity phosphatase PTEN also belongs to this last class. Upon oxidative stress, disulfide bond formation occurs between its catalytic cysteine C124 with the spatially aligned cysteine C71^{82,83}. However, the structural consequences of disulfide formation remain elusive. Moreover, PTP1B (PDB 1OEO) and CDC25B (PDB 1YMD) experience the irreversible modification including sulfonic acid formation under extensive oxidation condition (Figure 9)^{122,123,126}.

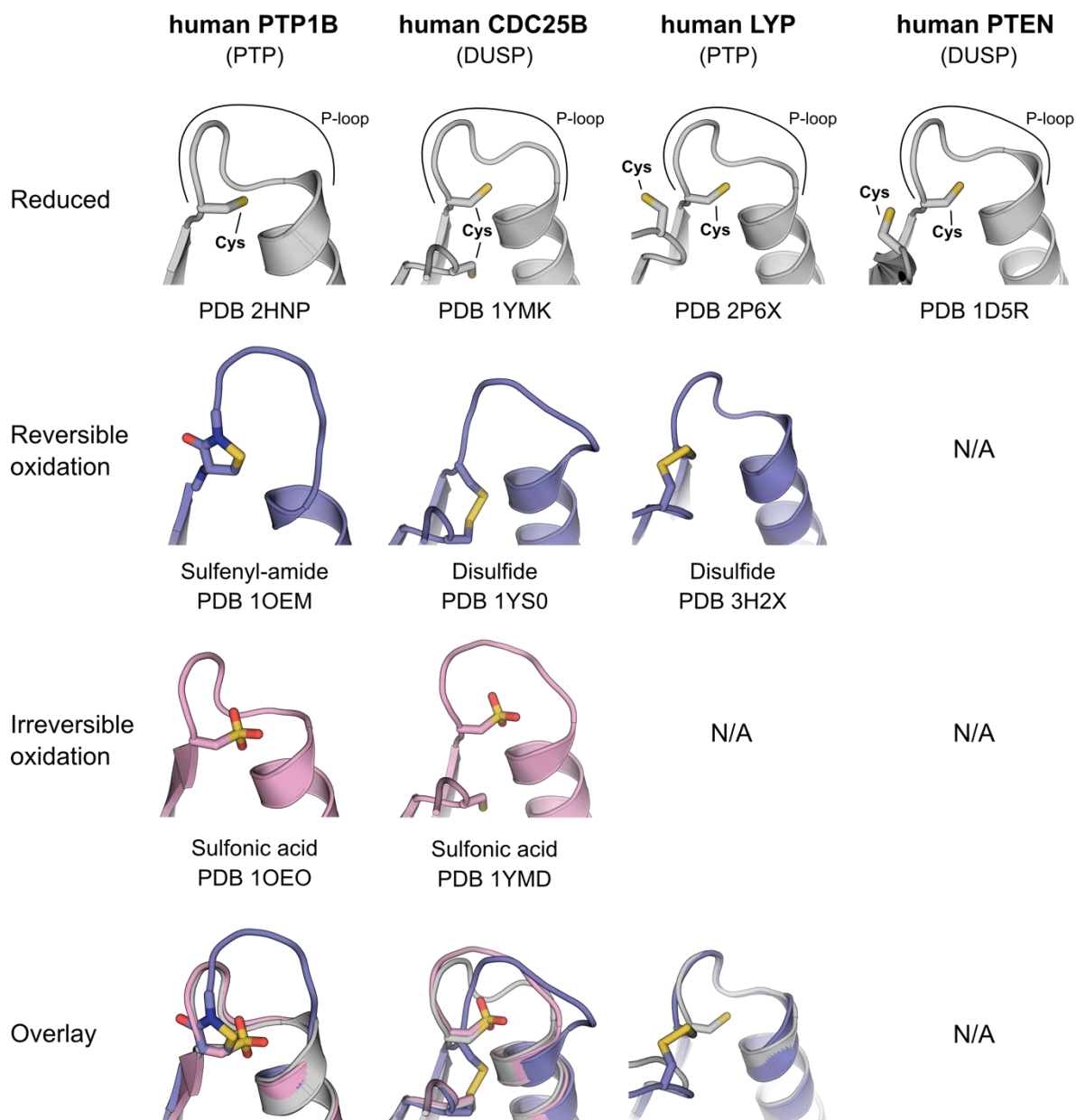


Figure 9 | Summary of oxidative modifications of the known human PTP crystal structures. Depending on the oxidizing conditions, catalytic cysteine of the reduced state (gray) undergoes reversible (blue; disulfide or sulfenyl-amide formation) or irreversible modification (red; sulfonic acid). Thereby, the conformation of the active site P-loop can be distorted to a large extent. PTP: protein tyrosine phosphatase, DUSP: dual-specific phosphatase, N/A: not available.

1.4 Bisperoxidovanadium-based PTEN inhibitors

As discussed above (Chapter 1.2.5), regenerative effects of PTEN inhibition provide new possibilities for acute treatment of stroke and nerve injury. Concerning PTEN inhibitors, there are both an organic compound (SF1670) and organovanadium complexes available. However, vanadium complexes are mainly used to study the effects of PTEN inhibition, due to their higher potency with sub-micromolar IC_{50} ranges. These vanadium-based PTEN inhibitors are categorized into two classes depending on the oxidation state. Vanadium (IV)-based VO-OHpic contains oxovanadium that is coordinated by a water molecule and two 3-hydroxypicolinic acid in a bidentate manner^{129,130}. The other compound class involves vanadium (V)-based bisperoxidovanadium (bpV) complexes¹³⁰⁻¹³³. In these organometallic molecules, a central oxovanadium is complexed with two peroxido ligands as well as an organic bidentate ligand in a pentagonal bipyramidal geometry^{134,135}. The widely used PTEN inhibitors in this class include an aromatic ligand such as phenanthroline (phen), picolinic acid (pic), 5-hydroxypicolinic acid (HOpic) (Figure 10). In addition, pharmacological inhibition of PTEN has been demonstrated in CNS/cardiomyocyte-injury and stroke using bpV-complexes¹³⁶⁻¹⁴¹. Consistent with physiological effects resulting from the genetic deletion, PTEN inhibition by these compounds enhanced PI3-K/Akt signaling and revealed neuronal and cardiac protection in earlier *in vitro* and *in vivo* studies¹³⁶⁻¹⁴¹. However, the mode of action of bpV-complexes on PTEN is still under debate^{132,133}. Its elucidation could support further optimization of these compound class to achieve improved efficacy.

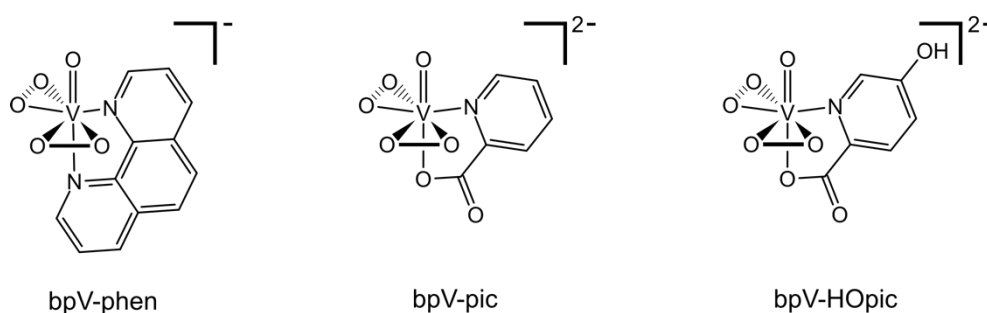


Figure 10 | Bisperoxidovanadium-based PTEN inhibitors. Central oxovanadium is coordinated by two peroxides and an organic ligand involving phenanthroline (phen), picolinic acid (pic), or 5-hydroxypicolinic acid (HOpic).

2 Aim of the thesis

As a central tumor suppressor, tight regulation of PTEN phosphatase activity is crucial for cellular homeostasis. In the physiological context, PTEN activity is inhibited by H_2O_2 produced in the redox signaling and oxidative stress^{82,83,109}. Thereby, PTEN renders disulfide formation between the catalytic cysteine C124 and the proximal cysteine C71⁸². However, structure-based implications of PTEN inhibition remain elusive, which would provide better understanding of its oxidative regulation. On the other side, pharmacological inhibition of PTEN phosphatase activity by bisperoxidovanadium (bpV) complexes has been shown to have cellular regenerative effects involving potential application for treatments after nerve and cardiac injury¹³⁶⁻¹⁴¹. So far, the mode of action of these compounds is still unclear. Its elucidation would contribute to further development of this compound class. Therefore, inhibition of PTEN phosphatase activity shall be investigated in this study using biochemical and structural biology methods. H_2O_2 and bpV-phen are selected as representative model compounds for physiologically relevant and synthetic PTEN inhibitors, respectively.

Different PTEN constructs shall be produced using recombinant protein expression. Due to the post-translational modification-dependent conformational change, PTEN shall be overexpressed in *E.coli* and insect cells following molecular cloning of the protein constructs. Subsequently, structural consequences of H_2O_2 -mediated disulfide formation shall be studied using X-ray crystallography to compare the effects with other PTP structures. Given that two other members of the PTP superfamily, PTP1B¹²² and CDC25B¹²⁶, experience irreversible modifications (*e.g.* sulfonic acid formation) under extensive treatment of H_2O_2 , it shall be tested, if the catalytic cysteine of PTEN also shows irreversible oxidation at physiologically relevant H_2O_2 concentrations. Furthermore, the mode of action of bpV-phen shall be studied. Knowing that PTP1B is oxidatively inhibited by peroxidovanadate¹⁵³, an oxidative mechanism of bpV-phen-mediated PTEN inhibition is considered. Potential chemical modifications of PTEN shall be determined using mass spectrometry and X-ray crystallography. ⁵¹V-NMR spectroscopy will be used to determine the vanadium species involved. In addition, protein-ligand-interactions between PTEN and other activity modulators (*e.g.* PIP_2 , $nhPIP_3$) will be studied. Biochemical and structural biology methods will be utilized to characterize their binding modes on PTEN.

3 Results and discussion

3.1 Protein expression and purification

3.1.1 Protein expression and purification of the various constructs

To characterize biochemical effects of activity modulators on PTEN, human PTEN (UniProt¹⁴² P60484) was recombinantly produced using heterologous protein expression systems. Thereby, protein expression of eight different constructs in the presence and absence of regulatory domains was performed to study protein-ligand interaction (Figure 11). Protein constructs containing *N*-terminal regulatory domain were divided into the full-truncation (Δ residues 1-16) and the presence of PIP₂ binding motif (Δ residues 1-6). The absence of *C*-terminal regulatory domain involved the entire *C*-tail region with 52 amino acids (Δ residues 352-403, Figure 3b and Figure 11b). In addition, a protein construct (PTEN 7-353 Δ 286-309) was produced based on the available crystal structure of PTEN (PDB 1D5R)⁴³. This construct served to study structural effects of activity modulators on PTEN. Protein expression was carried out using insect cells, due to its capability of introducing post-translational modifications. However, expression of the full-length PTEN was additionally performed in the prokaryotic host organism *Escherichia coli* to represent its open state⁵¹. This is due to the fact that intrinsic activity modulation of PTEN depends on the phosphorylation-mediated conformational change (Chapter 1.2.3) and *E. coli* lacks background phosphorylation by intrinsic kinases¹⁴³.

Initially, production of full-length PTEN was performed with *E. coli* using BL21 derivative Rosetta host strain, since this cell line is supplemented with an additional plasmid pRARE encoding tRNAs for rare codons. After transformation with the sequence-verified human wild-type *pten*, Rosetta cells produced the protein construct at 20 °C to facilitate proper protein folding. Full-length PTEN was overexpressed in a soluble form and isolated from cell lysate. The purified protein exhibits lipid phosphatase activity. However, this protein construct tends to form undefined multiple protein complexes during overexpression in *E. coli*, which does not demonstrate the physiologically relevant PTEN species (PTEN, 47 kDa). Formation of the protein complexes was detected by size exclusion chromatography (Figure 12). The majority of the protein was eluted at the void volume, indicating a protein size larger than the largest protein standard (Thyroglobulin, 669 kDa) used for comparison (Figure 12, upper panel). In order to obtain a monomeric species, the isolated protein was

treated with various detergents (Triton, NP-40, CHAPS) and incubated under high ionic strength environment (2 M NaCl). Besides, diverse protein tags (His₆, GST, MBP) were employed for improvement. Overall, His₆-THB-PTEN construct^{III} encoded in pET28a vector delivered the best result with a small fraction of monomeric species (Figure 12), although treatments with detergents or salt were unsuccessful for improvement. However, the following His₆-tag cleavage resulted in unspecific degradation of this protein construct (Figure 12, lower right). Altering the protease cleavage site, His₆-TEV-PTEN construct^{IV} was subsequently overexpressed. Nearly all protein was obtained in the form of multiple protein complexes, together with a significantly lower expression level.

| a | | | | |
|-------------------|------------------|----------------------|----------------------------------|-----------------------------|
| | | | | |
| Constructs | 1 - 403 | 1 - 403 | 6 - 403 | 16 - 403 |
| Expression System | <i>E.coli</i> | High Five | High Five | High Five |
| Characteristics | Full-length open | Full-length closed | ΔN | ΔN lacking PBM |
| b | | | | |
| | | | | |
| Constructs | 1 - 353 | 6 - 353 | 16 - 353 | 7 - 353 Δ 286-309 |
| Expression System | High Five | High Five | High Five | High Five |
| Characteristics | ΔC | $\Delta N, \Delta C$ | $\Delta N, \Delta C$ lacking PBM | Crystallization construct |

Figure 11 | Summary of PTEN constructs for the biochemical assays and the structural biology investigation. Depending on the presence of *N*- and *C*-terminal regulatory domains, various PTEN constructs were overexpressed in insect cells due to post-translational modifications *e.g.* phosphorylation. Only full-length construct was additionally produced in *E. coli*, representing its open active conformation. PTEN constructs (a) harboring and (b) lacking *C*-tail are varied with the presence of *N*-terminal PIP₂ binding motif (residues 6-15). PTEN 7-353 Δ 286-309 was used for the crystallographic analysis with activity modulators. PBM: PIP₂ binding motif.

^{III} THB: Thrombin protease cleavage site (LVPR|GS).

^{IV} TEV: *tobacco etch virus* protease cleavage site (ENLYFQ|G/S).

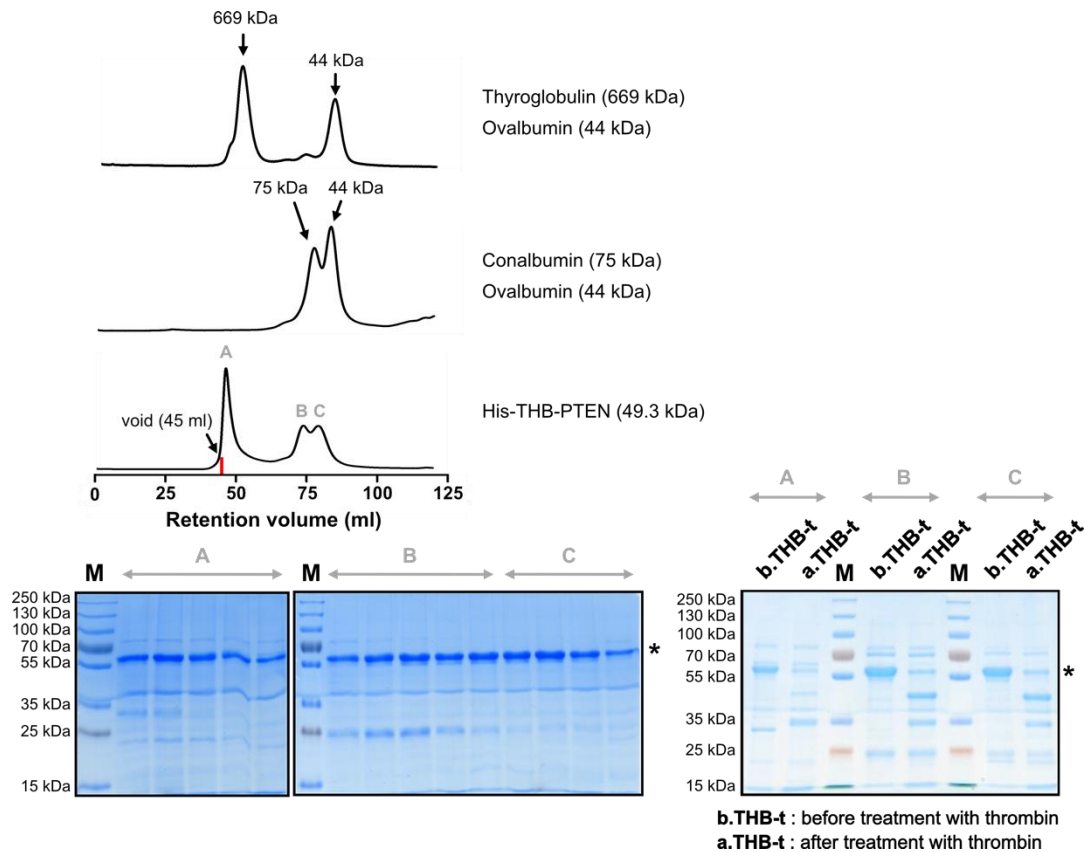


Figure 12 | Protein purification of His₆-THB-PTEN 1-403 from *E. coli*.^V Size exclusion chromatography (SEC, HiLoad Superdex S200 16/60) and the corresponding SDS-PAGE reveals the multiple protein complex formation of the full-length PTEN overexpressed in the prokaryotic host organism. A significant amount of the protein is eluted at the void volume (45 ml), indicating a protein size larger than 669 kDa. In addition, proteolytic cleavage of His₆-tag using thrombin protease leads to unspecific degradation of the protein. (THB: thrombin protease cleavage site; *: His₆-THB-PTEN 1-403)

Furthermore, full-length PTEN was overexpressed in High Five insect cells using baculovirus. The recombinantly produced PTEN construct contained an additional *N*-terminal His₆-tag and TEV-protease cleavage site for efficient protein purification. Due to the occurrence of numerous phosphorylation patterns during protein expression (Figure 23), the different PTEN species were not separated for the biochemical studies. PTEN was first purified with Ni²⁺-beads via IMAC (Figure 13a, lane E), followed by proteolytic cleavage of His₆-tag with TEV-protease (Figure 13a, lane TEV). Thereby, the redundant region including the protein affinity tag (His₆-TEV) was removed proteolytically. Only a glycine was left as an

^V Protein purification of His₆-THB-PTEN 1-403 from *E. coli* was performed by Sandra Bäcker for her Master's Thesis (Fakultät für Chemie und Chemische Biologie, TU Dortmund)¹⁴⁴.

artifact originating from the TEV-protease cleavage site (ENLYFQ[G]). The successful cleavage was demonstrated by the protein band shift in SDS-PAGE towards the lower molecular weight after treatment with TEV-protease. Full-length PTEN was furthermore purified with size exclusion chromatography as a final purification step (Figure 13b). Compared to the chromatograms of protein standards, the retention volume of the full-length PTEN indicates its monomeric nature. Overall, the purified PTEN shows high purity, as determined by SDS-PAGE analysis. The yield of full-length PTEN averages out at about 25 mg from 1 liter culture volume in the final purity.

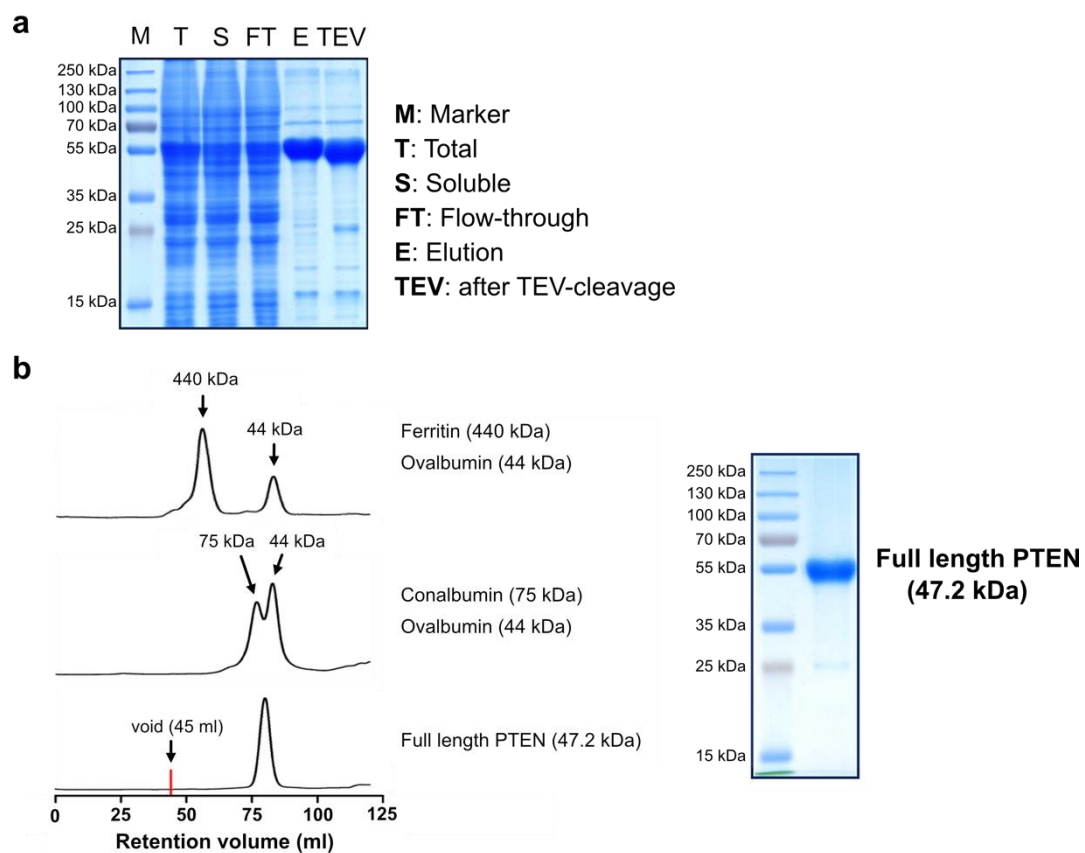


Figure 13 | Protein expression and purification of His₆-TEV-PTEN 1-403 from insect cells. (a) SDS-PAGE analysis of protein expression, affinity chromatography and His₆-tag cleavage. **(b)** SEC chromatogram (HiLoad Superdex S200 16/60) and SDS-PAGE analysis of the full-length construct in final purity. Its retention volume indicates the monomeric species compared with protein standards. For information about expression and purification of other PTEN constructs, see chapter 7.3 (TEV: *tobacco etch virus* protease). This figure is from the reference No. 171, © 2015 The Authors. Published by Wiley-VCH Verlag GmbH & Co. KGaA.

Four additional recombinant PTEN constructs were produced and purified (Figure 14). Analogous to the full-length PTEN from insect cells, these protein constructs containing His₆-tags were overexpressed in High Five insect cells and purified via IMAC, proteolytic cleavage of His₆-tag, and size exclusion chromatography. The corresponding chromatograms and SDS-PAGE analyses are found in Figure 46 – Figure 50.

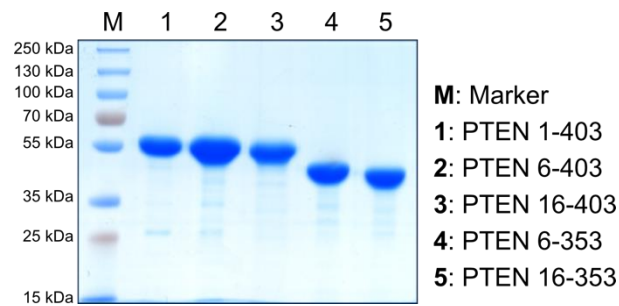


Figure 14 | SDS-PAGE analysis of PTEN constructs. The isolated five PTEN constructs overexpressed in insect cells are represented with final purity. The proteins were initially purified with affinity chromatography via His₆-tag, which was subsequently removed by treatment with TEV-protease. Size exclusion chromatography served as final purification.

Recombinant PTEN 1-353 could not be isolated by heterologous protein expression. Western blot analysis confirms the overexpression of this protein construct in insect cells (Figure 15). However, His₆-TEV-PTEN 1-353 appears to be insoluble. Given the possibility of strong interaction with the cell membrane and the following sedimentation, several detergents such as Triton X-100, NP-40, CHAPS, and sodium cholate were added during lysis. Nevertheless, the solubility of His₆-TEV-PTEN 1-353 was not improved, implicating precipitation during protein expression.

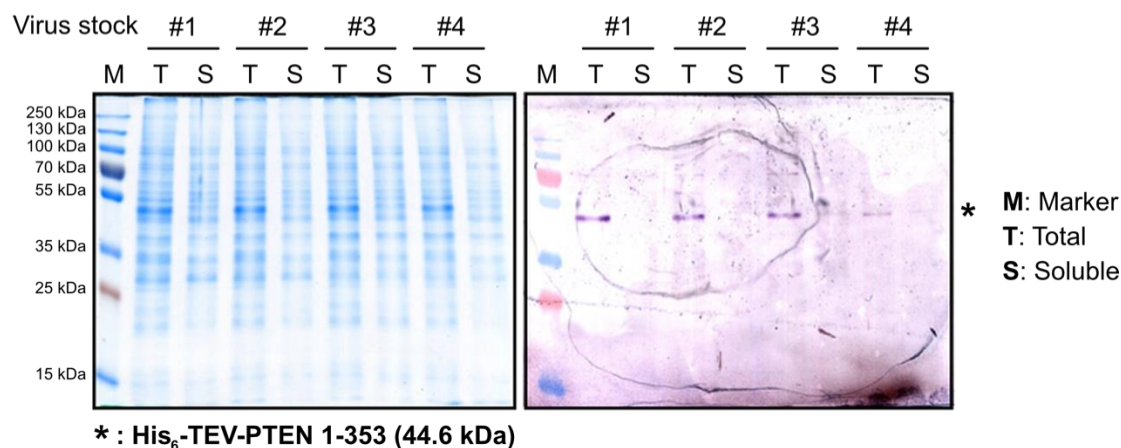


Figure 15 | PTEN 1-353 is overexpressed in insoluble form.^{VI} Analogous to other constructs, protein production of PTEN 1-353 was induced in insect cells using baculovirus-mediated expression system. Due to its insolubility, western-blot analysis was employed to validate the protein expression. The overexpression is confirmed in insect cell cultures infected with four independently produced virus stocks. However, protein bands specific for PTEN are missing in the soluble fraction indicating protein production in insoluble form. (*: His₆-TEV-PTEN 1-353, Mr = 44.6 kDa; TEV: *tobacco etch virus* protease recognition site)

3.1.2 Truncated version of PTEN (*t*PTEN) for protein crystallization

To study structural impact of activity modulators on PTEN, X-ray crystallography was employed. This method requires a well-ordered protein crystal, which is formed by regular packing of the protein of interest through intermolecular non-covalent interactions. Thereby, the target protein should be designed preferably as a rigid body to facilitate the crystallization process, since flexible regions may disturb proper crystal packing and consequently results in failure of crystallization or low data quality. In addition, a successful crystallographic effort frequently includes optimization of the recombinant protein expression and purification. This is due to the fact that formation of a protein crystal is promoted by high purity and concentration of the protein of interest.

^{VI} Western-blot analysis of PTEN 1-353 was performed by Sandra Bäcker for her Master's Thesis (Fakultät für Chemie und Chemische Biologie, TU Dortmund)¹⁴⁴.

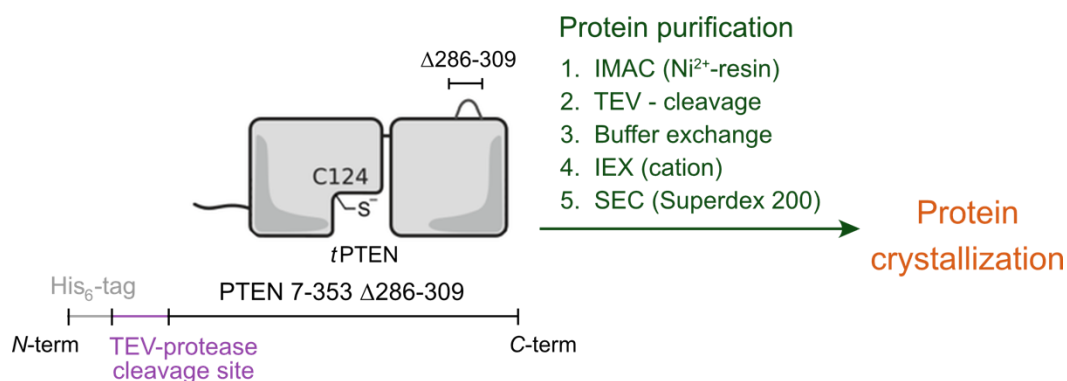


Figure 16 | Crystallization construct of *t*PTEN and its purification strategy. The crystallization construct PTEN 7-353 Δ286-309 adopted by the aforementioned crystal structure comprises PIP₂ binding motif, phosphatase and C2-domain. The flexible loop region Δ286-309 and the C-tail domain are not included. Following the serial purification steps, PTEN undergoes protein crystallization. (IMAC: immobilized metal ion affinity chromatography, TEV: *tobacco etch virus* protease, IEX: ion exchange chromatography, SEC: size exclusion chromatography)

For the crystallographic effort, the available crystal structure of PTEN was adopted. Lee *et al.* (1999) solved the structure with a truncated version including PTEN 7-353 Δ286-309 (*t*PTEN, PDB 1D5R), after they identified a rigid body using limited proteolysis with subtilisin^{43,47}. This protein construct comprises PIP₂ binding motif, phosphatase and C2-domain and exhibits active site cysteine in the reduced state⁴³ (Figure 16). However, this protein construct lacks flexible regions such as the entire C-tail region with 50 amino acids (residues 354-403) and D-loop with 24 amino acids (residues 286-309), which were deleted for proper crystal formation. In this study, *t*PTEN was produced containing an additional N-terminal His₆-tag and TEV-protease cleavage site (His₆-TEV-*t*PTEN) for efficient protein purification. Analogous to the preceding crystal structure and the full-length PTEN, His₆-TEV-*t*PTEN was produced in High Five insect cells via baculovirus. Following cell lysis, *t*PTEN was purified over five steps, including IMAC, proteolytic cleavage of His₆-tag, buffer exchange, ion exchange chromatography and size exclusion chromatography. After the serial purifications, *t*PTEN was subjected to protein crystallization.

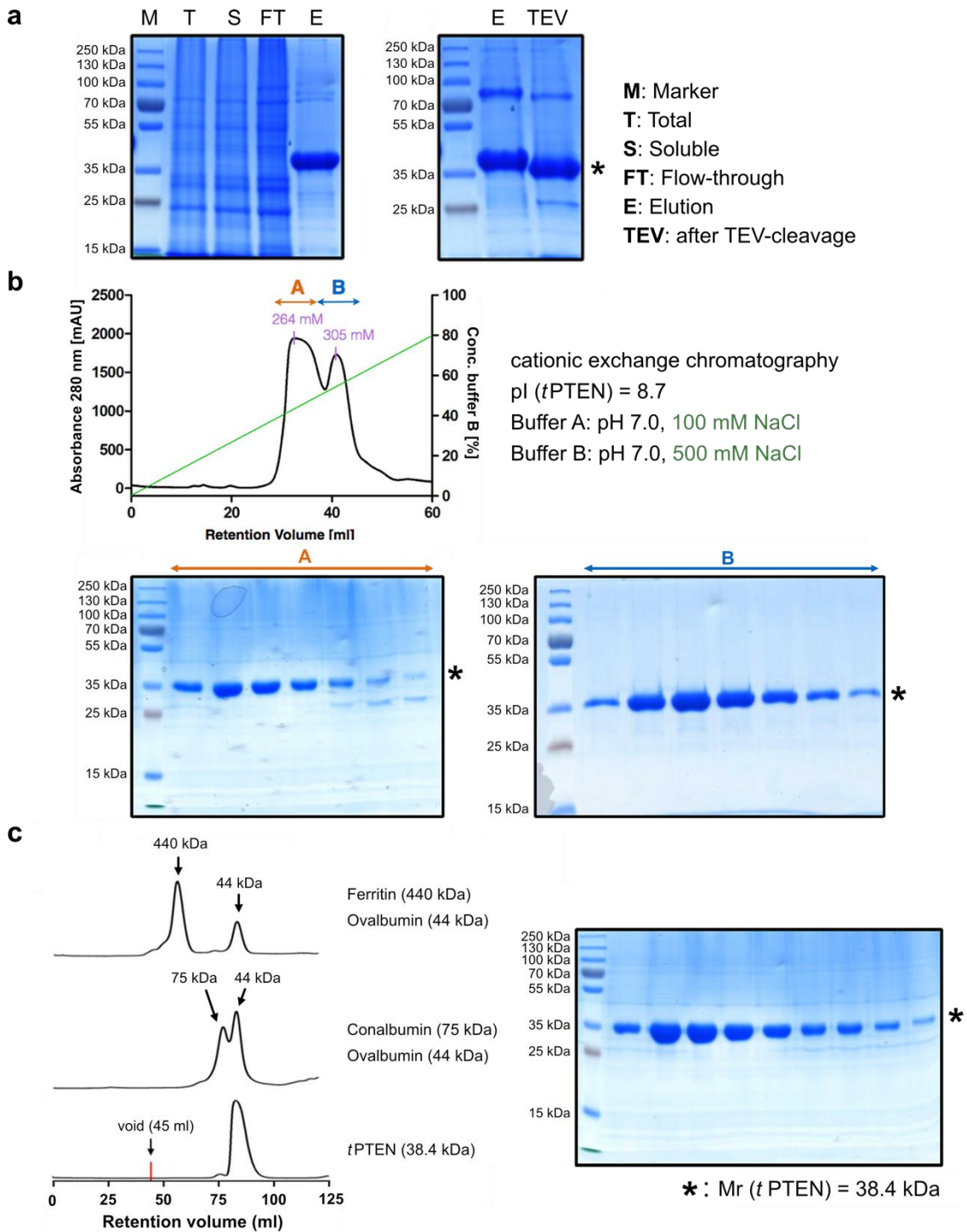
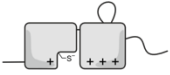
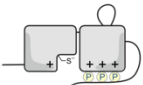
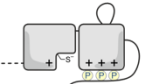
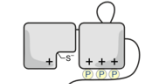
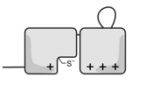
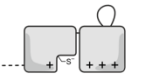
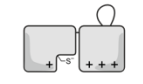
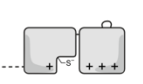


Figure 17 | Protein purification of PTEN 7-353 Δ 286-309. (a) SDS-PAGE analysis of protein expression, affinity chromatography and His₆-tag cleavage. (b) IEX chromatogram (HiTrap SP HP) and SDS-PAGE analysis. Two *t*PTEN species are separated by overall charge differences. (NaCl concentration; A: 264 mM, B: 305 mM) (c) SEC chromatogram (HiLoad Superdex S200 16/60) and SDS-PAGE analysis of the crystallization construct in final purity (species A, Figure 17b). Its retention volume indicates the monomeric species compared with protein standards. (TEV: *tobacco etch virus* protease)

His₆-TEV-*t*PTEN was initially isolated using affinity chromatography with Ni²⁺-beads, followed by treatment with TEV-protease (Figure 17a). The evident protein band shift in SDS-PAGE analysis indicates successful removal of the redundant region (His₆-tag and TEV-protease cleavage site; Figure 17a, lane E and TEV). The subsequent protein buffer exchange allowed to separate variably charged *t*PTEN species with ion exchange chromatography, which are engendered by the post-translational modification (Figure 17b). Since the isoelectric point of the crystallization construct (pI = 8.7) is above the pH-value of the running buffer (pH = 7.0), cation exchange chromatography was employed with increasing salt concentration, from 100 mM to 400 mM over 12 column volumes (CV). As demonstrated in the chromatogram, two *t*PTEN species could be isolated using this method (NaCl concentrations: 264 mM for species A, 305 mM for species B). These two species were treated separately in the subsequent purification and crystallization steps. As a final step, *t*PTEN was purified by size exclusion chromatography. Given the fact that this method allows us to change the buffer environment along with purification, the buffer used in this step is the final protein storage buffer prior to crystallization set-up. The buffer composition was modified by employing a lower salt concentration (150 mM NaCl instead of 400 mM NaCl in the previous report⁴³), as the reduced ionic strength decreases solubility and thereby promotes the crystallization process. As seen in the chromatogram, *t*PTEN manifests its monomeric nature compared to protein standards (Figure 17c). In addition, high protein purity was validated by SDS-PAGE analysis. 18 mg and 8 mg of the species A and B (Figure 17b) were yielded in the final purity from 1l insect cell culture, respectively. Protein expression and purification of various PTEN constructs are summarized in Table 1.

Table 1 | Summary of protein expression and purification. Eight different PTEN constructs in the presence and absence of regulatory domains were recombinantly expressed to study protein-ligand interaction. Six PTEN constructs have been successfully isolated. (IMAC: immobilized metal ion affinity chromatography, TEV: *tobacco etch virus* protease, IEX: ion exchange chromatography, SEC: size exclusion chromatography)

| | Constructs | Expression System | Characteristics | Protein expression & purification |
|---|-----------------------------|------------------------------|----------------------------------|---|
|  | 1 - 403 | <i>E. coli</i> | Full-length open | Formation of undefined multiple protein complex |
|  | 1 - 403 | insect cells (High Five) | Full-length closed | 1. IMAC (Ni ²⁺ - resin) 2. TEV - cleavage 3. SEC (Superdex 200) |
|  | 6 - 403 | insect cells (High Five) | ΔN | 1. IMAC (Ni ²⁺ - resin) 2. TEV - cleavage 3. SEC (Superdex 200) |
|  | 16 - 403 | insect cells (High Five) | ΔN lacking PBM | 1. IMAC (Ni ²⁺ - resin) 2. TEV - cleavage 3. SEC (Superdex 200) |
|  | 1 - 353 | insect cells (Sf9/High Five) | ΔC | Precipitation during protein expression |
|  | 6 - 353 | insect cells (High Five) | $\Delta N, \Delta C$ | 1. IMAC (Ni ²⁺ - resin) 2. TEV - cleavage 3. SEC (Superdex 200) |
|  | 16 - 353 | insect cells (High Five) | $\Delta N, \Delta C$ lacking PBM | 1. IMAC (Ni ²⁺ - resin) 2. TEV - cleavage 3. SEC (Superdex 200) |
|  | 7 - 353 $\Delta 286-309$ | insect cells (High Five) | Crystallization construct | 1. IMAC (Ni ²⁺ - resin) 2. TEV - cleavage 3. IEX (cation) 4. SEC (Superdex 200) |

3.2 Effects of PIP₂/PIP₃-derivatives on phosphatase activity

The enzymatic activities of five successfully isolated PTEN constructs (Figure 14) were furthermore determined using malachite green assay¹⁴⁵. This standard phosphatase assay takes advantage of the colorimetric change upon the orthophosphate released by phosphatases. The resulting phosphate molecule forms a malachite green phosphomolybdate complex under acidic condition. This green-colored inorganic complex exhibits an absorption range at 620-650 nm and thereby the amount of released phosphate can be quantified. Particularly, this assay allows us to use PTEN's natural substrate PIP₃. In this study, PI(3,4,5)P₃-diC8, a derivative of PIP₃ with truncated lipid acid side chains (C8 instead of C18-20), was employed to ensure solubility of the substrate and homogeneous assay conditions (Figure 18c). Phosphatase activity was measured at 1, 5, and 10 min after addition of PIP₃ (75 μM) to PTEN (50 nM) at 25 °C. Since the enzymatic activities show logarithmic curves, the relative PTEN activity was determined using the initial conversion rate. PTEN activities of the five constructs were plotted in normalized values, setting the phosphatase activity of the full-length PTEN 1-403 to 100 % (Figure 18a). Notably, there is a limitation of this assay. In this experimental setup, enzymatic reaction of PTEN occurs in solution, and not at the plasma membrane. In this regard, PTEN activity illustrated herein may not reflect the entire physiological events upon PTEN activation, involving subcellular localization and protein-protein interaction at the plasma membrane. Nevertheless, this assay is sufficient to compare the construct-dependent relative phosphatase activities of PTEN.

Consistent with an earlier *in vitro* study⁴⁸, the *N*-terminal domain appears to be essential for the PTEN activity (Figure 18a, gray). Compared with the full-length PTEN 1-403 (100 ± 3 %), the absence of the *N*-terminal domain leads to almost complete loss of enzymatic activity (PTEN 16-403: 12 ± 8 %), implicating its involvement in enzymatic reaction. Notably, a significant reduction of phosphatase activity is observed in PTEN 6-403 (25 ± 1 %), even though this construct still includes the entire PIP₂ binding motif (residues 6-KEIVSRNKRR-15). This observation implies a potential hydrophobic interaction of *N*-terminal five amino acids (residues 1-MTAII-5) with fatty acid side chains of phosphatidylinositol. The contribution of *N*-terminal domain to PTEN's enzymatic activity is also shown in the *C*-terminal truncated versions *e.g.* PTEN 6-353 (163 ± 1 %) and PTEN 16-353 (1 ± 1 %). In the latter construct, the absence of the entire *N*-terminal domain diminishes phosphatase activity of PTEN.

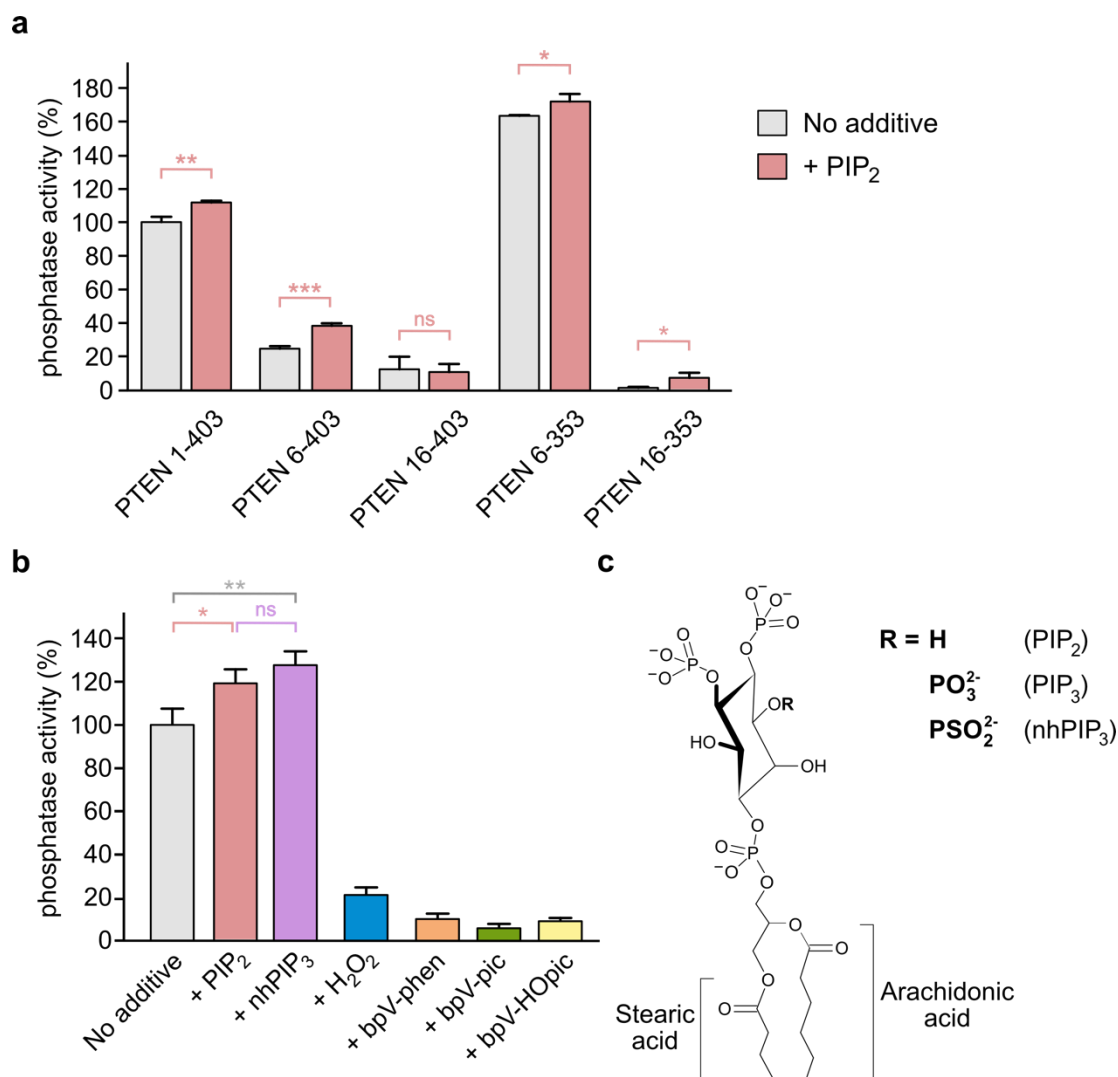


Figure 18 | Phosphatase activity of PTEN depends on the protein constructs and can be modulated by small molecules. (a) Using malachite green assay, phosphatase activity of various PTEN constructs was determined depending on the presence of *N*- and *C*-terminal regulatory domains. (gray, no addition of additives; for more information about protein constructs, see Figure 11). Due to its autocatalytic property, the construct-dependent activating effect was investigated performing the same assay with the addition of PIP₂ (red; 50 nM PTEN, 75 μM PI(3,4,5)P₃-diC8 as substrate, 50 μM PI(4,5)P₂-diC8, T = 25 °C, t = 30 min; triplicates, errors represent ± SD, * *P* < 0.05, ** *P* < 0.01, *** *P* < 0.001, ns: not significant) (b) Effects of activity modulators on the phosphatase activity of PTEN were demonstrated. Full-length PTEN (50 nM) was pre-incubated for 10 min with either PIP₂ (50 μM, red), nhPIP₃ (50 μM, purple), H₂O₂ (400 μM, blue), bpV-phen (1 μM, orange), bpV-pic (1 μM, yellow), or bpV-HOpic (1 μM, green), followed by addition of PIP₃ (75 μM, T = 25 °C, t = 30 min; triplicates, errors represent ± SD, * *P* < 0.05, ** *P* < 0.01, ns: not significant). (c) Chemical structures of PIP-derivatives.

The C-terminal domain (residues 352-403) has an inhibitory effect on the phosphatase activity of PTEN (Figure 18a, gray). Under our assay conditions, it is validated that PTEN 6-353 shows significantly higher activity than PTEN 6-403 and the full length construct, which is in agreement with previous reports^{55,71}.

As previously mentioned (Chapter 1.2.1), PTEN catalyzes hydrolysis reaction of PIP₃ and releases PIP₂. However, an activating effect of the reaction product PIP₂ on PTEN has been reported in an earlier *in vitro* study, indicating an autocatalytic mechanism⁴⁸. This property of PIP₂ is also validated in this study (Figure 18a, red). The presence of additional PIP₂ (50 μM) increases the enzymatic reaction rate in PTEN constructs including N-terminal domains (PTEN 1-403, PTEN 6-403, PTEN 6-353). Only a slight increase of the reaction rate in PTEN 6-353 is ascribed to a very high hydrolysis rate under this condition that was optimized to ensure the activity differences of PTEN constructs. Under this assay condition, almost complete conversion of PIP₃ by PTEN 6-353 was observed in the absence of additional PIP₂, even at the first measurement point (1 min).

Next, phosphatase activity of full-length PTEN (50 nM) was determined in the presence of different activity modulators (Figure 18b). Incubation with PIP₂ or nhPIP₃^{VII} (50 μM for each) increases enzymatic activity of PTEN (100 ± 7.5 %) to 119.3 ± 6.4 % and 127.7 ± 6.4 %, respectively, implicating a potential allosteric binding site for PIP₂ or nhPIP₃, and no selectivity for PIP₂ or PIP₃. Activity modulation of PTEN was subsequently measured with its inhibitors. Under our assay conditions, H₂O₂ (400 μM), bpV-phen, bpV-pic and bpV-HOpic (1 μM for each bpV-complex) shows efficient inhibition (H₂O₂: 21.4 ± 3.5 %, bpV-phen: 10.3 ± 2.5 %, bpV-pic: 6.0 ± 2.0 %, bpV-HOpic: 9.3 ± 1.5 %).

Having characterized the activity modulating effects of the regulatory domains of PTEN and the available modulators, fluorescence polarization (FP) assay was employed to identify the binding domain of PIP₂ (Figure 19). Fluorescein-labeled PIP₂ (20 nM) was incubated with six different PTEN constructs in serial dilution and the fluorescence polarization was measured¹⁴⁶. Notably, FP assay result shows no effective binding of PTEN constructs containing C-tail with PIP₂, while PTEN constructs lacking C-tail shows higher affinity for this activity modulator. Concerning that phosphatase activity of PTEN constructs containing C-tail is increased in the presence of PIP₂, this result may implicate the competition of

^{VII} nhPIP₃ is a non-hydrolyzable version of PIP₃ involving a thiophosphate at D3-position (Figure 18c).

intramolecular C-tail with interaction between PTEN's core domains and PIP₂ (Figure 18a, Figure 18b and Figure 19a). In addition, PIP₂ affinity of PTEN 16-353, which lacks PIP₂ binding motif, appears comparable to PTEN 6-353 (Figure 19b), indicating PIP₂ binding motif-independent interaction between PIP₂ and the core domains. Giving the possibility of PIP₂ interaction with either the active site or an allosteric binding site, phosphatase and C2 domains (Figure 3) were separately expressed using *E. coli* and insect cells^{VIII147}. However, it was not possible to obtain the single domains in soluble and monomeric forms. Therefore, investigation of PTEN interaction with PIP₂ and nhPIP₃ was discontinued.

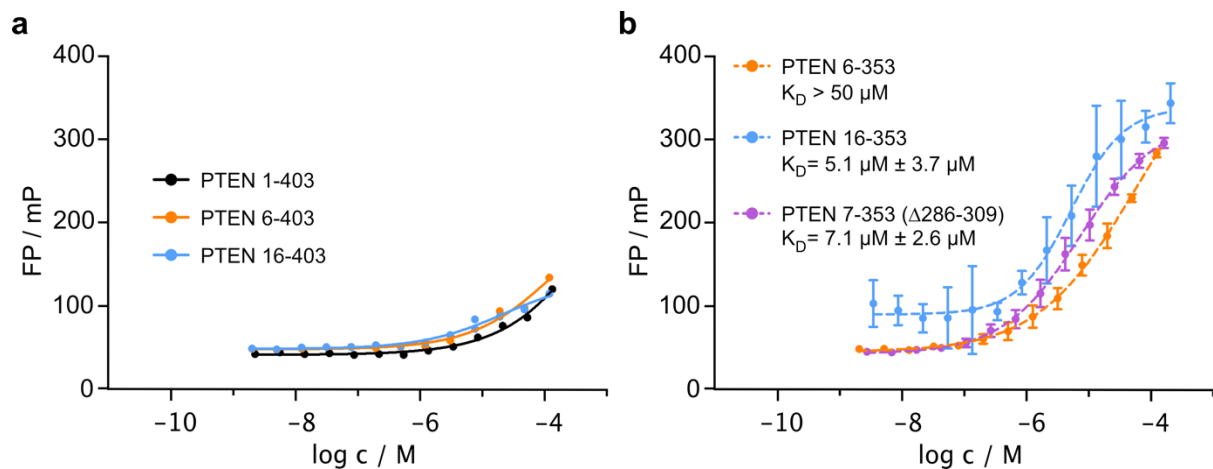


Figure 19 | C-tail of PTEN may compete with interaction between PTEN's core domain and PIP₂.^{IX} Fluorescence polarization (FP) assay served to determine the interaction of various PTEN constructs with fluorescein-labeled PIP₂ (20 nM, measured at 494 nm). (a) PTEN constructs including C-tail show very low affinity for PIP₂ ($K_D > 500 \mu\text{M}$, single point measurements). (b) PTEN constructs lacking C-tail show higher affinity for PIP₂ compared to those with C-tail. PTEN 16-353 devoid of the putative PIP₂-binding motif shows comparable PIP₂ affinity to PTEN 6-353 and PTEN 7-353 ($\Delta 286-309$) (triplicates, errors represent \pm SD).

^{VIII} Recombinant protein expression of phosphatase and C2 domains was performed by Carolin Müller for her Master's Thesis (Fakultät für Chemie und Chemische Biologie, TU Dortmund)¹⁴⁷.

^{IX} FP-assay of PTEN in the presence of PIP₂ was performed by Arne Küpper for his Master's Thesis (Fakultät für Chemie und Chemische Biologie, TU Dortmund)¹⁴⁶.

3.3 Oxidative modification of PTEN by hydrogen peroxide and bpV-phen

3.3.1 Determination of half-maximal inhibitory concentration

Initially, biochemical effects of H₂O₂ and bpV-complexes on full-length PTEN were validated by determining the half-maximal inhibitory concentrations (IC₅₀) of both compounds. Analogous to the previous phosphatase activity measurement (Chapter 3.2), malachite green assay was performed using the truncated version of PIP₃, PI(3,4,5)P₃-diC8¹⁴⁵.

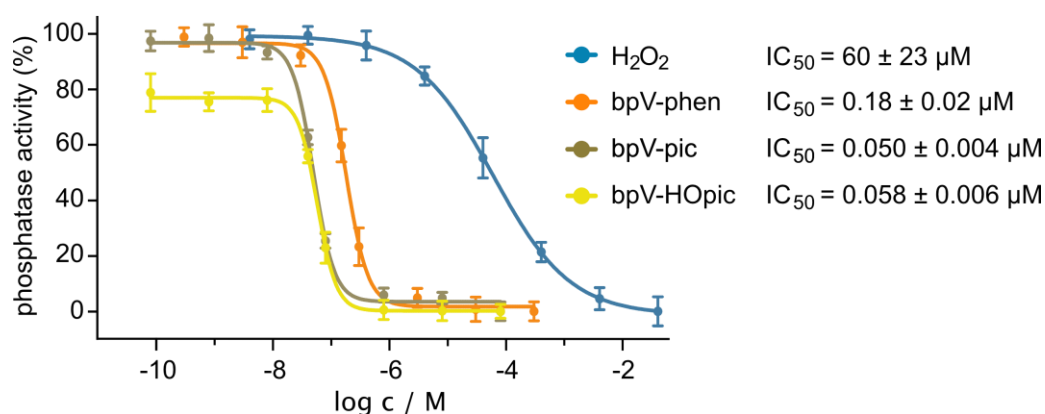


Figure 20 | H₂O₂ and bpV-inhibitors inhibit phosphatase activity of PTEN. Half-maximal inhibitory concentrations (IC₅₀) of H₂O₂ (blue), bpV-phen (orange), bpV-pic (green) and bpV-HOpic (yellow) were determined by phosphatase activity measurements using malachite green assay. (50 nM full-length PTEN, 75 μM PI(3,4,5)P₃-diC8 as substrate, T = 25 °C, t = 30 min; triplicates, errors represent ± SD.)

Applying 50 nM PTEN and 75 μM substrate, PTEN exhibited the expected phosphatase activity. In the presence of H₂O₂, bpV-phen, bpV-pic, and bpV-HOpic with serial dilution, IC₅₀ were subsequently determined to be 60 ± 23 μM, 0.18 ± 0.02 μM, 0.050 ± 0.004 μM, and 0.058 ± 0.006 μM, respectively. The values are in agreement with the previously reported range^{82,131}. Remarkably, IC₅₀ of H₂O₂ is significantly higher than its intracellular concentration in mammals, which varies from 0.001 to 0.7 μM for the redox signaling in the basal state^{148X}. Given oxidation of PTEN observed in the growth factor-mediated redox signaling¹⁰⁹ (Chapter 1.3.2), this physiological event is implicated to occur in response to local high concentration of H₂O₂.

^X IC₅₀ (H₂O₂) is higher by about 85 times compared to its maximal intracellular concentration.

3.3.2 Reactivation assay

Oxidative inhibition of PTEN by H₂O₂ via disulfide formation and its reactivation under reductive conditions have already been shown in previous studies^{82,83}. Prior to structural characterization, the reversible character of PTEN inhibition by H₂O₂ was confirmed using malachite green assay. PTEN was pre-incubated with H₂O₂ (3.5 mM), followed by dilution with buffer either containing or lacking reducing agent (mock). The residual phosphatase activity was subsequently determined. Effective inhibition was demonstrated in the absence of the reducing agent (residual activity = 8 ± 4 %), whereas PTEN reveals complete reactivation upon dilution with dithiothreitol (DTT, 4 mM; residual activity = 99 ± 3 %). In addition, the presence of physiologically relevant reducing agents (*e.g.* glutathione (GSH, 4 mM), thioredoxin system (5 μ M thioredoxin 1, 0.1 μ M thioredoxin reductase and 200 μ M NADPH)) also resulted in significant restoration of phosphatase activity (73 ± 4 % and 75 ± 2 %, respectively)^{XI}. These observations are in agreement with previous reports and validate the reversible character of PTEN inhibition by H₂O₂⁸².

Concerning bpV-based PTEN inhibitors, bpV-phen was chosen for further studies due to its highest stability in aqueous solution¹⁵². Inhibitory effect of bpV-phen was validated in the aforementioned chapter (Chapter 3.3.1). However, it is so far unknown, how these compounds exert inhibition upon PTEN. According to Huyer et al. (1997), treatment with peroxidovanadate, a chemically related compound harboring peroxide ligands, promotes hyperoxidation of the catalytic cysteine in PTP1B to sulfonic acid¹⁵³. Hence, the question shall be answered, whether bpV-phen exerts non-covalent or oxidative inhibition on PTEN. Given the latter case, it was worthwhile to discern two possible modifications: Disulfide bond (reversible) vs. hyperoxidation (irreversible). For that reason, the reactivation test of phosphatase activity was performed, analogous to the preceding assay with H₂O₂. The effective inhibition (residual activity = 4 ± 4 %) was determined by treatment of bpV-phen (400 μ M) and subsequent dilution without any reducing agents (mock). In analogy to H₂O₂-treated PTEN, DTT, GSH and the Trx system restored the phosphatase activity to 95 ± 7 %, 69 ± 5 % or 15 ± 5 %, respectively. This result indicates the oxidative inhibition and supports disulfide formation of PTEN upon bpV-phen treatment.

^{XI} Concentrations of glutathione and thioredoxin 1 applied in this assay were chosen according to the endogenous concentrations of both molecules (GSH: 0.5 – 10 mM, TRX1: 1 – 10 μ M)^{149,150,151}.

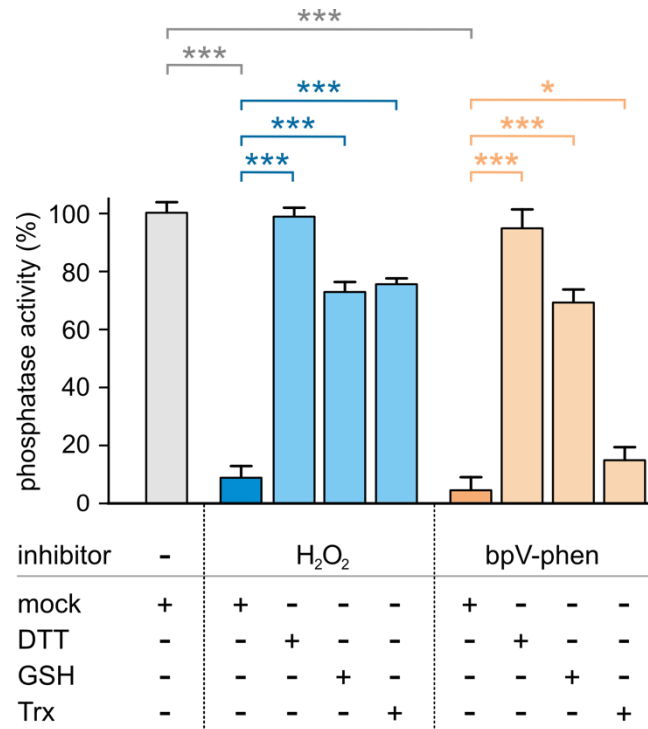


Figure 21 | PTEN inhibition by H₂O₂ and bpV-phen is reversed under reductive conditions.

Following the incubation with 3.5 mM H₂O₂ (blue) or 400 μM bpV-phen (orange), treatment of 5 μM full-length PTEN with 4 mM DTT, 4 mM GSH or thioredoxin system (Trx) reactivates its phosphatase activity. (Trx is composed of 5 μM thioredoxin, 0.1 μM thioredoxin reductase and 200 μM NADPH.; triplicates, errors represent ± SD, * $P < 0.05$, ** $P < 0.01$, *** $P < 0.001$)

3.3.3 Mass-spectrometric analysis

Next, chemical modification of PTEN upon oxidative inhibition was studied. Upon treatment with H₂O₂, PTEN undergoes disulfide formation involving the active site cysteines C124 and C71⁸². However, it remains elusive, if bpV-phen treatment induces the same disulfide bond. For this purpose, HPLC-coupled high resolution MS and MS/MS analysis were applied to investigate covalent protein modification of PTEN upon oxidative inhibition in cooperation with Dr. Tanja Bange (MPI Dortmund). Sample preparation was performed by the author of this thesis. Measurements and data analysis were carried out by Dr. Tanja Bange and Franziska Müller. Full-length PTEN samples were first treated with H₂O₂ or bpV-phen. Subsequent incubation with iodoacetamide allowed to prevent the free cysteine thiols from further modifications as well as thiol-disulfide shuffling. The following tryptic digestion was performed in the absence of reducing agents to maintain the disulfide bond. The resulting peptide fragments were separated and analyzed using HPLC-MS. Treatment with H₂O₂ or bpV-phen provided a new tryptic fragment with a monoisotopic mass of 930.918 Th (MH⁴⁺) (Figure 22a and b, upper panel)^{XII}. In both cases, MS/MS sequencing of this peak revealed a peptide fragment harboring a disulfide bond crosslinked between C71 and C124 (Figure 52). Notably, subsequent treatment of the oxidized sample with 10 mM DTT diminished the corresponding isotopic pattern (Figure 22b, lower panel), supporting the occurrence of disulfide bond upon H₂O₂ or bpV-phen treatment. Concerning the irreversible hyperoxidation of PTP1B by peroxidovanadate treatment instead of reversible oxidative sulfenyl-amide formation^{122,123,153,154,173} (Figure 8 and Figure 9), the disulfide bond formation of PTEN by bpV-phen underpins the proposed protective mechanism from irreversible inactivation^{10,116}. Prior to structural analysis of PTEN upon oxidative modification, the applicability of the crystallization construct (*t*PTEN) was confirmed for the following X-ray crystallography study. Treatment of *t*PTEN with H₂O₂ and bpV-phen resulted in tryptic fragments involving the same disulfide formation (Figure 53 and Figure 54).

^{XII} For more spectral data, please see Figure 51 – Figure 54.

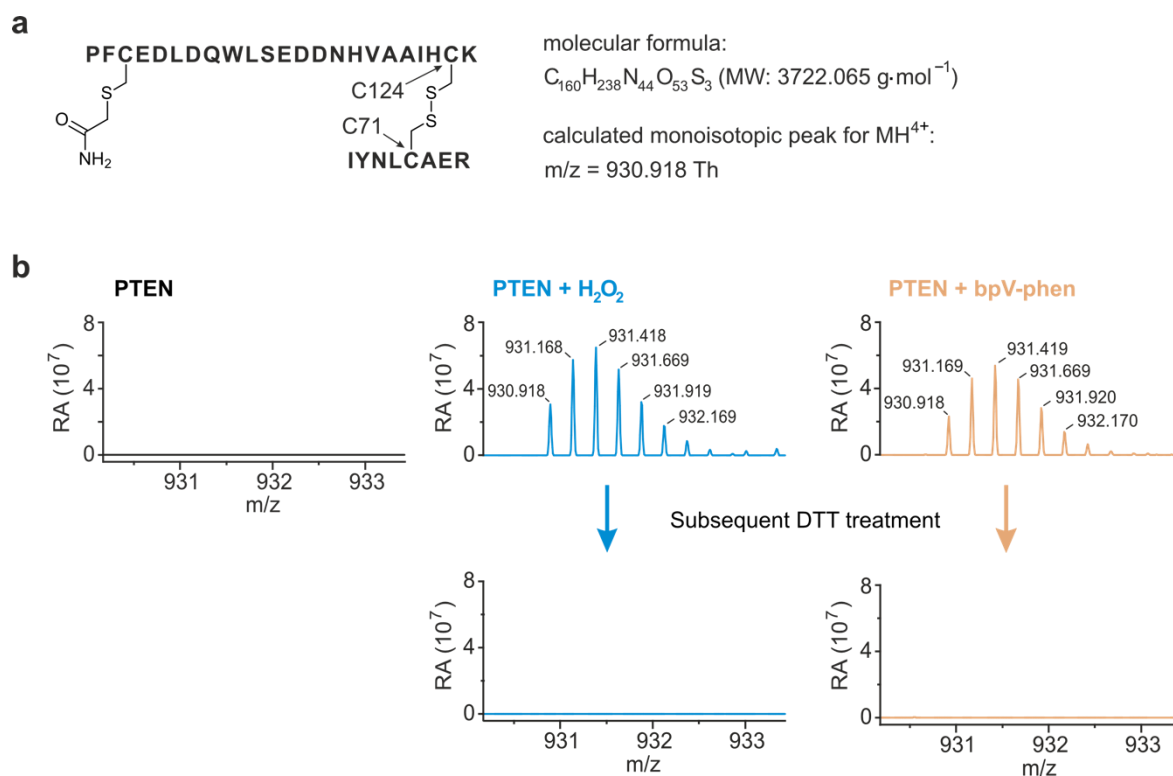


Figure 22 | H₂O₂ and bpV-phen-induced oxidative inactivations result in disulfide formation^{XIII}.

(a) The resulting peptide fragment of PTEN after H₂O₂ or bpV-phen treatment and the subsequent incubation with iodoacetamide and trypsin. The disulfide bond is formed between C71 and C124 (Th: Thomson = *Da* / *e*). (b) Compared to the untreated control (black), high-resolution MS validates the disulfide formation after H₂O₂ (1 mM, blue) or bpV-phen (1 mM, orange) treatment (upper panel; T = 25 °C, 100 μM PTEN, t = 10 min), detecting the corresponding monoisotopic pattern of the tryptic fragment. Consistent with the reversible property of disulfide bond, subsequent incubation with DTT (10 mM, 10 min) diminishes the signal (lower panel). This figure is reconstructed based on Lee *et al.* (2015)¹⁷¹.

^{XIII} Measurements of HPLC-MS and MS/MS and the following data analysis were carried out by Dr. Tanja Bange and Franziska Müller (MPI Dortmund, Germany).

3.4 Crystal structure of reduced PTEN

3.4.1 Protein crystallization of the full-length PTEN and reduced *t*PTEN

Structural effects of activity modulators on PTEN were furthermore investigated. For this purpose, full-length PTEN was initially subjected to protein crystallization. So far, structural information of the full-length PTEN remains elusive, which would additionally allow us to understand its functional regulation. Given that phosphorylation-mediated “closed” conformation of PTEN is facilitated by electrostatic interaction between globular domains and the phosphorylated C-tail^{55,70,71} (Chapter 1.2.3), full-length PTEN in the autoinhibited state might be crystallized as a rigid body. For the successful crystallization, the host organism for protein production should be able to phosphorylate PTEN. The recombinantly expressed full-length PTEN should also be isolated with a single phosphorylation pattern in high purity.

Full-length PTEN was overexpressed in High Five insect cells and initially purified with Ni²⁺-beads via IMAC. After His₆-tag cleavage and buffer exchange, different phosphorylation species were separated by ion exchange chromatography. Since the isoelectric point of the crystallization construct (pI = 5.95) is below pH-value of the running buffer (pH = 8.0), anion exchange chromatography was employed with increasing salt concentration from 50 mM to 500 mM (Figure 23a). Concerning the multiple phosphorylation sites (Figure 4), a flat salt gradient over 125 CV was employed. Nonetheless, merged pattern of peaks was observed, indicating numerous post-translationally modified species. Protein fractions from two “quasi peaks” were isolated and purified separately using size exclusion chromatography (species A and B, Figure 23b). Large-scale screening was performed for protein crystallization of both species using pre-mixed crystallization buffers (Qiagen[®] NeXtal JCSG Core Suites) (Table 2). Protein drops containing three different PTEN concentrations (20, 15, 10 mg/ml) and reservoir solution (ratio 1:1) were set up implementing the sitting drop vapor diffusion crystallization method²⁰⁶. Notably, crystalline formation was observed only from one condition (Qiagen[®] NeXtal JCSG Core I, No. 5^{XIV}, T = 20 °C; species A) including 1,6-hexanediol (Figure 23c). However, its reproduction for the further optimization was unsuccessful in the grid screening format, in which pH and 1,6-Hexanediol concentration of the reservoir solution were varied.

^{XIV} Composition: 100 mM Tris (pH 8.5), 200 mM MgCl₂, 3.4 M 1,6-Hexanediol

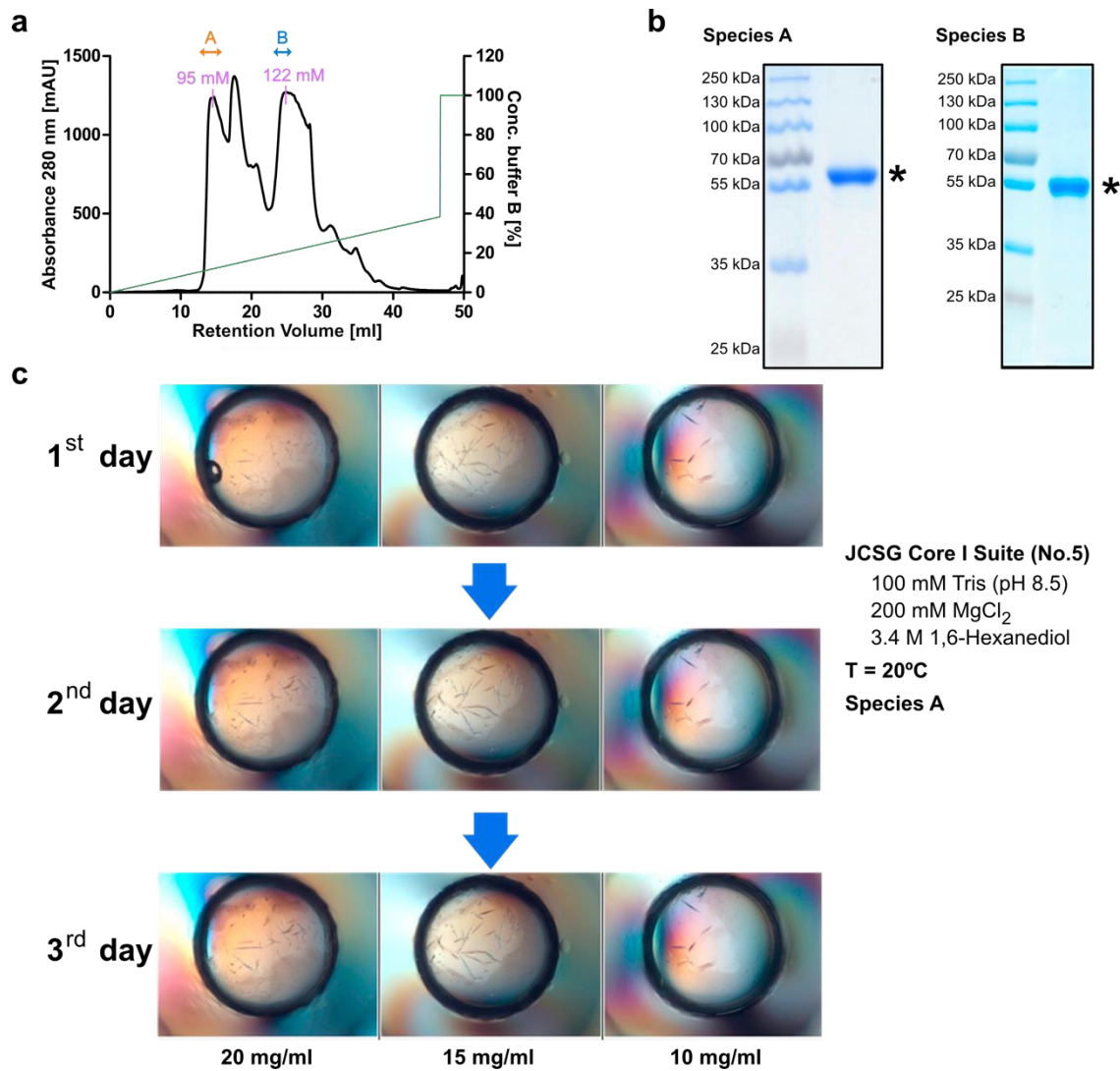


Figure 23 | Protein crystallization of the full-length PTEN. (a) IEX chromatogram (MonoQ 5/50 GL). Two PTEN species were isolated. (NaCl concentration; A: 95 mM, B: 122 mM) (b) SDS-PAGE analysis of the full-length construct in final purity. (c) Time course of crystallization. Crystalline formation was observed in one condition only (Qiagen[®] NeXtal JCSG Core I Suite, No. 5, T = 20 °C; species A).

Table 2 | Crystallization conditions used for the full-length PTEN. The isolated species A and B were subjected to initial protein crystallization using JCSG Core screening suites (Qiagen® NeXtal). Protein drops containing three different PTEN concentrations ($c = 20, 15$ and 10 mg/ml) and reservoir solution (ratio 1:1) were set up employing the sitting drop vapor diffusion crystallization method²⁰⁶. Protein crystallization was performed at 20 and 4 °C.

| Species A | | Species B | |
|-----------|----------|-----------|----------|
| 20 °C | 4 °C | 20 °C | 4 °C |
| Core I | Core I | Core I | Core I |
| - | Core II | Core II | Core II |
| Core III | Core III | Core III | Core III |
| - | Core IV | - | Core IV |

Next, protein crystallization of the truncated construct *t*PTEN (PTEN 7-353 Δ 286-309) was established based on the previous crystal structure of PTEN. As previously shown in the chapter 3.1.2, protein production of *t*PTEN in high purity allowed us to perform both large-scale and grid crystallization screenings. For the latter method, parameters (*e.g.* pH, concentration of precipitant and additive, temperature) were varied to find the optimum around the known crystallization condition^{XV} (PDB 1D5R)⁴³. Although the large-scale screening did not deliver a suitable protein crystal^{XVI}, box-like protein crystals of *t*PTEN appeared in the grid screen after two days, but only from species A (Figure 17b), and grew over five days at 20 °C (Figure 24). *t*PTEN crystals tend to grow in fewer numbers but larger under lower concentrations of the precipitant (L-tartrate) and the additive (glycerol). The best diffracting crystals were obtained under slightly acidic condition with lower tartrate concentration^{XVII}. After optimization of the crystallization condition, protein composition of *t*PTEN crystals was additionally confirmed by SDS-PAGE analysis. Proteins in the crystals showed highest purity, as crystallization is a sort of purification process (Figure 24). Prior to

^{XV} 100 mM Tris-HCl, 1.3M Na/K L(+)-tartrate, 5 % – 10 % (v/v) glycerol, 10 mM DTT (pH 8.0), $T = 20$ °C, $c(t$ PTEN) = 20 mg/ml⁴³

^{XVI} Protein crystallization of *t*PTEN was set up using Qiagen® NeXtal suites (JCSG Core Suites I, II, III, IV, Classics Suites I, II, Cryo Suite, MPD Suite, PEGs Suites I, II, Protein Complex Suite). Implementing the sitting drop vapor diffusion crystallization method²⁰⁶, *t*PTEN (20, 10 and 5 mg/ml) was incubated with reservoir solution (ratio 1:1) at 4 °C.

^{XVII} 100 mM MES (pH 6.5), 1.25M Na/K L(+)-tartrate, 7.5 % (v/v) glycerol, $T = 20$ °C, $c(t$ PTEN) = 20 mg/ml

data collection at synchrotron, *t*PTEN crystals were soaked in reservoir solution supplemented with higher glycerol concentration^{XVIII} and flash-frozen.

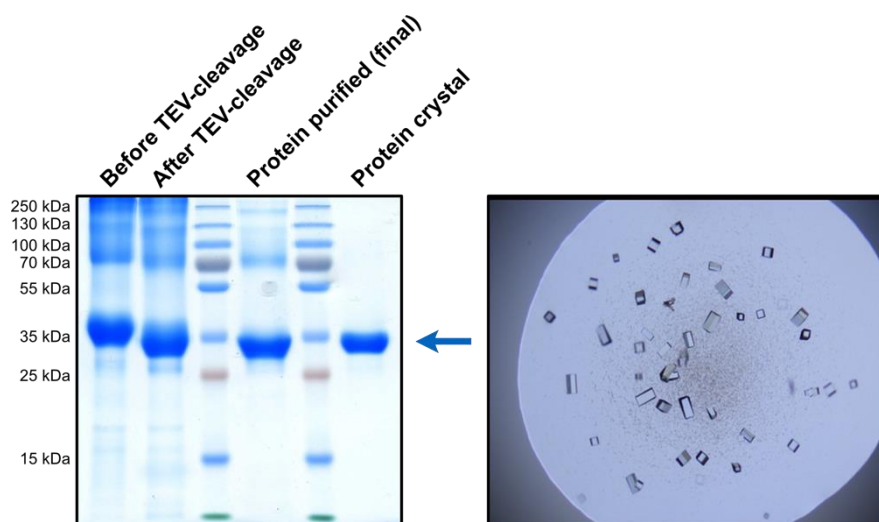


Figure 24 | SDS-PAGE analysis of PTEN 7-353 Δ 286-309 and its protein crystals. Protein purity of each purification step is represented with SDS-PAGE analysis. Protein crystals (right) were confirmed using SDS-PAGE ($M_r = 38.4$ kDa). This figure is from the reference No. 171, © 2015 The Authors. Published by Wiley-VCH Verlag GmbH & Co. KGaA.

3.4.2 Structure determination

Protein crystals of PTEN allowed us to analyze its 3D-structure using X-ray crystallography. At first, monochromatic diffraction data of a *t*PTEN crystal (Chapter 3.4.1) were collected under cryogenic condition at a synchrotron radiation source (Swiss Light Source, Villigen, Switzerland) implementing the rotating-crystal method^{155,156}. The wavelength of 1.000 Å was utilized for data collection. 1440 frames of X-ray diffraction patterns were recorded at every 0.25°, as the *t*PTEN crystal was gradually rotated by 360°. The diffraction dataset was furthermore processed using X-ray detector software XDS¹⁵⁷ by analyzing the diffraction pattern, which originates from the position and intensity of reflections on the detector. XSCALE¹⁵⁷ was used to reduce the data to the lowest resolution of 2.2 Å (Table 3)^{XIX}. The scaled dataset involves overall 99.9 % of data completeness.

^{XVIII} 100 mM MES (pH 6.5), 1.25M Na/K L(+)-tartrate, 25 % (v/v) glycerol

^{XIX} Criteria for selection of the lowest resolution were data completeness (> 95 %), signal-noise ratio ($I/\sigma(I) > 1$) and correlation coefficient ($CC_{1/2} > 70$ %)¹⁵⁸.

Table 3 | Dataset statistics of reduced *t*PTEN crystal. I/σ states signal to noise ratio of unique reflections. R_{meas} is a redundancy-independent R-factor¹⁵⁹. $CC_{1/2}$ is indicative of the correlation percentage between reflection intensities from random half-datasets¹⁵⁸. Correlation significant at the 0.1 % level is highlighted by an asterisk.

| Resolution [Å] | Number of reflections | | | Completeness [%] | $I/\sigma(I)$ | R_{meas} [%] | $CC_{1/2}$ [%] |
|-------------------|-----------------------|--------|----------|---------------------|---------------|--------------------------|-------------------|
| | Observed | Unique | Possible | | | | |
| 20.0 | 1595 | 152 | 168 | 90.5 | 49.07 | 5.2 | 99.9* |
| 15.0 | 2465 | 191 | 191 | 100.0 | 56.02 | 3.8 | 99.9* |
| 10.0 | 10456 | 787 | 787 | 100.0 | 61.54 | 3.4 | 99.9* |
| 8.0 | 11729 | 1022 | 1023 | 99.9 | 51.87 | 3.8 | 99.9* |
| 6.0 | 37679 | 2852 | 2853 | 100.0 | 42.13 | 5.1 | 99.9* |
| 4.0 | 149789 | 11368 | 11368 | 100.0 | 41.87 | 5.5 | 99.9* |
| 3.1 | 249220 | 18387 | 18391 | 100.0 | 22.27 | 11.5 | 99.8* |
| 3.0 | 47158 | 3510 | 3511 | 100.0 | 9.53 | 32.0 | 98.9* |
| 2.9 | 55999 | 4062 | 4062 | 100.0 | 8.64 | 36.2 | 99.0* |
| 2.8 | 64274 | 4620 | 4621 | 100.0 | 6.49 | 51.2 | 98.0* |
| 2.6 | 161522 | 11530 | 11534 | 100.0 | 4.21 | 80.8 | 95.5* |
| 2.5 | 96191 | 7198 | 7203 | 99.9 | 2.65 | 129.9 | 88.8* |
| 2.4 | 107706 | 8435 | 8436 | 100.0 | 2.05 | 163.2 | 83.2* |
| 2.3 | 134037 | 9953 | 9961 | 99.9 | 1.63 | 203.3 | 81.3* |
| 2.2 | 163197 | 11832 | 11843 | 99.9 | 1.17 | 273.9 | 72.7* |
| Total | 1293017 | 95899 | 95952 | 99.9 | 13.96 | 15.6 | 99.9* |

Data processing generates a reflection data containing information about the experimental data, which serves to calculate an electron density map with structure factor amplitudes. By default, this software automatically determines and suggests the highest probable crystallographic parameters such as space group and the unit cell constants based on the diffraction patterns during the data processing. However, the intrinsic twinning character of the *t*PTEN crystal (two twin fractions, ratio: 0.49 and 0.51) hindered to find the correct parameters with the software XDS, which consequently resulted in high R-factor in the later refinement step (Eq. 5)^{xx}. Since a twinned crystal is a composition of single crystals that are arranged with different orientations in a crystal, mathematical operators should be applied to solve the structure after determination of correct crystallographic parameters (Table 4). This issue was resolved by processing the diffraction data with implementation of a lower

^{xx} R-factor is a measure of agreement between the structure model and the experimental data (Eq. 5). High R-factor indicates that the structural solution is in accordance with the experimental data with low probability.

symmetry^{XXI} and applying detwinning functions (operators: k, h, -l and h, k, l) in the model refinement process. Following data processing, electron density map was generated to determine the structure solution. This requires structure factors of the crystallized protein including amplitude and phase information for calculation. However, the experimental data provides only amplitude but lacks phase information. Among various approaches to solve the “phase problem”, molecular replacement was applied in this study. This method is based on utilizing the phase term of the available structure that exhibits high sequence homology. Molecular replacement was performed with the reflection data against the known PTEN structure (PDB 1D5R)^{43XXII}. In a unit cell, the structure solution contains eight asymmetric units, which are the smallest units that can be used to reproduce a complete unit cell by applying symmetry operations. The asymmetric unit of *t*PTEN consists of four protomers (Chain A – D, Figure 25). The structure model was subsequently built in the electron density and refined in the iterative way^{XXIII}, until the discrepancy (R-factor) between crystallographic structure model and experimental X-ray diffraction data reached a minimum ($R_{\text{work}} = 0.19$ and $R_{\text{free}} = 0.22$). Crystallographic parameters and refinement statistics of *t*PTEN crystal (reduced, PDB 5BZZ) are summarized in Table 4.

In the final structure model, electron density is resolved from 14 to 351 in all four protomers of *t*PTEN (PDB 5BZZ). The missing electron density (Δ residues: 7-13 and 352-353) implicates flexible nature of *N*- and *C*-termini in the structure. In addition, four protomers of *t*PTEN in the asymmetric unit were compared using the final structure model. Discrepancies were calculated based on root-mean-square deviation (RMSD). As a rule of thumb, RMSD under 2 Å manifests a similar three-dimensional structure. The maximal RMSD value is represented with 1.46 Å (314 C_{α} atoms), indicating very similar structures.

^{XXI} XDS suggested space groups P4 and its subunits (SG 89 – 96), which comprises two PTEN protomers per asymmetric unit. The correct space group is determined to be C222₁ (SG 20) involving four PTEN molecules in the asymmetric unit.

^{XXII} Molecular replacement was performed using PhaserMR (CCP4 suite^{200,201}).

^{XXIII} Coot¹⁹⁵ and Refmac¹⁹⁶ were utilized for manual correction and automatic refinement of the structure model, respectively.

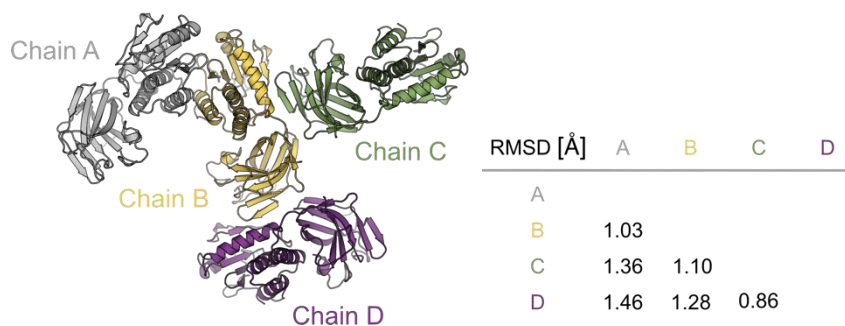


Figure 25 | Arrangement of four PTEN molecules in the asymmetric unit shows intermolecular contacts in the protein crystal. Each protomer in the asymmetric unit is represented with different colors. RMSD values (314 C_{α} atoms) under 2 Å reflect high similarity to each other (Chain A: gray; chain B: yellow; chain C: green; D: purple; RMSD: root-mean-square deviation). This figure is from the reference No. 171, © 2015 The Authors. Published by Wiley-VCH Verlag GmbH & Co. KGaA.

Table 4 | Crystallographic data collection and refinement statistics of reduced *t*PTEN crystal. Structure coordinates have been deposited in the RCSB Protein Data Bank⁴² with the accession code 5BZZ. Values in the parenthesis involve the highest resolution shell. R_{Free} was calculated from 5 % of the reflections omitted from refinement process.

| | <i>t</i>PTEN |
|---------------------------------------|----------------------------|
| PDB code | 5BZZ |
| Data Collection | |
| Space group | C222 ₁ |
| Unit-cell parameters | |
| a, b, c (Å) | 207.17, 207.39, 87.78 |
| α, β, γ (°) | 90, 90, 90 |
| Wavelength (Å) | 1.000010 |
| Resolution limits (Å) | 46.36 - 2.20 (2.30 - 2.20) |
| No. of unique reflections | 95899 (11832) |
| Completeness (%) | 99.9 (99.9) |
| Multiplicity | 13.48 (13.79) |
| $I/\sigma(I)$ | 13.96 (1.17) |
| CC _{1/2} | 99.9 (72.7) |
| R _{obs} | 15.0 (263.7) |
| Refinement | |
| Resolution limits (Å) | 46.36 - 2.20 (2.30 - 2.20) |
| R _{Work} / R _{Free} | 0.1920 / 0.2207 |
| R.m.s.d. | |
| Bond length (Å) | 0.0094 |
| Bond angles (°) | 1.567 |
| B-factors (Å ²) | 61.4 |
| No. atoms | |
| Protein | 10338 |
| Ligand | 40 |
| Water | 890 |
| Ramachandran plot (%) | |
| Favored regions | 92.9 |
| Allowed regions | 6.2 |
| Disallowed regions | 0.9 |

3.4.3 PTEN structure in the reduced form

*t*PTEN structure (PDB 5BZZ) consists of phosphatase and C2 domains (Figure 26). The phosphatase domain is composed of five central beta strands, which are surrounded by five alpha helices. The active site in the phosphatase domain is facing to the putative membrane binding region. The active site pocket contains conserved structural motifs of PTPs (*e.g.* WPD loop and P-loop). In particular, D92 in WPD loop, C124 and R130 in P-loop are essential components for hydrolysis reaction of a phosphorylated substrate (Figure 1, Figure 26a and Figure 26b)¹¹. Importantly, reduced form of the catalytic cysteine C124 is confirmed by $2F_o - F_c$ electron density map (Figure 26c). In addition, a molecule of tartrate is bound to the active site in the crystal structure, which originates from the crystallization solution (Figure 26b). The following C2 domain involving antiparallel β -sandwich structure has been reported to be crucial for membrane binding⁴³. This domain contains CBR3 loop and Ca2 region, which are enriched with lysine residues. Notably, side chains of two lysines in CBR3 loop are not resolved implicating their flexible nature. The tandem phosphatase and C2 domains are stabilized by an extensive interface ($\sim 1400 \text{ \AA}^2$)⁴³. Seven aromatic and hydrophobic residues are involved in hydrophobic interactions. Nine residues contribute to hydrogen bond networks via side chains and backbone groups (Figure 26a).

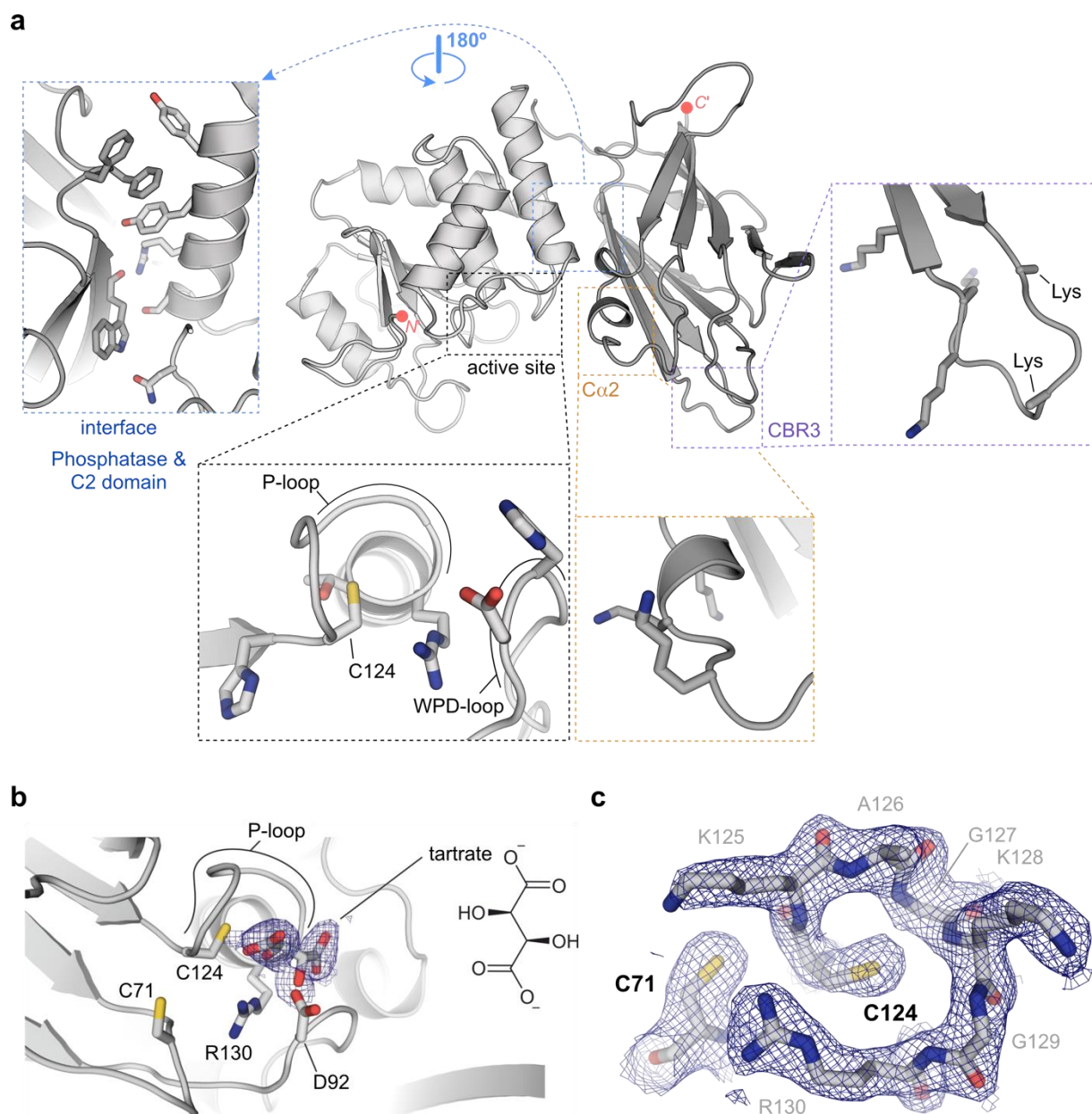


Figure 26 | Crystal structure of reduced *t*PTEN. (a) Crystal structure of *t*PTEN comprises phosphatase and C2 domains. Phosphatase domain harbors the active site decorated with WPD-loop as well as the catalytic cysteine in P-loop. C2-domain contains C α 2 and CBR3 loops, which are enriched with lysines and crucial for membrane binding. The interface of both domains is stabilized by extensive hydrophobic interactions and hydrogen bond networks. (b) Tartrate bound to the active site is represented with $2F_o - F_c$ electron density omit map (mesh, contoured at 1σ). Side chains of C71, D92, C124, and R130 are shown with stick representations. (c) Active site P-loop with $2F_o - F_c$ electron density map. (mesh: contoured at 1σ) The figures 26b and 26c are from the reference No. 171, © 2015 The Authors. Published by Wiley-VCH Verlag GmbH & Co. KGaA.

3.4.4 Structural comparison of PDB 5BZZ with PDB 1D5R

Prior to studying the structural alteration upon H₂O₂ or bpV-phen treatment, reduced *t*PTEN crystal structure (PDB 5BZZ) was compared to the previous reported one (PDB 1D5R). Notably, only one *t*PTEN molecule is available in PDB 1D5R, although two protomers should be present in the asymmetric unit according to the crystallographic parameter applied in this study⁴³. Structural discrepancies were calculated in RMSD by comparing each protomer in the novel structure (Chain A – D) to this available *t*PTEN molecule PDB 1D5R (Figure 27a). The maximal RMSD value is represented with 1.29 Å (314 C_α atoms), indicating overall comparable crystal structures to each other. Importantly, the active site P-loops of both structures are closely superimposed (Figure 27b).

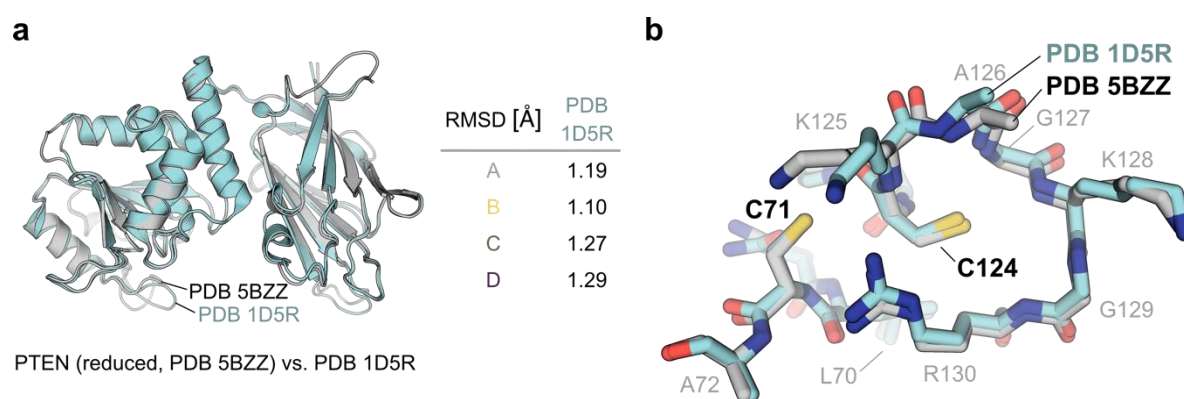
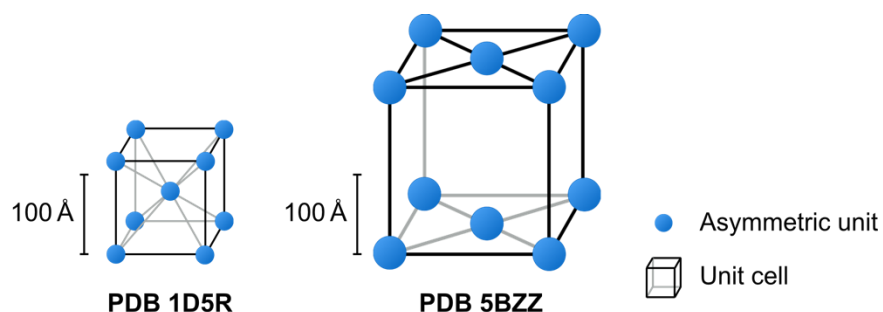


Figure 27 | PTEN (reduced) exhibits high similarity to the preceding structure. (a) Structural overlay of reduced *t*PTEN (gray, PDB 5BZZ, chain A) and PDB 1D5R (cyan, chain A). RMSD (307 C_α atoms) under 2 Å reflects high overall similarity. (b) The active site P-loop of the reduced *t*PTEN (gray, chain A) is closely superimposed on PDB 1D5R (cyan, chain A). This figure is from the reference No. 171, © 2015 The Authors. Published by Wiley-VCH Verlag GmbH & Co. KGaA.

Despite the analogy of the crystallization conditions and the structures, the crystal structure (PDB 5BZZ) was solved with different crystallographic parameters, implicating distinct molecule packing in the protein crystal (Figure 28 and Figure 29). PDB 5BZZ and PDB 1D5R harbor four and two protomers in the asymmetric unit, respectively. Each asymmetric unit is arranged in a unit cell with a base-centered orthorhombic and body-centered tetragonal character involving two-fold and four-fold rotations, as reflected in distinguished space groups (PDB 5BZZ: C222₁; PDB 1D5R: I4) (Figure 28). In addition, the unit cell of PDB 5BZZ is determined to be five times larger than PDB 1D5R (unit cell constants | reduced *t*PTEN: 206 X 206 X 89 Å; PDB 1D5R: 113 X 113 X 59 Å). Compared to PDB 1D5R (Figure

29a), PDB 5BZZ is packed with big solvent channels (Figure 29b). Taking advantage of this feature, soaking experiment with small molecules might be beneficial for the further structural investigations.



| | | | |
|--|--------|--|--|
| Lattice type | | tl Body-centered | oC Base-centered |
| Crystal system | | Tetragonal | Orthorhombic |
| Space group | | I4 | C222 ₁ |
| Unit cell | Length | 113 Å X 113 Å X 59 Å $a = b \neq c$ | 206 Å X 206 Å X 89 Å $a \neq b \neq c$ |
| | Angles | 90° X 90° X 90° $\alpha = \beta = \gamma$ | 90° X 90° X 90° $\alpha = \beta = \gamma$ |
| Protomers in an asymmetric unit | | 2 | 4 |
| Solvent content | | 49.6 % | 59.7 % |

Figure 28 | Geometric comparison of lattice types of PTEN 7-353 Δ 286-309 crystal structures.

The lattice packing of PDB 5BZZ is different from the preceding PTEN structure (PDB 1D5R) in spite of the analogous crystallization condition. The asymmetric units represented by blue spheres are positioned with a base-centered orthorhombic character in PDB 5BZZ, compared to the body-centered tetragonal lattice type of PDB 1D5R.

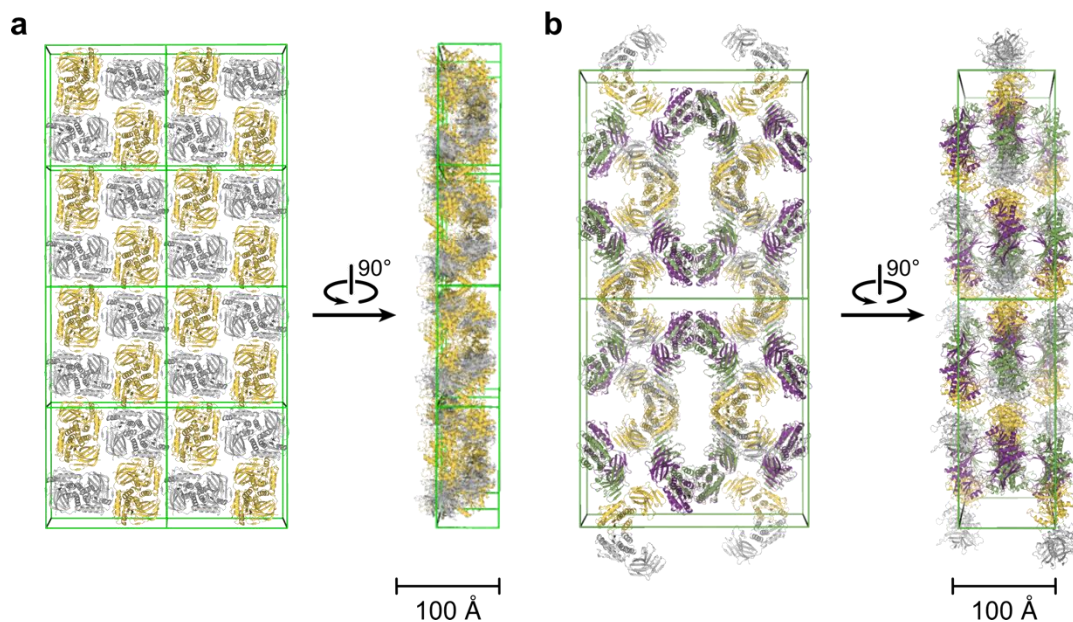


Figure 29 | Crystal packing of reduced *t*PTEN in unit cells compared with PDB 1D5R. (a) Front and side views of the lattice packing of PDB 1D5R. Two molecules (chain A – B) are assigned to an asymmetric unit with space group I4. (chain A: gray; chain B: yellow) (b) Front and side views of the lattice packing of reduced PTEN construct. Four Protomers (chain A – D) are present in an asymmetric unit with space group C222₁. (chain A: gray; chain B: yellow; chain C: green; D: purple) A green outlined lattice displays a unit cell. The size of the unit cells is adjusted to the scale shown with bars. This figure is from the reference No. 171, © 2015 The Authors. Published by Wiley-VCH Verlag GmbH & Co. KGaA.

3.4.5 Protein crystallization of *t*PTEN complexed with PIP₂/PIP₃-derivatives

Having established protein crystallization of *t*PTEN (Chapter 3.4.1), ligand-soaking experiments were employed to study the interaction between PTEN and PIP₂ and PIP₃-derivatives. Since the physiologically relevant natural products harbor long flexible fatty acid side chains (C₁₆) and may interfere with crystallization, those truncated versions with octanoic acids (C₈) were used. The soaking experiments were performed by transferring the protein crystals to a reservoir solution involving high concentration of the ligand (Table 5). The incubation time was adjusted to the crystal stability during soaking experiments. To ensure sufficient diffusion through the protein crystals, ligand concentration and incubation time were chosen as high and long as possible. 20 mM PIP₂ and nhPIP₃ were incubated with *t*PTEN crystals for 3.5 h and 7 h, respectively. PTEN substrate PIP₃ was also utilized with and without the preceding oxidation of the active site using H₂O₂ (1 mM, 1 h). In case of PIP₃, relatively low concentration (1 mM) and a short incubation time (< 60 min) were chosen due to the potential enzymatic digestion. The corresponding crystal structures were solved applying the same crystallographic parameters previously used for reduced *t*PTEN (Table 4). However, none of the ligand-soaking attempts yielded additional electron density indicating the presence of a ligand.

Table 5 | Ligand-soaking strategies for PIP₂/PIP₃-derivatives into *t*PTEN protein crystals.

| Ligands | Strategy | Ligand concentration | Comments |
|---|----------|--|--|
| PI-(4,5)-P ₂ -diC8 (alias PIP ₂) | Soaking | 20 mM, 3.5 h No back-soaking | Crystals dissolve after 3.5 h. |
| PI-(3,4,5)-P ₃ -diC8 (alias PIP ₃) | Soaking | 1 mM, 40 min | |
| H ₂ O ₂ , followed by PI-(3,4,5)-P ₃ -diC8 (alias PIP ₃) | Soaking | 1 mM, 60 min, then 1 mM, 60 min back-soaking | Crystals dissolve after the given time. |
| 3S-PI-(3,4,5)-P ₃ -diC8 (alias nhPIP ₃) | Soaking | 20 mM, 7 h No back-soaking | |

3.5 Crystal structure of H₂O₂-treated PTEN

Ligand-soaking experiments were furthermore employed to elucidate structural alteration upon H₂O₂ treatment. Protein crystals of *t*PTEN were incubated with 1 mM H₂O₂ for 1 h and flash-frozen. Data collection and processing were performed in analogy to the initial structure determination of *t*PTEN (PDB 5BZZ). However, 1280 out of 1440 frames were used for data processing, as signal-noise ratio (I/σ) has decreased with the last 160 frames. Dataset of H₂O₂-treated *t*PTEN crystal was reduced to the lowest resolution of 2.4 Å, which yielded data completeness of 100 % (Table 6 and Table 7). The final structure model exhibits R_{work} and R_{free} of 0.18 and 0.21, respectively (PDB 5BUG, Table 7). The overall structure shows high similarity to the reduced state of *t*PTEN (maximal RMSD = 1.57 Å for 314 C α atoms, Figure 30a). However, minor structural alterations are observed within the active site. Compared to the clearly separated electron density between the catalytic cysteine C124 and the proximal C71 in the protein crystal without oxidative treatment (Figure 30b), the evidently connected electron density confirms disulfide formation in the H₂O₂-treated crystal (Figure 30c and Figure 31a). Disulfide bonds are observed consistently in all four protomers of the asymmetric unit (Figure 31b). This is in agreement with the high-resolution MS result (Chapter 3.3.3). H₂O₂-triggered disulfide formation is promoted by rotation of the side chain in catalytic cysteine C124 towards the back-door cysteine C71. Notably, there is no significant change of C α -distance between C71 and C124 (reduced: 5.2 Å vs. reduced: 5.0 Å). This distance is in the expected range of a disulfide bond (4.4 Å – 6.8 Å)¹¹⁵. Most importantly, the entire active site including P-loop experiences only small conformational changes (RMSD = 0.37 Å for 10 C α atoms, Figure 31c). In addition, analogous to the reduced state, H₂O₂-treated crystal structure of *t*PTEN harbors a molecule of tartrate bound to the active site (Figure 31d). The bound tartrate moves slightly deeper into the active site, due to the space rendered by disulfide formation. Concerning the bound tartrate in the reduced and oxidized *t*PTEN structures, it was furthermore investigated, if tartrate has an influence on the oxidative inhibition and reactivation of PTEN. Full-length PTEN was pre-incubated with H₂O₂ (5 mM), followed by dilution with buffer either containing or lacking DTT (4 mM). In order to reflect the crystal soaking condition, high tartrate concentration ($c = 1.5$ M) was maintained during oxidation and reduction steps. Phosphatase activity of PTEN was monitored using malachite green assay¹⁴⁵, providing comparable enzymatic activities to the

control samples lacking tartrate (Figure 55)^{XXIV}. This indicates that tartrate does not have an effect on PTEN oxidation and reactivation, which may be due to the low affinity of tartrate for PTEN (IC_{50} (tartrate) = 337 ± 9.5 mM; Figure 56).

Table 6 | Dataset statistics of H₂O₂-phen-treated tPTEN crystal. I/σ states signal to noise ratio of unique reflections. R_{meas} is a redundancy-independent R-factor¹⁵⁹. $CC_{1/2}$ is indicative of the correlation percentage between reflection intensities from random half-datasets¹⁵⁸. Correlation significant at the 0.1 % level is highlighted by an asterisk.

| Resolution [Å] | Number of reflections | | | Completeness [%] | $I/\sigma(I)$ | R_{meas} [%] | $CC_{1/2}$ [%] |
|-------------------|-----------------------|--------|----------|---------------------|---------------|-------------------|-------------------|
| | Observed | Unique | Possible | | | | |
| 20.0 | 1258 | 153 | 167 | 91.6 | 58.28 | 3.8 | 100.0* |
| 15.0 | 2110 | 192 | 192 | 100.0 | 59.7 | 3.5 | 99.9* |
| 10.0 | 9154 | 777 | 777 | 100.0 | 75.95 | 3.0 | 100.0* |
| 8.0 | 10471 | 1017 | 1018 | 99.9 | 64.77 | 2.9 | 100.0* |
| 6.0 | 33239 | 2824 | 2824 | 100.0 | 50.76 | 4.1 | 99.9* |
| 4.0 | 133147 | 11293 | 11294 | 100.0 | 49.98 | 4.3 | 100.0* |
| 3.1 | 220671 | 18232 | 18233 | 100.0 | 24.19 | 9.7 | 99.9* |
| 3.0 | 41674 | 3477 | 3477 | 100.0 | 9.16 | 28.6 | 98.8* |
| 2.9 | 49418 | 4043 | 4043 | 100.0 | 7.86 | 33.0 | 98.8* |
| 2.8 | 56363 | 4570 | 4570 | 100.0 | 5.86 | 45.0 | 97.7* |
| 2.7 | 66226 | 5327 | 5327 | 100.0 | 4.18 | 64.3 | 96.2* |
| 2.6 | 76859 | 6126 | 6128 | 100.0 | 3.18 | 85.8 | 91.8* |
| 2.5 | 85407 | 7119 | 7120 | 100.0 | 2.18 | 122.5 | 86.3* |
| 2.4 | 95199 | 8347 | 8348 | 100.0 | 1.59 | 166.0 | 77.6* |
| Total | 881196 | 73497 | 73518 | 100.0 | 19.82 | 10.4 | 99.9* |

^{XXIV} Inhibition with H₂O₂: residual activities = 6.7 ± 2.1 % (lacking tartrate) vs. 7.1 ± 1.6 % (containing tartrate)

Reactivation with DTT: residual activities = 96.5 ± 3.8 % (lacking tartrate) vs. 92.8 ± 2.5 % (containing tartrate)

Table 7 | Crystallographic data collection and refinement statistics of H₂O₂-treated tPTEN crystal. Structure coordinates have been deposited in the RCSB Protein Data Bank⁴² with the accession code 5BUG. Values in the parenthesis involve the highest resolution shell. R_{Free} was calculated from 5 % of the reflections omitted from refinement process.

| | tPTEN + H₂O₂ |
|---------------------------------------|---|
| PDB code | 5BUG |
| Data Collection | |
| Space group | C222 ₁ |
| Unit-cell parameters | |
| a, b, c (Å) | 206.87, 206.83, 87.43 |
| α, β, γ (°) | 90, 90, 90 |
| Wavelength (Å) | 1.000010 |
| Resolution limits (Å) | 48.76 - 2.40 (2.50 - 2.40) |
| No. of unique reflections | 73497 (8347) |
| Completeness (%) | 100 (100) |
| Multiplicity | 11.99 (11.41) |
| I/σ(I) | 19.82 (1.59) |
| CC _{1/2} | 99.9 (77.6) |
| R _{obs} | 10.0 (158.5) |
| Refinement | |
| Resolution limits (Å) | 48.76 - 2.4 (2.5 - 2.4) |
| R _{Work} / R _{Free} | 0.1751 / 0.2106 |
| R.m.s.d. | |
| Bond length (Å) | 0.0100 |
| Bond angles (°) | 1.6794 |
| B-factors (Å ²) | 70.2 |
| No. atoms | |
| Protein | 10338 |
| Ligand | 40 |
| Water | 751 |
| Ramachandran plot (%) | |
| Favored regions | 93.5 |
| Allowed regions | 5.7 |
| Disallowed regions | 0.8 |

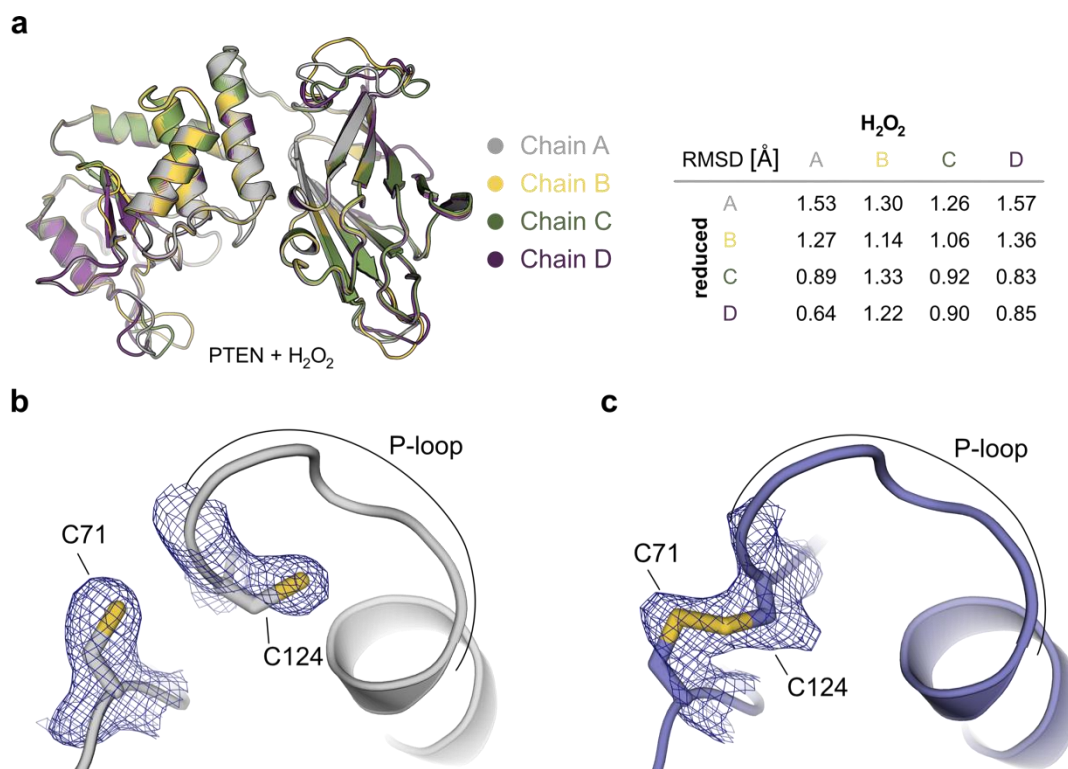


Figure 30 | Disulfide formation upon H₂O₂-treatment has a minor structural impact on PTEN.

(a) Overlay representation demonstrates that four protomers per asymmetric unit are structurally comparable. (Chain A: gray; chain B: yellow; chain C: green; D: purple). Implicated by low RMSD values, H₂O₂-treatment does not induce significant conformational change in the overall structure of PTEN. (b, c) Active site P-loop and the adjacent cysteine of reduced (b: gray, chain A) and H₂O₂-treated PTEN (c: blue, chain A). Side chains of C71 and C124 are shown explicitly with $2 F_o - F_c$ electron density omit map (mesh, contoured at 1σ). This figure is from the reference No. 171, © 2015 The Authors. Published by Wiley-VCH Verlag GmbH & Co. KGaA.

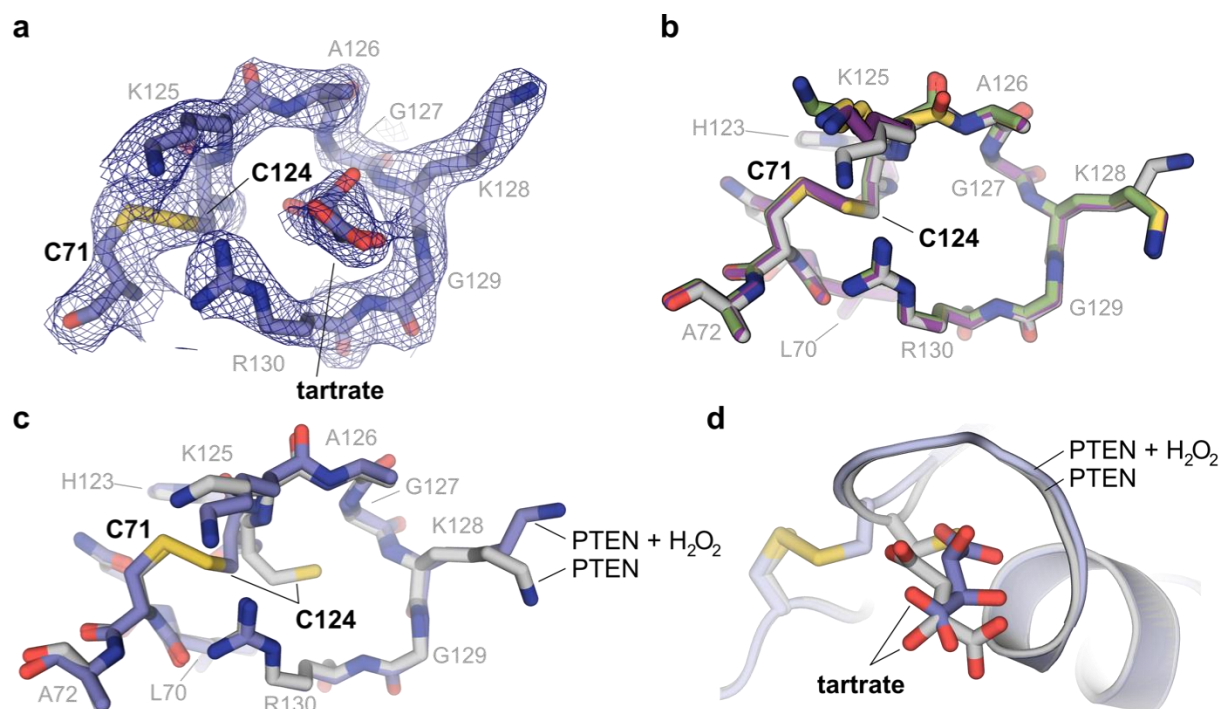


Figure 31 | Structural alteration of the active site P-loop upon exposure to H₂O₂. (a) The active site of H₂O₂-treated PTEN (blue, chain A) with 2 $F_o - F_c$ electron density map (mesh: contoured at 1 σ). (b) Close alignment of four protomers per asymmetric unit demonstrates high similarity at the active sites of H₂O₂-treated PTEN (Chain A: gray; chain B: orange; chain C: green; D: purple). (c) Structural overlay of the active sites in reduced (gray, chain A) and H₂O₂-treated PTEN (blue, chain A). Disulfide formation has a minor structural impact on the active site of PTEN. (d) Superimposition of the active sites in reduced (gray, chain A) and H₂O₂-treated PTEN (blue, chain A). The position of the bound tartrate changes upon disulfide formation. Tartrates and side chains of C71 and C124 are shown with stick representations. This figure is from the reference No. 171, © 2015 The Authors. Published by Wiley-VCH Verlag GmbH & Co. KGaA.

Conformational changes at the active site of PTEN were compared with other available PTP structures exhibiting reversible oxidative modification. Minor structural change of PTEN P-loop is analogous to human lymphoid tyrosine phosphatase, which also involves disulfide formation^{118,160} (LYP, RMSD = 0.39 Å, Figure 32a and 32b). Interestingly, LYP reveals a substantial change of WPD-loop at its active site upon disulfide formation, whereas the entire active site in PTEN remains unaffected during this process. In contrast, CDC25B (disulfide, RMSD = 2.48 Å, Figure 32c)¹²⁶ and PTP1B (sulfenyl-amide, RMSD = 2.38 Å, Figure 32d)¹²² show a significant structural alteration in the active site P-loop upon reversible oxidative

modification. Notably, irreversible modification (*e.g.* sulfinic or sulfonic acid) was also observed at the catalytic cysteine of these PTPs upon long incubation time with H_2O_2 ($t > 20$ min)^{122,126}. Concerning the potential hyperoxidation with intensive H_2O_2 treatment, tolerance of the reversible modification was tested in PTEN under stringent oxidative conditions. Full-length PTEN was first treated with H_2O_2 in the time- and concentration-dependent manner (Figure 33), followed by dilution with buffer lacking (mock) or containing DTT (10 mM, 20 min). Remarkably, phosphatase activity of PTEN was restored upon DTT treatment up to 20 mM H_2O_2 and 80 min incubation time. Such robust reactivation implies a very efficient protective mechanism of PTEN from irreversible catalytic impairment under oxidative stress.

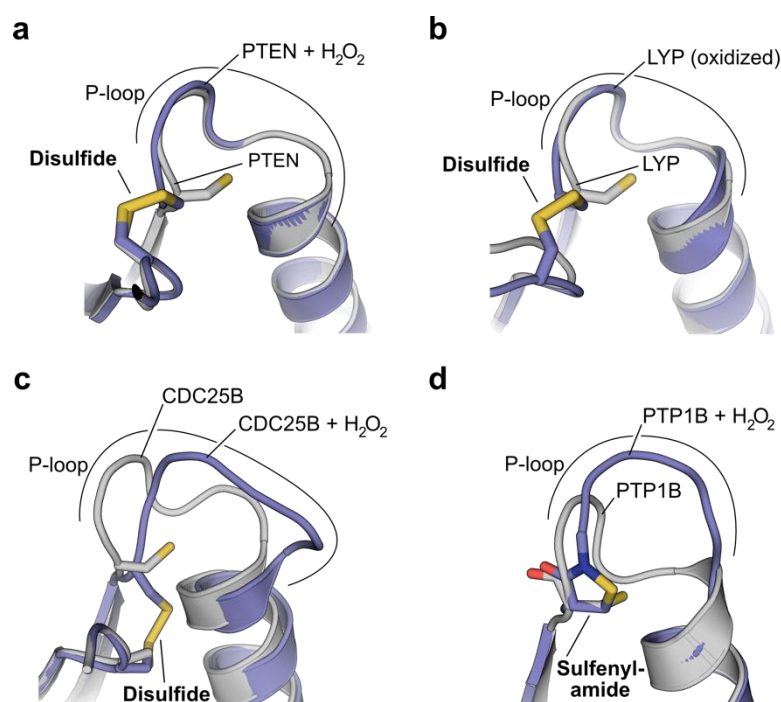


Figure 32 | Structural comparison of active site P-loops upon reversible oxidative modification.

(a) Superimposition of reduced and oxidized PTEN structures shows conservation of backbone conformation of the P-loop. (b) Analogous to PTEN, disulfide formation of lymphoid tyrosine phosphatase does not alter its P-loop conformation (PDB: 2P6X, 3H2X)^{118,160}. (c) Significant structural change of CDC25B upon disulfide formation (PDB: 1YMK, 1YS0)¹²⁶. (d) H_2O_2 treatment promotes sulfenyl-amide formation of PTP1B resulting in structural distortion in the P-loop (PDB: 2HNP, 1OEM)^{120,122}. This figure is from the reference No. 171, © 2015 The Authors. Published by Wiley-VCH Verlag GmbH & Co. KGaA.

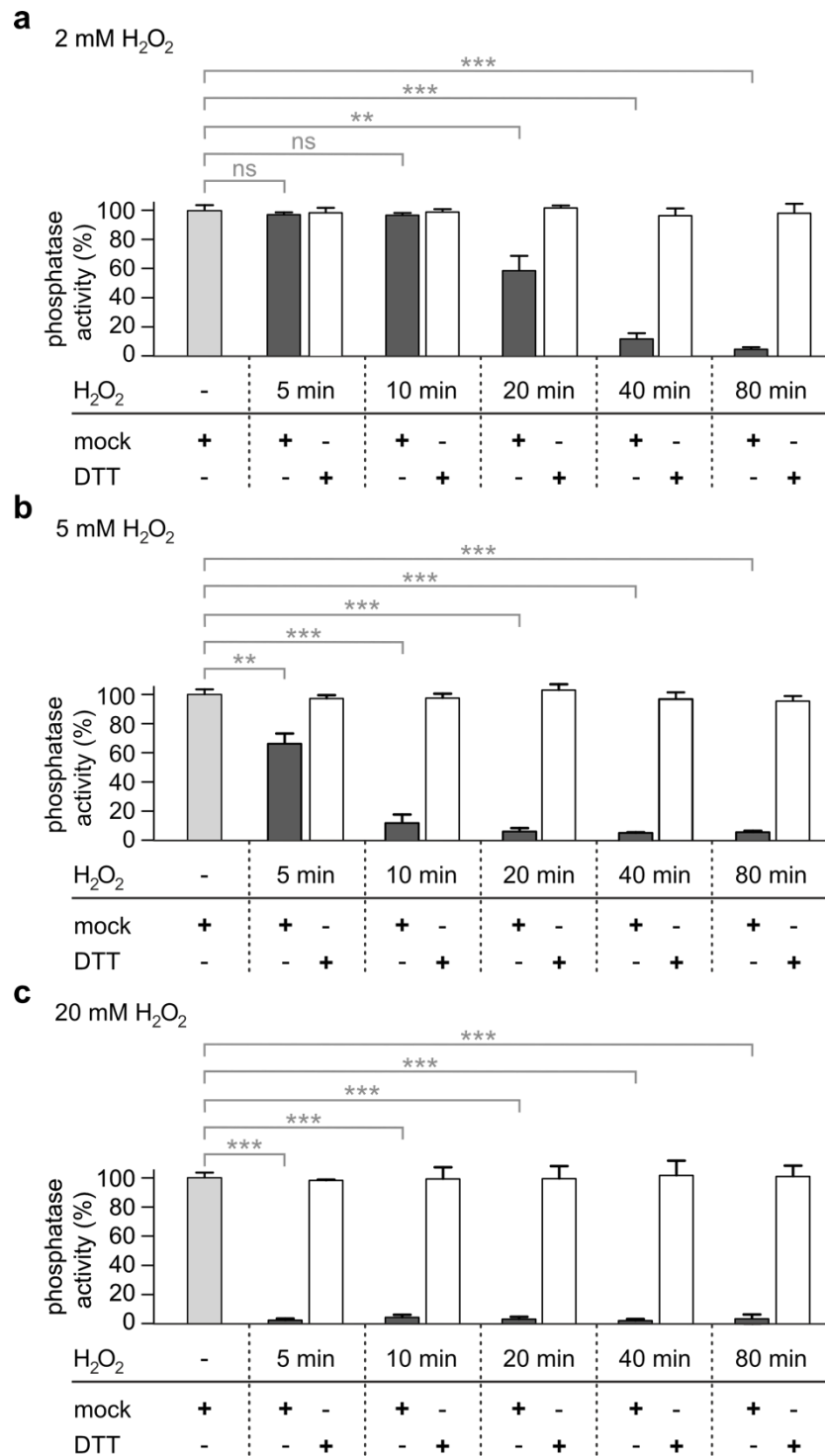


Figure 33 | Kinetic measurements of PTEN oxidation by H₂O₂ and its reactivation under reductive condition. (a – c) PTEN inhibition by H₂O₂ was studied in the concentration- and time-dependent manner. PTEN (100 μM) was treated with H₂O₂ (a: 2 mM, b: 5 mM, c: 20 mM) during the given time ranges, followed by incubation (20 min) with buffer lacking or containing DTT (10 mM). Errors represent ± SD. (triplicate of triplicates; ns: $P > 0.05$, * $P < 0.05$, ** $P < 0.01$, *** $P < 0.001$) This figure is reconstructed based on Lee *et al.* (2015)¹⁷¹.

3.6 Structural impact of PTEN inhibition by bpV-phen

3.6.1 Reaction product of bpV-phen

The preceding results implicate an oxidative mode of action of bpV-phen, which results in inhibition of PTEN phosphatase activity via disulfide bond formation (Chapters 3.3.2 and 3.3.3). However, it remains elusive, which vanadium species is formed as a reaction product. In addition, it is not clear whether the oxidized form of PTEN differs between H₂O₂ and bpV-phen treatments.

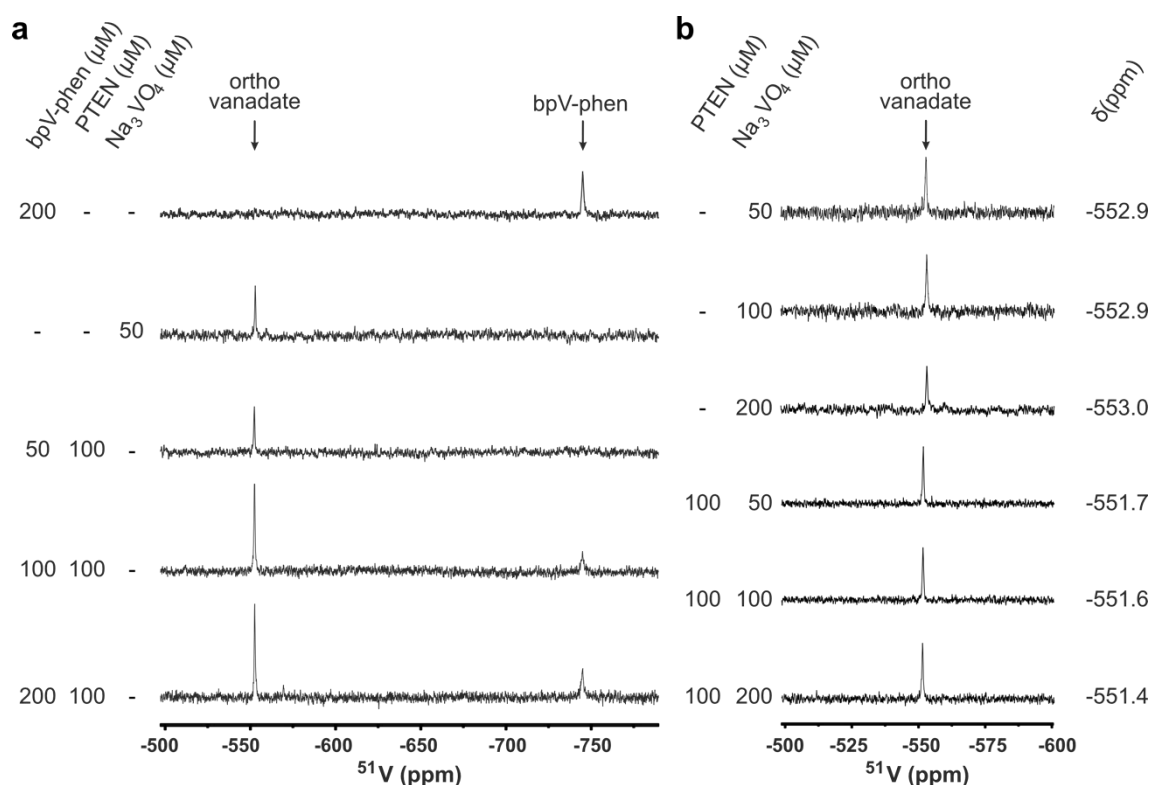


Figure 34 | Orthovanadate is a reaction product of bpV-phen treatment upon PTEN and exhibits low affinity for the pre-oxidized PTEN^{XXV}. (a) ⁵¹V-NMR titration measurements demonstrate the conversion of bpV-phen (50 – 200 μM) to orthovanadate in the presence of PTEN (100 μM). (b) The binding property was determined using ⁵¹V-NMR measurements. Na₃VO₄ (50 – 200 μM) was titrated in the presence and absence of 100 μM pre-oxidized full-length PTEN. This figure is from the reference No. 171, © 2015 The Authors. Published by Wiley-VCH Verlag GmbH & Co. KGaA.

^{XXV} ⁵¹V-NMR spectroscopic analysis was carried out by Jonas Hanske and Dr. Christoph Rademacher at Max Planck Institute of Colloids and Interfaces, Berlin, Germany.

To elucidate the reaction product of bpV-phen upon PTEN inhibition, ^{51}V -NMR spectroscopic analysis^{XXVI} was performed in cooperation with the group of Dr. Christoph Rademacher (Max Planck Institute of Colloids and Interfaces, Berlin, Germany). This method provides an excellent platform for the investigation of vanadate species with a very wide chemical shift range. For the efficient workflow, sample preparation was performed by the author of this thesis. NMR spectroscopic analysis was carried out by Dr. Christoph Rademacher and Jonas Hanske. In initial tests, bpV-phen proved to be stable under assay conditions (pH 8.0, 25 °C), yielding a signal in the expected range ($\delta = -744$ ppm, Figure 34a)¹⁶¹. Full-length PTEN (100 μM) was then titrated with increasing bpV-phen concentrations ranging from 50 to 200 μM . Notably, bpV-phen peak rapidly disappeared at low bpV-phen concentration (50 μM , complete conversion: < 15 min), providing a concurrent occurrence of a new peak ($\delta = -553$ ppm). This new signal was assigned to be dihydrogen orthovanadate (H_2VO_4^-) by direct comparison with Na_3VO_4 titration (Figure 34a)¹⁶². In addition, a residual bpV-phen signal detected at its increased concentrations (100 and 200 μM) demonstrates the quantitative oxidation of PTEN by bpV-phen under these conditions.

Given that disulfide formation is promoted by bpV-phen and orthovanadate is a phosphate mimicry, binding affinity of the reaction product orthovanadate for oxidized PTEN was studied. Full-length PTEN pre-oxidized with H_2O_2 (100 μM) was titrated with sodium orthovanadate (50 – 200 μM)^{XXVII} (Figure 34b). Upon ligand binding, a chemical shift change is expected and the corresponding signal should exhibit line-broadening¹⁶³. However, no significant chemical shift or line broadening was observed indicating low affinity of orthovanadate for pre-oxidized PTEN ($K_D > 1$ mM). Given that orthovanadate inhibits some human phosphatases at sub-micromolar concentrations (*e.g.* PTP1B ($K_i = 0.38$ μM)¹⁵³, alkaline phosphatase ($K_i = 0.6$ μM)¹⁶⁴), it was furthermore investigated, if the formed orthovanadate has an influence on PTEN activity. For that purpose, phosphatase activity of PTEN was monitored in the presence of orthovanadate using malachite green assay (Figure

^{XXVI} ^{51}V -NMR spectroscopic analysis was carried out by Jonas Hanske and Dr. Christoph Rademacher at Max Planck Institute of Colloids and Interfaces, Berlin, Germany.

^{XXVII} Full-length PTEN was oxidized with H_2O_2 and purified using size exclusion chromatography to remove residual H_2O_2 in the protein buffer. Oxidation yielded two species detected in the chromatogram. Protein fractions corresponding to monomeric species (the second peak) were used for ^{51}V -NMR experiments. For more details about chromatograms and inhibitory as well as reactivating properties, see Figure 57.

35). Compared with efficient inhibition by bpV-phen, only 20 % PTEN inhibition was observed at 1 mM orthovanadate. Given that 1 mM orthovanadate is equivalent to over 5000-fold higher concentration than IC_{50} of bpV-phen, inhibition of PTEN phosphatase activity is mainly induced by bpV-phen-mediated disulfide formation.

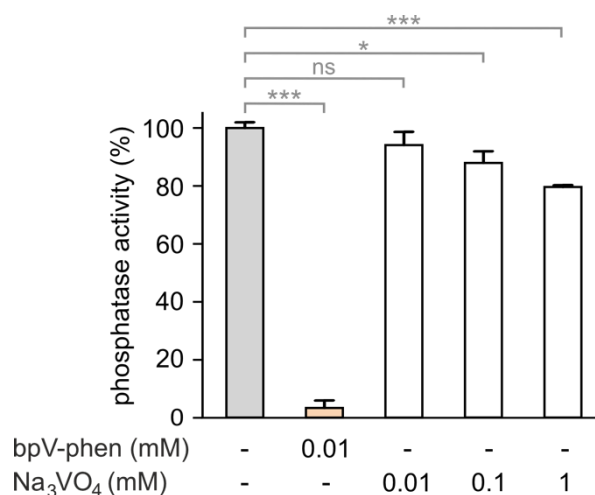
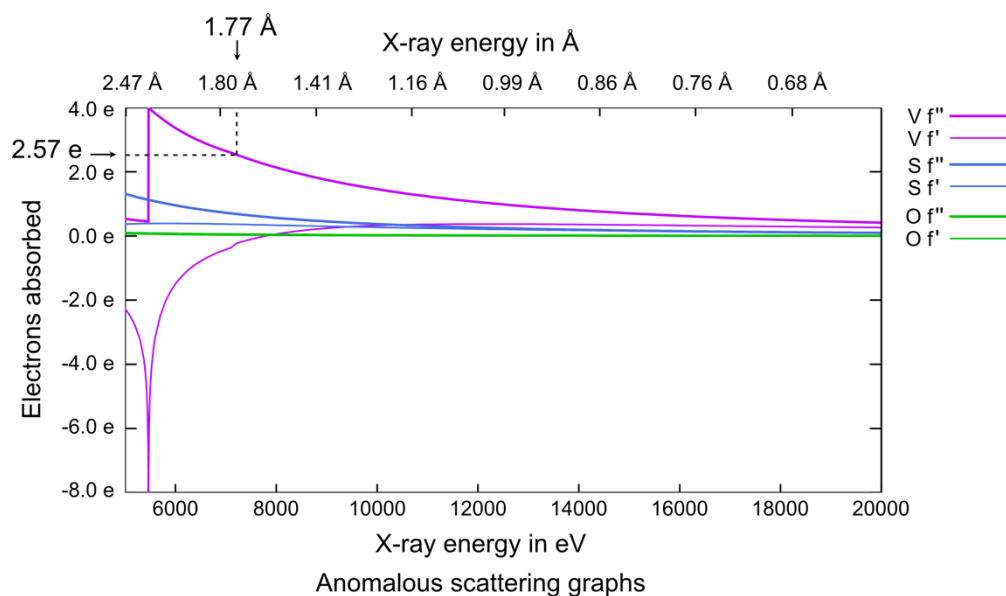


Figure 35 | Catalytic impairment of PTEN is not affected by orthovanadate. Phosphatase activity of PTEN was determined using malachite green assay. Full-length PTEN (50 nM) was incubated either with bpV-phen or Na₃VO₄ (T = 25 °C, t = 10 min; triplicates, errors represent \pm SD; ns: not significant, * P < 0.05, ** P < 0.01, *** P < 0.001). This figure is from the reference No. 171, © 2015 The Authors. Published by Wiley-VCH Verlag GmbH & Co. KGaA.

3.6.2 Crystal structure of bpV-phen-treated PTEN

Next, structural consequences of bpV-phen-mediated PTEN inhibition were studied using X-ray crystallography. Analogous to structural investigation upon H₂O₂-treated PTEN, soaking experiments were employed. A *t*PTEN crystal in the reduced state was treated with 1 mM bpV-phen for 4 h and flash-frozen prior to data collection. Compared to the aforementioned H₂O₂-treated PTEN structure ($\lambda = 1.000$ Å), dataset was collected at a longer wavelength ($\lambda = 1.771$ Å). This allows to utilize specific elemental character such as anomalous scattering and consequently provides the precise localization of potential vanadium species. As represented in Figure 36, absorbance of incident X-ray photons increases with longer wavelength up to an absorption edge. This elemental property is intensified in elements involving higher atomic numbers, which results in more intensive anomalous scattering. In addition, elemental components of amino acids except for sulfur hardly contribute to the anomalous scattering even at a longer wavelength. Taking advantage

of this property, an additional electron density map can be generated, which provides a specific density map representing potential vanadium species and thiols.



| | C | H | N | O | P | S | V |
|---------------|--------|-------|--------|--------|--------|---------------|---------------|
| 1.00 Å | ~ 0 e | ~ 0 e | 0.01 e | 0.01 e | 0.19 e | 0.24 e | 0.93 e |
| 1.77 Å | 0.01 e | ~ 0 e | 0.02 e | 0.04 e | 0.56 e | 0.71 e | 2.57 Å |

Figure 36 | Anomalous scattering property facilitates an electron density map yielded from vanadium and sulfur. X-ray absorbance of vanadium (purple) and sulfur (blue) increases with longer wavelength up to absorption edge (upper panel, vanadium absorption edge = 2.27 Å). These elements largely contribute to anomalous scattering, compared to other elemental components (*e.g.* C, H, N, O) present in the protein and buffer. This is represented with f'' scattering coefficients (lower panel). f' and f'' are real and imaginary components of scattering coefficients, respectively. The theoretical plot is generated based on *S Brennan and PL Cowan (1992)*^{165, XXVIII}.

^{XXVIII} The figure is modified based on the plot which is generated on the following homepage:

<http://skuld.bmsc.washington.edu/scatter/> (Jan. 2016)

Following data collection of the bpV-phen-treated *t*PTEN crystal, data processing was performed in analogy to the reduced *t*PTEN (PDB 5BZZ) to determine structure factor amplitude and to generate $2F_o - F_c$ electron density map. Dataset of the bpV-phen-treated *t*PTEN crystal was reduced to the lowest resolution of 2.5 Å, which yielded data completeness of 100 % (1440 frames, Table 8 and Table 9). The final structure model was built with R_{work} and R_{free} of 0.18 and 0.20, respectively (PDB 5BZX, Table 9). Close alignment of four protomers in the asymmetric unit confirms high structural similarity among symmetry-relevant structures (Figure 37). The overall structures are determined to be very similar to the reduced and H₂O₂-treated PTEN (maximal RMSD = 1.42 Å and 1.37 Å for 314 C α atoms). Consistent with the previous high resolution MS results upon bpV-phen treatment, disulfide formation at the active site is observed in all protomers involving connected electron densities between C71 and C124 ($2F_o - F_c$ omit map, Figure 38).

Table 8 | Dataset statistics of bpV-phen-treated *t*PTEN crystal. I/σ states signal to noise ratio of unique reflections. R_{meas} is a redundancy-independent R-factor¹⁵⁹. $CC_{1/2}$ is indicative of the correlation percentage between reflection intensities from random half-datasets¹⁵⁸. Correlation significant at the 0.1 % level is highlighted by an asterisk.

| Resolution [Å] | Number of reflections | | | Completeness [%] | $I/\sigma(I)$ | R_{meas} [%] | $CC_{1/2}$ [%] |
|-------------------|-----------------------|--------|----------|---------------------|---------------|--------------------------|-------------------|
| | Observed | Unique | Possible | | | | |
| 20.0 | 1552 | 152 | 167 | 91.0 | 52.51 | 3.7 | 100.0* |
| 15.0 | 2476 | 192 | 192 | 100.0 | 59.43 | 4.1 | 100.0* |
| 10.0 | 10715 | 778 | 778 | 100.0 | 65.55 | 3.6 | 100.0* |
| 8.0 | 13692 | 1024 | 1024 | 100.0 | 57.69 | 3.6 | 100.0* |
| 6.0 | 35011 | 2832 | 2833 | 100.0 | 39.73 | 5.4 | 99.9* |
| 4.0 | 149571 | 11341 | 11341 | 100.0 | 39.86 | 5.7 | 99.9* |
| 3.1 | 248426 | 18311 | 18312 | 100.0 | 18.51 | 13.5 | 99.8* |
| 3.0 | 42575 | 3496 | 3497 | 100.0 | 6.56 | 39.6 | 98.0* |
| 2.9 | 49248 | 4049 | 4049 | 100.0 | 5.71 | 44.2 | 97.8* |
| 2.8 | 58498 | 4590 | 4591 | 100.0 | 4.34 | 60.0 | 96.0* |
| 2.7 | 67403 | 5341 | 5341 | 100.0 | 3.04 | 85.4 | 92.1* |
| 2.6 | 77080 | 6142 | 6144 | 100.0 | 2.25 | 114.7 | 85.1* |
| 2.5 | 87652 | 7145 | 7147 | 100.0 | 1.53 | 161.9 | 73.1* |
| Total | 843899 | 65393 | 65416 | 100.0 | 17.43 | 12.3 | 99.9* |

Table 9 | Crystallographic data collection and refinement statistics of bpV-phen-treated tPTEN crystal. Structure coordinates have been deposited in the RCSB Protein Data Bank⁴² with the accession code 5BZX. Values in the parenthesis involve the highest resolution shell. R_{Free} was calculated from 5 % of the reflections omitted from refinement process.

| | tPTEN + bpV-phen |
|-------------------------------------|----------------------------|
| PDB code | 5BZX |
| Data Collection | |
| Space group | C222 ₁ |
| Unit-cell parameters | |
| a, b, c (Å) | 207.06, 206.90, 87.67 |
| α, β, γ (°) | 90, 90, 90 |
| Wavelength (Å) | 1.771190 |
| Resolution limits (Å) | 46.29 - 2.50 (2.60 - 2.50) |
| No. of unique reflections | 65393 (7145) |
| Completeness (%) | 100 (100) |
| Multiplicity | 12.91 (12.27) |
| $I/\sigma(I)$ | 17.43 (1.53) |
| $CC_{1/2}$ | 99.9 (73.1) |
| R_{obs} | 11.8 (155.2) |
| Refinement | |
| Resolution limits (Å) | 46.29 - 2.50 (2.60 - 2.50) |
| $R_{\text{Work}} / R_{\text{Free}}$ | 0.1752 / 0.2037 |
| R.m.s.d. | |
| Bond length (Å) | 0.0094 |
| Bond angles (°) | 1.5376 |
| B-factors (Å ²) | 72.0 |
| No. atoms | |
| Protein | 10310 |
| Ligand | 40 |
| Water | 880 |
| Ramachandran plot (%) | |
| Favored regions | 92.8 |
| Allowed regions | 6.7 |
| Disallowed regions | 0.6 |

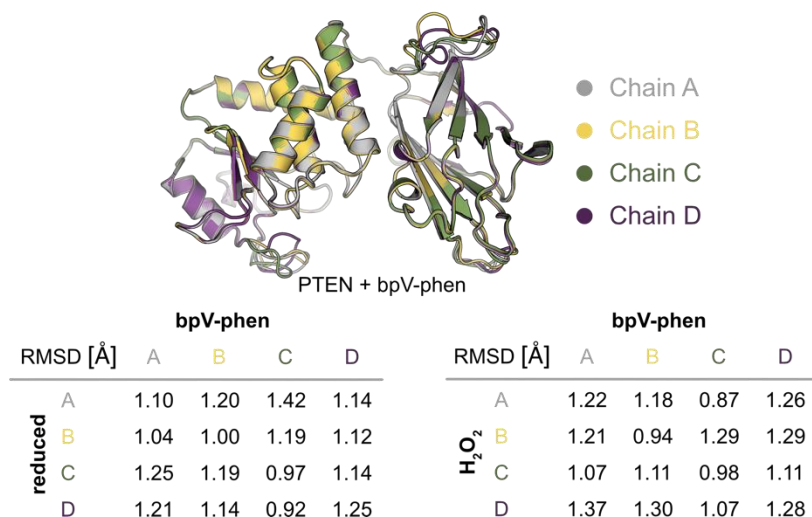


Figure 37 | There is no overall significant structural change of *t*PTEN upon bpV-phen treatment.

Structural overlay represents close alignment of four protomers of bpV-phen-treated *t*PTEN structures in an asymmetric unit (PDB 5BZX, upper panel; chain A: gray; chain B: orange; chain C: green; D: purple). As reflected by RMSD values, the crystal structure incubated with bpV-phen shows high similarity to reduced and H₂O₂-treated crystal structures (lower panel). This figure is from the reference No. 171, © 2015 The Authors. Published by Wiley-VCH Verlag GmbH & Co. KGaA.

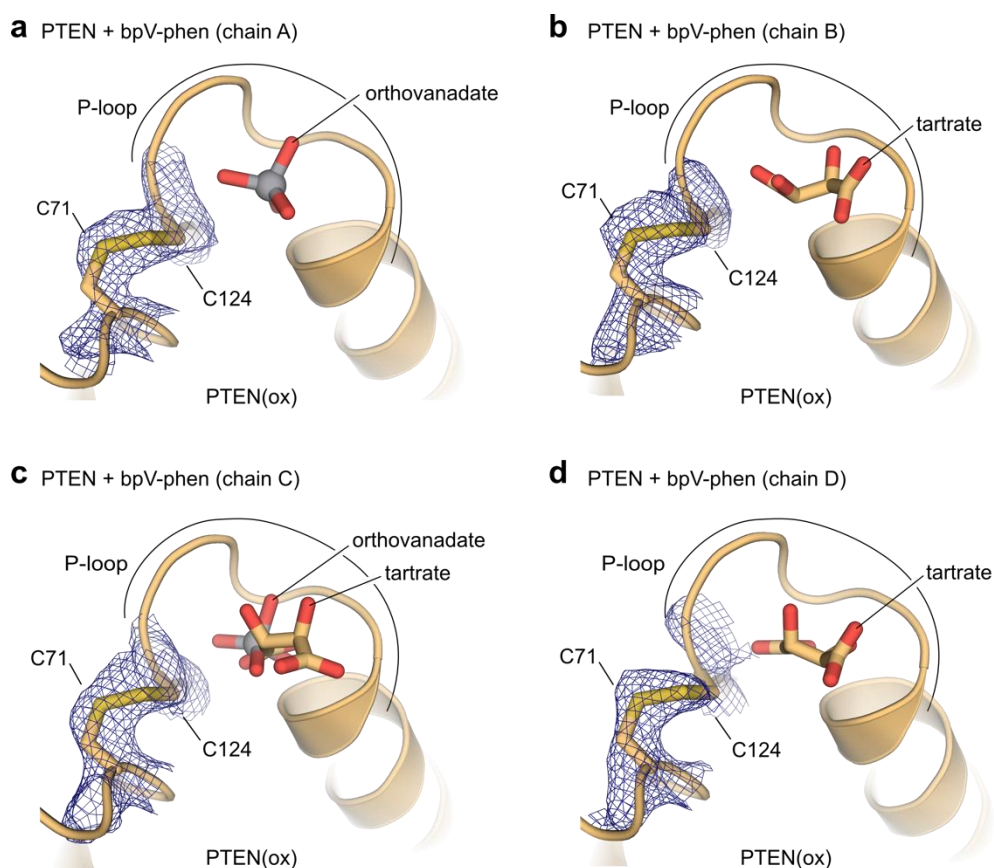


Figure 38 | bpV-Phen exerts oxidative modification on tPTEN via disulfide formation. (a – d) The crosslinked $2F_o - F_c$ omit map (mesh: contoured at 1σ) validates the disulfide formations between C71 and C124 in all protomers of the bpV-phen-treated crystal structure. Orthovanadate, tartrate, and side chains of C71 and C124 are shown with stick representations. This figure is from the reference No. 171, © 2015 The Authors. Published by Wiley-VCH Verlag GmbH & Co. KGaA.

Next, an additional electron density map was generated based on the anomalous scattering signal applying the Bijvoet-difference Fourier method¹⁶⁶. Oxidation of thiol group to disulfide by bpV-phen is, again, confirmed in all protomers with the anomalous density map (Figure 39a and b). The evidently connected density of C71 and C124 in bpV-phen-treated PTEN is distinct from the reduced PTEN, indicating disulfide bond formation (Figure 39). Interestingly, different density map patterns are observed in the middle of the active site, which implicates varied occupancy of vanadium species. Taking ratio of density size (disulfide vs. vanadium species) and their anomalous scattering contribution into account (Figure 36), ligand populations were determined. Chain A harbors primarily orthovanadate, whereas both chain B and D contain one molecule of tartrate analogous to H_2O_2 -treated PTEN. Chain C exhibits a partial occupancy of tartrate and orthovanadate (~70:30) (Figure

38). Different ligands bound to the active site are also validated by their differing density pattern in $2F_o - F_c$ electron density map (Figure 40a, b and c). This X-ray crystallographic observation involving mixed ligand occupancy is consistent with low affinity of orthovanadate for the active site of pre-oxidized PTEN, as demonstrated by ^{51}V -NMR spectroscopic analysis (Figure 34b). Notably, in spite of the distinctions in four protomers, close overlay of the P-loops and overall structures implicates low structural impact of the bound ligands on the active site conformation (Figure 40d).

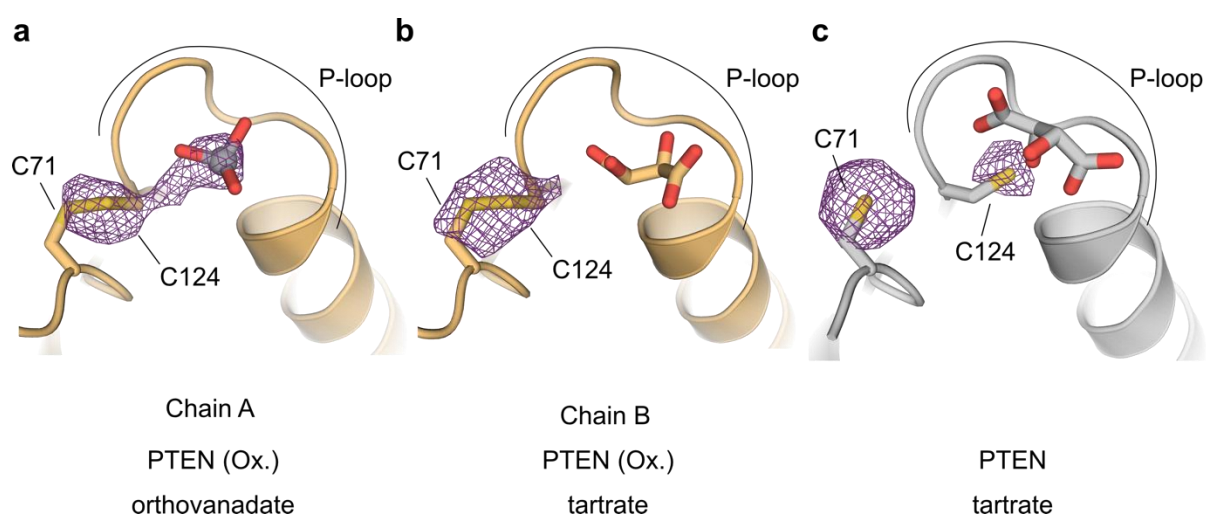


Figure 39 | bpV-phen-treated PTEN crystal structure exhibits disulfide bond and harbors partial occupancy of orthovanadate at the active site. Active sites of bpV-phen-treated (orange; **a**: chain A, **b**: chain B) and reduced PTEN (gray; **c**: chain A). Orthovanadate, tartrate and side chains of C71 and C124 are shown with stick representations. Anomalous scattering property of vanadium and sulfur facilitates generation of an electron density map (resolution: 5.0 Å, mesh: contoured at 3.4 σ), which shows specific locations of both elements. The intensity of the electron density allows to determine varied orthovanadate occupancies at the active sites of bpV-phen-treated PTEN. This figure is from the reference No. 171, © 2015 The Authors. Published by Wiley-VCH Verlag GmbH & Co. KGaA.

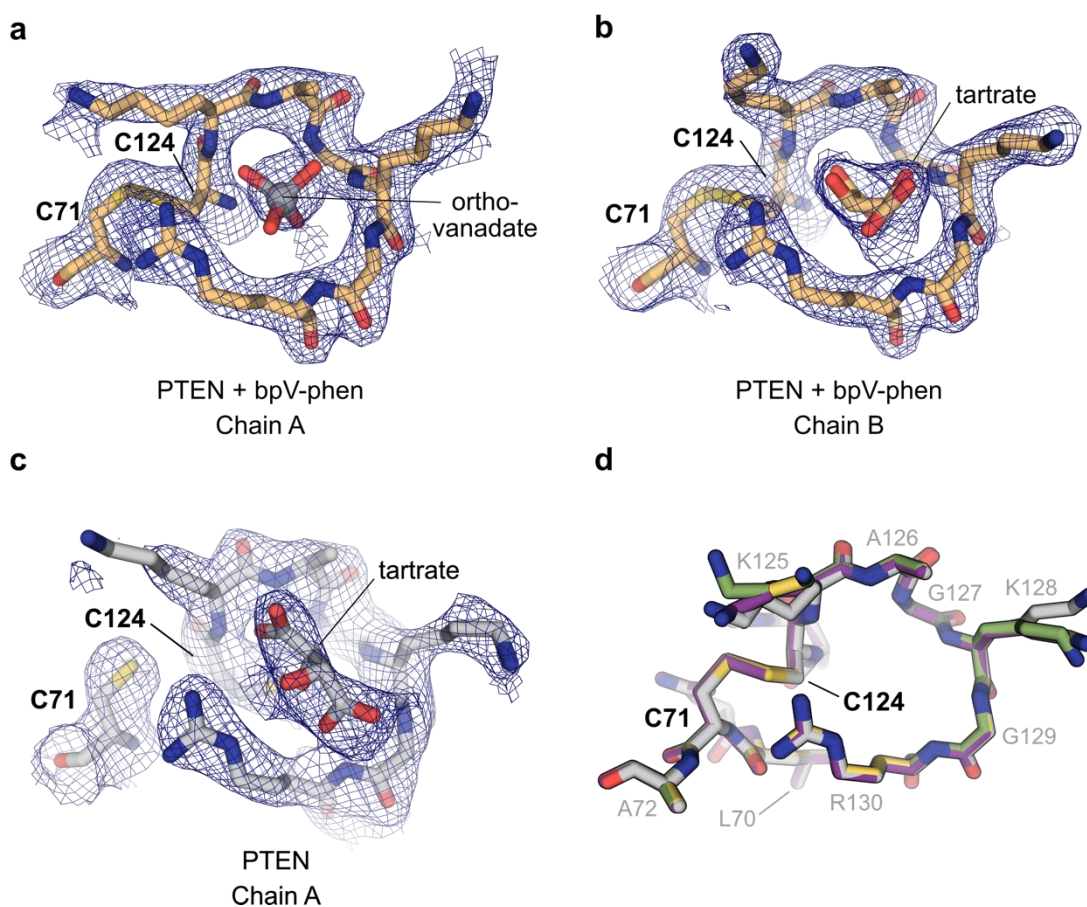


Figure 40 | $2 F_o - F_c$ electron density confirms disulfide formation and different ligand occupancy at the active site of bpV-phen-treated PTEN. (a, b) $2 F_o - F_c$ electron density map of bpV-phen-treated PTEN (orange) is clearly resolved at the active site exhibiting varied ligand occupancy and connected density for disulfide bond. Active sites of chain A and B are shown representatively. (c) Compared to the disulfide structure, electron density is separated between C71 and C124 at the active site of reduced PTEN (gray). $2 F_o - F_c$ electron density map is represented in mesh and contoured at 1σ . (d) Superimposition of bpV-phen-treated PTEN active sites shows high structural similarity among four protomers present in the asymmetric unit (Chain A: gray; chain B: yellow; chain C: green; D: purple). This figure is from the reference No. 171, © 2015 The Authors. Published by Wiley-VCH Verlag GmbH & Co. KGaA.

3.7 Discussion

Herein, modulation of PTEN phosphatase activity was investigated using biochemical and structural biology methods. This study was divided into two sections involving investigation of activation by phosphatidylinositol derivatives and inhibition by the second messenger H₂O₂ as well as a synthetic inhibitor bpV-phen.

Upon activation, PTEN is localized to the plasma membrane and catalyzes dephosphorylation of PIP₃ to PIP₂^{25,32,33}. Thereby, the *N*-terminal domain (residues 1-15, Figure 3) containing a PIP₂-binding motif (PBM, residues 6-KEIVSRNKRR-15) not only plays a crucial role for membrane association, but also is essential for PTEN phosphatase activity^{48,73}. In addition, the dephosphorylation product PIP₂ promotes membrane binding of PTEN and increases the phosphatase activity via autocatalytic mechanism^{48,73}. In this context, earlier studies have proposed that the flexible *N*-terminal sequence of PTEN serves as an allosteric binding site of PIP₂ for the preceding membrane activation^{174,175}. However, it remains elusive, how PTEN is activated by PIP₂ and which protein site is responsible for protein-ligand interaction. In order to elucidate the underlying mechanism mediated by PIP₂, various PTEN constructs were recombinantly produced in the presence and absence of *N*- and *C*-terminal regulatory sequences (Figure 11). Consistent with previous studies^{48,55,71}, subsequent phosphatase activity measurements of the constructs showed that the *N*-terminus (residues 1-15) is essential for PTEN activity, whereas the *C*-terminal tail (residues 352-403) has an inhibitory effect (Figure 18). It is an important finding that the absence of the *N*-terminal hydrophobic amino acids (residues 1-MTAAI-5) reduces the phosphatase activity significantly, although the entire PBM is present. This implicates potential hydrophobic interaction with the hydrocarbon chains of PIP₂/PIP₃. In addition, autocatalytic property of PIP₂ demonstrated herein is in agreement with the previous *in vitro* study⁴⁸ (Figure 18). Importantly, comparable activating effect of the substrate analog nhPIP₃ implicates the presence of an allosteric binding site and no selectivity for PIP₂/PIP₃-mediated enzymatic activation.

The FP-measurements show that PTEN constructs containing the *C*-tail have low affinity for PIP₂. Given that phosphatase activity of the corresponding constructs is increased in the presence of PIP₂, this may implicate the competition of PTEN *C*-tail with PTEN-PIP₂ interaction (Figure 19a). In addition, PIP₂ affinity of PTEN 16-353 lacking PBM appears comparable to PTEN 6-353, indicating PBM-independent interaction between PIP₂ and the PTEN core domains (Figure 19b). Concerning the significance of lysine-enriched CBR3 loop

(residues 260-269) on the phosphatase activity and its potential interaction with PTEN C-tail implicated by earlier reports^{71,167}, phosphatase and C2 domain were separately expressed using *E. coli* and insect cells to identify the allosteric binding site of PIP₂/nhPIP₃¹⁴⁷. However, it was not possible to obtain the isolated domains in soluble and monomeric forms. It might be ascribed to the extensive hydrophobic interface between phosphatase and C2 domain, which hinders stable overexpression as single species (Figure 26a). Thereby, investigation of PTEN interaction with PIP₂ and nhPIP₃ was discontinued.

To investigate inhibition of PTEN phosphatase activity, X-ray crystallography can provide an excellent platform to study structural alteration upon inhibition. Based on the known crystal structure (PDB 1D5R), protein crystallization of PTEN core domains (*t*PTEN) was established for ligand-soaking experiments (Figure 24). Structure determination of the corresponding protein crystal (PDB 5BZZ) is comparable to PDB 1D5R and shows the sulfhydryl group of the active site cysteine in the reduced state. Notably, PDB 5BZZ exhibits distinct protein packing from the original crystal structure (PDB 1D5R), involving different crystallographic parameters (*e.g.* space group, unit cell constants and the number of protomers in the asymmetric unit; Figure 28 and Figure 29). In this respect, it is an interesting finding that different protein packing is observed for analogous crystallization conditions. In addition to *t*PTEN, full-length PTEN was subjected to crystallization, since structural elucidation of the full-length PTEN would provide additional information of its autoinhibitory mechanism. However, no suitable crystal was obtained in spite of the large scale crystallization screening (Chapter 3.4.1). This is possibly attributed to two major factors. First, a single homogenous protein species could not be isolated due to extensive post-translational modifications produced during protein expression (Figure 23). Assuming the presence of only one conformation for a defined phosphorylation pattern, protein production with phosphomimicry mutations or native chemical ligation of a phosphorylated peptide may allow to resolve this issue. Second, the flexible region of the C-tail (50 amino acids) and the D-loop (24 amino acids) may be too long so that it could disturb the protein crystallization. In this respect, various truncated PTEN constructs should be tested to find a suitable length for crystallization.

Inhibition of PTEN phosphatase activity by H₂O₂ was investigated in detail. H₂O₂ is not only involved in cellular oxidative stress as a major component of ROS, but also plays a crucial role in the redox signaling as a second messenger^{99,104}. In the signal transduction, growth

factor-mediated cell stimulation promotes production of H_2O_2 , which inhibits phosphatase activity of PTEN and reinforces PI3-K/Akt signaling^{105,109}. Thereby, selective on/off switching of PTEN phosphatase activity and protection from irreversible inactivation constitute highly desirable features for the efficient regulation of the signaling^{10,115}. In this regard, PTEN exhibits an active site cysteine (C124) susceptible to oxidation^{8,9,10}. PTEN undergoes reversible inactivation via disulfide formation between this cysteine C124 and the proximal C71, which prevents irreversible oxidation^{10,82,83} (Figure 8a). In this study, reversible oxidative inhibition and disulfide formation of PTEN were confirmed employing phosphatase activity assay and mass spectrometric analysis, respectively. Notably, IC_{50} of H_2O_2 determined herein ($60 \pm 23 \mu\text{M}$) is significantly higher than the intracellular H_2O_2 concentration in mammals ($0.001 - 0.7 \mu\text{M}$ in the basal state)¹⁴⁸. This suggests that PTEN oxidation occurs in response to local high concentration of H_2O_2 and supports its role as a second messenger in the redox signaling. Structural consequences of PTEN inhibition by H_2O_2 were studied using ligand-soaking experiments. The subsequent X-ray crystallographic analysis revealed only small structural alterations in oxidized PTEN involving disulfide formation (Figure 41). Remarkably, earlier studies have shown that PTEN oxidation abolishes the interaction between the core domain and the phosphorylated C-tail peptide⁷⁰. Its nuclear localization occurs in the open conformation and is promoted under oxidative stress (Figure 5)^{84,168}. Moreover, nuclear PTEN is also known to contribute to reduction of ROS production⁸⁴. Taken together, nuclear PTEN may preserve the conformation of the central domains for the phosphatase-independent tumor suppressing effect, which is facilitated by protein-protein interaction via C2 domain^{21,85,86}. In addition, this implicates a role of PTEN in a feedback mechanism for the regulation of cellular ROS concentration.

So far, reversible oxidation of the catalytic cysteine has been found in PTPs such as PTP1B¹⁶⁹, LYP¹¹⁸, VHR¹⁶⁹, SHP-1/2^{108,170}, LMW-PTP¹²⁴, CDC25B¹²⁸ and PTEN⁸². Among them, phosphatase domains of PTP1B^{122,123}, CDC25B¹²⁶, LYP¹¹⁸ and now PTEN¹⁷¹ have been structurally characterized in reduced and oxidized forms (Figure 32). Upon oxidation, PTP1B and CDC25B experience profound conformational changes of the active site P-loop with the formation of sulfenyl-amide and disulfide, respectively. It has been proposed that these structural changes may disrupt the interaction with their substrates and facilitate selective reduction by antioxidants^{10,122,126}. For instance, sulfenyl-amide formation maintains the active site cysteine in a solvent-exposed manner, which enables the reductive reactivation by thioredoxin and GSH^{122,150}. However, the disulfide bond of CDC25B is buried at the bottom

of the active site, which results in selective reduction by thioredoxin, but not by GSH^{126,128}. In this context, minimal structural changes of PTEN's active site upon oxidation are consistent with reactivation by physiologically relevant small-molecular reducing agents (*e.g.* GSH)^{82,150,171}. Nevertheless, it remains to be seen, if the structural alteration of oxidized PTEN has an influence on its substrate binding and its subcellular localization^{70,84,168}. Another remarkable aspect of PTEN is implicated with its robust protection from irreversible oxidation by H₂O₂. Compared to PTP1B and CDC25B (Figure 9), PTEN restores the phosphatase activity under reductive conditions even after intensive H₂O₂ treatment (Figure 33). This finding supports the efficient protection from irreversible catalytic impairment by ROS.

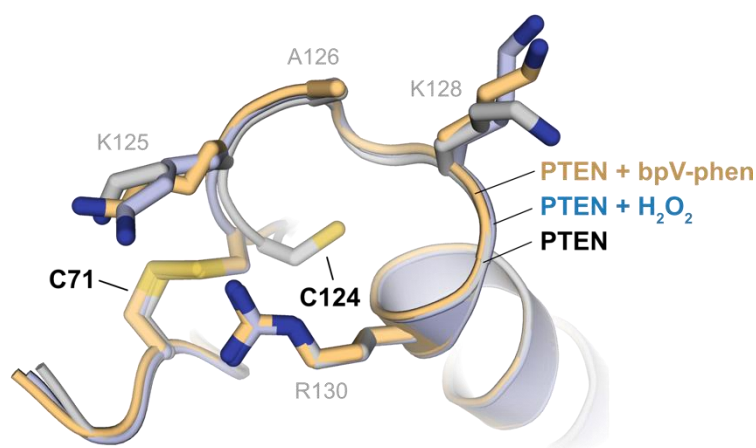


Figure 41 | Oxidative modification does not induce significant conformational change. H₂O₂ (blue, chain A) or bpV-phen (orange, chain A) treatment of PTEN promotes disulfide formation by rotating the catalytic cysteine C124 to the back-door cysteine C71. Structural overlay with reduced PTEN (gray, chain A) demonstrates maintenance of backbone conformation upon oxidation. This figure is reconstructed based on Lee *et al.* (2015)¹⁷¹.

In addition, PTEN inhibition was investigated using bpV-complexes. These are the most frequently used tool compounds to study *in cellulo* and *in vivo* inhibition of PTEN. In earlier studies, bpV-complexes have shown cellular regenerative effects in neuronal and cardiac injury¹³⁶⁻¹⁴¹. However, the mode of action of bpV-complexes on PTEN has been unclear – It was speculated that bpV-mediated PTEN inhibition occurs in the non-covalent or oxidative manner. The latter case may occur via disulfide formation (reversible) or hyperoxidation (irreversible)^{132,133}. So far, oxidative inhibition of PTP1B phosphatase activity has been demonstrated with peroxidovanadate¹⁵³. Notably, formation of sulfonic acid was only

observed at the active site cysteine, implicating high potency of peroxidovanadium species for irreversible modification¹⁵³. Herein, reversible oxidative inhibition of PTEN by bpV-phen was verified applying phosphatase activity assays and mass spectrometric analysis. Analogous to H₂O₂, bpV-phen induces the same disulfide bond, also with only minor conformational changes in the active site (Figure 41). However, the underlying mechanisms of both compounds are suggested to be different. Compared to intermediate sulfenic acid formation by H₂O₂ (Figure 8), peroxidovanadium-mediated thiol oxidation has been proposed to involve radical one-electron transfer steps¹⁷².

In addition, NMR titration experiment performed herein identified the formation of orthovanadate as a reaction product of bpV-phen (Figure 34). This is an important finding, since orthovanadate resulting from *in vivo* bpV-phen treatment may exert a secondary effect as an inhibitor of additional human enzymes (*e.g.* PTP1B¹⁵³, alkaline phosphatase¹⁶⁴ and ATPase¹⁷⁷). Earlier studies showed cytoprotective effects of orthovanadate in ischemia and reperfusion injury^{178,179,180}. Further cell-based studies are required to understand, whether orthovanadate has a synergetic effect with bpV-phen on neuronal and cardiac protection together.

In this study, X-ray crystallographic analysis of PTEN was used to obtain structural insights into H₂O₂- and bpV-phen-mediated inhibition of PTEN phosphatase activity. In addition, the mode of action of PTEN inhibition by bpV-phen elucidated herein will help to evaluate the therapeutic potential of bisperoxidovanadium complexes. Importantly, the reversible oxidative inhibition of PTEN by these complexes may represent a highly beneficial feature, since irreversible impairment of this central tumor suppressor can cause systemic disturbance.

4 Summary

PTEN is a dual-specificity protein tyrosine phosphatase. PTEN has a significant impact on cell fate determination between survival and apoptosis depending on its phosphatase activity in the PI3-K/Akt signaling. Therefore, tight regulation of its phosphatase activity is very important for cellular homeostasis. In this context, both selective on/off switching of PTEN's phosphatase activity and protection from irreversible inactivation constitute highly desirable features. The second messenger H_2O_2 , which is produced under both growth factor-mediated signal transduction and oxidative stress, transiently inactivates PTEN in an oxidative manner. Under oxidative conditions, PTEN undergoes disulfide bond formation between the catalytic cysteine C124 and the proximal cysteine C71. The structural impact of disulfide formation on PTEN's structure was unclear. Given the potential structural change and presence of other active site cysteine modifications, structural characterization of oxidized PTEN would facilitate a better understanding of its regulation and proposed protective mechanism as a central tumor suppressor.

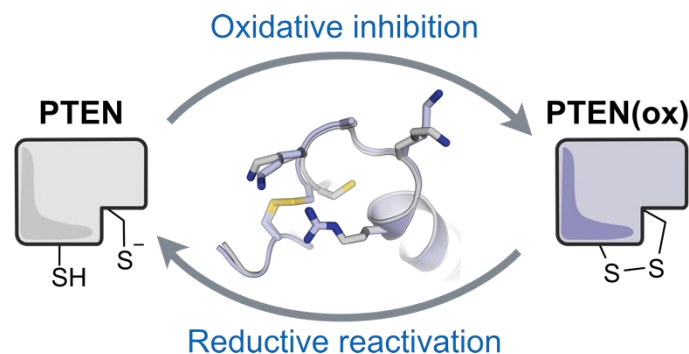


Figure 42 | Reversible oxidative modification of PTEN's active site by H_2O_2 . The active site cysteine of PTEN (gray) is oxidatively inhibited upon exposure to H_2O_2 (blue). This inhibitory process results in disulfide bond formation without significant conformational change. Due to its reversible character, the catalytic activity of PTEN can be reversed under reductive condition.

H_2O_2 -triggered oxidative inhibition and the reductive reactivation of PTEN were investigated using the malachite green phosphatase activity assay. HPLC-coupled high resolution mass spectrometry confirmed disulfide formation between cysteines C71 and C124. Structural alteration induced by PTEN oxidation was investigated applying X-ray crystallography. Reduced *t*PTEN (PDB 5BZZ) was treated with H_2O_2 using soaking experiment. The resulting oxidized *t*PTEN (PDB 5BUG) verifies disulfide bond formation at the active site (Figure 42). In comparison with two other members of the PTP superfamily, PTP1B and CDC25B, PTEN

exhibits only a small structural change and a very robust reactivation after stringent H_2O_2 treatment. This indicates a very efficient protection from irreversible modifications which may represent a crucial feature of this important tumor suppressor.

In addition, the structural consequences of PTEN inhibition by bisperoxidovanadium (bpV) complexes were studied using bpV-phen (bisperoxido (1,10-phenanthroline) oxovanadate (V)) as model compound. Importantly, it was previously shown that after nerve and cardiac injury, treatment with bpV-complexes can trigger cellular regeneration. However, the precise mode of action is still under debate. In this study, the reversible oxidative inhibition of PTEN by bpV-phen via disulfide formation was shown applying phosphatase activity assays and mass spectrometric analysis (Figure 43). ^{51}V -NMR spectroscopy allowed the identification of orthovanadate as the reaction product of bpV-phen-mediated PTEN inhibition. Furthermore, X-ray crystallographic analysis was applied to study structural impact of disulfide formation in bpV-phen-treated PTEN (PDB 5BZX). Analogous to H_2O_2 -treatment, PTEN inhibition by bpV-phen results in minor structural alteration at the active site. An additional electron density map based on the scattering property of vanadium verified the presence of orthovanadate in the active site. Varying occupancy in each protomer indicates a low affinity for the active site of oxidized PTEN, which was also validated by ^{51}V -NMR titration experiments. Overall, this study successfully elucidated the mode of action of bpV-phen and the structural impact of disulfide formation on PTEN. The reversible oxidative inhibition of PTEN by bpV-phen may represent a highly beneficial feature, since irreversible impairment of this central tumor suppressor may cause systemic disturbance. The mode of action of bpV-phen elucidated in this study can contribute to the further development of bpV-complexes as PTEN inhibitors.

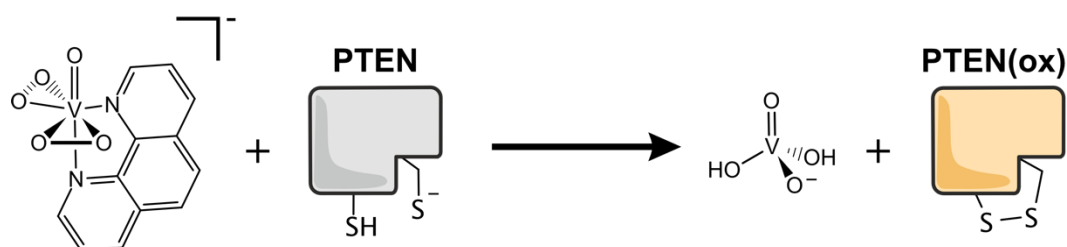


Figure 43 | Mode of action of bpV-phen. bpV-Phen inhibits reduced PTEN (gray) in an oxidative manner by promoting disulfide formation (orange). Orthovanadate is a reaction product originating from bpV-phen.

5 Material and methods

5.1 Materials and equipments

5.1.1 List of chemicals and materials

The following chemicals and materials were used for the experiments performed in this thesis.

Table 10 | List of chemicals and materials generally used for experiments.

| Chemicals and materials | Manufacturer |
|---|---|
| Acetic acid | J. T. Baker |
| Conical tube (15 ml, 50 ml) | Sarstedt |
| Dithiothreitol (DTT) | Serva Electrophoresis GmbH |
| Eppendorf tubes (0.5 ml, 1.5 ml, 2 ml) | Eppendorf |
| Ethanol (abs.) | Sigma-Aldrich |
| Ethylenediaminetetraacetic acid (EDTA) | Sigma-Aldrich |
| Glycerol | GERBU Biotechnik GmbH |
| Hydrochloric acid (HCl) | J. T. Baker |
| Isopropanol | J. T. Baker |
| Syringe needle 100 Sterican [®] | B. Braun Melsungen AG |
| Culture test tubes (sterile, 13 ml, 100 x 16 mm) | Sarstedt |
| Nalgene [®] Bottle Top Filter with PES Membrane | Thermo Scientific |
| Sodium chlorid (NaCl) | AnalaR [®] NORMAPUR [®] VWR |
| Sodium hydroxide | J. T. Baker |
| Pipette tips (10 µl, 200 µl, 1250 µl) | Nerbe Plus |
| Syringes (1 ml, 2 ml, 5 ml, 10 ml, 20 ml) | B. Braun Melsungen AG |
| Serological pipettes (2 ml, 5 ml, 10 ml, 25 ml) | Sarstedt |
| Syringe filter Filtropur S (0.2 µm, 0.45 µm) | Sarstedt |
| Tris (tris(hydroxymethyl)aminomethane) | Roth |
| Falcon [®] cell culture plate (10 cm) | Corning |
| Falcon [®] cell culture plate (6 well) | Corning |

Table 11 | List of chemicals and materials used for molecular cloning.

| Chemicals and materials | Manufacturer |
|---|-------------------------------------|
| GelRed Nucleic Acid Stain (10.000x in DMSO) | Biotium |
| Gene Ruler 1 kb Plus DNA Ladder (#SM1333) | Thermo Scientific |
| Gentamycin sulfate | Serva Electrophoresis GmbH |
| Kanamycin A disulfate | GERBU Biotechnik GmbH |
| LB agar plates | |
| (LB-Media und 1.5 % (w/v) agar): | |
| - gentamycin plate | |
| containing gentamycin (10 µg/ml) | |
| - kanamycin plate | |
| containing kanamycin (50 µg/ml) | MPI-Medienküche |
| - kanamycin + chloramphenicol plate | (<i>engl.</i> Culture media supply |
| containing kanamycin (50 µg/ml), | service) |
| chloramphenicol (34 µg/ml) | |
| - blue-white-screening plate | |
| containing kanamycin (50 µg/ml), | |
| gentamycin (7 µg/ml), tetracycline | |
| (10 µg/ml), X-gal (100 µg/ml) | |
| and IPTG (40 µg/ml) | |
| LB-Media | MPI-Medienküche |
| For 1 l: | (<i>engl.</i> Culture media supply |
| 10 g tryptone, 5 g yeast extract, 10 g NaCl | service) |
| PCR-Tubes (8er Kette) | Sarstedt |
| Phusion Flash PCR Master Mix | Thermo Scientific® |
| Surgical Disposable Scalpel | B. Braun Melsungen AG |
| Ultra Pure™ Agarose | Invitrogen |
| 6x DNA Loading Dye (#R0611) | Thermo Scientific |
| 10x Fast Digest® Buffer | Fermentas |
| 10x T4 DNA Ligase Buffer | Fermentas |

Table 12 | List of chemicals and materials used for protein expression, purification and analytics.

| Chemicals and materials | Manufacturer |
|---|--------------------------------|
| Acrylamide 4K-Solution (30 %) Mix 37.5:1 | PanReac AppliChem |
| Amicon [®] Ultra-Filter, 10 kDa (15 ml, 0,5 ml) | Merck Millipore |
| Amicon [®] Ultra-Filter, 30 kDa (15 ml, 0,5 ml) | Merck Millipore |
| Ammonium persulfate (APS) | ChemCruz [™] |
| β -Mercaptoethanol | Serva Electrophoresis GmbH |
| Bradford - reagent 5x | Serva Electrophoresis GmbH |
| Bromophenol blue - sodium salt | Serva Electrophoresis GmbH |
| DNA-Transfection reagent (X-tremeGENE HP) | Roche Diagnostics GmbH |
| Gibco [®] heat inactivated <i>Fetal Bovine Serum</i> (FBS) | Life Technologies [™] |
| Glycine | Roth |
| Imidazole | Roth |
| Sodium dodecylsulfate (SDS) | GERBU Biotechnik GmbH |
| Nickel-NTA-Superflow | Qiagen [®] |
| Page Ruler [™] Plus Prestained Protein Ladder (#26019) | Thermo Scientific |
| Phenylmethylsulfonylfluorid (PMSF) | Serva Electrophoresis GmbH |
| Protein-free insect cell media Spodopan L-Glutamine, 0,35 g/l NaHCO ₃ , sterile | PAN [™] Biotech GmbH |
| Tetramethylethylenediamine (TEMED) | Roth |
| Tris(2-carboxyethyl)phosphine (TCEP) | Serva Electrophoresis GmbH |
| Trypan Blue solution (0.4 %) | Sigma-Aldrich |

5.1.2 Equipments and apparatus

The following equipments and apparatus were used for the experiments performed in this thesis.

Table 13 | List of equipments and apparatus used for experiments.

| Equipments / Apparatus | Manufacturer |
|---|---------------------------------|
| Äkta-FPLC | GE Healthcare Life Sciences |
| Horizontal electrophoresis apparatus | Bio-Rad |
| AlphaImager [®] | Biozym |
| Analog Dry Block Heaters | VWR [®] |
| Avanti [™] J-25 Centrifuge | |
| Rotor JA-25.50 | |
| Rotor JLA-8.1000 | Beckman Coulter [™] |
| Centrifuge tube | |
| Incubator | BINDER |
| Centrifuge 5415 R | Eppendorf |
| Centrifuge 5804 R | Eppendorf |
| Digital Sonifier [®] Cell Disruptor mit 102-C Converter | Branson Ultrasonics Corporation |
| Drigalski-Spatula (glass) | Roth |
| Epson Perfection 2400 photo scanner | Epson [®] |
| Falcon [™] EXPRESS Pipet-aid | BD Biosciences |
| Sample comb (horizontal electrophoresis apparatus) | Bio-Rad |
| GFL [®] -3005 Orbital shaker | Gesellschaft für Labortechnik |
| Glass plates (SDS-PAGE) | Bio-Rad |
| High Performance UV Transilluminator | UVP |
| HiLoad [™] 16/60 Superdex [™] 200 preparative grade | GE Healthcare Life Sciences |
| HiTrap SP HP, 5 ml | GE Healthcare Life Sciences |
| Hot plate magnetic stirrer | IKA [®] |
| Microflow Class II advanced biological safety cabinet | Nalge Nunc International |
| Microscope: Olympus CX41 RF | Olympus |
| Microplate reader Safire2 [™] | Tecan [®] |
| Microwave (700 Watt) | Severin |
| Millipore Q-water system Q-POD [™] | Merck Millipore |

| Equipments / Apparatus (Continued) | Manufacturer |
|---|-----------------------------|
| Mini Gyro-rocker S SM3 Orbital shaker | Stuart® |
| MiniSpin® | Eppendorf |
| Multifuge 3 S-R | Heraeus / Thermo Scientific |
| NanoDrop® 2000c Spectrophotometer | PEQLAB Biotechnologie GmbH |
| Neubauer chamber (0,0025 mm ² , depth: 0,1 mm) | Marienfeld-Superior |
| PCR-Thermo-Cycler (Mastercycler EP Gradient) | Eppendorf |
| pH-Meter inoLab® with pH Electrode SenTix® 81 Plus | WTW |
| Pipettes (2.5, 10, 20, 100, 200, 1000 µl) | Eppendorf |
| Electrophoresis chamber (SDS-PAGE) | Bio-rad |
| Q-Exactive-MS mit Nano-HPLC | Thermo Scientific |
| Rotator SB3 | Stuart® |
| SartoPac basic SPb-LA230P | Sartorius |
| Shaking incubator Ecotron | Infors HAT |
| Shaking incubator Innova® 42 | New Brunswick Scientific |
| Shaking incubator Innova® 4430 | New Brunswick Scientific |
| SDS-gel hand casting apparatus | Bio-Rad |
| PowerPac™ HC und Basic | Bio-Rad |
| Thermomixer comfort | Eppendorf |
| Vortex Genie 2 Vortexer | Scientific Industries |
| Centrifuge Universal 320R | Hettich GmbH |
| 96-Well Deep Well Plate | VWR |

5.1.3 Buffer and solution

The following buffers and solutions were used for the experiments performed in this thesis. They were prepared with deionized water.

Table 14 | List of buffer used for protein purification.

| Used for protein purification | |
|--|--|
| Description | Composition |
| Lysis buffer | 50 mM Tris-HCl (pH 8.0), 500 mM NaCl, 5 % Glycerol, 5 mM β -Mercaptoethanol |
| Washing buffer (<i>batch</i> mode) | 50 mM Tris-HCl (pH 8.0), 500 mM NaCl, 5 % Glycerol, 5 mM β -Mercaptoethanol, 20 mM Imidazol |
| Elution buffer (<i>batch</i> mode) | 50 mM Tris-HCl (pH 8.0), 500 mM NaCl, 5 % Glycerol, 5 mM β -Mercaptoethanol, 300 mM Imidazol |
| IEX running buffer A (<i>t</i> PTEN purification) | 25 mM Tris-HCl (pH 7.0), 100 mM NaCl, 2 mM DTT |
| IEX running buffer B (<i>t</i> PTEN purification) | 25 mM Tris-HCl (pH 7.0), 500 mM NaCl, 2 mM DTT |
| IEX running buffer A (Full-length purification) | 25 mM Tris-HCl (pH 8.0), 50 mM NaCl, 2 mM DTT |
| IEX running buffer B (Full-length purification) | 25 mM Tris-HCl (pH 8.0), 500 mM NaCl, 2 mM DTT |
| SEC running buffer (Biochemical Assay) | 25 mM Tris-HCl (pH 8.0), 200 mM NaCl, 2 mM TCEP |
| SEC running buffer (Protein crystallization) | 20 mM Tris-HCl (pH 7.5), 150 mM NaCl, 5 mM DTT |

Table 15 | Buffer used for agarose gel electrophoresis.

| Used for agarose gel electrophoresis | |
|--------------------------------------|---|
| Description | Composition |
| 50 x TAE-buffer | 50 mM EDTA, 2 M Tris-HCl (pH 8.5), 5.71 % Acetic acid |

Table 16 | List of buffer used for SDS-PAGE.

| Used for SDS-PAGE | |
|--------------------------------|---|
| Description | Composition |
| Tris buffer for separating gel | 1.5 M Tris-HCl (pH 8.8), 0.4 % SDS |
| Tris buffer for stacking gel | 500 mM Tris-HCl (pH 6.8), 0.4 % SDS |
| 5 x SDS-PAGE sample buffer | 0.6 ml 1 M Tris-HCl (pH 6.8), 5 ml 50 % Glycerol, 2 ml 10 % SDS (w/v), 0.5 ml β -Mercaptoethanol, 1 ml 1 % Bromphenol blue, 0.9 ml ddH ₂ O |
| SDS-PAGE running buffer | 25 mM Tris-HCl (pH 8.3), 200 mM Glycine, 0,1 % SDS |
| Coomassie-Staining solution | 10 % Acetic acid, 0,006 % (w/v) Coomassie Brilliant Blue G250 |

Table 17 | List of solution used for protein crystallization.

| Used for protein crystallization | |
|---|--|
| Description | Composition |
| Protein crystallization solution | 100 mM MES (pH 6.5), 1250 mM K/Na-(L)-tartrate, 7.5 % Glycerol |
| Cryo solution | 100 mM MES (pH 6.5), 1250 mM K/Na-(L)-tartrate, 25 % Glycerol |
| Crystal-soaking solution (H ₂ O ₂) | 100 mM MES (pH 6.5), 1250 mM K/Na-(L)-tartrate, 7.5 % Glycerol, 1 mM H ₂ O ₂ |
| Crystal-soaking solution (bpV-phen) | 100 mM MES (pH 6.5), 1250 mM K/Na-(L)-tartrate, 7.5 % Glycerol, 1 mM bpV-phen |
| Crystal-soaking solution (PIP ₃) | 100 mM MES (pH 6.5), 1250 mM K/Na-(L)-tartrate, 7.5 % Glycerol, 1 mM PI-(3,4,5)-P ₃ diC8 |
| Crystal-soaking solution (PIP ₂) | 100 mM MES (pH 6.5), 1250 mM K/Na-(L)-tartrate, 7.5 % Glycerol, 20 mM PI-(4,5)-P ₂ diC8 |
| Crystal-soaking solution (nhPIP ₃) | 100 mM MES (pH 6.5), 1250 mM K/Na-(L)-tartrate, 7.5 % Glycerol, 20 mM 3S-PI-(3,4,5)-P ₃ diC8 |

5.1.4 Enzymes

The following enzymes were used for the experiments performed in this thesis.

Table 18 | List of enzymes used for experiments.

| Enzyme | Manufacturer |
|--|--|
| Fast Digest [®] <i>Nde</i> I (#FD0583) | Fermentas |
| Fast Digest [®] <i>Sal</i> I (#FD0644) | Fermentas |
| Phusion Flash II DNA Polymerase | Thermo Scientific |
| TEV-Protease (1,8 mg/ml) | Dortmund Protein Facility (MPI Dortmund) |
| T4 DNA Ligase (1000 units/ μ l) (#EL0011) | Thermo Scientific |

5.1.5 Reagent kits

The following reagent kits were used for the experiments performed in this thesis. They were employed in accordance with the manufacturer's instructions.

Table 19 | List of reagent kits used for experiments.

| Reagent kits | Manufacturer |
|---|----------------------------------|
| Cycle Pure Kit | Omega Bio-Tek |
| Gel Extraction Kit | Omega Bio-Tek |
| Malachite Green Assay Kit | Echelon [®] BioSciences |
| QIA prep [®] Spin Miniprep Kit | QIAGEN [®] |

5.1.6 Microorganisms and cells

Table 20 | List of microorganisms and cells used for experiments.

| Taxonomy | Strain/line | Genotype | Source |
|---|-----------------------------------|--|---|
| <i>E. coli</i> | OmniMax™ | F' { <i>proAB lacIq lacZ</i> ΔM15 <i>Tn10</i> (TetR) Δ(<i>ccdAB</i>)} <i>mcrA</i> Δ(<i>mrr hsdRMS-mcrBC</i>) Φ 80(<i>lacZ</i>)ΔM15 Δ(<i>lacZYA-argF</i>)U169 <i>endA1 recA1 supE44</i> <i>thi-1 gyrA96 relA1 tonA panD</i> | MPI, Dortmund (Originally from Invitrogen™) |
| <i>E. coli</i> | DH10Bac™ | F- , <i>mcr A</i> , Δ(<i>mrr-hsd RMS-mcr</i> BC), φ80 <i>lacZ</i> ΔM15, Δ <i>lacX74</i> , <i>deoR</i> , <i>recA1</i> , <i>endA1</i> , <i>araD139</i> , Δ(<i>ara</i> , <i>leu</i>)7697, <i>galU</i> , <i>galKλ-rpsL</i> , <i>nupG/ bMON14272/ pMON7124</i> | MPI, Dortmund (Originally from Invitrogen™) |
| <i>E. coli</i> | Rosetta™ | F- <i>ompT hsdSB</i> (rB- mB-) <i>gal dcm</i> pRARE (CamR) | MPI, Dortmund (Originally from Merck Millipore™) |
| <i>Spodoptera</i> <i>frugiperda</i> (fall armyworm) | IPLB-Sf-21-AE (Sf-9) | - | DPF, Dortmund (Originally from Invitrogen™) |
| <i>Trichoplusia ni</i> (Cabbage looper) | BTI-TN-5B1-4 (High Five cells) | - | DPF, Dortmund (Originally from Invitrogen™) |

5.2 Quantative analytical methods

5.2.1 Photometric determination of DNA concentration

Concentrations of the purified DNA including plasmids and linear PCR-products are determined photometrically using NanoDrop[®] 2000c spectrophotometer. The absorption values are measured at 260 nm, of which DNA shows the absorption maximum. This equipment calculates the DNA concentration proportionally, applying the absorption value of 1 for 50 ng/μl double-stranded DNA as a standard measurement value.

5.2.2 Photometric determination of protein concentration

NanoDrop[®] 2000c spectrophotometer is applied to determine the protein concentration. Analogous to the measurement of DNA concentration (Chapter 5.2.1), the principle is based on Beer-Lambert law that states the proportional relationship of absorbance to the sample concentration in diluted solution (Eq. 1). The absorption values are monitored at 280 nm. For the concentration measurement of protein including significant amount of impurity, absorbance of 1 is set to the protein concentration of 1 mg/ml. After final purification, the extinction coefficient and molecular weight of the protein construct are given for the precise determination. Both values have been calculated using the ProtParam tool (ExpPASy) in advance (Table 21)¹⁸¹.

$$A = \log \left(\frac{I_0}{I} \right) = \varepsilon \cdot c \cdot d \quad (\text{Eq. 1})$$

A: Absorbance, I_0 : Incident intensity of the light, I: Transmitted intensity, ε : molar extinction coefficient [$\text{M}^{-1} \text{cm}^{-1}$], c: concentration of the sample [mol l^{-1}], d: Length of the light path through the sample [cm].

Extinction coefficients and molecular weights of PTEN constructs used for the protein concentration measurements are summarized as follows (Table 21).

Table 21 | Extinction coefficients and molecular weights of PTEN constructs. The values are calculated using the ProtParam tool¹⁸¹.

| PTEN constructs | Extinction coefficient [M ⁻¹ cm ⁻¹] | Molecular weight [kDa] |
|-----------------------|---|---------------------------|
| PTEN (1-403) | 45270 | 47.22 |
| PTEN (6-403) | 45270 | 46.69 |
| PTEN (16-403) | 45270 | 45.42 |
| PTEN (6-353) | 42290 | 41.13 |
| PTEN (16-353) | 42290 | 39.86 |
| PTEN (7-353) Δ286-309 | 42290 | 38.39 |

5.3 Molecular biological methods

5.3.1 Polymerase chain reaction (PCR)

Polymerase chain reaction^{182,183} is employed to amplify a specific DNA sequence in a plasmid for recombinant protein expression. This method requires forward and reverse primers^{XXIX}, template DNA, dNTPs, Mg²⁺-containing reaction buffer, and thermophilic DNA polymerase (Table 22). The reaction mixture is prepared by pipetting the components together. In this study, a commercially available premixed reagent, 2 x Phusion[®] master mix is used, which contains dNTPs, reaction buffer with Mg²⁺ and DNA polymerase.

Table 22 | Component scheme for polymerase chain reaction.

| Component | Volume [μl] preparative | Volume [μl] analytical | Final Concentration |
|-------------------------------------|----------------------------|---------------------------|--|
| Primer (forward) | 5 | 1 | 1 μM |
| Primer (reverse) | 5 | 1 | 1 μM |
| Template DNA | 1 | 0.2 | ~ 100 ng (preparative) ~ 20 ng (analytical) |
| 2 x Phusion [®] Master Mix | 25 | 5 | 1x |
| ddH ₂ O | 14 | 2.8 | - |
| Total | 50 | 10 | - |

Polymerase chain reaction is carried out using a thermocycler with the reaction mixture mentioned above. Thermocycling conditions have been programmed in advance with the

^{XXIX} Forward and reverse primers are also called sense and antisense primers, respectively.

following temperature/time profile (Table 23). Elongation time varies depending on the polymerase utilized in the reaction. In spite of a different manufacturer's instructions, elongation time of 60s per 1kb is applied in this study. Moreover, the number of PCR cycles is set not to exceed 25 cycles to avoid the potential introduction of mutation, as though the utilized polymerase had a proof-reading function.

Table 23 | Thermocycling profiles for polymerase chain reaction.

| Steps | Temperature [°C] | Time [s] | No. of cycles |
|----------------------|------------------|-------------|---------------|
| Initial denaturation | 94 | 120 | 1 |
| Denaturation | 94 | 30 | |
| Annealing | 53 | 30 | 25 |
| Elongation | 72 | 60 per 1 kb | |
| Final extension | 72 | 600 | 1 |
| Cooling down / Hold | 4 | ∞ | - |

Afterwards, the crude product is purified with a purification kit ("Cycle Pure Kit, Omega Bio-tek") following the manufacturer's instruction. The concentration of the purified PCR-product is determined using NanoDrop[®] (Chapter 5.2.1) and stored at -20 °C until further use.

5.3.2 Overlap extension PCR

As a methodological variant, overlap extension PCR¹⁸⁴ is especially useful to extend a PCR product by combining two fragments. Alternatively, this method can be applied to bring a target-oriented mutation into the sequence during the molecular cloning. Overlap extension PCR is achieved over two steps. First, two primer-directed PCR should be carried out. Thereby, the resulting two PCR products should include an overlapping sequence. Second, PCR-products from the first step serve as a primer and simultaneously as a DNA-template for the second polymerization. The following components (Table 24) are mixed together in a reaction tube and subjected to a subsequent thermocycling program.

Table 24 | Component scheme for overlap extension PCR.

| Component | Volume [μ l] | Final Concentration |
|-------------------------------------|-------------------|---------------------|
| Primer (forward) | 5 | 1 μ M |
| Primer (reverse) | 5 | 1 μ M |
| Template DNA 1 | 0.5 | ~ 50 ng |
| Template DNA 2 | 0.5 | ~ 50 ng |
| 2 x Phusion [®] Master Mix | 25 | 1 x |
| ddH ₂ O | 14 | - |
| Total | 50 | - |

Overlap extension PCR is performed using thermocycler with the same temperature/time profile as the standard PCR (Table 23). The crude reaction product is purified by using agarose gel electrophoresis (Chapter 5.3.3). Concentration of the purified PCR-product is determined using NanoDrop[®] (Chapter 5.2.1) and stored at -20 °C until further use.

5.3.3 Agarose gel electrophoresis

Agarose gel electrophoresis^{185,186} is employed to analyze and purify the DNA fragments after PCR, colony PCR and restriction digest. In this study, 1 % (w/v) agarose gel is made with TAE-buffer (1x) as a standard gel density. 3 g of agar is boiled in 300 ml of TAE-buffer (1x) by microwave. 30 μ l of the fluorescence stain called Gel Red[®] Nucleic Acid Stain (10,000 x) is added to the agarose suspension, which is subsequently poured onto a tray. The gel is hardened in the presence of a comb that involves suitable pocket sizes.

The samples for the agarose gel electrophoresis are prepared by mixing DNA-solution with 6 x DNA loading buffer. The mixture and a DNA marker are given to each pocket in the gel that has been transferred to the TAE-buffer (1x) in the running chamber beforehand. Purification is run under 80 V (constant voltage) for 40 min. The DNA bands are visualized with UV light and cut using a scalpel. The DNA fragment is extracted from the agarose gel with "Gel Extraction Kit" (Chapter 5.1.5) following the manufacturer's instruction.

5.3.4 Restriction digest

For the recombinant protein expression, plasmids should be modified by insertion of the gene of interest. Plasmids are cleaved by specific restriction enzymes in the multiple cloning sites¹⁸⁷⁻¹⁸⁹, followed by ligation of plasmid DNA and the gene of interest using a ligase.

According to the Table 25, plasmid DNA or PCR product is resuspended with reaction buffer, ddH₂O and restriction enzymes for the restriction digest. The reaction mixture is subsequently incubated for 1h at 37 °C. The crude product is furthermore purified using agarose gel electrophoresis (Chapter 5.3.3) in order to remove restriction enzymes and excised redundant DNA fragments. Concentration of the purified PCR-product is determined using NanoDrop[®] (Chapter 5.2.1) and stored at -20 °C until further use.

Table 25 | Component scheme for restriction digest.

| Component | Volume [μl] Plasmid DNA | Volume [μl] PCR product | Final Concentration |
|--------------------------------------|----------------------------|----------------------------|------------------------|
| Plasmid DNA | 10 | 0 | 50 - 100 ng/μl |
| PCR product | - | 15 | ca. 60 ng/μl |
| 10 x Fast Digest [®] Buffer | 2 | 3 | 1 x |
| Restriction enzyme (5'-end) | 1 | 1.5 | |
| Restriction enzyme (3'-end) | 1 | 1.5 | |
| ddH ₂ O | 6 | 9 | |
| Total | 20 | 30 | |

5.3.5 Ligation

Through ligation¹⁹⁰⁻¹⁹², two nucleic acid fragments are joined covalently to create a recombinant DNA molecule, in that phosphodiester bond formation is catalyzed by a ligase between 3'-hydroxyl of one DNA terminus and 5'-phosphate end of another. A linearized vector is incubated with a PCR product (from Chapter 5.3.4) in the presence of T4-ligase under the appropriate buffered condition (Table 26). After ligation at 25 °C for 1h, the reaction product is immediately subjected to the transformation (Chapter 5.3.6).

Table 26 | Component scheme for ligation of PCR product and linearized vector.

| Component | Volume [μ l] | Final Concentration |
|---|-------------------|---------------------|
| Linearized vector DNA | 2 | 3- 5 ng/ μ l |
| PCR product (After restriction digest) | 7 | ca. 20 ng/ μ l |
| 10 x T4-ligase Buffer | 2 | 1 x |
| T4-ligase | 1 | |
| ddH ₂ O | 8 | |
| Total | 20 | |

5.3.6 Transformation of the chemically competent cells^{xxx}

Cellular transformation is a genetic alteration of the host organism by direct uptake or incorporation of the exogenous genetic materials. In laboratory practice, transformation serves to deliver genetically modified colonies harboring a homogenous genetic material. Depending on the host *E. coli* strains, transformed cells can be utilized to amplify plasmids or to produce recombinant proteins. In this study, commercially available *E. coli*-strain OmniMAX and BL21(DE3)-derivatives are used for the plasmid amplification and protein production, respectively. For the cellular transformation, *E. coli* cells should be made artificially competent prior to the DNA-uptake process. The corresponding *E. coli* cells have been prepared chemically competent using calcium chloride in advance¹⁹³.

50 – 100 μ l of competent *E. coli* cells are thawed on ice. 10 μ l of ligation product or 1 μ l of a plasmid is added to the cells and incubated subsequently for 30 min on ice. The cells are exposed to heat shock at 42 °C for 1 min, transferred immediately back onto ice and furthermore incubated for 1.5 – 2 min. The cells are supplied with 900 μ l LB-media and incubated at 37 °C and 600 rpm for 1 h. Following recovery from the heat shock, 100 μ l of cells are transferred to an LB-agar plate supplemented with a selection antibiotic (Chapter 5.1.1) and spread using a Drigalski-spatula. The LB-agar plate is incubated overnight at 37 °C.

^{xxx} Transformation of DH10-Bac for bacmid production will be discussed in the following chapter Transposition (Chapter 5.4.1)

5.3.7 Colony PCR

Colony PCR^{194,195} is a variant of PCR methods to amplify a targeted gene sequence directly from bacterial colonies. This method is particularly useful during molecular cloning to verify successful ligation of the gene of interest in the vector. Colony PCR utilizes the same principle as the standard PCR (Chapter 5.3.1). The major difference is to use randomly selected colonies instead of an isolated DNA template. In addition, primers are frequently designed to bind upstream and downstream regions of the multiple cloning sites in the vector backbone to ensure the experimental success (Table 27). Consequently, colonies with the successful insertion of the gene of interest are differentiated from the counterparts by size of the amplified PCR products.

Table 27 | Sequencing primers for pFH1 vector.

| Primer | Oligonucleotide sequences |
|--------------|--|
| pFH1 forward | 5' - GTA ACA GTT TTG TAA TAA AAA AAC C - 3' |
| pFH1 reverse | 5' - GTT TCA GGT TCA GGG GGA GGT GTG GG - 3' |

During the procedure, each colony is carefully resuspended with 10 μ l sterile ddH₂O in a reaction tube using a sterile pipette tips. The resuspension is heated at 95 °C for 10 min. The cell lysate is subsequently centrifuged at > 10,000 g for 2 min. 1 μ l of the supernatant is added to the colony PCR master mix that has been prepared in advance (Table 28).

Table 28 | Component scheme for colony PCR master mix. Volume scaled to 1 colony.

| Component | Volume [μ l] | Final Concentration |
|-------------------------------------|-------------------|---------------------|
| Primer (forward) | 1 | 1 μ M |
| Primer (reverse) | 1 | 1 μ M |
| 2 x Phusion [®] Master Mix | 5 | 1 x |
| ddH ₂ O | 3 | - |
| Total | 10 | - |

Colony PCR is run with the following program (Table 29). The number of PCR cycles is set to 30 in order to ensure amplification of the DNA insert. Afterwards, the samples are subjected to agarose gel electrophoresis (Chapter 5.3.3) to confirm success of the previous ligation step (Chapter 5.3.5).

Table 29 | Thermocycling profiles for colony PCR.

| Steps | Temperature [°C] | Time [s] | No. of cycles |
|----------------------|------------------|-------------|---------------|
| Initial denaturation | 94 | 120 | 1 |
| Denaturation | 94 | 30 | |
| Annealing | 53 | 30 | 30 |
| Elongation | 72 | 60 per 1 kb | |
| Final extension | 72 | 600 | 1 |
| Cooling down / Hold | 4 | ∞ | - |

5.3.8 Isolation of the recombinant plasmid DNA

After the successful insertion of the gene of interest, the recombinant plasmid DNA is isolated from the transformed cells. A colony of the transformed *E. coli* strain OmniMAX is inoculated into 5 ml LB-media with appropriate antibiotics and cultured overnight at 37 °C. The cell culture is centrifuged at > 10,000 g for 2 min. The isolation of the plasmid is carried out using QIAprep[®] Spin Miniprep Kit (QIAGEN[®]) following the manufacturer's instruction. The principle is based on the alkaline cell lysis¹⁹⁶.

The cell pellet is resuspended with 250 µl resuspension buffer (P1) in which RNase has been added in advance. After addition of 250 µl lysis buffer (P2) and inversion of the sample for several times, the mixture is incubated for 5 min. After treatment with 350 µl neutralization buffer (N3) and subsequent inversion, plasmid in solution is separated by centrifugation (10 min, 16,100 rcf) from the genomic DNA, endogenous proteins, and other cellular components. The supernatant is given to the DNA-affinity column including a silica membrane, which is supplied in the kit. Plasmid DNA is bound to the membrane through centrifugation (16,100 rcf, 1 min), followed by addition of 500 µl binding buffer (PB). The silica column is washed twice by centrifugation with 750 µl washing buffer (PE). Prior to elution of the plasmid DNA, the spin column is centrifuged without any buffer to remove trace of ethanol, which might influence the following experiments. Finally, plasmid DNA is eluted with 30 – 50 µl elution buffer (EB) by centrifugation. The concentration of the obtained plasmid DNA is determined photometrically by NanoDrop[®] (Chapter 5.2.1).

5.3.9 Sequence identification

Validation of the sequence identity is performed by a DNA sequencing process. During the molecular cloning experiments, the insert fragment is amplified using PCR-procedures. This

might be a potential error-prone step with sequence mutations, in spite of the intrinsic proof-reading function of the DNA polymerases used. Therefore, plasmids produced recombinantly are monitored by this sequencing step before further use. The sequence identification is carried out by an external company StarSeq[®] (Mainz, Germany). The samples are prepared with the total volume of 7 μ l including plasmid DNA (600-800 ng) and primer (10 pmol; either forward or reverse). The sequencing results are aligned with the wild-type PTEN sequence (*homo sapiens*) from Uniprot¹⁴² (Uniprot-ID: P60484) using an online tool ClustalW2¹⁹⁷. The results of the sequence identification are found in the Chapter 7.2.

5.4 Protein expression using Bac-to-Bac[®] baculovirus expression system

5.4.1 Transposition

Recombinant protein expression using insect cells is performed based on Bac-to-Bac[®] baculovirus expressions system¹⁹⁸ (Figure 44). The gene of interest is transformed into bacmid DNA by transposition in DH10Bac *E. coli* cells. The resulting recombinant bacmid DNA is used for transfection of insect cells to generate recombinant baculovirus particles, which in turn are used for subsequent infection of insect cell expression culture to produce the protein of interest.

To generate the recombinant bacmid DNA harboring the gene of interest, 50 μ l chemically competent DH10bacTM *E. coli* cells are transformed with 1 – 10 ng sequence-verified PTEN construct in the pFH1 vector by heat shock transformation (Chapter 5.3.6.). Compared to the heat shock protocol described above, cells are treated differently after heat shock and re-cooling. 150 μ l LB-Medium are added to the cells and incubated at 37 °C for 4 h. Following the incubation in which transposition of the gene of interest takes place, cells are spread out on a blue-white-screening plate containing IPTG and X-gal (5-bromo-4-chloro-3-indolyl- β -D-galactopyranoside)¹⁹⁹ (Chapter 5.1.1) and incubated at 37 °C for 2 days. Upon successful transposition, colonies show white color, since the cells are not able to produce β -galactosidase, which conveys conversion of X-gal to indigo derivatives (5,5'-dibromo-4,4'-dichloro-indigo). Four positive (white) and one negative (blue) colonies are transferred to a new blue-white-screening agar plate to ensure the assay result.

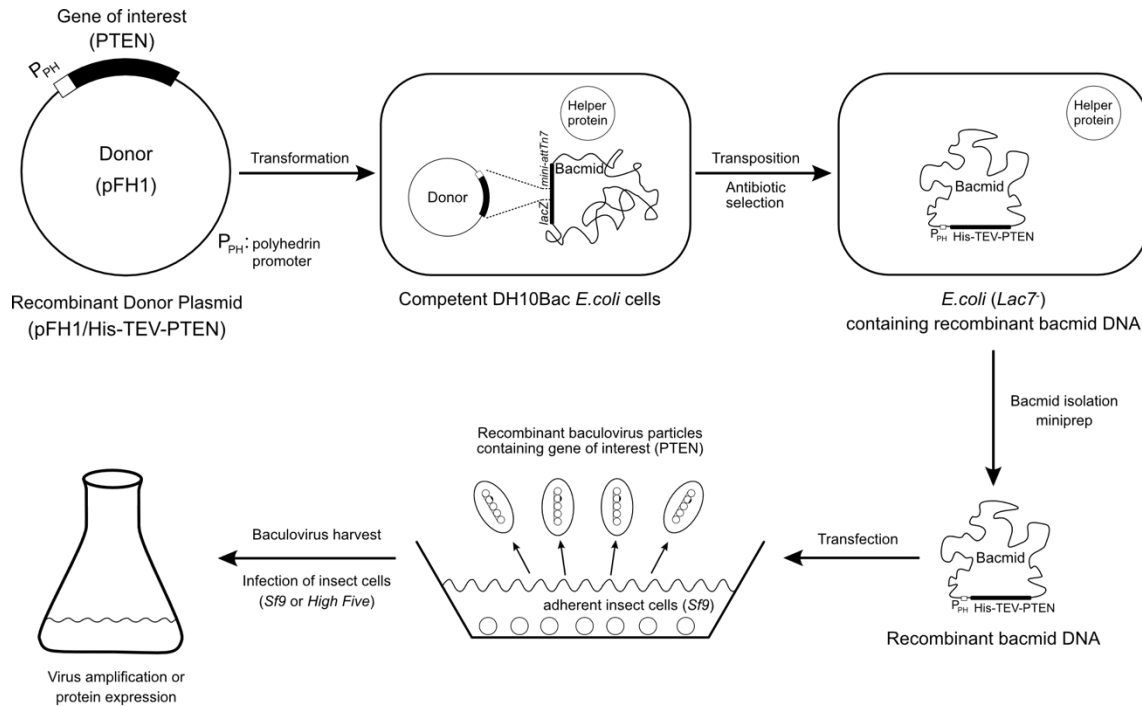


Figure 44 | General scheme of Bac-to-Bac[®] baculovirus expressions system. Gene of interest from the donor plasmid is transferred to bacmid DNA by transposition, which is subsequently isolated and used for transfection. Insect cells that carry the bacmid DNA serve to amplify baculovirus and produce the protein of interest. This figure is reconstructed based on Bac-to-Bac[®] Baculovirus Expression System manual (Invitrogen[™], 2010)¹⁷⁶.

5.4.2 Isolation of the recombinant bacmid DNA

Following the previous selection step (Chapter 5.4.1), the positive colonies (white) are used for the bacmid amplification. Each colony is inoculated in 5 ml LB media containing kanamycin (50 $\mu\text{g/ml}$), gentamycin (7 $\mu\text{g/ml}$), tetracycline (10 $\mu\text{g/ml}$) and incubated overnight at 37 °C and 160 rpm. The cell pellet is harvested by centrifugation (16,400 rcf, 2 min). The supernatant is discarded. Cell lysis is carried out using solutions supplied in a commercially available kit, QIAprep[®] Spin Miniprep Kit (QIAGEN[®]). Herein, the protocol is differentiated as follows. The cell pellet is resuspended with 300 μl *Resuspension buffer* (P1) in which RNase has been given in advance. The cell suspension is treated with 300 μl *Lysis buffer* (P2) and inverted several times. The reaction mixture is subsequently incubated for 5 min. Finally, lysis is stopped by adding 300 μl *Neutralization buffer* (N3). The mixture is incubated for 10 min on ice, followed by centrifugation for 30 min (16,400 rcf, 4 °C). 1100 μl ice-cold isopropanol is added to the supernatant fraction. Bacmid DNA is precipitated by incubation at -20 °C for 2 h and separated by centrifugation for 30 min (16,400 rcf, 4 °C). The

obtained bacmid DNA pellet is washed with 900 μ l ethanol (80 %). After the final centrifugation for 15 min (16,400 rcf, 4 °C), the supernatant is discarded and the bacmid DNA is dried on the sterile bench. Bacmid DNA is dissolved in the sterile elution buffer (40 μ l, EB, QIAprep[®] Spin Miniprep Kit). The harvested bacmid DNA is subsequently used for the transfection (Chapter 5.4.3).

5.4.3 Transfection and baculovirus amplification

Sf9 cells (insect cell line derived from *spodoptera frugiperda*) are appropriately diluted to 0.5×10^6 cells/ml with cell culture media (Spodopan, PAN[™] BIOTECH GmbH). Cells are counted using a Neubauer cell-counting chamber and trypan blue solution. 2 ml cell suspension is given to each well in 6-well cell culture plate. Thereby, one well is supplied with media only and serves as a contamination test. Cells in the culture plate are incubated for 30 min at room temperature to make them adherent to the plate. Among the remaining five wells, one well serves as a negative control for the transfection. On the other side, cells are treated with the transfection mixture that has been prepared beforehand incubating 20 μ l isolated bacmid DNA (Chapter 5.4.2), 10 μ l X-tremeGENE[™] HP DNA Transfection Reagent (Roche[®]) and 200 μ l Spodopan (PAN[™] BIOTECH GmbH) for 20 min at room temperature. The transfected cells are subsequently incubated for 3 days at 27 °C. Afterwards, cells in each well are transferred to 10 ml *Sf9* cells (1×10^6 cells/ml) which have been separately prepared in 10 cm cell culture plates. Following incubation for 4 days at 27 °C, cells are harvested and sedimented by centrifugation (500 rcf, 10 min). The baculovirus-containing supernatant is sterile filtered and supplied with 10 % (v/v) sterile fetal bovine serum (FBS). The harvested baculovirus (The first passage, V0-stock) is stored at 4 °C until further use.

The high titer baculovirus (V1) is produced for protein expression. 50 ml *Sf9* cells are prepared with the cell density of 1×10^6 cells/ml and infected with 500 μ l baculovirus (V0-stock)^{XXXI}. The cells are subsequently incubated for 5 days (27 °C, 110 rpm). Harvest of the V1-stock is carried out same as that of V0-stock.

5.4.4 Recombinant protein expression in High Five[™] insect cells.

High Five[™] cells, derived from *trichoplusia ni*, are used for overexpression of PTEN constructs. Prior to infection, cells are counted and diluted appropriately to 1×10^6 cells/ml.

^{XXXI} 500 ml Erlenmeyer flask is used for 50 ml culture volume during virus amplification.

Subsequently, High FiveTM cells are infected with 1 % (v/v) of V1 baculovirus harboring the gene of interest and incubated for 3 days at 27 °C and 110 rpm^{xxxii}. Cells are harvested by centrifugation at 4 °C (600 rcf, 20 min). The supernatant is discarded. The cell pellet is resuspended with lysis buffer (35 ml lysis buffer for 800 ml insect cell culture volume, Table 14), shock-frozen in liquid N₂ and stored at -80 °C until further use.

5.5 Recombinant protein expression in *Escherichia coli*

PTEN constructs are overexpressed in the prokaryotic host organism *E. coli*. RosettaTM (NovagenTM), a BL21 (DE3) derivative. This cell line carries an additional chloramphenicol-resistant plasmid encoding the tRNAs that are rarely used in *E. coli* (rare codons).

Competent cells of RosettaTM cell line are transformed with pET28a vector that contains the full-length PTEN construct (Chapter 5.3.6). The transformed cells are inoculated in 100 ml TB media (supplied with 50 µg/ml kanamycin and 34 µg/ml chloramphenicol) and grown overnight at 37 °C (160 rpm). On the following day, the cells are diluted 1:100 in fresh TB media (supplied with 50 µg/ml kanamycin and 34 µg/ml chloramphenicol) in a large scale and grown up to the optical density (OD₆₀₀) of ~ 0.8 (37 °C, 120 rpm). The cells are cooled down to 20 °C and treated with 0.4 mM IPTG to induce protein expression. Full-length PTEN protein is produced for the next 16 h at 20 °C (120 rpm), followed by cell harvest through centrifugation at 4 °C (20 min, 4000 rcf). The cell pellet is resuspended with lysis buffer (30 ml per 1 l cell culture, Table 14), shock-frozen in liquid N₂ and stored at -80 °C until further use.

5.6 Isolation of the recombinantly expressed proteins and their purification

5.6.1 Cell lysis

The overexpressed proteins are isolated by cell lysis and subsequent protein purification. *E. coli* cells from large-scale expression are generally disrupted by Microfluidizer[®], whereas insect cells are sonicated. In the first step, the frozen cell pellets from the previous steps (Chapters 0 and 5.5) are thawed at room temperature. A universal protease inhibitor PMSF and a reducing agent β-mercaptoethanol are added up to 1 mM and 5 mM, respectively.

^{xxxii} 2000 ml Erlenmeyer flask is used for 400 ml culture volume during protein expression.

Microfluidizer[®] - Prior to cell lysis by Microfluidizer[®], 0.05 % (v/v) DNase (10 mg/ml) is additionally given to the cell suspension. The appliance, pre-equilibrated with lysis buffer and cooled down with ice in advance, disrupts the cells by passing them through a narrow reaction chamber. Thereby, the chamber is first exposed to high pressure, then the pressure is abruptly released. This induces a shearing force in the reaction chamber. Cells are lysed in consequence. To ensure complete disruption, the cells passed through Microfluidizer[®] four times.

Sonication - Thawed High Five[™] cells are disrupted by sonication. The insect cells are treated on ice with pulsed sonication (Sonifier Cell Disruptor, Branson Sonic Power Co.) as follows: 6 x 60 s at 45 % intensity, 1 s pulse on, 1 s pulse off.

In both cases, a protein sample of the total fraction is spared for SDS-PAGE (Chapter 5.6.7) after the cell disruption. The soluble fraction containing the protein of interest is isolated by centrifugation at 4 °C (60 min, 64,000 rcf) and used to perform the following Ni-NTA affinity chromatography. A protein sample from this fraction is also taken for SDS-PAGE.

5.6.2 Ni-NTA immobilized metal ion affinity chromatography

Protein constructs discussed in this thesis harbor an *N*-terminal His₆-tag involving six histidine residues. This protein tag can be utilized for protein purification, since it has an affinity for Ni²⁺ that is immobilized to the carrier material (Nitrilotriacetic acid, NTA). Taking advantage of the affinity property, the protein of interest is bound and washed on the column, followed by elution from the column using imidazole. In general, there are two different methods to perform affinity chromatography. The first one is to employ the pre-packed column and the other is to use the column material (Ni²⁺-beads). In this study, both methods are utilized as described below.

HisTrap[™] column - Recombinant proteins produced from *E. coli* are purified at 4 °C using a peristaltic pump and 5 ml pre-packed HisTrap[™] HP-column (GE[®] Healthcare Lifesciences). The column is first equilibrated with 5 CV of the lysis buffer at 1 ml/min. The supernatant fraction of the cell lysate (Chapter 5.6.1) is subsequently flown into the column at the same flow rate. Next, the column is washed with 10 CV of the washing buffer including low concentration of imidazole (30 mM). Thereby, unspecifically bound proteins are washed out. Finally, protein of interest is collected by flowing the elution buffer including high concentration of imidazole (300 mM).

Batch-purification - Recombinant proteins produced from High Five™ cells are purified using Ni²⁺-NTA beads (QIAGEN® Superflow) in a 50 ml conical centrifuge tube. This method takes advantage of accelerated sedimentation and isolation of bead materials by centrifugation (700 rcf, 10 min, 4 °C). In the first step, Ni²⁺-NTA beads (1 ml Ni²⁺-NTA beads slurry per 1 l insect cell culture) are equilibrated with 50 ml ddH₂O and lysis buffer consecutively. After equilibration, buffer is discarded. The conical centrifuge tube including the beads is subsequently filled up with the supernatant fraction of the cell lysate, followed by incubation overnight at 4 °C and 3 rpm. Afterwards, beads are sedimented by centrifugation (700 rcf, 10 min, 4 °C). The supernatant is discarded. Beads are washed twice with 15 ml washing buffer containing 20 mM imidazole. Finally, the protein of interest is eluted with 10 ml elution buffer containing 300 mM imidazole.

In both cases, purified proteins from the elution step are furthermore subjected to the following purification step after determination of protein concentration (Chapter 5.2.2) and SDS-PAGE analysis (Chapter 5.6.7).

5.6.3 Proteolytic cleavage of the protein affinity tag

Following the affinity chromatography, His₆-tag is removed from the protein construct by protease-mediated proteolytic cleavage. In this study, proteins produced by insect cells contained a recognition sequence of TEV-protease between *N*-terminal His₆-tag and PTEN. TEV-protease cleaves its recognition site (ENLYFQ|G) specifically and leaves the protein construct without cloning artifacts except for an *N*-terminal glycine residue. His₆-tagged TEV-protease is supplied by DPF (Dortmunder Protein Facility, MPI Dortmund). According to the manufacturer's data sheet, 1 mg of protein (75 kDa) harboring the TEV-recognition sequence is suggested to be digested with 0.06 mg TEV-protease. Concerning different protease concentrations in every purification batch, the concentration statement of the TEV-protease is not provided in this thesis. The elution fraction from the affinity chromatography is treated with an appropriate amount of TEV-protease and incubated overnight at 4 °C. The success of the cleavage is determined by SDS-PAGE (Chapter 5.6.7).

5.6.4 Ion exchange chromatography

Proteins can be separated by their overall charges using ion exchange chromatography. The purification principle is based on the electrostatic interaction between mobile phase (proteins) and immobilized one (ligands linked with a column matrix). Proteins can be eluted separately

with increasing ionic strength of the running buffer (*e.g.* salt gradient or changing pH). Depending on the charge of the ligands, ion exchange chromatography columns are categorized into cation (anionic ligands on the bead material) and anion (cationic ligands) exchangers. Cation exchanger can be used for purification in the case of theoretical isoelectric points (pI values) higher than pH of the running buffer and vice versa. In this study, theoretical isoelectric points (pI values) of each protein construct have been calculated using ProtParam tool¹⁸¹ in advance (Table 30). PTEN constructs including the C-terminal tail show lower pI than pH of the running buffer, due to the acidic residues in the tail region. Therefore, anion exchanger is employed. In contrast, cation exchanger is the choice for PTEN core domains (*t*PTEN).

Table 30 | Theoretical isoelectric points calculated by ProtParam tool¹⁸¹. The calculation is based on the amino acid property. Post-translational modification such as phosphorylation is not considered in the calculation.

| PTEN constructs | Isoelectric points (pI-values) |
|-----------------------|--------------------------------|
| PTEN (1-403) | 5.95 |
| PTEN (7-353) Δ286-309 | 8.69 |

Full-length PTEN is purified using MonoQTM 5/50 GL column (CV, 1 ml; GE[®] Healthcare Lifesciences). The column is first equilibrated with 5 CV of IEX-buffer A containing 100 mM NaCl. Subsequently, full-length PTEN is loaded onto the column at a flow rate of 1 ml/min. The column is subsequently washed with 5 CV of IEX-buffer A. Protein of interest is eluted by increasing the NaCl concentration from 100 mM to 500 mM over 125 CV with linear gradient. For the protein elution, 0.5 ml/min is used as a flow rate. *t*PTEN is purified using HiTrapTM SP HP (CV, 5 ml; GE[®] Healthcare Lifesciences). General procedure is same as the description for anion exchange chromatography, except the gradient setting. NaCl concentration is increased from 100 mM to 400 mM over 12 CV. In both cases, protein elution is detected by absorbance at 280 nm and subsequently analyzed by SDS-PAGE (Chapter 5.6.7). Ion exchange chromatography columns are connected with Äkta FPLC (GE[®] Healthcare Lifesciences) during purification and controlled via Unicorn software (GE[®] Healthcare Lifesciences).

5.6.5 Protein Ultrafiltration

PTEN is concentrated before the size exclusion chromatography and after the final purification. Utilizing the centrifugal force, proteins are concentrated on the filter membrane, which is supplied with different pore sizes involving the molecular weight cut-off. In preparation for protein concentration, Amicon[®] Ultra Centrifugal Filter Unit (Merck Millipore) with 10 kDa cut-off is equilibrated by passing buffer through the filter membrane. It is facilitated by centrifuging the Amicon[®] Ultra Centrifugal Filter Unit for 10 min at 3,000 rcf and 4 °C. Thereby, trace of glycerol can be removed in the membrane. After discarding the buffer passed through, protein solution is transferred onto the filter membrane and centrifugation is run as mentioned above. Duration of the concentration depends on the total volume, molecular weight of the protein, purity, mono-dispersity, and the final protein concentration. Finally, protein concentration is determined by NanoDrop[®] (Chapter 5.2.2).

5.6.6 Size exclusion chromatography

Final protein purification is performed using size exclusion chromatography. Its principle is based on the separation of molecules by size. Together with its purification property, this method allows to determine protein size in the native state and to change the buffer environment of the protein of interest.

Prior to running size exclusion chromatography, protein constructs are concentrated (Chapter 5.6.5) and subsequently centrifuged in order to remove any precipitation (16,400 rcf, 4 °C, 15 min), while the corresponding column is equilibrated with 1.5 CV of the filtered and degassed buffer (Table 14). Next, the prepared protein sample is injected onto the column and 1 CV of the buffer is run with flow rate of 1 ml/min (preparative, HiLoad[™] 16/60 Superdex[™] 200 preparative grade) or 0.5 ml/min (analytical, Superdex[™] 200 10/30 GL analytical grade) at 4 °C. Protein elution is detected by absorbance at 280 nm and analyzed using SDS-PAGE (Chapter 5.6.7). Size exclusion chromatography columns are connected with Äkta FPLC (GE[®] Healthcare Lifesciences) and controlled via Unicorn software (GE[®] Healthcare Lifesciences).

5.6.7 SDS-Polyacrylamide gel electrophoresis (SDS-PAGE)

SDS-PAGE^{xxxiii} is employed to analyze the protein overexpression and its purity during protein purification. During the electrophoresis, protein samples run through polyacrylamide gel and can be separated by size. The ratio of acrylamide used for polymerization varies depending on size of the protein of interest. Since PTEN constructs used in this study lie between 30 and 50 kDa, 12 % SDS gels are utilized for the separating gel (Table 31). Prior to the electrophoresis, protein samples are prepared by incubating with 5 x SDS sample buffer (Table 16) at 95 °C for 10 min.

Table 31 | Component scheme for the SDS polyacrylamide gel preparation.

| Component | Volume Separating gel (12 %) (Two gels) | Volume Stacking gel (Two gels) |
|--------------------------------|---|--------------------------------------|
| ddH ₂ O | 4.9 ml | 4.2 ml |
| 30 % Acrylamide (4K solution) | 6.0 ml | 1.0 ml |
| Tris buffer for separating gel | 3.8 ml | |
| Tris buffer for stacking gel | | 760 µl |
| 10 % SDS (w/v) | 150 µl | 60 µl |
| 10 % APS (w/v) | 150 µl | 60 µl |
| TEMED | 6 µl | 6 µl |

10 µl of prepared samples and 4 µl of prestained protein standard marker (Page RulerTM Plus Prestained Protein Ladder, FermentasTM) are given to each pocket in the gel that has been soaked in the SDS running buffer in advance. The electrophoresis is run under 160 V (constant voltage) for 70 min. SDS gels are transferred to the staining buffer (Table 16), boiled via microwave and incubated for 20 min at room temperature. Stained SDS gels are furthermore destained in boiling water, until the protein bands are clearly visible and the background blue staining is no longer present. The destained gels are documented with a scanner.

^{xxxiii} In this study, Tris-Glycine SDS-PAGE is used based on Laemmli et al. (1970)²⁰⁵.

5.7 Protein crystallization and structure determination

5.7.1 Protein crystallization

Full-length PTEN (PTEN 1-403) is used for protein crystallization with commercially available pre-mixed crystallization buffers (Qiagen[®] NeXtal JCSG Core Suites, Chapter 3.4.1). Each suite involves 96 conditions. Initial crystallization condition screening is carried out in 96-unit plate format (3553, Corning[®]), in which one large well for the reservoir solution and three small wells for protein drops make up one unit. Applying the sitting-drop vapor diffusion method²⁰⁶, protein solution containing PTEN is incubated with each reservoir solution of the suite. Reservoir solution (70 μ l) of each crystallization condition is transferred to the large well of each unit on the 96-unit plate. The three small wells per unit are filled with protein solution (100 nl) involving three different concentrations (7, 14 and 21 mg/ml), followed by transfer of the corresponding reservoir solution (100 nl) onto the protein drops (ratio 1:1). This was carried out at 20 °C using the pipetting robot Mosquito (TTP Labtech). The 96-unit plate is sealed with a transparent film and incubated in a Rock Imager 1000 (Formulatrix) at 20 or 4 °C, respectively. The crystallization process of each well is automatically recorded as an image in the regular terms and monitored using software Rock Maker 2.0 (Formulatrix).

*t*PTEN (PTEN 7-353 Δ 286-309) is crystallized based on the known crystallization condition (100 mM Tris, 1.3 M Na/K L(+)-tartrate and 5 – 10 % glycerol, 10 mM DTT (pH 8.0)). Applying the hanging-drop vapor diffusion method²⁰⁶, protein solution containing *t*PTEN is incubated with the reservoir solution in the 24-well plate format (Crystalgen 24 Well SuperClear[™] Plates, pregreased, Jena Bioscience). Thereby, pH (pH 6 – 10)^{xxxiv}, temperature (20 or 4 °C), tartrate (1.2 – 1.35 M) and glycerol concentration (5 – 20 %) are varied to find the optimal condition. DTT is not added for the following soaking experiments. Reservoir solution of each crystallization condition (700 μ l) is given to the well in a corresponding position. Protein solution of *t*PTEN (20 mg/ml, 1 μ l) is mixed with 1 μ l of the reservoir solution on 22 mm cover slides (ratio 1:1). The cover slide is turned upside down, sealed on each well and incubated. Crystal growth is monitored everyday.

^{xxxiv} For the range of each pH, different buffer is utilized. pH 6 – 6.5: MES, pH 7 – 8.5: TRIS, pH 9 – 10: CAPS.

5.7.2 Freezing of protein crystals

Prior to data collection, protein crystals are frozen for protection from radiation damage. However, freezing process of biological macromolecules leads to formation of crystalline ice, which results in crystal damage. Therefore, protein crystals should be frozen in a cryo solution, which is supplemented with frost protection agent (*e.g.* glycerol, ethylene glycol, xylitol) and facilitates vitreous freezing of water and crystallization solution. In the case of *t*PTEN, protein crystals are incubated in reservoir solution supplemented with 25 % glycerol (cryo solution, Table 17) for 2 min. *t*PTEN crystals are subsequently flash-frozen in liquid N₂.

5.7.3 Ligand-soaking experiment

The crystal structures of H₂O₂- and bpV-phen-treated *t*PTEN (Ox) are obtained by soaking the protein crystals (reduced, Chapter 5.7.1) in the crystallization buffers supplemented with 1 mM H₂O₂ (*t* = 1 h) and 1 mM bpV-phen (*t* = 4 h), respectively. After incubation, the protein crystals are back-soaked with cryo solution (Table 17, Chapter 5.7.2) for 10 min and flash-frozen in liquid N₂.

5.7.4 Data collection

X-ray dataset is collected at synchrotron (beamline PXII, Swiss Light Source, Villigen, Switzerland). During data collection, protein crystals are kept under the cryo stream at 100 K (-173 °C)¹⁵⁵. Crystals are rotated by 360° with an oscillation range of 0.25°¹⁵⁶ and exposed to 20 % attenuation of radiation with 0.1 s exposure time for one frame. PILATUS detector is employed for detection and positioned with a distance of 345. For reduced and H₂O₂-treated PTEN crystals, monochromatic radiation is set at the wavelength of 1.000 Å, while the wavelength of 1.771 Å is applied for reduced and bpV-phen-treated PTEN crystals, in which anomalous scattering is utilized.

5.7.5 Data processing

Data collection results in a set of detection images (frames), which involves a pattern of reflections occurring from X-ray diffraction of the protein crystal. Each frame represents a small wedge of structural information generated by the rotation of the crystal in the X-ray beam. In addition, reflections on the detector images are distorted due to projection on the two-dimensional detector. For that reason, data processing serves to reconstruct the undistorted three-dimensional lattice. The underlying Bravais Lattice, space group symmetry

and unit cell geometries are determined from the reflection positions. A corresponding Miller index (h, k, l) is assigned to each reflection, followed by quantification of its intensity. Afterwards, symmetry-related reflections must be put on the same intensity. This is due to possible incidences such as change of the X-ray intensity during data collection, potential difference of sensitivity in different regions of the detector and the crystal larger in one direction than another. Finally, the structure factor amplitudes are calculated, which are the essential terms to generate electron density maps.

The software XDS¹⁵⁷ serves to calculate intensities of all reflections and index them. The scaling of intensities is performed with the software XSCALE¹⁵⁷. XDSCONV¹⁵⁷ is furthermore applied to calculate the structure factor amplitudes of the scaled intensities. For tPTEN structures, space group C222₁ (SG No. 20) and unit cell constants (a = 206 Å, b = 206 Å, c = 89 Å; α = 90°, β = 90° γ = 90°) are given for data processing.

5.7.6 Computer-aided structure determination

The structure factor $\mathbf{F}(\mathbf{hkl})$ is a mathematical description of diffracted X-ray radiation that produces reflections at a detector. $\mathbf{F}(\mathbf{hkl})$ accounts for scattering property of hkl as a Fourier-series and can be decomposed into the sum of simple oscillating functions. Every single term in the factor corresponds to contribution of an atom to reflections hkl. $\mathbf{F}(\mathbf{hkl})$ is composed of amplitude $|F(\mathbf{hkl})|$ and phase term $\exp(i\alpha(\mathbf{hkl}))$ as described in Eq. 2.

$$\mathbf{F}(\mathbf{hkl}) = |F(\mathbf{hkl})| \cdot \exp(i\alpha(\mathbf{hkl})) \quad (\text{Eq. 2})$$

$\mathbf{F}(\mathbf{hkl})$: structure factor; $|F(\mathbf{hkl})|$: structure factor amplitude; $\exp(i\alpha(\mathbf{hkl}))$: phase term of the structure factor

The structure factor $\mathbf{F}(\mathbf{hkl})$ allows to calculate electron density around the atoms in a unit cell. The electron density ρ at position x, y, z in the Cartesian coordinate system of the unit cell can be determined with following equations (Eq. 3 and 4).

$$\rho(xyz) = \frac{1}{V} \sum_{\mathbf{hkl}} \mathbf{F}(\mathbf{hkl}) \cdot \exp(-2\pi i(hx + ky + lz)) \quad (\text{Eq. 3})$$

$$= \frac{1}{V} \sum_{\mathbf{hkl}} |F(\mathbf{hkl})| \cdot \exp(i\alpha(\mathbf{hkl})) \cdot \exp(-2\pi i(hx + ky + lz)) \quad (\text{Eq. 4})$$

$\rho(xyz)$: electron density in the Cartesian coordinate system at the position x, y, z; V: volume of the unit cell; $\mathbf{F}(\mathbf{hkl})$: structure factor; $|F(\mathbf{hkl})|$: structure factor amplitude; $\exp(i\alpha(\mathbf{hkl}))$: phase term of the structure factor

Although the structure factor amplitude $|F(hkl)|$ can be calculated using measured intensities of the diffraction pattern, the phase term $\exp(i\alpha(hkl))$ cannot be derived directly from the measurement, while this term is an indispensable factor to calculate the electron density. This is also known as “phase problem”. In this study, the phase problem is resolved using molecular replacement (MR) method²⁰⁷. This method is based on utilizing phase term of the available crystal structure as a template. Therefore, it is prerequisite that the template structure involves high sequence homology to the crystallized protein. However, such template structures are frequently crystallized in a distinguished packing involving different crystallographic parameters (*e.g.* space group, unit cell constants etc.). Hence, MR method rotates and translates the template molecule within the unit cell. The structure factor amplitude of the template structure ($|F_{\text{cal}}|$) is determined at each position and compared with the observed one ($|F_{\text{obs}}|$). This method runs, until the maximal likelihood of its position and orientation is reached. In the case of *t*PTEN, a structural solution is yielded by the software PhaserMR (CCP4 suite^{200,201}). The previously reported PTEN crystal structure (PDB⁴²: 1D5R⁴³) is employed as a template.

Applying the measured structure factor amplitude $|F_{\text{obs}}(hkl)|$ and the phase term α_{hkl} obtained from molecular replacement, the electron density map can be generated. This allows to build the structure model *t*PTEN in its electron density, which is facilitated by the software Coot²⁰². The following refinement process using Refmac²⁰³ corrects geometric parameters of the structure model (*e.g.* bond lengths and angles between atoms) and approximates the calculated structural factor amplitude of the current model $|F_{\text{calc}}(hkl)|$ to the observed one $|F_{\text{obs}}(hkl)|$. In the case of *t*PTEN, structure refinement is performed with the detwin function, due to the twinned character of the crystals. The refinement process provides a new refined model and structure factor. The structure model can be subsequently improved by manual structure correction, followed by repeated refinement in the iterative way, until both structure factor amplitudes ($|F_{\text{obs}}(hkl)|$ and $|F_{\text{calc}}(hkl)|$) have reached the maximal agreement. As a measure of model quality, crystallographic R-factor R_{cryst} is applied to demonstrate the discrepancy between the observed data and the structure model. The smaller R_{cryst} is, the better the model is in accordance with the measured data. Since new structure factor is calculated based on the refined structure, erroneously refined region in the model can influence the calculation of the phase and results in biased model. Therefore, 5 % of the measured reflections are not included for the refinement process. Analogous to R_{cryst} (also called R_{work}), R_{free} is additionally calculated, which reflects the debiased R-factor. Difference

of both values should not be larger than 5 %^{208,209}. Processing and refinement statistics are summarized in Table 4, Table 7 and Table 9.

$$R_{cryst} = \frac{\sum ||F_{obs}| - |F_{calc}||}{\sum |F_{obs}|} \quad (\text{Eq. 5})$$

R: R-factor; F_{obs} : observed structural factor (experimental data); F_{calc} : calculated structural factor.

Generation of $2 F_o - F_c$ omit maps is carried out using Sfcheck (CCP4 suite^{200,201}). The anomalous scattering electron density maps are rendered by performing an additional data processing without adhering to Friedel's law, followed by calculation using Refmac, Cad, and FFT (CCP4 suite^{200,201}). All figures involving crystal structures are generated using Pymol²⁰⁴.

Table 32 | Summary of utilized softwares for X-ray crystallographic analysis.

| Package | Software | Usage |
|------------|---------------|----------------------------------|
| XDS suite | XDS | Data processing |
| | XSCALE | Scaling of dataset |
| | XDSCONV | File format conversion |
| CCP4 suite | CAD | Anomalous density map |
| | FFT | Map generation |
| | Sfcheck | Omit map calculation |
| | Matthews_coef | Matthews coefficient calculation |
| | PhaserMR | Molecular replacement |
| | Refmac | Structure refinement |
| | - | Pymol |
| - | Coot | Model building |

5.8 Malachite green activity assay

5.8.1 Determination of phosphatase activity

Phosphatase activity of PTEN is investigated using PI(3,4,5)P₃ diC8 as a substrate. This compound is a natural substrate PIP₃ derivative truncated at fatty acid side chains. It is used to ensure the solubility and homogeneity of the assay. 60 nM PTEN is pre-treated with buffer either lacking or containing additives *e.g.* 50 μM PIP₂, 50 μM nhPIP₃, 400 μM H₂O₂, 1 μM bpV-phen, 1 μM bpV-pic, or 1 μM bpV-HOpic for 10 min (Figure 18). Phosphatase reaction is initiated by addition of PIP₃ (final: 50 nM PTEN, 75 μM PIP₃). The reaction mixture is incubated at 25 °C for 30 min. The reaction is quenched by transferring the reaction mixture

($V = 25 \mu\text{l}$) to malachite green solution ($V = 100 \mu\text{l}$, Echelon Biosciences[®]) that has been prepared in 96-well plate (transparent, flat bottom) beforehand. Following color development for 30 min, absorbance of each well is measured at 620 nm employing a plate reader Safire2[™]. The absorption values are converted to the released orthophosphate amount by extrapolating from the standard phosphate-malachite green curve. Relative PTEN activity is determined relative to untreated wild-type PTEN (devoid of activity modulators). Measurements are carried out in triplicates. GraphPad Prism[™] is used to calculate the relative PTEN activity including standard deviation.

For clarity, substrate and additives are denoted in simplified forms. All phosphoinositide-derived compounds *e.g.* PIP₂, PIP₃, nhPIP₃ involve truncated fatty acid side chains diC8.

5.8.2 IC₅₀ determination of PTEN inhibitors

Half maximal concentrations (IC₅₀) of H₂O₂, bpV-phen, bpV-pic and bpV-HOpic are determined. Full-length PTEN is treated with the inhibitors at 25 °C for 10 min, which have been prepared with a 10-fold serial dilution beforehand. Concentrations of PTEN and the inhibitors during the treatment are as follows. PTEN: 60 nM; H₂O₂: 40 mM to 4 nM; bpV-phen: 0.3 mM to 0.3 nM – 150 nM bpV-phen is included; bpV-pic / bpV-HOpic: 0.08 mM to 0.08 nM – 1 μM and 40 nM bpV-pic / bpV-HOpic are included (Figure 20). The subsequent addition of PI(3,4,5)P₃ diC8 triggers the phosphatase reaction. The reaction mixture is incubated at 25 °C for 30 min (final: 50 nM PTEN, 75 μM PI(3,4,5)P₃ diC8). The reaction is quenched by transferring the reaction mixture ($V = 25 \mu\text{l}$) to malachite green solution ($V = 100 \mu\text{l}$, Echelon Biosciences[®]). Following color development for 30 min, absorbance of each well is measured at 620 nm employing a plate reader Safire2[™]. The absorption values are converted to the released orthophosphate amount to determine the relative phosphatase activity. Measurements are carried out in triplicates. GraphPad Prism[™] is used to calculate the relative PTEN activity including standard deviation.

5.8.3 Characterization of reversible property of phosphatase inhibition

For initial phosphatase inhibition, 100 μM full-length PTEN is incubated with either 3.5 mM H₂O₂ or 400 μM bpV-phen for 10 min. Each reaction sample is subsequently diluted with reaction buffer lacking reducing agents (mock) or containing DTT, GSH or Trx system to the following concentrations for 10 min: 5 μM PTEN, 4 mM DTT or GSH, Trx system (5 μM thioredoxin, 0.1 μM thioredoxin reductase and 200 μM NADPH). The following addition of

PI(3,4,5)P₃ diC8 triggers the phosphatase reaction (final: 1 μM PTEN, 75 μM PI(3,4,5)P₃ diC8). The reaction mixture is incubated at 25 °C for 30 min. The reaction is quenched by transferring the reaction mixture (V = 25 μl) to malachite green solution (V = 100 μl, Echelon Biosciences®). Following color development for 30 min, absorbance of each well is measured at 620 nm employing a plate reader Safire2™. The absorption values are converted to the released orthophosphate amount to determine the relative phosphatase activity. Measurements are carried out in triplicates. GraphPad Prism™ is used to calculate the relative PTEN activity including standard deviation.

5.8.4 Characterization of inhibitory effect of orthovanadate on PTEN

60 nM Full-length PTEN is pre-incubated with either reaction buffer, 0.01 mM bpV-phen or sodium orthovanadate (0.01, 0.1, 1 mM) for 10 min. PI(3,4,5)P₃ diC8 is added to each reaction mixture, followed by incubation for 30 min at 25 °C (final: 50 nM PTEN, 75 μM PI(3,4,5)P₃ diC8). The reaction is quenched by transferring the reaction mixture (V = 25 μl) to malachite green solution (V = 100 μl, Echelon Biosciences®). Following color development for 30 min, absorbance of each well is measured at 620 nm employing a plate reader Safire2™. The absorption values are converted to the released orthophosphate amount to determine the relative phosphatase activity. Measurements are carried out in triplicates. GraphPad Prism™ is used to calculate the relative PTEN activity including standard deviation.

5.8.5 Impact of tartrate on redox-mediated inhibition and reactivation of PTEN

To explore the impact of tartrate under ligand-soaking condition, redox-mediated inhibition and reactivation are tested in the presence of K/Na L(+)-tartrate and compared to tartrate-lacking samples. 50 μM full-length PTEN is first incubated with reaction buffer lacking or containing 5 mM H₂O₂ in the presence or absence of 1.5 M K/Na L(+)-tartrate for 20 min. Each reaction sample is subsequently treated with buffer containing or lacking DTT (final: 2.5 μM PTEN, 4 mM DTT) for 10 min. The concentration of K/Na L(+)-tartrate is maintained at 1.5 M for the tartrate-containing samples during dilution. The following addition of PI(3,4,5)P₃ diC8 triggers the phosphatase reaction (final: 50 nM PTEN, 75 μM PI(3,4,5)P₃ diC8). The reaction mixture is incubated at 25 °C for 30 min. The reaction is quenched by transferring the reaction mixture (V = 25 μl) to malachite green solution (V = 100 μl, Echelon Biosciences®). Following color development for 30 min, absorbance of each well is measured

at 620 nm employing a plate reader Safire2TM. The absorption values are converted to the released orthophosphate amount to determine the relative phosphatase activity. Measurements are carried out in triplicates. GraphPad PrismTM is used to calculate the relative PTEN activity including standard deviation.

5.8.6 Kinetic measurement of phosphatase inhibition by H₂O₂

For initial oxidative inhibition, 100 μM full-length PTEN is treated with H₂O₂ (2, 5 or 20 mM) for the following time ranges: 5, 10, 20, 40 or 80 min (Figure 33). Each reaction sample is subsequently diluted with reaction buffer in the absence (mock) or presence of DTT (final: 5 μM PTEN, 10 mM DTT). The samples are incubated at 25 °C for 20 min. The following addition of PI(3,4,5)P₃ diC8 triggers the phosphatase reaction (final: 1 μM PTEN, 75 μM PI(3,4,5)P₃ diC8). The reaction mixture is incubated at 25 °C for 30 min. The reaction is quenched by transferring the reaction mixture (V = 25 μl) to malachite green solution (V = 100 μl, Echelon Biosciences[®]). Following color development for 30 min, absorbance of each well is measured at 620 nm employing a plate reader Safire2TM. The absorption values are converted to the released orthophosphate amount to determine the relative phosphatase activity. Measurements are carried out in triplicate of triplicates. GraphPad PrismTM is used to calculate the relative PTEN activity including standard deviation.

5.9 Sample preparation for mass-spectrometric methods

100 μM PTEN constructs (full-length PTEN or PTEN 7-353 Δ286-309) are incubated with either reaction buffer, 1 mM H₂O₂ or 1 mM bpV-phen for 10 min at 25 °C. Subsequently, each sample is treated with iodoacetamide (2 mM, T = 25 °C, t = 10 min) for alkylation of free thiols and denatured in 8 M Urea. The following tryptic digest, HPLC-MS, MS/MS measurements and the corresponding data analysis are carried out by Dr. Tanja Bange and Franzisk Müller (MPI Dortmund). For more details about procedures, see reference No. 171.

6 References

1. Cohen, P. The origins of protein phosphorylation. *Nature* **4**, E127–E130 (2002).
2. Bialy, L. & Waldmann, H. Inhibitors of protein tyrosine phosphatases: next-generation drugs? *Angew. Chem. Int. Ed. Engl.* **44**, 3814–3839 (2005).
3. Hunter, T. & Cooper, J. A. Protein-tyrosine kinases. *Annu. Rev. Biochem.* **54**, 897–930 (1985).
4. Hunter, T. Signaling - 2000 and beyond. *Cell* **100**, 113–127 (2000).
5. Hunter, T. & Sefton, B. M. Transforming gene product of Rous sarcoma virus phosphorylates tyrosine. *Proceedings of the National Academy of Sciences* **77**, 1311–1315 (1980).
6. Zhang, Z.-Y. Protein tyrosine phosphatases: structure and function, substrate specificity, and inhibitor development. *Annu. Rev. Pharmacol. Toxicol.* **42**, 209–234 (2002).
7. Picotti, P. Phosphoproteomics takes it easy. *Nat Biotechnol* **33**, 929–930 (2015).
8. Zhang, Z. Y. & Dixon, J. E. Active site labeling of the Yersinia protein tyrosine phosphatase: the determination of the pKa of the active site cysteine and the function of the conserved histidine 402. *Biochemistry* **32**, 9340–9345 (1993).
9. Peters, G. H., Frimurer, T. M. & Olsen, O. H. Electrostatic evaluation of the signature motif (H/V)CX5R(S/T) in protein-tyrosine phosphatases. *Biochemistry* **37**, 5383–5393 (1998).
10. Tonks, N. K. Protein tyrosine phosphatases: from genes, to function, to disease. *Nat. Rev. Mol. Cell Biol.* **7**, 833–846 (2006).
11. Zhao, S., Sedwick, D. & Wang, Z. Genetic alterations of protein tyrosine phosphatases in human cancers. *Oncogene* **34**, 3885–3894 (2014).
12. Alonso, A. *et al.* Protein tyrosine phosphatases in the human genome. *Cell* **117**, 699–711 (2004).
13. Zhao, S., Sedwick, D. & Wang, Z. Genetic alterations of protein tyrosine phosphatases in human cancers. *Oncogene* **34**, 3885–3894 (2015).
14. Li, X. *et al.* Eya protein phosphatase activity regulates Six1-Dach-Eya transcriptional effects in mammalian organogenesis. *Nature* **426**, 247–254 (2003).
15. Tootle, T. L. *et al.* The transcription factor Eyes absent is a protein tyrosine phosphatase. *Nature* **426**, 299–302 (2003).
16. Rayapureddi, J. P. *et al.* Eyes absent represents a class of protein tyrosine

- phosphatases. *Nature* **426**, 295–298 (2003).
17. Steck, P. A. *et al.* Identification of a candidate tumour suppressor gene, MMAC1, at chromosome 10q23.3 that is mutated in multiple advanced cancers. *Nat. Genet.* **15**, 356–362 (1997).
 18. Li, J. *et al.* PTEN, a putative protein tyrosine phosphatase gene mutated in human brain, breast, and prostate cancer. *Science* **275**, 1943–1947 (1997).
 19. Myers, M. P. *et al.* The lipid phosphatase activity of PTEN is critical for its tumor suppressor function. *Proc. Natl. Acad. Sci. U.S.A.* **95**, 13513–13518 (1998).
 20. Singh, G. & Chan, A. Post-Translational Modifications of PTEN and their Potential Therapeutic Implications. *CCDT* **11**, 536–547 (2011).
 21. Song, M. S., Salmena, L. & Pandolfi, P. P. The functions and regulation of the PTEN tumour suppressor. *Sci. Rep.* **13**, 283–296 (2012).
 22. Park, K. K. *et al.* Promoting axon regeneration in the adult CNS by modulation of the PTEN/mTOR pathway. *Science* **322**, 963–966 (2008).
 23. Liu, K. *et al.* PTEN deletion enhances the regenerative ability of adult corticospinal neurons. *Nat. Neurosci.* **13**, 1075–1081 (2010).
 24. Sun, F. *et al.* Sustained axon regeneration induced by co-deletion of PTEN and SOCS3. *Nature* **480**, 372–375 (2011).
 25. Stambolic, V. *et al.* Negative regulation of PKB/Akt-dependent cell survival by the tumor suppressor PTEN. *Cell* **95**, 29–39 (1998).
 26. Vivanco, I. & Sawyers, C. L. The phosphatidylinositol 3-Kinase AKT pathway in human cancer. *Nat. Rev. Cancer* **2**, 489–501 (2002).
 27. Taniguchi, C. M., Emanuelli, B. & Kahn, C. R. Critical nodes in signalling pathways: insights into insulin action. *Nat. Rev. Mol. Cell Biol.* **7**, 85–96 (2006).
 28. Alessi, D. R. *et al.* Characterization of a 3-phosphoinositide-dependent protein kinase which phosphorylates and activates protein kinase B alpha. *Curr. Biol.* **7**, 261–269 (1997).
 29. Franke, T. F. *et al.* The protein kinase encoded by the Akt proto-oncogene is a target of the PDGF-activated phosphatidylinositol 3-kinase. *Cell* **81**, 727–736 (1995).
 30. Burgering, B. M. & Coffey, P. J. Protein kinase B (c-Akt) in phosphatidylinositol-3-OH kinase signal transduction. *Nature* **376**, 599–602 (1995).
 31. Laplante, M. & Sabatini, D. M. mTOR signaling at a glance. *J. Cell. Sci.* **122**, 3589–3594 (2009).
 32. Maehama, T. & Dixon, J. E. The tumor suppressor, PTEN/MMAC1,

- dephosphorylates the lipid second messenger, phosphatidylinositol 3,4,5-trisphosphate. *Journal of Biological Chemistry* **273**, 13375–13378 (1998).
33. Sun, H. *et al.* PTEN modulates cell cycle progression and cell survival by regulating phosphatidylinositol 3,4,5,-trisphosphate and Akt/protein kinase B signaling pathway. *Proceedings of the National Academy of Sciences* **96**, 6199–6204 (1999).
 34. Myers, M. P. *et al.* P-TEN, the tumor suppressor from human chromosome 10q23, is a dual-specificity phosphatase. *Proc. Natl. Acad. Sci. U.S.A.* **94**, 9052–9057 (1997).
 35. Tamura, M. *et al.* PTEN interactions with focal adhesion kinase and suppression of the extracellular matrix-dependent phosphatidylinositol 3-kinase/Akt cell survival pathway. *Journal of Biological Chemistry* **274**, 20693–20703 (1999).
 36. Lietha, D. *et al.* Structural basis for the autoinhibition of focal adhesion kinase. *Cell* **129**, 1177–1187 (2007).
 37. Tamura, M. *et al.* Inhibition of cell migration, spreading, and focal adhesions by tumor suppressor PTEN. *Science* **280**, 1614–1617 (1998).
 38. Tamura, M., Gu, J., Takino, T. & Yamada, K. M. Tumor suppressor PTEN inhibition of cell invasion, migration, and growth: differential involvement of focal adhesion kinase and p130Cas. *Cancer Res.* **59**, 442–449 (1999).
 39. Shi, Y. *et al.* PTEN is a protein tyrosine phosphatase for IRS1. *Nat Struct Mol Biol* **21**, 522–527 (2014).
 40. Tibarewal, P. *et al.* PTEN protein phosphatase activity correlates with control of gene expression and invasion, a tumor-suppressing phenotype, but not with AKT activity. *Sci Signal* **5**, ra18–ra18 (2012).
 41. Keniry, M. & Parsons, R. The role of PTEN signaling perturbations in cancer and in targeted therapy. *Oncogene* **27**, 5477–5485 (2008).
 42. Bernstein, F. C. *et al.* The Protein Data Bank: a computer-based archival file for macromolecular structures. *Ann. Rev. Biochem.* **112**, 535–542 (1977).
 43. Lee, J. O. *et al.* Crystal structure of the PTEN tumor suppressor: implications for its phosphoinositide phosphatase activity and membrane association. *Cell* **99**, 323–334 (1999).
 44. Yuvaniyama, J., Denu, J. M., Dixon, J. E. & Saper, M. A. Crystal structure of the dual specificity protein phosphatase VHR. *Science* **272**, 1328–1331 (1996).
 45. Maehama, T., Taylor, G. S. & Dixon, J. E. PTEN and myotubularin: novel phosphoinositide phosphatases. *Annu. Rev. Biochem.* **70**, 247–279 (2001).
 46. Torres, J. *et al.* Phosphorylation-regulated cleavage of the tumor suppressor PTEN by

- caspace-3: implications for the control of protein stability and PTEN-protein interactions. *Journal of Biological Chemistry* **278**, 30652–30660 (2003).
47. Trotman, L. C. *et al.* Ubiquitination regulates PTEN nuclear import and tumor suppression. *Cell* **128**, 141–156 (2007).
 48. Campbell, R. B., Liu, F. & Ross, A. H. Allosteric activation of PTEN phosphatase by phosphatidylinositol 4,5-bisphosphate. *Journal of Biological Chemistry* **278**, 33617–33620 (2003).
 49. Funamoto, S., Meili, R., Lee, S., Parry, L. & Firtel, R. A. Spatial and temporal regulation of 3-phosphoinositides by PI 3-kinase and PTEN mediates chemotaxis. *Cell* **109**, 611–623 (2002).
 50. Iijima, M. & Devreotes, P. Tumor suppressor PTEN mediates sensing of chemoattractant gradients. *Cell* **109**, 599–610 (2002).
 51. McConnachie, G., Pass, I., Walker, S. M. & Downes, C. P. Interfacial kinetic analysis of the tumour suppressor phosphatase, PTEN: evidence for activation by anionic phospholipids. *Biochem. J.* **371**, 947–955 (2003).
 52. Iijima, M., Huang, Y. E., Luo, H. R., Vazquez, F. & Devreotes, P. N. Novel mechanism of PTEN regulation by its phosphatidylinositol 4,5-bisphosphate binding motif is critical for chemotaxis. *Journal of Biological Chemistry* **279**, 16606–16613 (2004).
 53. Walker, S. M., Leslie, N. R., Perera, N. M., Batty, I. H. & Downes, C. P. The tumour-suppressor function of PTEN requires an N-terminal lipid-binding motif. *Biochem. J.* **379**, 301–307 (2004).
 54. Vazquez, F. *et al.* Tumor suppressor PTEN acts through dynamic interaction with the plasma membrane. *Proc. Natl. Acad. Sci. U.S.A.* **103**, 3633–3638 (2006).
 55. Odriozola, L., Singh, G., Hoang, T. & Chan, A. M. Regulation of PTEN activity by its carboxyl-terminal autoinhibitory domain. *J. Biol. Chem.* **282**, 23306–23315 (2007).
 56. Vazquez, F., Ramaswamy, S., Nakamura, N. & Sellers, W. R. Phosphorylation of the PTEN tail regulates protein stability and function. *Mol. Cell. Biol.* **20**, 5010–5018 (2000).
 57. Torres, J. & Pulido, R. The tumor suppressor PTEN is phosphorylated by the protein kinase CK2 at its C terminus. Implications for PTEN stability to proteasome-mediated degradation. *Journal of Biological Chemistry* **276**, 993–998 (2001).
 58. Wu, X. *et al.* Evidence for regulation of the PTEN tumor suppressor by a membrane-

- localized multi-PDZ domain containing scaffold protein MAGI-2. *Proceedings of the National Academy of Sciences* **97**, 4233–4238 (2000).
59. Valiente, M. *et al.* Binding of PTEN to specific PDZ domains contributes to PTEN protein stability and phosphorylation by microtubule-associated serine/threonine kinases. *Journal of Biological Chemistry* **280**, 28936–28943 (2005).
60. Hopkins, B. D. *et al.* A secreted PTEN phosphatase that enters cells to alter signaling and survival. *Science* **341**, 399–402 (2013).
61. Liang, H. *et al.* PTEN α , a PTEN Isoform Translated through Alternative Initiation, Regulates Mitochondrial Function and Energy Metabolism. *Cell Metabolism* **19**, 836–848 (2014).
62. Pulido, R. *et al.* A unified nomenclature and amino acid numbering for human PTEN. *Sci Signal* **7**, pe15–pe15 (2014).
63. Malaney, P., Uversky, V. N. & Davé, V. Identification of intrinsically disordered regions in PTEN and delineation of its function via a network approach. *Methods* **77-78**, 69–74 (2015).
64. Shi, Y., Paluch, B. E., Wang, X. & Jiang, X. PTEN at a glance. *J. Cell. Sci.* **125**, 4687–4692 (2012).
65. Worby, C. A. & Dixon, J. E. PTEN. *Annu. Rev. Biochem.* **83**, 641–669 (2014).
66. Miller, S. J., Lou, D. Y., Seldin, D. C., Lane, W. S. & Neel, B. G. Direct identification of PTEN phosphorylation sites. *FEBS Letters* **528**, 145–153 (2002).
67. Al-Khouri, A. M., Ma, Y., Togo, S. H., Williams, S. & Mustelin, T. Cooperative phosphorylation of the tumor suppressor phosphatase and tensin homologue (PTEN) by casein kinases and glycogen synthase kinase 3 β . *Journal of Biological Chemistry* **280**, 35195–35202 (2005).
68. Maccario, H., Perera, N. M., Davidson, L., Downes, C. P. & Leslie, N. R. PTEN is destabilized by phosphorylation on Thr366. *Biochem. J.* **405**, 439–444 (2007).
69. Okahara, F., Ikawa, H., Kanaho, Y. & Maehama, T. Regulation of PTEN phosphorylation and stability by a tumor suppressor candidate protein. *Journal of Biological Chemistry* **279**, 45300–45303 (2004).
70. Rahdar, M. *et al.* A phosphorylation-dependent intramolecular interaction regulates the membrane association and activity of the tumor suppressor PTEN. *Proc. Natl. Acad. Sci. U.S.A.* **106**, 480–485 (2009).
71. Bolduc, D. *et al.* Phosphorylation-mediated PTEN conformational closure and deactivation revealed with protein semisynthesis. *Elife* **2**, e00691 (2013).

72. Vazquez, F. *et al.* Phosphorylation of the PTEN tail acts as an inhibitory switch by preventing its recruitment into a protein complex. *Journal of Biological Chemistry* **276**, 48627–48630 (2001).
73. Das, S., Dixon, J. E. & Cho, W. Membrane-binding and activation mechanism of PTEN. *Proc. Natl. Acad. Sci. U.S.A.* **100**, 7491–7496 (2003).
74. Li, Z. *et al.* Regulation of PTEN by Rho small GTPases. *Nature* **7**, 399–404 (2005).
75. Yim, E.-K. *et al.* Rak functions as a tumor suppressor by regulating PTEN protein stability and function. *Cancer Cell* **15**, 304–314 (2009).
76. Maddika, S. *et al.* WWP2 is an E3 ubiquitin ligase for PTEN. *Nature* **13**, 728–733 (2011).
77. Wang, X. *et al.* NEDD4-1 is a proto-oncogenic ubiquitin ligase for PTEN. *Cell* **128**, 129–139 (2007).
78. Amodio, N. *et al.* Oncogenic role of the E3 ubiquitin ligase NEDD4-1, a PTEN negative regulator, in non-small-cell lung carcinomas. *Am. J. Pathol.* **177**, 2622–2634 (2010).
79. Van Themsche, C., Leblanc, V., Parent, S. & Asselin, E. X-linked inhibitor of apoptosis protein (XIAP) regulates PTEN ubiquitination, content, and compartmentalization. *J. Biol. Chem.* **284**, 20462–20466 (2009).
80. Okumura, K. *et al.* PCAF modulates PTEN activity. *Journal of Biological Chemistry* **281**, 26562–26568 (2006).
81. Ikenoue, T., Inoki, K., Zhao, B. & Guan, K.-L. PTEN acetylation modulates its interaction with PDZ domain. *Cancer Res.* **68**, 6908–6912 (2008).
82. Lee, S. R. *et al.* Reversible Inactivation of the Tumor Suppressor PTEN by H₂O₂. *Journal of Biological Chemistry* **277**, 20336–20342 (2002).
83. Leslie, N. R. *et al.* Redox regulation of PI 3-kinase signalling via inactivation of PTEN. *EMBO J.* **22**, 5501–5510 (2003).
84. Chang, C.-J. *et al.* PTEN nuclear localization is regulated by oxidative stress and mediates p53-dependent tumor suppression. *Mol. Cell. Biol.* **28**, 3281–3289 (2008).
85. Shen, W. H. *et al.* Essential role for nuclear PTEN in maintaining chromosomal integrity. *Cell* **128**, 157–170 (2007).
86. Bassi, C. *et al.* Nuclear PTEN controls DNA repair and sensitivity to genotoxic stress. *Science* **341**, 395–399 (2013).
87. Song, M. S. *et al.* Nuclear PTEN regulates the APC-CDH1 tumor-suppressive complex in a phosphatase-independent manner. *Cell* **144**, 187–199 (2011).

88. Freeman, D. J. *et al.* PTEN tumor suppressor regulates p53 protein levels and activity through phosphatase-dependent and -independent mechanisms. *Cancer Cell* **3**, 117–130 (2003).
89. Tang, Y. PTEN Autoregulates Its Expression by Stabilization of p53 in a Phosphatase-Independent Manner. *Cancer Res.* **66**, 736–742 (2006).
90. Li, A. G. *et al.* Mechanistic insights into maintenance of high p53 acetylation by PTEN. *Mol. Cell* **23**, 575–587 (2006).
91. Yiu, G. & He, Z. Glial inhibition of CNS axon regeneration. *Nat. Rev. Neurosci.* **7**, 617–627 (2006).
92. Harel, N. Y. & Strittmatter, S. M. Can regenerating axons recapitulate developmental guidance during recovery from spinal cord injury? *Nat. Rev. Neurosci.* **7**, 603–616 (2006).
93. Soltoff, S. P., Rabin, S. L., Cantley, L. C. & Kaplan, D. R. Nerve growth factor promotes the activation of phosphatidylinositol 3-kinase and its association with the trk tyrosine kinase. *Journal of Biological Chemistry* **267**, 17472–17477 (1992).
94. Korhonen, J. M., Saïd, F. A., Wong, A. J. & Kaplan, D. R. Gab1 mediates neurite outgrowth, DNA synthesis, and survival in PC12 cells. *Journal of Biological Chemistry* **274**, 37307–37314 (1999).
95. Christie, K. J., Webber, C. A., Martinez, J. A., Singh, B. & Zochodne, D. W. PTEN inhibition to facilitate intrinsic regenerative outgrowth of adult peripheral axons. *J. Neurosci.* **30**, 9306–9315 (2010).
96. Fujio, Y., Nguyen, T., Wencker, D., Kitsis, R. N. & Walsh, K. Akt promotes survival of cardiomyocytes in vitro and protects against ischemia-reperfusion injury in mouse heart. *Circulation* **101**, 660–667 (2000).
97. Mocanu, M. M. & Yellon, D. M. PTEN, the Achilles' heel of myocardial ischaemia/reperfusion injury? *Br. J. Pharmacol.* **150**, 833–838 (2007).
98. Keyes, K. T. *et al.* Pharmacological inhibition of PTEN limits myocardial infarct size and improves left ventricular function postinfarction. *Am. J. Physiol. Heart Circ. Physiol.* **298**, H1198–208 (2010).
99. Winterbourn, C. C. Reconciling the chemistry and biology of reactive oxygen species. *Nat Chem Biol* **4**, 278–286 (2008).
100. Cairns, R. A., Harris, I. S. & Mak, T. W. Regulation of cancer cell metabolism. *Nat. Rev. Cancer* **11**, 85–95 (2011).
101. Shi, X., Zhang, Y., Zheng, J. & Pan, J. Reactive oxygen species in cancer stem cells.

- Antioxid. Redox Signal.* **16**, 1215–1228 (2012).
102. Na, A. R. *et al.* A critical role for Romo1-derived ROS in cell proliferation. *Biochem. Biophys. Res. Commun.* **369**, 672–678 (2008).
103. Gupta, S. C. *et al.* Upsides and downsides of reactive oxygen species for cancer: the roles of reactive oxygen species in tumorigenesis, prevention, and therapy. *Antioxid. Redox Signal.* **16**, 1295–1322 (2012).
104. D'Autréaux, B. & Toledano, M. B. ROS as signalling molecules: mechanisms that generate specificity in ROS homeostasis. *Nat. Rev. Mol. Cell Biol.* **8**, 813–824 (2007).
105. Paulsen, C. E. & Carroll, K. S. Orchestrating redox signaling networks through regulatory cysteine switches. *ACS Chem. Biol.* **5**, 47–62 (2010).
106. Cumming, R. C. *et al.* Protein disulfide bond formation in the cytoplasm during oxidative stress. *Journal of Biological Chemistry* **279**, 21749–21758 (2004).
107. Bretón-Romero, R. & Lamas, S. Hydrogen peroxide signaling in vascular endothelial cells. *Redox Biol* **2**, 529–534 (2014).
108. Meng, T.-C., Fukada, T. & Tonks, N. K. Reversible oxidation and inactivation of protein tyrosine phosphatases in vivo. *Mol. Cell* **9**, 387–399 (2002).
109. Kwon, J. *et al.* Reversible oxidation and inactivation of the tumor suppressor PTEN in cells stimulated with peptide growth factors. *Proc. Natl. Acad. Sci. U.S.A.* **101**, 16419–16424 (2004).
110. Gupta, V. & Carroll, K. S. Sulfenic acid chemistry, detection and cellular lifetime. *Biochim. Biophys. Acta* **1840**, 847–875 (2014).
111. Kim, H.-J., Ha, S., Lee, H. Y. & Lee, K.-J. ROSics: chemistry and proteomics of cysteine modifications in redox biology. *Mass Spectrom Rev* **34**, 184–208 (2015).
112. Marino, S. M. & Gladyshev, V. N. Analysis and functional prediction of reactive cysteine residues. *J. Biol. Chem.* **287**, 4419–4425 (2012).
113. Besse, D., Siedler, F., Diercks, T., Kessler, H. & Moroder, L. The Redox Potential of Selenocystine in Unconstrained Cyclic Peptides. *Angew. Chem. Int. Ed. Engl.* **36**, 883–885 (1997).
114. Lohse, D. L., Denu, J. M., Santoro, N. & Dixon, J. E. Roles of aspartic acid 181 and serine-222 in intermediate formation and hydrolysis of the mammalian protein-tyrosine-phosphatase PTP1. *Biochemistry* **36**, 4568–4575 (1997).
115. Cho, S.-H. *et al.* Redox regulation of PTEN and protein tyrosine phosphatases in H₂O₂ mediated cell signaling. *FEBS Letters* **560**, 7–13 (2004).
116. Tonks, N. K. Redox redux: revisiting PTPs and the control of cell signaling. *Cell* **121**,

- 667–670 (2005).
117. Veal, E. A., Day, A. M. & Morgan, B. A. Hydrogen peroxide sensing and signaling. *Mol. Cell* **26**, 1–14 (2007).
118. Tsai, S. J. *et al.* Crystal structure of the human lymphoid tyrosine phosphatase catalytic domain: insights into redox regulation. *Biochemistry* **48**, 4838–4845 (2009).
119. Lee, S. R., Kwon, K. S., Kim, S. R. & Rhee, S. G. Reversible inactivation of protein-tyrosine phosphatase 1B in A431 cells stimulated with epidermal growth factor. *Journal of Biological Chemistry* **273**, 15366–15372 (1998).
120. Barford, D., Flint, A. J. & Tonks, N. K. Crystal structure of human protein tyrosine phosphatase 1B. *Science* **263**, 1397–1404 (1994).
121. Barford, D., Das, A. K. & Egloff, M. P. The structure and mechanism of protein phosphatases: Insights into catalysis and regulation. *Annu Rev Biophys Biomol Struct* **27**, 133–164 (1998).
122. Salmeen, A. *et al.* Redox regulation of protein tyrosine phosphatase 1B involves a sulphenyl-amide intermediate. *Nature* **423**, 769–773 (2003).
123. van Montfort, R. L. M., Congreve, M., Tisi, D., Carr, R. & Jhoti, H. Oxidation state of the active-site cysteine in protein tyrosine phosphatase 1B. *Nature* **423**, 773–777 (2003).
124. Caselli, A. *et al.* The inactivation mechanism of low molecular weight phosphotyrosine-protein phosphatase by H₂O₂. *Journal of Biological Chemistry* **273**, 32554–32560 (1998).
125. Chiarugi, P. *et al.* Two vicinal cysteines confer a peculiar redox regulation to low molecular weight protein tyrosine phosphatase in response to platelet-derived growth factor receptor stimulation. *Journal of Biological Chemistry* **276**, 33478–33487 (2001).
126. Buhrman, G., Parker, B., Sohn, J., Rudolph, J. & Mattos, C. Structural mechanism of oxidative regulation of the phosphatase Cdc25B via an intramolecular disulfide bond. *Biochemistry* **44**, 5307–5316 (2005).
127. Fauman, E. B. *et al.* Crystal structure of the catalytic domain of the human cell cycle control phosphatase, Cdc25A. *Cell* **93**, 617–625 (1998).
128. Sohn, J. & Rudolph, J. Catalytic and chemical competence of regulation of cdc25 phosphatase by oxidation/reduction. *Biochemistry* **42**, 10060–10070 (2003).
129. Mak, L. H., Vilar, R. & Woscholski, R. Characterisation of the PTEN inhibitor VO-OHpic. *J Chem Biol* **3**, 157–163 (2010).

130. Mak, L. H. & Woscholski, R. Targeting PTEN using small molecule inhibitors. *Methods* **77-78C**, 63–68 (2015).
131. Schmid, A. C., Byrne, R. D., Vilar, R. & Woscholski, R. Bisperoxovanadium compounds are potent PTEN inhibitors. *FEBS Letters* **566**, 35–38 (2004).
132. Rosivatz, E. *et al.* A small molecule inhibitor for phosphatase and tensin homologue deleted on chromosome 10 (PTEN). *ACS Chem. Biol.* **1**, 780–790 (2006).
133. Spinelli, L., Lindsay, Y. E. & Leslie, N. R. PTEN inhibitors: an evaluation of current compounds. *Adv Biol Regul* **57**, 102–111 (2015).
134. Shaver, A., Ng, J. B., Hynes, R. C. & Posner, B. I. Potassium (5-nitro-1,10-phenanthroline-N1,N10)oxodiperoxovanadate(V) dihydrate: an insulin-mimetic peroxovanadate. *Acta Crystallogr C Cryst Struct Commun* **50**, 1044–1046 (1994).
135. Thompson, K. H. & Orvig, C. Coordination chemistry of vanadium in metallopharmaceutical candidate compounds. *Coordination Chemistry Reviews* **219**, 1033–1053 (2001).
136. Zhang, Q.-G., Wu, D.-N., Han, D. & Zhang, G.-Y. Critical role of PTEN in the coupling between PI3K/Akt and JNK1/2 signaling in ischemic brain injury. *FEBS Letters* **581**, 495–505 (2007).
137. Guo, J.-Y. *et al.* Dose-Dependent Protective Effect of Bisperoxovanadium against Acute Cerebral Ischemia in a Rat Model of Ischemia/Reperfusion Injury. *Int J Mol Sci* **14**, 12013–12022 (2013).
138. Chen, Y. *et al.* Administration of a PTEN inhibitor BPV(pic) attenuates early brain injury via modulating AMPA receptor subunits after subarachnoid hemorrhage in rats. *Neurosci. Lett.* **588C**, 131–136 (2015).
139. Walker, C. L. *et al.* Systemic Bisperoxovanadium Activates Akt/mTOR, Reduces Autophagy, and Enhances Recovery following Cervical Spinal Cord Injury. *PLoS ONE* **7**, e30012 (2012).
140. Walker, C. L. & Xu, X.-M. PTEN inhibitor bisperoxovanadium protects oligodendrocytes and myelin and prevents neuronal atrophy in adult rats following cervical hemicontusive spinal cord injury. *Neurosci. Lett.* **573**, 64–68 (2014).
141. Tian, Y., Daoud, A. & Shang, J. Effects of bpV(pic) and bpV(phen) on H9c2 cardiomyoblasts during both hypoxia/reoxygenation and H₂O₂-induced injuries. *Mol Med Rep* **5**, 852–858 (2012).
142. UniProt Consortium. UniProt: a hub for protein information. *Nucleic Acids Res.* **43**, D204–12 (2015).

143. Clegg, R. A. & Holt, C. An *E. coli* over-expression system for multiply-phosphorylated proteins and its use in a study of calcium phosphate sequestration by novel recombinant phosphopeptides. *Protein Expr. Purif.* **67**, 23–34 (2009).
144. Bäcker, S. *Untersuchung des Phosphorylierungsgrades verschiedener PTEN-Varianten (Master's Thesis)*. (TU Dortmund, 2013).
145. Carter, S. G. & Karl, D. W. Inorganic phosphate assay with malachite green: an improvement and evaluation. *J. Biochem. Biophys. Methods* **7**, 7–13 (1982).
146. Kuepper, A. *Investigation of the flexible terminal sequences of Phosphatase and TENsin homolog deleted on chromosome ten (Master's Thesis)*. (TU Dortmund, 2013).
147. Müller, C. *Expression und Charakterisierung verschiedener PTEN-Konstrukte (Master's Thesis)*. (TU Dortmund, 2014).
148. Stone, J. R. & Yang, S. Hydrogen peroxide: a signaling messenger. *Antioxid. Redox Signal.* **8**, 243–270 (2006).
149. Holmgren, A. & Luthman, M. Tissue distribution and subcellular localization of bovine thioredoxin determined by radioimmunoassay. *Biochemistry* **17**, 4071–4077 (1978).
150. Schwertassek, U. *et al.* Reactivation of oxidized PTP1B and PTEN by thioredoxin 1. *FEBS J.* **281**, 3545–3558 (2014).
151. Meister, A. & Anderson, M. E. Glutathione. *Annu. Rev. Biochem.* **52**, 711–760 (1983).
152. Hwang, J. H., Larson, R. K. & Abu-Omar, M. M. Kinetics and mechanistic studies of anticarcinogenic bisperoxovanadium(V) compounds: ligand substitution reactions at physiological pH and relevance to DNA interactions. *Inorg Chem* **42**, 7967–7977 (2003).
153. Huyer, G. *et al.* Mechanism of inhibition of protein-tyrosine phosphatases by vanadate and pervanadate. *Journal of Biological Chemistry* **272**, 843–851 (1997).
154. Butler, A., Clague, M. J. & Meister, G. E. Vanadium Peroxide Complexes. *Chemical reviews* **94**, 625–638 (1994).
155. Rodgers, D. W. Cryocrystallography. *Structure* **2**, 1135–40 (1994).
156. Arndt, U. W. & Wonacott, A. J. The rotation method in crystallography. North Holland Publishing Co, Amsterdam. (1977).
157. Kabsch, W. XDS. *Acta Crystallogr. D Biol. Crystallogr.* **66**, 125–132 (2010).
158. Karplus, P. A. & Diederichs, K. Linking crystallographic model and data quality.

- Science* **336**, 1030–1033 (2012).
159. Diederichs, K. & Karplus, P. A. Improved R-factors for diffraction data analysis in macromolecular crystallography. *Nat Struct Mol Biol* **4**, 269–275 (1997).
160. Barr, A. J. *et al.* Large-scale structural analysis of the classical human protein tyrosine phosphatome. *Cell* **136**, 352–363 (2009).
161. Cerovac, Z. *et al.* Activation of MAPK by potassium bisperoxo(1,10-phenanthroline)oxovanadate (V). *Neurochem. Int.* **34**, 337–344 (1999).
162. Jaswal, J. S. & Tracey, A. S. Formation and decomposition of peroxovanadium(V) complexes in aqueous solution. *Inorg Chem* **30**, 3718–3722 (1991).
163. Rehder, D., Časný, M. & Grosse, R. A vanadium-51 NMR study of the binding of vanadate and peroxovanadate to proteins. *Magn Reson Chem* **42**, 745–749 (2004).
164. Seargeant, L. E. & Stinson, R. A. Inhibition of human alkaline phosphatases by vanadate. *Biochem. J.* **181**, 247–250 (1979).
165. Brennan, S. & Cowan, P. L. A Suite of Programs for Calculating X-Ray Absorption, Reflection, and Diffraction Performance for a Variety of Materials at Arbitrary Wavelengths. *Review of Scientific Instruments* **63**, 850–853 (1992).
166. Strahs, G. & Kraut, J. Low-resolution electron-density and anomalous-scattering-density maps of Chromatium high-potential iron protein. *Ann. Rev. Biochem.* **35**, 503–512 (1968).
167. Shenoy, S. S., Nanda, H. & Lösche, M. Membrane association of the PTEN tumor suppressor: electrostatic interaction with phosphatidylserine-containing bilayers and regulatory role of the C-terminal tail. *J. Struct. Biol.* **180**, 394–408 (2012).
168. Nguyen, H.-N. *et al.* Opening the conformation is a master switch for the dual localization and phosphatase activity of PTEN. *Scientific reports* **5**, 12600 (2015).
169. Denu, J. M. & Tanner, K. G. Specific and reversible inactivation of protein tyrosine phosphatases by hydrogen peroxide: evidence for a sulfenic acid intermediate and implications for redox regulation. *Biochemistry* **37**, 5633–5642 (1998).
170. Cunnick, J. M., Dorsey, J. F., Mei, L. & Wu, J. Reversible regulation of SHP-1 tyrosine phosphatase activity by oxidation. *Biochem. Mol. Biol. Int.* **45**, 887–894 (1998).
171. Lee, C.-U. *et al.* Redox Modulation of PTEN Phosphatase Activity by Hydrogen Peroxide and Bisperoxidovanadium Complexes. *Angew. Chem. Int. Ed. Engl.* **54**, 13796–13800 (2015).
172. Ballistreri, F. P., Barbuzzi, E. G., Tomaselli, G. A. & Toscano, R. M. Insulin mimesis

- of vanadium derivatives. Oxidation of cysteine by V(V) oxo diperoxo complexes. *J. Inorg. Biochem.* **80**, 173–176 (2000).
173. Paulsen, C. E. & Carroll, K. S. Cysteine-mediated redox signaling: chemistry, biology, and tools for discovery. *Chemical reviews* **113**, 4633–4679 (2013).
174. Leslie, N. R., Batty, I. H., Maccario, H., Davidson, L. & Downes, C. P. Understanding PTEN regulation: PIP2, polarity and protein stability. *Oncogene* **27**, 5464–5476 (2008).
175. Wei, Y., Stec, B., Redfield, A. G., Weerapana, E. & Roberts, M. F. Phospholipid-binding Sites of Phosphatase and Tensin Homolog (PTEN): exploring the mechanism of phosphatidylinositol 4,5-bisphosphate activation. *J. Biol. Chem.* **290**, 1592–1606 (2015).
176. Invitrogen™, Bac-to-Bac® Baculovirus Expression System - An efficient site-specific transposition system to generate baculovirus for high-level expression of recombinant proteins, *User Manual Version F*, (2010).
177. Cantley, L. C. *et al.* Vanadate is a potent (Na,K)-ATPase inhibitor found in ATP derived from muscle. *Journal of Biological Chemistry* **252**, 7421–7423 (1977).
178. Hasegawa, Y. *et al.* Neuroprotective effect of postischemic administration of sodium orthovanadate in rats with transient middle cerebral artery occlusion. *J Cereb Blood Flow Metab* **23**, 1040–1051 (2003).
179. Kawano, T. *et al.* Neuroprotective effect of sodium orthovanadate on delayed neuronal death after transient forebrain ischemia in gerbil hippocampus. *J Cereb Blood Flow Metab* **21**, 1268–1280 (2001).
180. Takada, Y., Hashimoto, M., Kasahara, J., Aihara, K. & Fukunaga, K. Cytoprotective effect of sodium orthovanadate on ischemia/reperfusion-induced injury in the rat heart involves Akt activation and inhibition of fodrin breakdown and apoptosis. *Journal of Pharmacology and Experimental Therapeutics* **311**, 1249–1255 (2004).
181. Wilkins, M. R. *et al.* Protein identification and analysis tools in the ExPASy server. *Methods Mol. Biol.* **112**, 531–552 (1999).
182. Saiki, R. K. *et al.* Enzymatic amplification of beta-globin genomic sequences and restriction site analysis for diagnosis of sickle cell anemia. *Science* **230**, 1350–1354 (1985).
183. Saiki, R. K. *et al.* Primer-directed enzymatic amplification of DNA with a thermostable DNA polymerase. *Scientific reports* **239**, 487–491 (1988).
184. Shevchuk, N. A. *et al.* Construction of long DNA molecules using long PCR-based

- fusion of several fragments simultaneously. *Nucleic Acids Res.* **32**, e19 (2004).
185. Aaij, C. & Borst, P. The gel electrophoresis of DNA. *Biochim. Biophys. Acta* **269**, 192–200 (1972).
186. Southern, E. M. Detection of specific sequences among DNA fragments separated by gel electrophoresis. *Ann. Rev. Biochem.* **98**, 503–517 (1975).
187. Kelly, T. J. & Smith, H. O. A restriction enzyme from *Hemophilus influenzae*. II. *Ann. Rev. Biochem.* **51**, 393–409 (1970).
188. Smith, H. O. & Wilcox, K. W. A restriction enzyme from *Hemophilus influenzae*. I. Purification and general properties. *Ann. Rev. Biochem.* **51**, 379–391 (1970).
189. Mertz, J. E. & Davis, R. W. Cleavage of DNA by R 1 restriction endonuclease generates cohesive ends. *Proc. Natl. Acad. Sci. U.S.A.* **69**, 3370–3374 (1972).
190. Jackson, D. A., Symons, R. H. & Berg, P. Biochemical method for inserting new genetic information into DNA of Simian Virus 40: circular SV40 DNA molecules containing lambda phage genes and the galactose operon of *Escherichia coli*. *Proc. Natl. Acad. Sci. U.S.A.* **69**, 2904–2909 (1972).
191. Cohen, S. N., Chang, A. C., Boyer, H. W. & Helling, R. B. Construction of biologically functional bacterial plasmids in vitro. *Proc. Natl. Acad. Sci. U.S.A.* **70**, 3240–3244 (1973).
192. Lehman, I. R. DNA ligase: structure, mechanism, and function. *Science* **186**, 790–797 (1974).
193. Dagert, M. & Ehrlich, S. D. Prolonged incubation in calcium chloride improves the competence of *Escherichia coli* cells. *Gene* **6**, 23–28 (1979).
194. Holmes, D. S. & Quigley, M. A rapid boiling method for the preparation of bacterial plasmids. *Anal. Biochem.* **114**, 193–197 (1981).
195. Zon, L. I., Dorfman, D. M. & Orkin, S. H. The polymerase chain reaction colony miniprep. *BioTechniques* **7**, 696–698 (1989).
196. Birnboim, H. C. & Doly, J. A rapid alkaline extraction procedure for screening recombinant plasmid DNA. *Nucleic Acids Res.* **7**, 1513–1523 (1979).
197. Larkin, M. A. *et al.* Clustal W and Clustal X version 2.0. *Bioinformatics* **23**, 2947–2948 (2007).
198. Life Technologies, Growth and Maintenance of Insect Cell Lines. **5.0**, 1–41 (2013).
199. Vilen, H., Aalto, J.-M., Kassinen, A., Paulin, L. & Savilahti, H. A direct transposon insertion tool for modification and functional analysis of viral genomes. *J. Virol.* **77**, 123–134 (2003).

200. Potterton, E., Briggs, P., Turkenburg, M. & Dodson, E. A graphical user interface to the CCP4 program suite. *Acta Crystallogr. D Biol. Crystallogr.* **59**, 1131–1137 (2003).
201. Winn, M. D. *et al.* Overview of the CCP4 suite and current developments. *Acta Crystallogr. D Biol. Crystallogr.* **67**, 235–242 (2011).
202. Emsley, P., Lohkamp, B., Scott, W. G. & Cowtan, K. Features and development of Coot. *Acta Crystallogr. D Biol. Crystallogr.* **66**, 486–501 (2010).
203. Murshudov, G. N., Vagin, A. A. & Dodson, E. J. Refinement of macromolecular structures by the maximum-likelihood method. *Acta Crystallogr. D Biol. Crystallogr.* **53**, 240–255 (1997).
204. *The PyMOL Molecular Graphics System, Version 1.5.0.4 Schrödinger, LLC.*
205. Laemmli, U. K. Cleavage of Structural Proteins during the Assembly of the Head of Bacteriophage T4. *Nature* **227**, 680–685 (1970).
206. McPherson A. Current approaches to macromolecular crystallization. *Eur J Biochem.* **189**,1-23 (1990).
207. Rossmann, M. G. The molecular replacement method. *Acta Crystallogr. A* **46**, 73-82 (1990).
208. Brünger, A. T. Free R value: a novel statistical quantity for assessing the accuracy of crystal structures. *Nature* **355**, 472-475 (1992).
209. Brünger, A. T. Free R Value: Cross-Validation in Crystallography. *Methods in Enzymology* **277**, 366-396 (1997).

7 Appendices

7.1 pFH1-Vector

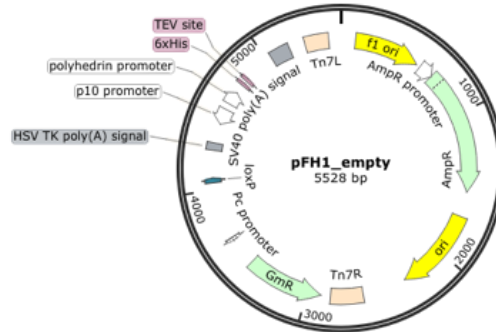


Figure 45 | Map of pFH1 vector used for the baculovirus-mediated protein expression.

TTCTCTGTACAGAATGAAAATTTTTCTGTCTATCTCTTCGTTATTAATGTTTGTAAATTGACTGAATATCAACGCT
TATTTGCAGCCTGAATGGCGAATGGGACGCGCCCTGTAGCGGCGCATTAAAGCGCGGGTGTGGTGGTTACGCG
CAGCGTGACCGCTACACTTGCCAGCGCCCTAGCGCCCGCTCCTTTTCGCTTTCTTCCCTTCCCTTTCTCGCCACGTT
CGCCGGCTTTCCCGTCAAGCTCTAAATCGGGGGCTCCCTTTAGGGTTCCGATTTAGTGCTTTACGGCACCTCGA
CCCCAAAAAATTGATTAGGGTGATGGTTCACGTAGTGGGCCATCGCCCTGATAGACGGTTTTTTCGCCCTTTGAC
GTTGGAGTCCACGTTCTTAATAGTGGACTCTTGTTCAAACTGGAACAACACTCAACCCTATCTCGGTCTATTTCT
TTTGATTTATAAGGGATTTTGCCGATTTTCGGCCTATTGGTTAAAAAATGAGCTGATTTAACAAAAATTTAACGG
AATTTTAACAAAAATTTAACGCTTACAATTTAGGTGGCACTTTTCGGGGAAATGTGCGCGGAACCCCTATTTGTT
TATTTTTCTAAATACATTTCAAATATGTATCCGCTCATGAGACAATAACCCTGATAAATGCTTCAATAATATTGAA
AAAGGAAGAGTATGAGTATTTCAACATTTCCGTGTCGCCCTTATTTCCCTTTTTTTCGCGCATTTTCCTTCTGTTT
TTGCTCACCCAGAAACGCTGGTGAAGTAAAAGATGCTGAAGATCAGTTGGGTGCACGAGTGGGTACATCGAAC
TGGATCTCAACAGCGGTAAGATCCTTGAGAGTTTTTCGCCCCGAAGAACGTTTTTCCAATGATGAGCACTTTTAAAG
TTCTGCTATGTGGCGCGGTATTATCCCGTATTGACGCCGGCAAGAGCAACTCGGTTCGCCGCATACACTATTCTC
AGAATGACTTGGTTGAGTACTCACCAGTCACAGAAAAGCATCTTACGGATGGCATGACAGTAAGAGAATTATGCA
GTGCTGCCATAACCATGAGTGATAACACTGCGGCCAACTTACTTCTGACAACGATCGGAGGACCGAAGGAGCTAA
CCGCTTTTTTGCACAACATGGGGGATCATGTAACCTCGCCTTGATCGTTGGGAACCGGAGCTGAATGAAGCCATAC
CAAACGACGAGCGTGACACCACGATGCCTGTAGCAATGGCAACAACGTTGCGCAAATTTAACTGGCGAACTAC
TTACTCTAGCTTCCCGCAACAATTAATAGACTGGATGGAGGCGGATAAAGTTGCAGGACCCTTCTGCGCTCGG
CCCTTCCGGCTGGCTGGTTTTATTGCTGATAAATCTGGAGCCGGTGAGCGTGGGTCTCGCGGTATCATTGCAGCAC
TGGGGCCAGATGGTAAGCCCTCCCGTATCGTAGTTATCTACACGACGGGGAGTCAGGCAACTATGGATGAACGAA
ATAGACAGATCGCTGAGATAGGTGCCTCACTGATTAAGCATTGGTAACTGTCAGACCAAGTTTACTCATATATAC
TTTAGATTGATTTAAAACCTTCATTTTTTAATTTAAAAGGATCTAGGTGAAGATCCTTTTTTGATAATCTCATGACCA
AAATCCCTTAACGTGAGTTTTTCGTTCCACTGAGCGTCAGACCCCGTAGAAAAGATCAAAGGATCTTCTTGAGATC
CTTTTTTCTGCGCGTAATCTGCTGCTTGCAAAACAAAAAACCACCGCTACCAGCGGTGGTTTGTGTGCCGGATC
AAGAGCTACCAACTCTTTTTCCGAAGGTAAGTGGCTTACAGAGAGCGCAGATACCAAATACTGTTCTTCTAGTGT
AGCCGTAGTTAGGCCACCCTTCAAGAACTCTGTAGCACCCGCTACATACTACCTCGCTCTGCTAATCTCTTACCAG
TGGCTGCTGCCAGTGGCGATAAGTCTGTCTTACCGGGTTGGACTCAAGACGATAGTTACCGGATAAGGCGCAGC
GGTCCGGCTGAACGGGGGGTTTCGTGCACACAGCCAGCTTGGAGCGAACGACCTACACCGAAGTACCTGAGATACCTAC
AGCGTGAGCTATGAGAAAGCGCCACGCTTCCCGAAGGGAGAAAGGCGGACAGGTATCCGGTAAGCGGCAGGGTCG
GAACAGGAGAGCGCACGAGGGAGCTTCCAGGGGAAACGCCTGGTATCTTTATAGTCTTGTGCGGGTTTCGCCACC
TCTGACTTGAGCGTCGATTTTTTGTGATGCTCGTCAGGGGGCGGAGCCTATGGAAAAACGCCAGCAACCGCGCCT
TTTTACGGTTCCTGGCCTTTTGCTGGCCTTTTGCTCACATGTTCTTTTCTGCGTTATCCCCTGATTTCTGTGGATA
ACCGTATTACCGCCTTTGAGTGAGCTGATACCGCTCGCCGAGCCGAACGACCGAGCGCAGCGAGTCACTGAGCG
AGGAAGCGGAAGAGCGCCTGATGCGGTATTTTTCTCCTTACGCATCTGTGCGGTATTTACACCGCATAGACCAGC
CGCGTAACCTGGCAAAATCGGTTACGGTTGAGTAATAAATGGATGCCCTGCGTAAGCGGGTGTGGGCGGACAATA
AAGTCTTAACTGAACAAAATAGATCTAAACTATGACAATAAAGTCTTAACTAGACAGAATAGTTGTAACCTGA
AATCAGTCCAGTTATGCTGTGAAAAAGCATACTGGACTTTTGTTATGGCTAAAGCAAACCTTTCATTTTCTGAAG
TGCAAAATTGCCCGTCGTATTAAGAGGGGGCGTGGCCAAGGGCATGGTAAAGACTATATTTCGCGGGCTTGTGACAA
TTTACCGAACAACCTCCGCGGCCGGGAAGCCGATCTCGGCTTGAACGAATTGTTAGGTGGCGGTACTTGGGTGCGAT

ATCAAAGTGCATCACTTCTTCCCGTATGCCCAACTTTGTATAGAGAGCCACTGCGGGATCGTACCCGTAATCTGC
 TTGCACGTAGATCACATAAGCACCAAGCGCGTTGGCCTCATGCTTGAGGAGATTGATGAGCGCGGTGGCAATGCC
 CTGCCTCCGGTGTCTCGCCGGAGACTGCGAGATCATAGATATAGATCTCACTACGCGGCTGCTCAAACTTGGGCAG
 AACGTAAGCCGCGAGAGCGCCAACAACCGCTTCTTGGTCTGAAGGCAGCAAGCGCGATGAATGTCTTACTACGGAG
 CAAGTTCCTCCGAGGTAATCGGAGTCCGGCTGATGTTGGGAGTAGGTGGCTACGTCTCCGAACTCACGACCGAAAAG
 ATCAAGAGCAGCCCGCATGGATTTGACTTGGTCAGGGCCGAGCCTACATGTGCGAATGATGCCATACTTGAGCC
 ACCTAACTTTGTTTTAGGGCGACTGCCCTGCTGCGTAACATCGTTGCTGCTGCGTAACATCGTTGCTGCTCCATA
 ACATCAAACATCGACCCACGGCGTAACGCGCTTGGTATGCCCGAGGCATAGACTGTACAAAAAACAGT
 CATAACAAGCCATGAAAACCGCCACTGCGCCGTTACCACCGCTGCGTTCGGTCAAGGTCTGGACCAGTTGCGTG
 AGCGCATACGCTACTTGCATTACAGTTTACGAACCGAACAGGCTTATGTCAACTGGGTTTCGTGCCTTCATCCGTT
 TCCACGGTGTGCGTACCCCGCAACCTTGGGCAGCAGCGAAGTCGAGGCATTTCTGTCTTGGCTGGCGAACGAGC
 GCAAGGTTTCGGTCTCCACGCATCGTCAGGCATTGGCGCCTTGGTGTCTTCTACGGCAAGGTGCTGTGCACGG
 ATCTGCCCTTGTCTCAGGAGATCGGTAGACCTCGGCCGTCGCGGCGCTTGCCGGTGGTGTGACCCCGGATGAAG
 TGGTTCGCATCCTCGGTTTTCTGGAAGGCGAGCATCGTTTTGTTTCGCCAGGACTCTAGCTATAGTTCTAGTGGTT
 GGCTACAGCTTTGTTTGTACTATCAACAGGTTGAACTGCTGATCAACAGATCCTCTACGCGGCCGCGGTACCATA
 ACTTCGTATAGCATAACATTATACGAAGTTATCTGGTTTTAAACGTACCCGTAGTGGCTATGGCAGGGCTTGCCGCC
 CCGACGTTGGCTGCGAGCCCTGGGCCTTACCCGAACTTGGGGGTTGGGGTGGGGAAAAGGAAGAAACGCGGGCG
 TATTGGTCCCAATGGGGTCTCGGTGGGGTATCGACAGAGTGCCAGCCCTGGGACCGAACCCCGCGTTTATGAACA
 AACGACCCAACACCCGTGCGTTTTATTCTGTCTTTTTATTGCCGTACATAGCGCGGGTTCCCTCCGGTATTGTCTC
 CTTCCGTGTTTTCAGTTAGCCTCCCCATCTCCCGGTACCGCATGCTATGCATCAGCTGCTAGCACCATGGCTCGA
 GATCCCGGGTATCAAGTCTTCGTCGAGTGATTGTAAATAAAATGTAATTTACAGTATAGTATTTAATTAATAT
 ACAAATGATTTGATAATAATTCTTATTTAACTATAATATATTGTGTTGGGTTGAATTAAGGTCCGTATACTAGT
 ATCGATTCGCGACCTACTCCGGAATATTAATAGATCATGGAGATAAATAAAATGATAACCATCTCGCAATAAAT
 AAGTATTTACTGTTTTTCGTAACAGTTTTGTAAATAAAAAAACCTATAAATATTCCGGATTATTCATACCGTCCCA
 CCATCGGGCGCGATCTACAACC**CATATG**TCGTACTAC**CATCACCATCACCATCAC**GATTACGATATCCCAACGA
 CC**GAAAACCTGTATTTTCAGGGC**GCCATG**GGATCC**GGAATTCAAAGGCCTAC**GTCGAC**GAGCTCACTAGTCGCGG
 CCGCTTTCGAATCTAGAGCCTGCAGTCTCGACAAGCTTGTGAGAAAGTACT**TAG**AGGATCATAATCAGCCATACCA
 CATTGTAGAGGTTTTACTTGTCTTAAAAAACCTCCACACCTCCCCCTGAACCTGAAAACATAAAATGAATGCAA
 TTGTTGTTGTTAACTTGTATTGTCAGCTTATAATGGTTACAAATAAAGCAATAGCATCACAAATTTACAAAATA
 AAGCATTTTTTTTTACTGCATTCTAGTTGTGGTTTTGTCCAACTCATCAATGTATCTTATCATGTCTGGATCTGAT
 CACTGCTTGAGCCTAGAAGATCCGGCTGCTAACAAAGCCCGAAAGGAAGCTGAGTTGGCTGCTGCCACCGCTGAG
 CAATAACTATCATAACCCCTAGGAGATCCGAACCAGATAAGTGAAATCTAGTTCCAACTATTTTGTCAATTTTA
 ATTTTCGTATTAGCTTACGACGCTACACCCAGTTCCCATCTATTTTGTCACTCTTCCCTAAATAATCTTAAAA
 CTCCATTTCCACCCCTCCAGTTCCCAACTATTTTGTCCGCCACAGCGGGGCATTTTTCTTCTTCTGTTATGTTTT
 TAATCAAACATCCTGCCAACTCCATGTGACAAACCGTCATCTTCGGCTACTTT

Table 33 | Sequence characteristics in the multiple cloning site. *NdeI* and *SalI* are used to insert the gene of interest.

| Nucleotide sequence | Description |
|------------------------------|-----------------------|
| CATATG | <i>NdeI</i> |
| ATG | Translation start |
| CATCACCATCACCATCAC | His ₆ -tag |
| GAAAACCTGTATTTTCAGGGC | TEV-site |
| GGATCC | <i>BamHI</i> |
| GTCGAC | <i>SalI</i> |
| TAG | Stop codon |

7.2 Sequencing results

Primer forward: 5' GTA ACA GTT TTG TAA TAA AAA AAC C 3'

Primer reverse: 5' GTT TCA GGT TCA GGG GGA GGT GTG GG 3'

Uniprot ID: P60484 (PTEN *Homo Sapiens*)

M: Translation start
HHHHHH: His₆-tag
ENLYFGQ: TEV-recognition site

7.2.1 His-TEV-PTEN 1-403

Plasmid description: pFH1/(*Nde*I)-His₆-TEV-PTEN 1-403-(*Sal*I)

Clone description: Mi-2

Forward

```

Mi-2_forw      MSYYHHHHHDYDIPTTENLYFQGMTAI IKEIVSRNKRRYQEDGFDDLTYIYPNIIAMG 60
PTEN_human    -----MTAI IKEIVSRNKRRYQEDGFDDLTYIYPNIIAMG 36
                *****

Mi-2_forw      FPAERLEGVYRNNIDDVVRFLDSKHKNHKYIYNLCAERHYDTAKFNCRVAQYPFEDHNPP 120
PTEN_human    FPAERLEGVYRNNIDDVVRFLDSKHKNHKYIYNLCAERHYDTAKFNCRVAQYPFEDHNPP 96
                *****

Mi-2_forw      QLELIKPFCELDLQWLSEDDNHVAAIHCKAGKGRGTGVMICAYLLHRGKFLKAQEALDFYG 180
PTEN_human    QLELIKPFCELDLQWLSEDDNHVAAIHCKAGKGRGTGVMICAYLLHRGKFLKAQEALDFYG 156
                *****

Mi-2_forw      EVRTRDKKGVTI PSQRRYVYYSYLLKNHLDYRPVALLFHKMMFETIPMFSGGTCNPQFV 240
PTEN_human    EVRTRDKKGVTI PSQRRYVYYSYLLKNHLDYRPVALLFHKMMFETIPMFSGGTCNPQFV 216
                *****

Mi-2_forw      VCQLKVKIYSSNSGPTREDKFMFYFEPQPLPVCVDIKVEFFHKQNKMLKKDKMFHFWVN 300
PTEN_human    VCQLKVKIYSSNSGPTREDKFMFYFEPQPLPVCVDIKVEFFHKQNKMLKKDKMFHFWVN 276
                *****

Mi-2_forw      TFFIPGPEETSE----- 312
PTEN_human    TFFIPGPEETSEKVENGLCDQEIDSICSIERADNDKEYLVLTLTKNLDKANKDKANRY 336
                *****

Mi-2_forw      -----
PTEN_human    FSPNFVKLYFTKTVEEPSNPEASSSTSVTPDVSDNEPDHYRSDTTSDPENEPFDEDQ 396

Mi-2_forw      -----
PTEN_human    HTQITKV 403

Reverse
PTEN_human    MTAI IKEIVSRNKRRYQEDGFDDLTYIYPNIIAMGFPAERLEGVYRNNIDDVVRFLDSK 60
Mi-2_rev      -----

PTEN_human    HKNHYKIYNLCAERHYDTAKFNCRVAQYPFEDHNPPQLELIKPFCELDLQWLSEDDNHVA 120
Mi-2_rev      -----

PTEN_human    AIHCKAGKGRGTGVMICAYLLHRGKFLKAQEALDFYGEVTRDKKGVTI PSQRRYVYYSY 180
Mi-2_rev      -----RGKFLKAQEALDFYGEVTRDKKGVTI PSQRRYVYYSY 39
                *****

PTEN_human    LLKNHLDYRPVALLFHKMMFETIPMFSGGTCNPQFVVCQLKVKIYSSNSGPTREDKFMFY 240
Mi-2_rev      LLKNHLDYRPVALLFHKMMFETIPMFSGGTCNPQFVVCQLKVKIYSSNSGPTREDKFMFY 99
                *****

PTEN_human    FEFPQPLPVCVDIKVEFFHKQNKMLKKDKMFHFWVNTFFIPGPEETSEKVENGLCDQEI 300
Mi-2_rev      FEFPQPLPVCVDIKVEFFHKQNKMLKKDKMFHFWVNTFFIPGPEETSEKVENGLCDQEI 159
                *****

PTEN_human    DSICSIERADNDKEYLVLTLTKNLDKANKDKANRYFSPNFVKLYFTKTVEEPSNPEAS 360
Mi-2_rev      DSICSIERADNDKEYLVLTLTKNLDKANKDKANRYFSPNFVKLYFTKTVEEPSNPEAS 219
                *****

PTEN_human    SSTSVTPDVSDNEPDHYRSDTTSDPENEPFDEDQHTQITKV 403
Mi-2_rev      SSTSVTPDVSDNEPDHYRSDTTSDPENEPFDEDQHTQITKV 262
                *****

```


7.2.2 His₆-TEV-PTEN 6-403Plasmid description: pFH1/(NdeI)-His₆-TEV-PTEN 6-403-(Sall)

Clone description: Mi-26

Forward

```

PTEN_human      -----MTAIIKEIVSRNKRRYQEDGFDLDTYIYPNIIAMGFPAE 40
Mi-26_forw      HMSYYHHHHHDYDIPTTENLYFQKKEIVSRNKRRYQEDGFDLDTYIYPNIIAMGFPAE 60
                  :          *****

PTEN_human      RLEGVYRNNIDDVVRFLDSKHKNHKYIYNLCAERHYDTAKFNCRVAQYPFEDHNPPQLEL 100
Mi-26_forw      RLEGVYRNNIDDVVRFLDSKHKNHKYIYNLCAERHYDTAKFNCRVAQYPFEDHNPPQLEL 120
                  *****

PTEN_human      IKPFCEDLDQWLSEDDNHVAIIHCKAGKGRGTGVMICAYLLHRGKFLKAQEALDFYGEVRT 160
Mi-26_forw      IKPFCEDLDQWLSEDDNHVAIIHCKAGKGRGTGVMICAYLLHRGKFLKAQEALDFYGEVRT 180
                  *****

PTEN_human      RDKKGV TIP SQRRYVYYSYLLKNHLDYRPVALLFHKMMFETIPMFSGGTCNPQFVVCQL 220
Mi-26_forw      RDKKGV TIP SQRRYVYYSYLLKNHLDYRPVALLFHKMMFETIPMFSGGTCNPQFVVCQL 240
                  *****

PTEN_human      KVKIYSSNSGPTRRREDKFMFEFPQPLPVCGLKVEFFHKQNKMLKKDKMFHFWNTFFI 280
Mi-26_forw      KVKIYSSNSGPTRRREDKFMFEFPQPLPVCGLKVEFFHKQNK----- 283
                  *****

PTEN_human      PGPEETSEKVENGLCDQEIDSICSIERADNDKEYLVLTLTKNLDKANKDKANRYFSPN 340
Mi-26_forw      -----

PTEN_human      FVKVLYFTKTVEEPSNPEASSSTSVTPDVSDNEPDHYRYSDDTSDPENEPFDEDQHTQI 400
Mi-26_forw      -----

PTEN_human      TKV 403
Mi-26_forw      ---

```

Reverse

```

PTEN_human      MTAIIKEIVSRNKRRYQEDGFDLDTYIYPNIIAMGFPAERLEGVYRNNIDDVVRFLDSK 60
Mi-26_rev      -----

PTEN_human      HKNHXYIYNLCAERHYDTAKFNCRVAQYPFEDHNPPQLELIKPFCELDQWLSEDDNHVA 120
Mi-26_rev      -----

PTEN_human      AIHCKAGKGRGTGVMICAYLLHRGKFLKAQEALDFYGEVTRDKKGV TIP SQRRYVYYSY 180
Mi-26_rev      -----KFLKAQEALDFYGEVTRDKKGV TIP SQRRYVYYSY 37
                  *****

PTEN_human      LLKNHLDYRPVALLFHKMMFETIPMFSGGTCNPQFVVCQLKVKIYSSNSGPTRRREDKFM 240
Mi-26_rev      LLKNHLDYRPVALLFHKMMFETIPMFSGGTCNPQFVVCQLKVKIYSSNSGPTRRREDKFM 97
                  *****

PTEN_human      FEFPQPLPVCGLKVEFFHKQNKMLKKDKMFHFWNTFFIPGPEETSEKVENGLCDQEI 300
Mi-26_rev      FEFPQPLPVCGLKVEFFHKQNKMLKKDKMFHFWNTFFIPGPEETSEKVENGLCDQEI 157
                  *****

PTEN_human      DSICSIERADNDKEYLVLTLTKNLDKANKDKANRYFSPNFVKVLYFTKTVEEPSNPEAS 360
Mi-26_rev      DSICSIERADNDKEYLVLTLTKNLDKANKDKANRYFSPNFVKVLYFTKTVEEPSNPEAS 217
                  *****

PTEN_human      SSTSVPDVSDNEPDHYRYSDDTSDPENEPFDEDQHTQITKV 403
Mi-26_rev      SSTSVPDVSDNEPDHYRYSDDTSDPENEPFDEDQHTQITKV 260
                  *****

```

7.2.3 His₆-TEV-PTEN 16-403

Plasmid description: pFH1/(*Nde*I)-His₆-TEV-PTEN 16-403-(*Sal*I)

Clone description: Mi-33

Forward

```

PTEN_human      -----MTAI I KEI VSRNKRRYQEDGF DLDLTYI YPNIIAMGFPAERLEGVYRNNI 50
Mi-33_forw      HMSYYHHHHHDYDIPTTENLYFQGYQEDGF DLDLTYI YPNIIAMGFPAERLEGVYRNNI 60
                  * . : *****

PTEN_human      DDVVRFLDSKHKHNYKIYNLCAERHYDTAKFNCRVAQYPFEDHNPPQLELIKPFCELDLQ 110
Mi-33_forw      DDVVRFLDSKHKHNYKIYNLCAERHYDTAKFNCRVAQYPFEDHNPPQLELIKPFCELDLQ 120
                  *****

PTEN_human      WLSEDDNHVAAIHCKAGKGR TGVMICAYLLHRGKFLKAQEALDFYGEVTRDKKGV TIPS 170
Mi-33_forw      WLSEDDNHVAAIHCKAGKGR TGVMICAYLLHRGKFLKAQEALDFYGEVTRDKKGV TIPS 180
                  *****

PTEN_human      QRRYVYYYSYLLKNHLDYR PVALLFHKMMFETIPMFSGGTCNPQFVVCQLKVKIYSSNSG 230
Mi-33_forw      QRRYVYYYSYLLKNHLDYR PVALLFHKMMFETIPMFSGGTCNPQFVVCQLKVKIYSSNSG 240
                  *****

PTEN_human      PTRREDKFM YFEFPQPLVCGDIKVEFFHKQNKMLKKDKMFHFWNTFFIPGPEETSEKV 290
Mi-33_forw      PTRREDKFM YFEFPQPLVCGDIKVEFFHKQNKMLKKDKMFHFWNTFFIPGPEETSEKV 300
                  *****

PTEN_human      ENGLCDQEIDSICSIERADNDKEYLVLT LTKNDLDKANKDKANRYFSPNFVKLYFTKT 350
Mi-33_forw      ENGLCDQEIDSICSIERAD----- 320
                  *****

PTEN_human      VEEPSNPEASSSTSVTPDVSDNEPDHYRYS DTTDSDPENEPFDEDQHTQITKV 403
Mi-33_forw      -----

```

Reverse

```

PTEN_human      MTAI I KEI VSRNKRRYQEDGF DLDLTYI YPNIIAMGFPAERLEGVYRNNIDDVVRFLDSK 60
Mi-33_rev      -----

PTEN_human      HKNHYKIYNLCAERHYDTAKFNCRVAQYPFEDHNPPQLELIKPFCELDLQWLSEDDNHVA 120
Mi-33_rev      -----

PTEN_human      AIHCKAGKGR TGVMICAYLLHRGKFLKAQEALDFYGEVTRDKKGV TIPSQRRYVYYYSY 180
Mi-33_rev      -----

PTEN_human      LLKNHLDYR PVALLFHKMMFETIPMFSGGTCNPQFVVCQLKVKIYSSNSGPTREDKFM Y 240
Mi-33_rev      -----TIPMFSGGTCNPQFVVCQLKVKIYSSNSGPTREDKFM Y 39
                  *****

PTEN_human      FEFPQPLVCGDIKVEFFHKQNKMLKKDKMFHFWNTFFIPGPEETSEKVENGLCDQEI 300
Mi-33_rev      FEFPQPLVCGDIKVEFFHKQNKMLKKDKMFHFWNTFFIPGPEETSEKVENGLCDQEI 99
                  *****

PTEN_human      DSICSIERADNDKEYLVLT LTKNDLDKANKDKANRYFSPNFVKLYFTKTVEEPSNPEAS 360
Mi-33_rev      DSICSIERADNDKEYLVLT LTKNDLDKANKDKANRYFSPNFVKLYFTKTVEEPSNPEAS 159
                  *****

PTEN_human      SSTSVPDVSDNEPDHYRYS DTTDSDPENEPFDEDQHTQITKV 403
Mi-33_rev      SSTSVPDVSDNEPDHYRYS DTTDSDPENEPFDEDQHTQITKV 202
                  *****

```

7.2.4 His₆-TEV-PTEN 6-353Plasmid description: pFH1/(NdeI)-His₆-TEV-PTEN 6-353-(Sall)

Clone description: Mi-53

Forward

```

PTEN_human          -----MTAIIKEIVSRNKRRYQEDGFDLDLTYIYPNI IAMGFPAE 40
Mi-53_forw          HMSYYHHHHHDYDIPTTENLYFQKKEIVSRNKRRYQEDGFDLDLTYIYPNI IAMGFPAE 60
                    :          *****

PTEN_human          RLEGVYRNNIDDVVRFLDSKHKNHYKIYNLCAERHYDTAKFNCRVAQYPFEDHNPPQLEL 100
Mi-53_forw          RLEGVYRNNIDDVVRFLDSKHKNHYKIYNLCAERHYDTAKFNCRVAQYPFEDHNPPQLEL 120
                    *****

PTEN_human          IKPFCEDLDQWLSEDDNHVAIIHCKAGKGRGTGVMICAYLLHRGKFLKAQEALDFYGEVRT 160
Mi-53_forw          IKPFCEDLDQWLSEDDNHVAIIHCKAGKGRGTGVMICAYLLHRGKFLKAQEALDFYGEVRT 180
                    *****

PTEN_human          RDKKGVTIPSQRRYVYVYVSYLLKNHLDYRPVALLFHKMMFETIPMFSGGTCNPQFVVCQL 220
Mi-53_forw          RDKKGVTIPSQRRYVYVYVSYLLKNHLDYRPVALLFHKMMFETIPMFSGGTCNPQFVVCQL 240
                    *****

PTEN_human          KVKIYSSNSGPTRRREDKFMFEFPQPLPVCGLKVEFFHKQNKMLKKDKMFHFWNTFFI 280
Mi-53_forw          KVKIYSSNSGPTRRREDKFMFEFPQPLPVCGLKVEFFHKQNKMLKKDKMFHFWNTFFI 300
                    *****

PTEN_human          PGPEETSEKVENGLCDQEIDSICSIERADNDKEYLVLTLTKNLDKANKDKANRYFSPN 340
Mi-53_forw          PGPEET----- 306
                    *****

PTEN_human          FKVKLYFTKTVEEPSNPEASSSTSVTPDVSDNEPDHYRSDTTDSDPENEPFDEDQHTQI 400
Mi-53_forw          -----

PTEN_human          TKV 403
Mi-53_forw          ---

Reverse
PTEN_human          MTAI I KEIVSRNKRRYQEDGFDLDLTYIYPNI IAMGFPAERLEGVYRNNIDDVVRFLDSK 60
Mi-53_rev          -----

PTEN_human          HKNHYKIYNLCAERHYDTAKFNCRVAQYPFEDHNPPQLELIKPFCEDLDQWLSEDDNHVA 120
Mi-53_rev          -----EDDNHVA 7
                    *****

PTEN_human          AIHCKAGKGRGTGVMICAYLLHRGKFLKAQEALDFYGEVTRDKKGVTPSQRRYVYVYVSY 180
Mi-53_rev          AIHCKAGKGRGTGVMICAYLLHRGKFLKAQEALDFYGEVTRDKKGVTPSQRRYVYVYVSY 67
                    *****

PTEN_human          LLKNHLDYRPVALLFHKMMFETIPMFSGGTCNPQFVVCQLKVKIYSSNSGPTRRREDKFM 240
Mi-53_rev          LLKNHLDYRPVALLFHKMMFETIPMFSGGTCNPQFVVCQLKVKIYSSNSGPTRRREDKFM 127
                    *****

PTEN_human          FEFPQPLPVCGLKVEFFHKQNKMLKKDKMFHFWNTFFIPGPEETSEKVENGLCDQEI 300
Mi-53_rev          FEFPQPLPVCGLKVEFFHKQNKMLKKDKMFHFWNTFFIPGPEETSEKVENGLCDQEI 187
                    *****

PTEN_human          DSICSIERADNDKEYLVLTLTKNLDKANKDKANRYFSPNFVKVLYFTKTVEEPSNPEAS 360
Mi-53_rev          DSICSIERADNDKEYLVLTLTKNLDKANKDKANRYFSPNFVKVLYFTKTVEE----- 240
                    *****

PTEN_human          SSTSVTPDVSDNEPDHYRSDTTDSDPENEPFDEDQHTQITKV 403
Mi-53_rev          -----

```

7.2.5 His₆-TEV-PTEN 16-353Plasmid description: pFH1/(NdeI)-His₆-TEV-PTEN 16-353-(SalI)

Clone description: Mi-63

Forward

```

PTEN_human      -----MTAI I KEIVSRNKRRYQEDGF DLDLTYIYPNI IAMGFPAERLEGVYRNNI  50
Mi-63_forw      HMSYYHHHHHDYDIPTTENLYFQYQEDGF DLDLTYIYPNI IAMGFPAERLEGVYRNNI  60
                  *      .      : *****

PTEN_human      DDVVRFLDSKHKHNYKIYNLCAERHYDTAKFNCRVAQYPFEDHNPPQLELIKPFCELDLQ  110
Mi-63_forw      DDVVRFLDSKHKHNYKIYNLCAERHYDTAKFNCRVAQYPFEDHNPPQLELIKPFCELDLQ  120
                  *****

PTEN_human      WLSEDDNHVAAIHCKAGKGR TGVMICAYLLHRGKFLKAQEALDFYGEVTRDKKGV TIPS  170
Mi-63_forw      WLSEDDNHVAAIHCKAGKGR TGVMICAYLLHRGKFLKAQEALDFYGEVTRDKKGV TIPS  180
                  *****

PTEN_human      QRRYVYYYSYLLKNHLDYR PVALLFHKMMFETIPMFSGGTCNPQFVVCQLKVKIYSSNSG  230
Mi-63_forw      QRRYVYYYSYLLKNHLDYR PVALLFHKMMFETIPMFSGGTCNPQFVVCQLKVKIYSSNSG  240
                  *****

PTEN_human      PTRREDKFM YFEFPQPLPVC GDIKVEFFHKQNKMLKKDKMFHFWNTFFIPGPEETSEKV  290
Mi-63_forw      PTRREDKFM YFEFPQPLPVC GDIKVEFFHKQNKMLKKDKMFHFWNTFFIPGPEETSEKV  300
                  *****

PTEN_human      ENGLCDQEIDSICSIERADNDKEYLVLT LTKNDL DKANKDKANRYFSPNFVKLYFTKT  350
Mi-63_forw      ENGLCDQEIDSICSIER-----  318
                  *****

PTEN_human      VEEPSNPEASSSTSVTPDVSDNEPDHYRYS DTTDSDPENEPFDEDQHTQITKV  403
Mi-63_forw      -----

```

Reverse

```

PTEN_human      MTAI I KEIVSRNKRRYQEDGF DLDLTYIYPNI IAMGFPAERLEGVYRNNIDDVVRFLDSK  60
Mi-63_rev      -----

PTEN_human      HKNHYKIYNLCAERHYDTAKFNCRVAQYPFEDHNPPQLELIKPFCELDLQWLSEDDNHVA  120
Mi-63_rev      -----

PTEN_human      AIHCKAGKGR TGVMICAYLLHRGKFLKAQEALDFYGEVTRDKKGV TIPSQRRYVYYYSY  180
Mi-63_rev      -----DKKGV TIPSQRRYVYYYSY  19
                  *****

PTEN_human      LLKNHLDYR PVALLFHKMMFETIPMFSGGTCNPQFVVCQLKVKIYSSNSGPTREDKFM Y  240
Mi-63_rev      LLKNHLDYR PVALLFHKMMFETIPMFSGGTCNPQFVVCQLKVKIYSSNSGPTREDKFM Y  79
                  *****

PTEN_human      FEFPQPLPVC GDIKVEFFHKQNKMLKKDKMFHFWNTFFIPGPEETSEKVENGLCDQEI  300
Mi-63_rev      FEFPQPLPVC GDIKVEFFHKQNKMLKKDKMFHFWNTFFIPGPEETSEKVENGLCDQEI  139
                  *****

PTEN_human      DSICSIERADNDKEYLVLT LTKNDL DKANKDKANRYFSPNFVKLYFTKTVEEPSNPEAS  360
Mi-63_rev      DSICSIERADNDKEYLVLT LTKNDL DKANKDKANRYFSPNFVKLYFTKTVEE-----  192
                  *****

PTEN_human      SSTSVTPDVSDNEPDHYRYS DTTDSDPENEPFDEDQHTQITKV  403
Mi-63_rev      -----

```

7.2.6 His-TEV-PTEN 7-353 Δ286-309

Protein construct: His₆-TEV-PTEN 7-353 Δ286-309

Plasmid description: pFH1/(*Nde*I)-His-TEV-PTEN 7-353ID-(*Sal*I)

Clone description: Mi-41

Forward

```

PTEN_human      -----MTAIKEIVSRNKRRYQEDGFDDLTYIYPNIIAMGFPAER 41
Mi-41_forw      HMSYYHHHHHDYDIPTTENLYFQGEIVSRNKRRYQEDGFDDLTYIYPNIIAMGFPAER 60
                  : *****

PTEN_human      LEGVYRNNIDDVVRFLDSKHKHNYKIYNLCAERHYDTAKFNCRVAQYPFEDHNPPQLELI 101
Mi-41_forw      LEGVYRNNIDDVVRFLDSKHKHNYKIYNLCAERHYDTAKFNCRVAQYPFEDHNPPQLELI 120
                  *****

PTEN_human      KPFCEDLDQWLSDDNHVAAIHCKAGKGRGTGVMICAYLLHRGKFLKAQEALDFYGEVRTR 161
Mi-41_forw      KPFCEDLDQWLSDDNHVAAIHCKAGKGRGTGVMICAYLLHRGKFLKAQEALDFYGEVRTR 180
                  *****

PTEN_human      DKKGVTIPSRRYVYYYSYLLKNHLDYRPVALLFHKMMFETIPMFSGGTCNPQFVVCQLK 221
Mi-41_forw      DKKGVTIPSRRYVYYYSYLLKNHLDYRPVALLFHKMMFETIPMFSGGTCNPQFVVCQLK 240
                  *****

PTEN_human      VKIYSSNSGPTREDKFMYYFEFPQPLVCGDIKVEFFHKQNKMLKKDKMFHFWVNTFFIP 281
Mi-41_forw      VKIYSSN----- 247
                  *****

PTEN_human      GPEETSEKVENGSLCDQEIDSICSIERADNDKEYLVLTLTKNLDKANKDKANRYFSPNF 341
Mi-41_forw      -----

PTEN_human      KVKLYFTKTVEEPSNPEASSSTSVTPDVS DNEPDHYRYS DTTDSDPENEPFDEDQHTQIT 401
Mi-41_forw      -----

PTEN_human      KV 403
Mi-41_forw      --

Reverse
PTEN_human      MTAIKEIVSRNKRRYQEDGFDDLTYIYPNIIAMGFPAERLEGVYRNNIDDVVRFLDSK 60
Mi-41_rev      -----

PTEN_human      HKNHYKIYNLCAERHYDTAKFNCRVAQYPFEDHNPPQLELIKPFCELDQWLSDDNHVA 120
Mi-41_rev      -----NHVA 4
                  ****

PTEN_human      AIHCKAGKGRGTGVMICAYLLHRGKFLKAQEALDFYGEVRTRDKKGVTIPSRRYVYYYSY 180
Mi-41_rev      AIHCKAGKGRGTGVMICAYLLHRGKFLKAQEALDFYGEVRTRDKKGVTIPSRRYVYYYSY 64
                  *****

PTEN_human      LLKNHLDYRPVALLFHKMMFETIPMFSGGTCNPQFVVCQLKVKIYSSNSGPTREDKFMYY 240
Mi-41_rev      LLKNHLDYRPVALLFHKMMFETIPMFSGGTCNPQFVVCQLKVKIYSSNSGPTREDKFMYY 124
                  *****

PTEN_human      FEFPQPLVCGDIKVEFFHKQNKMLKKDKMFHFWVNTFFIPGPEETSEKVENGSLCDQEI 300
Mi-41_rev      FEFPQPLVCGDIKVEFFHKQNKMLKKDKMFHFWVNTFFIPGPEE----- 169
                  *****

PTEN_human      DSICSIERADNDKEYLVLTLTKNLDKANKDKANRYFSPNFKVKLYFTKTVEEPSNPEAS 360
Mi-41_rev      -----DNDKEYLVLTLTKNLDKANKDKANRYFSPNFKVKLYFTKTVEE----- 213
                  *****

PTEN_human      SSTSVTPDVS DNEPDHYRYS DTTDSDPENEPFDEDQHTQITKV 403
Mi-41_rev      -----

```

7.3 SDS-PAGE and SEC analyses of the protein purification

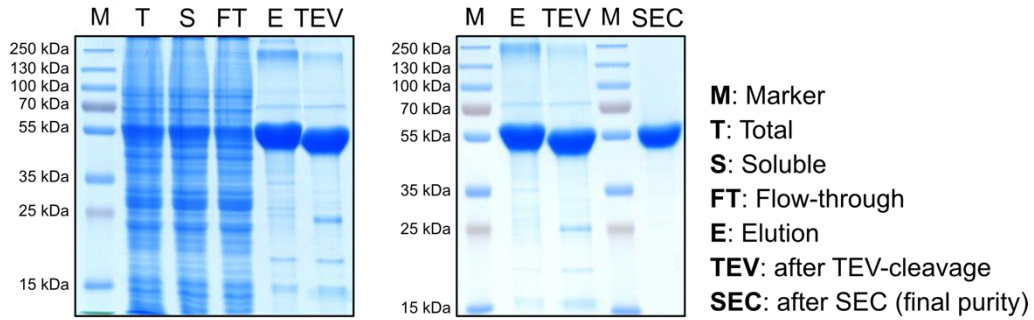


Figure 46 | SDS-analysis of protein purification (PTEN 6-403)

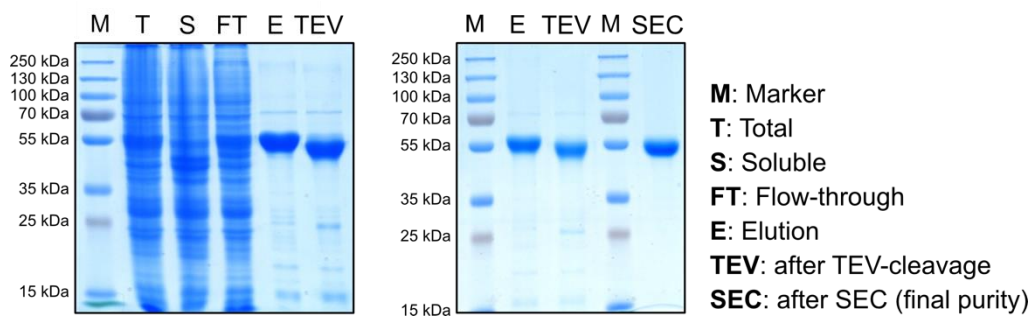


Figure 47 | SDS-analysis of protein purification (PTEN 16-403)

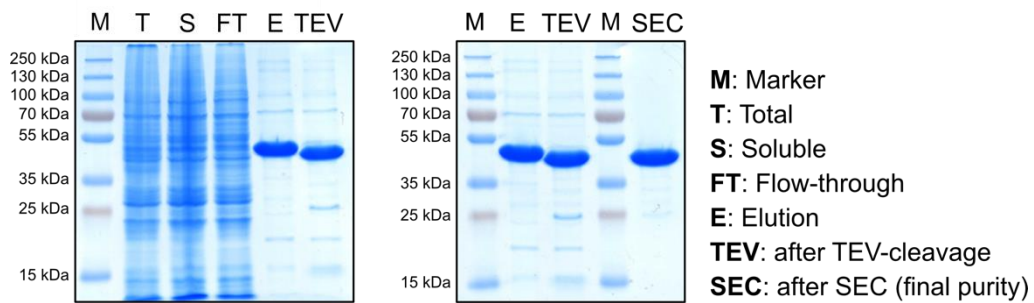


Figure 48 | SDS-analysis of protein purification (PTEN 6-353)

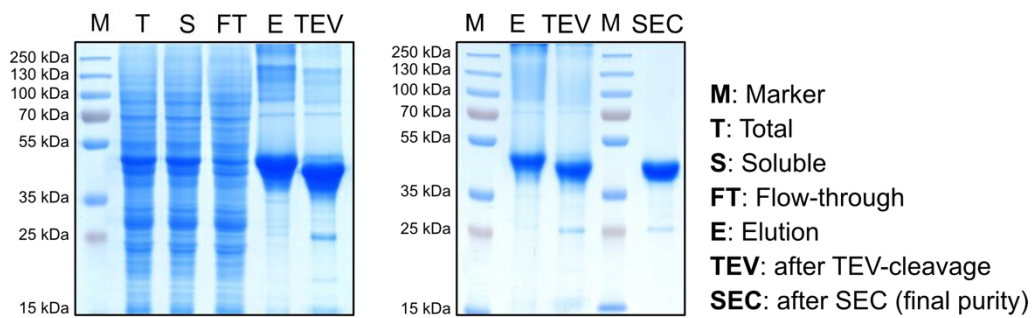


Figure 49 | SDS-analysis of protein purification (PTEN 16-353)

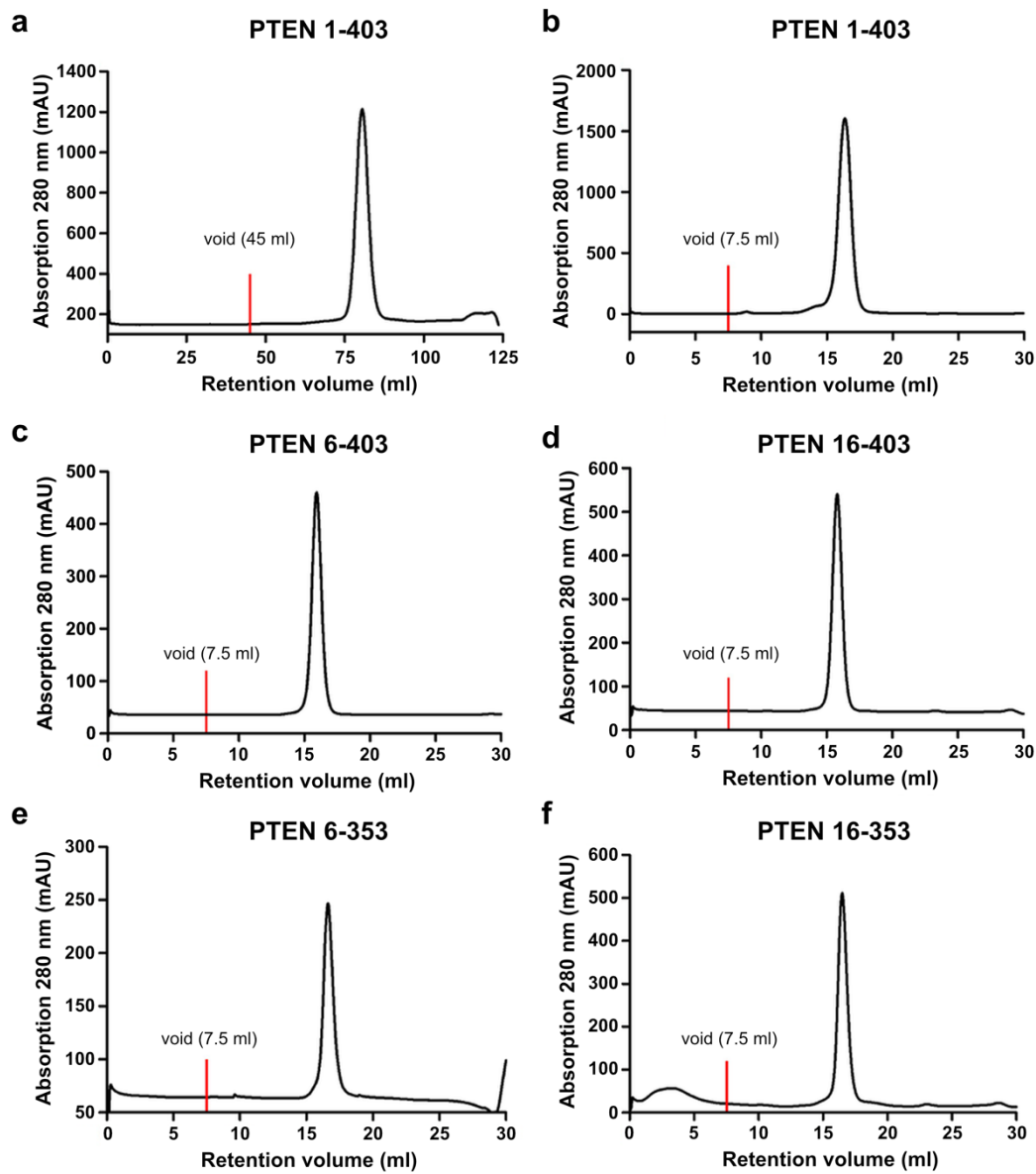


Figure 50 | Size exclusion chromatograms of PTEN constructs. (a) Preparative size exclusion chromatogram of full-length PTEN 1-403 using HiLoadTM SuperdexTM S200 16/60. (b – f) Analytical size exclusion chromatograms of various PTEN constructs using HiLoadTM SuperdexTM S200 10/30. Void volumes are marked with a red bar.

7.4 Detection of disulfide formation using HPLC-MS and MS/MS

Full-length PTEN

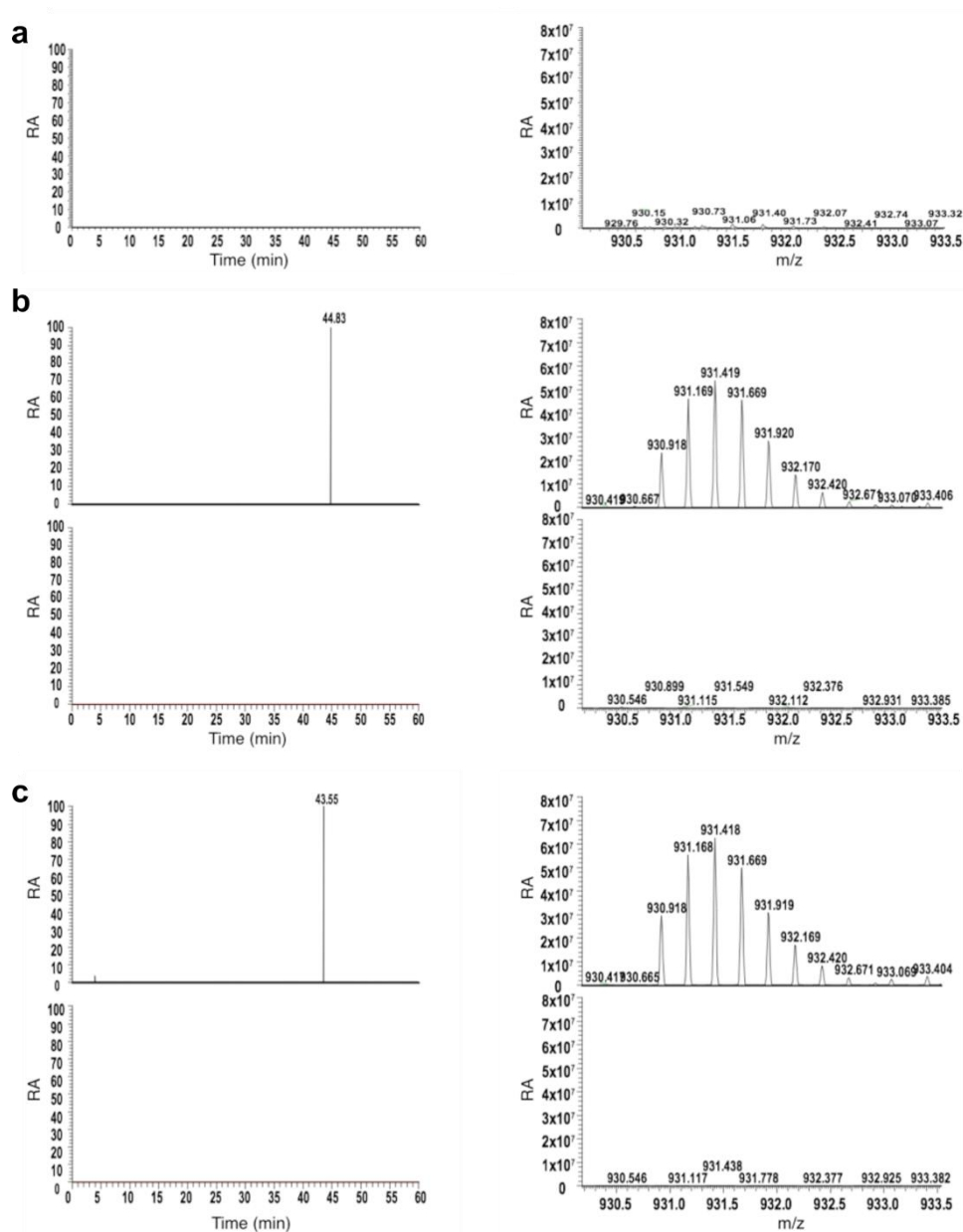


Figure 51 | Determination of disulfide formation between C71 and C124 in full-length PTEN using HPLC-coupled high resolution mass spectrometry. Compared to (a) buffer treatment, the disulfide-bridged tryptic fragment is detected after incubation with (b) 1 mM H₂O₂ or (c) 1 mM bpV-phen (T = 25 °C, 100 μM PTEN, t = 10 min). The corresponding peak in HPLC chromatogram and its high resolution MS-spectra (mass error < 1 ppm) are represented in the left and right panel, respectively. Treatment with 10 mM DTT diminishes the disulfide-bridged tryptic fragment (b and c, lower panel). Sample preparation is performed by the author of this thesis. The measurements and data analysis are carried out by Dr. Tanja Bange and Franziska Müller. This figure is from the reference No. 171, © 2015 The Authors. Published by Wiley-VCH Verlag GmbH & Co. KGaA.

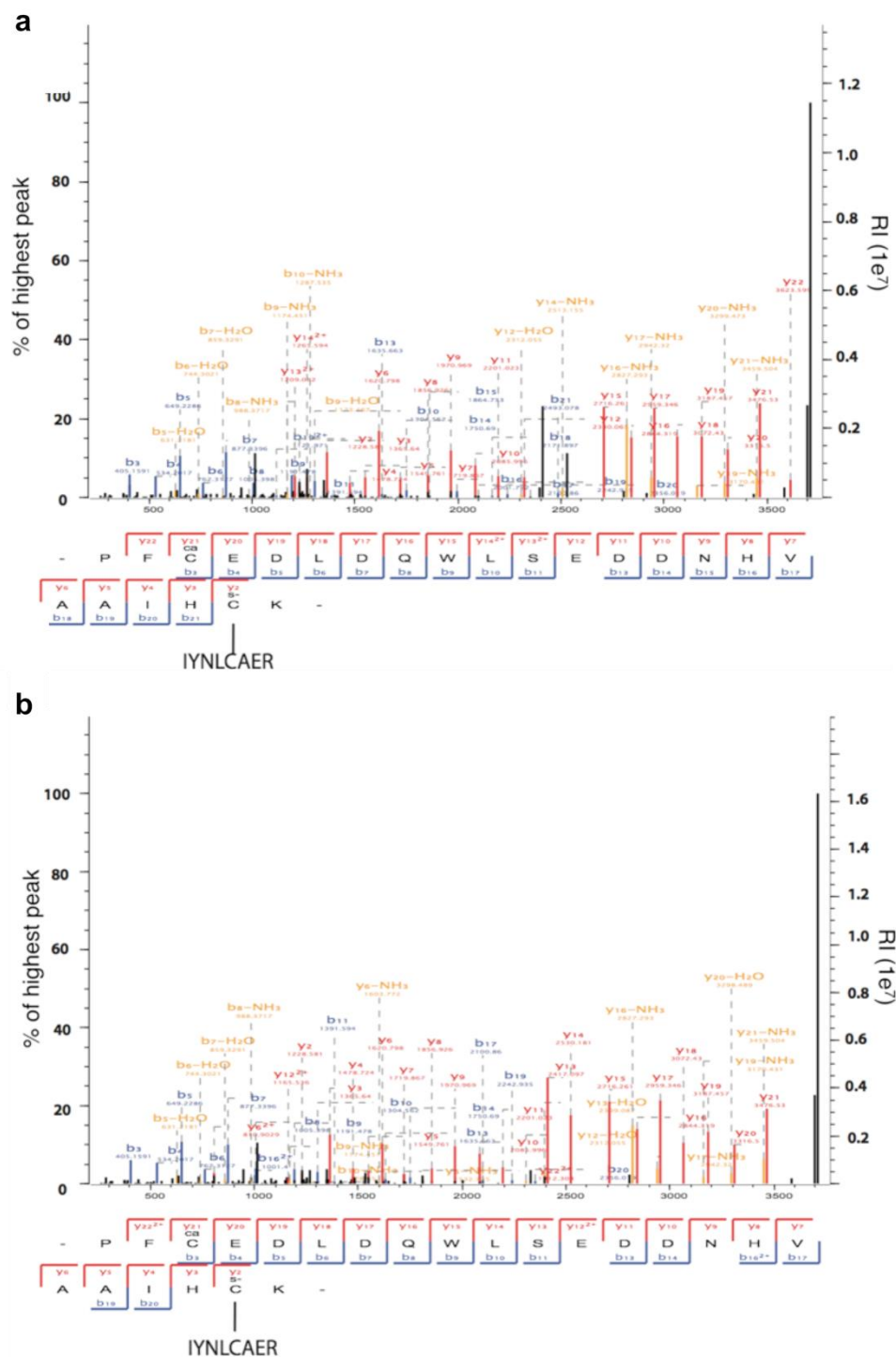


Figure 52 | MS/MS spectra confirms disulfide formation between C71 and C124 in full-length PTEN. Following treatment with (a) 1 mM H₂O₂ and (b) 1 mM bpV-phen (T = 25 °C, 100 μM PTEN, t = 10 min), MS/MS spectra of corresponding samples are searched giving the mass of C71-containing peptide (IYNLCAER) cross-linked to any peptide fragments including C124. The spectra show the annotated disulfide-bridged peptides. The tryptic fragment has been sequenced over 300 times. Sample preparation is performed by the author of this thesis. The measurements and data analysis are carried out by Dr. Tanja Bange and Franziska Müller. This figure is from the reference No. 171, © 2015 The Authors. Published by Wiley-VCH Verlag GmbH & Co. KGaA.

Truncated PTEN

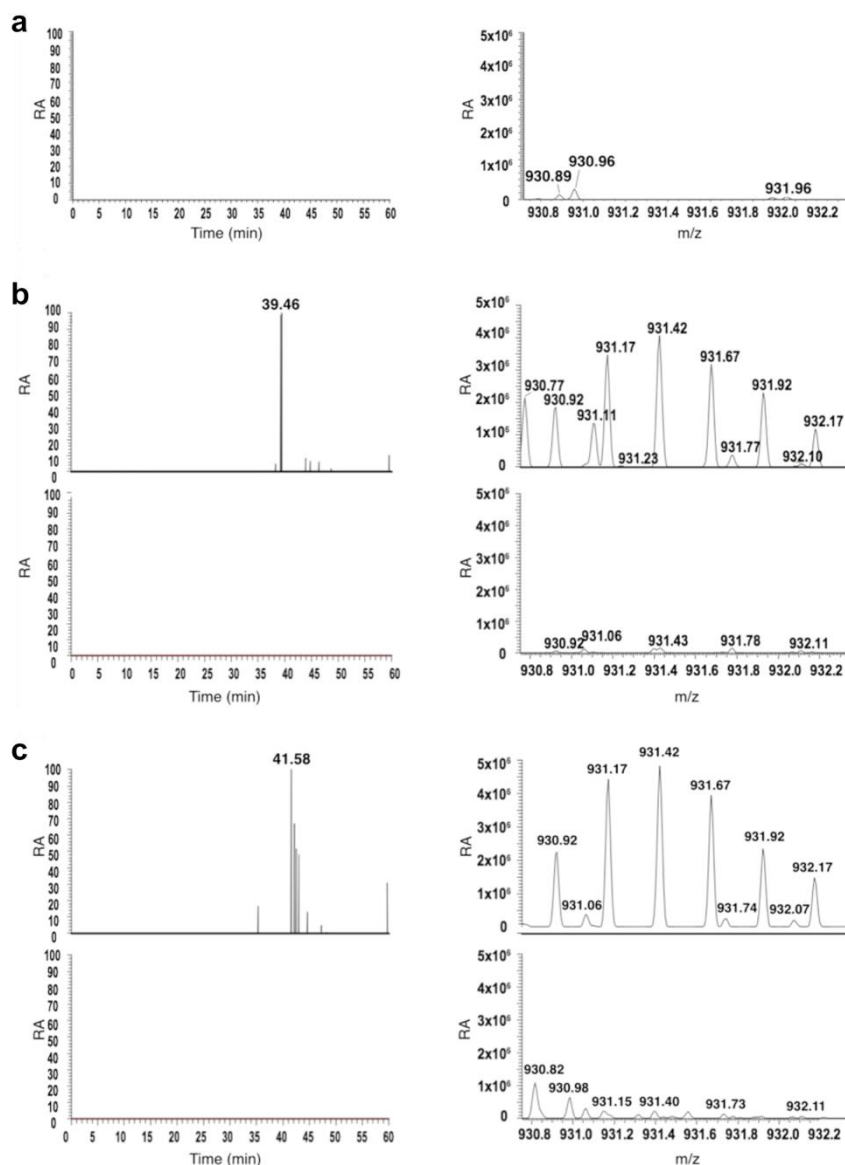


Figure 53 | Determination of disulfide formation between C71 and C124 in *t*PTEN using HPLC-coupled high resolution mass spectrometry. Compared to (a) buffer treatment, the disulfide-bridged tryptic fragment is detected after incubation with (b) 1 mM H₂O₂ or (c) 1 mM bpV-phen (T = 25 °C, 100 μM PTEN, t = 10 min). The corresponding peak in HPLC chromatogram and its high resolution MS-spectra (mass error < 1 ppm) are represented in the left and right panel, respectively. Treatment with 10 mM DTT diminishes the disulfide-bridged tryptic fragment (b and c, lower panel). Sample preparation is performed by the author of this thesis. The measurements and data analysis are carried out by Dr. Tanja Bange and Franziska Müller. This figure is from the reference No. 171, © 2015 The Authors. Published by Wiley-VCH Verlag GmbH & Co. KGaA.

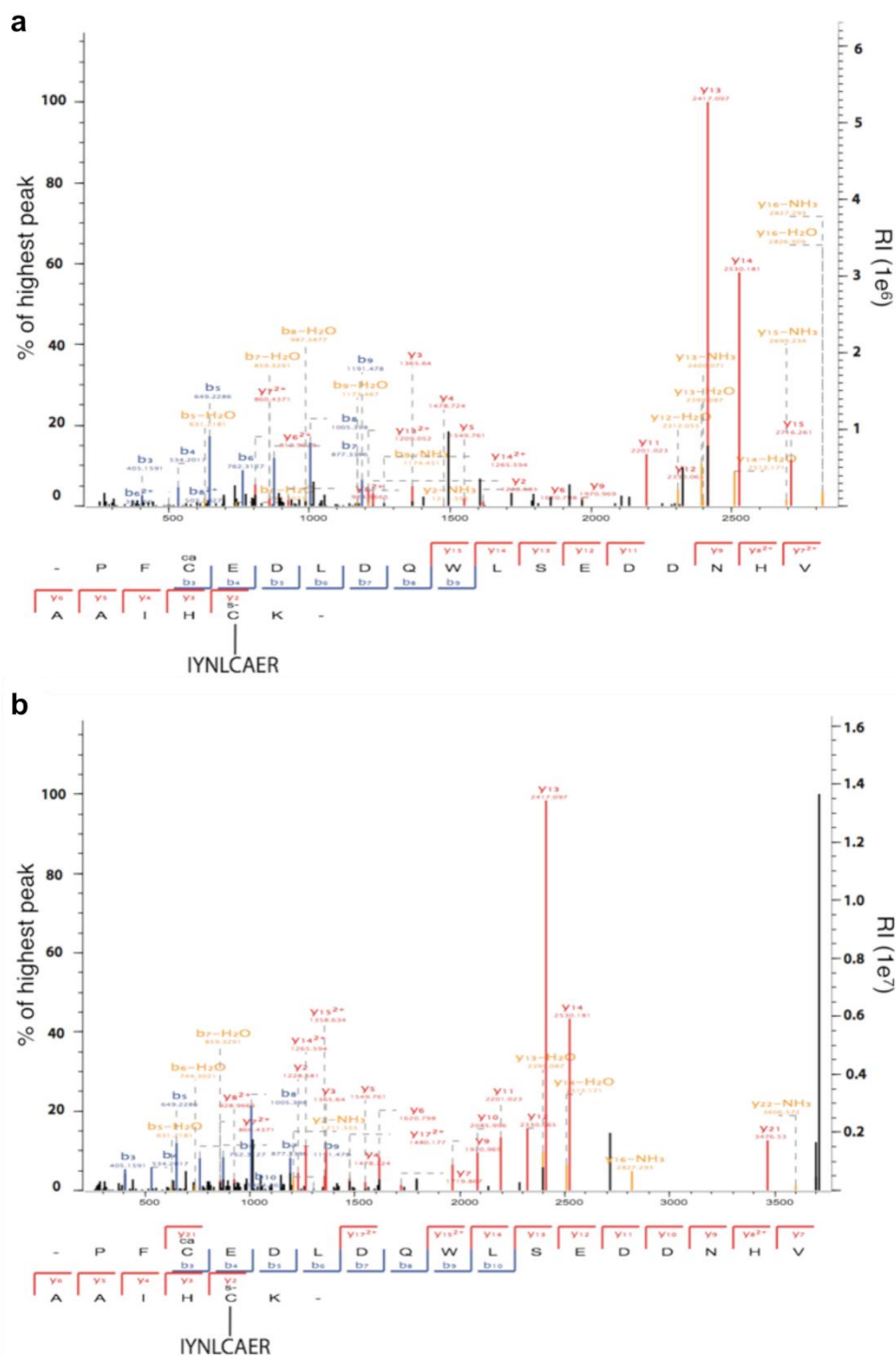


Figure 54 | MS/MS spectra confirms disulfide formation between C71 and C124 in *t*PTEN. Following treatment with (a) 1 mM H_2O_2 and (b) 1 mM bpV-phen ($T = 25^\circ\text{C}$, $100\ \mu\text{M}$ PTEN, $t = 10$ min), MS/MS spectra of corresponding samples are searched giving the mass of C71-containing peptide (IYNLCAER) cross-linked to any peptide fragments including C124. The spectra show the annotated disulfide-bridged peptides. The tryptic fragment has been sequenced over 300 times. Sample preparation is performed by the author of this thesis. The measurements and data analysis are carried out by Dr. Tanja Bange and Franziska Müller. This figure is from the reference No. 171, © 2015 The Authors. Published by Wiley-VCH Verlag GmbH & Co. KGaA.

7.5 Influence of tartrate on oxidative inhibition and reactivation

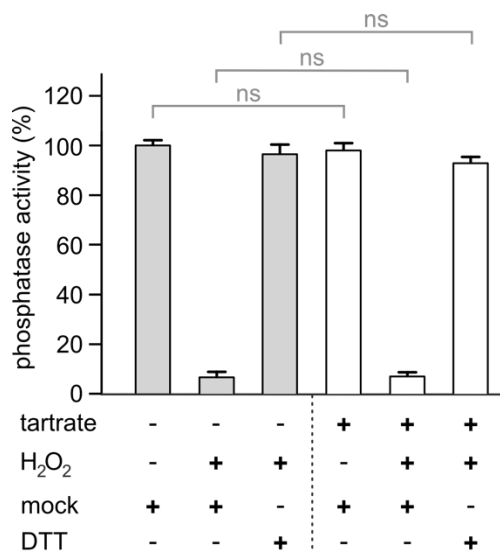


Figure 55 | Tartrate does not have a significant impact on oxidation and reactivation of PTEN.

In order to confirm the oxidative inhibition and reactivation of PTEN under the crystal soaking condition, phosphatase activity of PTEN is determined under high concentration tartrate. Full-length PTEN (50 μ M) is treated with H₂O₂ (5 mM, 20 min) in buffer (gray) or buffer containing tartrate (1.5 M, white). Following oxidation, 20-fold dilution (10 min) is performed with buffer lacking or containing 4 mM DTT. Phosphatase activities are given relative to the untreated protein sample (absence of H₂O₂, tartrate and DTT). Errors account for \pm SD (triplicates; ns: $P > 0.05$). This figure is from the reference No. 171, © 2015 The Authors. Published by Wiley-VCH Verlag GmbH & Co. KGaA.

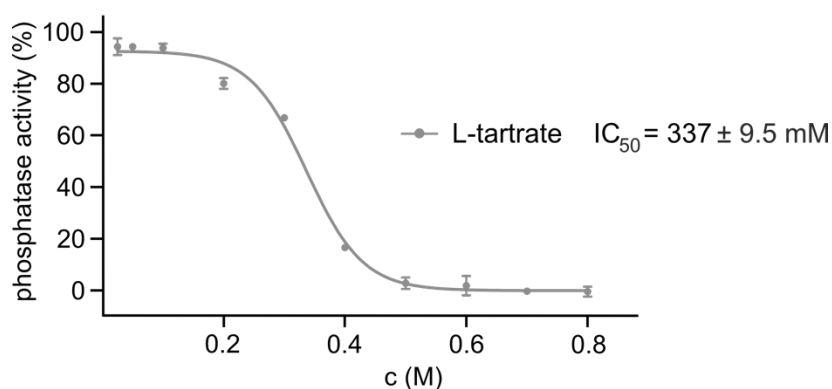


Figure 56 | Tartrate has low impact on the phosphatase activity of PTEN. Half-maximal concentration (IC_{50}) of tartrate is determined by enzymatic activity measurements using malachite green assay. (50 nM full-length PTEN, 75 μ M PI(3,4,5)P₃-diC8 as substrate, $T = 25$ °C, $t = 30$ min; triplicates, errors represent \pm SD.)

7.6 SDS-PAGE and SEC analyses of the protein purification

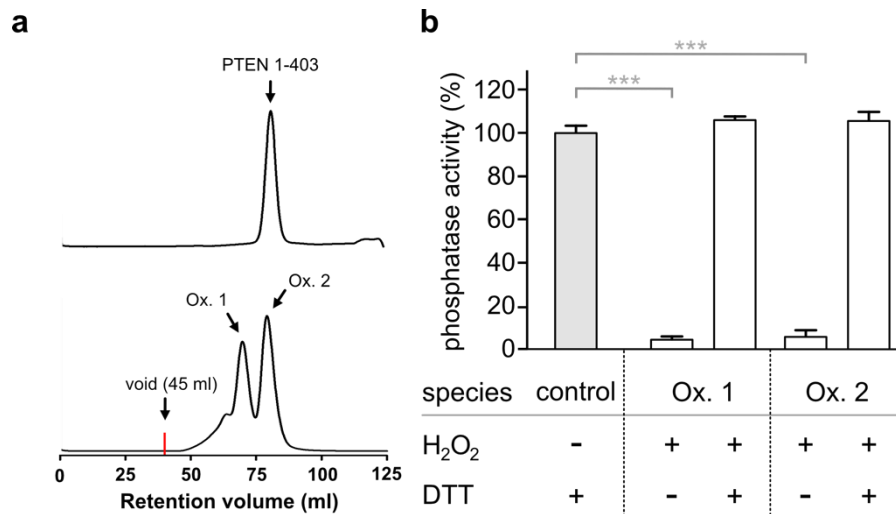


Figure 57 | Size exclusion chromatography chromatograms of H₂O₂-treated PTEN 1-403 and its phosphatase activity. (a) H₂O₂-treatment (2 mM) of the purified PTEN 1-403 (upper) results in two species, which are separated using the subsequent size exclusion chromatography (lower). HiLoad™ Superdex™ S200 16/60 prep grade is used. (b) Phosphatase activity of each species is determined using malachite green assay. H₂O₂-treated species show effective inhibition after the following purification, of which the phosphatase activity is restored completely in the presence of DTT (4 mM). (T = 25 °C, triplicates, errors account for 1σ; *** *P* < 0.001)

8 Abbreviations

| | | |
|--------------------|---|--|
| A (Base) | = | Adenine |
| Akt (PKB) | = | Protein kinase B |
| APC/C | = | Anaphase promoting complex / cyclosome |
| APS | = | Ammonium persulfate |
| ASU | = | Asymmetric unit |
| <i>Bam</i> HI | = | Restriction enzyme (recognition sequence G ^A GATCC) |
| bp | = | Base pair |
| bpV | = | Bisperoxidovanadium |
| bpV-HOpic | = | Bisperoxido (5-hydroxypyridine-2-carboxy) oxovanadate (V) |
| bpV-phen | = | Bisperoxido(1,10-phenanthroline) oxovanadate (V) |
| bpV-pic | = | Bisperoxido (picolinato) oxovanadate (V) |
| BSA | = | Bovine serum albumin |
| C (Base) | = | Cytosine |
| C' | = | C-terminus |
| C α | = | Carbon atom at the alpha position in an amino acid |
| ca. | = | Circa |
| CBP | = | CREB-binding protein |
| CBR3-loop | = | Calcium-binding region 3 loop |
| CC _{1/2} | = | Correlation coefficient of two half datasets |
| CDC25B | = | M-phase inducer phosphatase 2 |
| CDH1 | = | Adaptor protein of APC |
| CHAPS | = | 3-[(3-Cholamidopropyl)dimethylammonio]-1-propanesulfonate |
| CK2 | = | Casein kinase 2 |
| CV | = | Column volume |
| ddH ₂ O | = | Bidistilled water |
| DMSO | = | Dimethyl sulfoxide |
| DNA | = | Deoxyribonucleic acid |
| DNase | = | Desoxyribonuclease |
| dNTP | = | Deoxynucleotide triphosphate |
| DPF | = | Dortmund protein facility |
| DTT | = | Dithiothreitol |
| DUSP | = | Dual specificity phosphatase |

| | | |
|-----------------------|---|--|
| <i>E. coli</i> | = | <i>Escherichia coli</i> |
| EDTA | = | Ethylenediaminetetraacetic acid |
| <i>e.g.</i> | = | <i>exempli gratia</i> , for example |
| EGF | = | Epidermal growth factor |
| <i>et al.</i> | = | And others |
| FAK | = | Focal adhesion kinase |
| FBS | = | Fetal Bovine Serum |
| F _{cal} | = | Structure factor (calculated) |
| F _{obs} | = | Structure factor (observed) |
| FP | = | Fluorescence polarization |
| FPLC | = | Fast protein liquid chromatography |
| fw | = | Forward |
| G (Base) | = | Guanine |
| GSH | = | Glutathione reduced |
| GST | = | Glutathione S-transferase |
| GSK3 β | = | Glycogen synthase kinase 3 β |
| HIF-1 α | = | Hypoxia-induced factor-1 α |
| <i>High Five</i> | = | <i>Trichoplusia ni</i> |
| His ₆ -Tag | = | Affinity chromatography involving six histidine in a row |
| HPLC | = | High performance liquid chromatography |
| HPLC-MS | = | HPLC-coupled mass spectrometry |
| IC ₅₀ | = | half maximal inhibitory concentration |
| IEX | = | Ion exchange chromatography |
| IMAC | = | Immobilized metal ion affinity chromatography |
| IP ₃ | = | Inositol trisphosphate |
| IPTG | = | Isopropyl- β -D-thiogalactopyranoside |
| IRS | = | Insulin receptor substrate |
| JCSG | = | Joint Center for Structural Genomics |
| kb | = | Kilobase |
| kDa | = | Kilodalton |
| K _D | = | Dissociation constant |
| K _i | = | Inhibition constant |
| LB | = | Lysogeny broth |
| LMW-PTP | = | Low molecular weight protein tyrosine phosphatase |

| | | |
|-----------------------|---|---|
| LYP | = | Lymphoid tyrosine phosphatase |
| MBP | = | Maltose binding protein |
| MCS | = | Multiple cloning site |
| MES (buffer) | = | 2-(<i>N</i> -morpholino)ethanesulfonic acid |
| MPI | = | Max Planck Institute |
| Mr | = | Molecular mass |
| MS | = | Mass spectrometry |
| MS/MS | = | Tandem mass spectrometry |
| mTORC1/2 | = | Mammalian target of rapamycin complex 1/2 |
| m/z | = | Mass-to-charge ratio |
| <i>N</i> ' | = | <i>N</i> -terminus |
| NADPH | = | Nicotinamide adenine dinucleotide phosphate |
| <i>Nde</i> I | = | Restriction enzyme (recognition sequence CA [^] TATG) |
| NEDD4-1 | = | Ubiquitin Ligase |
| NF-κB | = | Nuclear factor kappa-light-chain-enhancer of activated B cells |
| nhPIP ₃ | = | Non-hydrolyzable variant of PIP ₃ , 3S-PI-(3,4,5)-P3 |
| Ni-NTA | = | Nickel-nitrilotriacetic acid |
| NMR | = | Nuclear magnetic resonance |
| NOX | = | NADPH oxidase |
| N/A | = | Not available |
| ns | = | Not significant |
| OD | = | Optical density |
| Ox. | = | Oxidized (species) |
| <i>P</i> (statistics) | = | P value |
| PBM | = | PIP ₂ -binding motif |
| PCAF | = | Lysine acetyltransferase 2B |
| PCR | = | Polymerase chain reaction |
| PDB | = | Protein Data Bank |
| PDGF | = | Platelet-derived growth factor |
| PDPK1 | = | Phosphoinositide dependent protein kinase 1 |
| PDZ | = | PSD95/SAP90, Discs large und Zonula occludentes-1 |
| pH | = | Potentia hydrogenii |
| pI | = | Isoelectric point |
| PIP ₂ | = | Phosphatidylinositol-4,5-bisphosphate |

| | | |
|------------------|---|--|
| PIP ₃ | = | Phosphatidylinositol-3,4,5-trisphosphate |
| PI3-K | = | Phosphoinositide-3-Kinase |
| P-loop | = | Phosphate-binding loop |
| PMSF | = | Phenylmethylsulfonyl fluoride |
| ppm | = | Parts per million |
| PTP | = | Protein tyrosine phosphatase |
| PTEN | = | Phosphatase and TENsin homolog deleted on chromosome 10 |
| RA | = | Relative abundance |
| RACK | = | fyn-related kinase (also known as FRK) |
| rcf | = | Relative centrifugal force |
| rev | = | Reversed |
| RMSD | = | Root-mean-square deviation |
| RNase A | = | Ribonuclease A |
| ROCK | = | rho-associated, coiled-coil-containing protein kinase |
| ROS | = | Reactive oxygen species |
| rpm | = | Rotation per minute |
| RTK | = | Receptor-tyrosine kinase |
| <i>SalI</i> | = | Restriction enzyme (recognition sequence G ^A TCGAC) |
| SD | = | Standard deviation |
| SDS | = | Sodium dodecylsulfate |
| SDS-PAGE | = | Sodium dodecylsulfate polyacrylamide gelelektrophorese |
| SEC | = | Size exclusion chromatography |
| <i>Sf9</i> | = | <i>Spodoptera frugiperda</i> |
| SG | = | Space group |
| SHP-1/2 | = | Src homology region 2 domain-containing phosphatase-1/2 |
| STAT3 | = | Signal transducer and activator of transcription 3 |
| T (Base) | = | Thymine |
| TAE (buffer) | = | Tris acetate EDTA buffer |
| TCEP | = | Tris-(2-carboxyethyl)-phosphine |
| TEMED | = | Tetramethylethylenediamine |
| TEV | = | <i>Tobacco Etch Virus</i> protease recognition site |
| Th | = | Thomson (Th = unified atomic mass unit / electric charge unit) |
| THB | = | Thrombin protease recognition site |
| ™ | = | Trademark |

| | | |
|------------------|---|--|
| <i>t</i> PTEN | = | PTEN 7-353 Δ 286-309 |
| Tris (buffer) | = | 2-Amino-2-(hydroxymethyl)-propane-1,3-diol |
| Trx | = | Thioredoxin |
| Ub | = | Ubiquitin |
| UV | = | Ultraviolet |
| VHR | = | Vaccinia H1-related phosphatase |
| v/v | = | Volume per volume |
| w/v | = | Weight per volume |
| WWP2 | = | NEDD4-like E3 ubiquitin ligase |
| XDS | = | X-ray Detector Software |
| X-gal | = | 5-Brom-4-chlor-3-indoxyl- β -D-galactopyranosid |
| XIAP | = | X-linked inhibitor of apoptosis protein |
| 3S-PI-(3,4,5)-P3 | = | PIP ₃ substituted with thiophosphate at D3 position |
| Δ | = | Delta; “deficient of” |
| © | = | Copyright |
| ® | = | Registered trademark |

Table 34 | Three- and one-letter codes of 20 canonical amino acids.

| Amino acid | Three-letter code | One-letter code |
|-------------------|--------------------------|------------------------|
| Alanine | Ala | A |
| Arginine | Arg | R |
| Asparagine | Asn | N |
| Aspartic acid | Asp | D |
| Cysteine | Cys | C |
| Glutamine | Gln | Q |
| Glutamic acid | Glu | E |
| Glycine | Gly | G |
| Histidine | His | H |
| Isoleucine | Ile | I |
| Leucine | Leu | L |
| Lysine | Lys | K |
| Methionine | Met | M |
| Phenylalanine | Phe | F |
| Proline | Pro | P |
| Serine | Ser | S |
| Threonine | Thr | T |
| Tryptophan | Trp | W |
| Tyrosine | Tyr | Y |
| Valine | Val | V |